SPECTRAL ATMOSPHERIC ENERGETICS DURING JANUARY 1959

SPECTRAL ATMOSPHERIC ENERGETICS DURING

JANUARY 1959

by

Gaston Paulin

A thesis submitted to the Faculty of Graduate Studies and Research in partial fulfilment of the requirements for the degree of Doctor of Philosophy.

Department of Meteorology,
McGill University,
Montreal, Canada.

March, 1968

Dédiée à mon épouse, Norma

ACKNOWLEDGEMENTS

The author wishes to thank his research supervisor, Professor B. W. Boville, for the learned and sustained assistance provided throughout the duration of this study. He is also grateful to Professor B. O'Reilly for the spontaneous help received and for the loan of some computer programmes. He is also indebted to many of his colleagues in the Arctic Meteorology Research Group, especially to Dr. R. A. D. Byron-Scott, for stimulating discussions and helpful suggestions.

Thanks are due to Miss Susan Hoblyn, who prepared the typescripts and Messrs. Chang-Chun Su and Yvon Bourassa who drafted the diagrams.

The author acknowledges the helpful cooperation of the staff of the McGill Computing Centre. He also wishes to acknowledge with gratitude the financial support received from the Canadian Meteorological Service while undertaking this research.

TABLE OF CONTENTS

Chapter

Chapter

LIST OF FIGURES

Figure Number	Description of figure
5.3.3	Correlation coefficient between the 25-500 mb heights for total, eddy and wave numbers 1, 2 and 3 cases.
5.4.1	Comparison of the mean January 12-16, 1959, profile of the stability against Gates (1961).
5.4.2	Comparisons of computed energy conversions between eddy modes of available to kinetic energy using the diabatic diagnostic method (CE) and the adiabatic thermodynamic method (CE*) for the 25-100 mb layer.
5.4.3	Comparisons of computed energy conversions between the zonal modes of available to kinetic energy using the diabatic diagnostic (CZ) method and the adiabatic thermodynamic (CZ*) method. The zonal generation GZ is given by the residual CZ - CZ*. The computations are valid for the 100-25 mb layer.
5.4.4	Spectral vectors for both vertical motion methods and temperature at 25 mb on Jan. 12, 1959.
5.5.1	Balance terms in the budget of zonal available energy AZ at 25 mb during January 1959.
5.5.2	Balance terms in the budget of the eddy available energy AE at 25 mb in January 1959.
5.5.3	Balance terms in the budget of the eddy kinetic energy KE at 25 mb in January 1959.
5.5.4	KZ budget at 25 mb
5.5.5	Time loci of energy transfer maxima in January 1959 at 25 and 500 mb.
5.6.1	Balance terms for the budget of the zonal available energy AZ at 100 mb during January 1959.
5.6.2	Balance terms of the eddy available energy AE at 100 mb during January 1959.
5.6.3	Balance terms of the eddy kinetic energy KE at 100 mb during January 1959.
5.6.4	Balance of the zonal kinetic energy KZ at 100 mb during January 1959.
5.7.1	Energy transfers at 500 mb in January 1959.
5.8.1	Mean January 1959 energy transfers at 25 mb.

LIST OF TABLES

LIST OF SYMBOLS

The symbol notation follows current usage as closely as possible. This list may remove some ambiguity in occasional duplication of symbols.

Symbol	Meaning	First appears in equation number
c_v	Specific heat of dry air at constant volume	
c_p	Specific heat of dry air at constant pressure	
T	Temperature	
Z	Geopotential height	
g	Acceleration of gravity	
P, p	Pressure	
p	Pressure	
$\overline{(X)}^{y}$	Mean of X averaged over y	
A	Available potential energy: zonal plus eddy averaged over a constant pressure surface	
K	Kinetic energy: zonal plus eddy averaged over a constant pressure surface	
AZ, AE	Zonal and eddy components of A	
KZ, KE	Zonal and eddy components of K	
AE(n)	Wave number "n" component of A	
KE(n)	Wave number "n" component of K	
CA	Conversion from zonal to eddy available energy	1.1.1
CZ	Conversion from zonal available to zonal kinetic energy	1.1.1
GZ, GE	Zonal and eddy generation of available energy	1.1.1
CE	Conversion from eddy available to eddy kinetic energy	1.1.2
DZ, DE	Zonal and eddy frictional dissipation of kinetic energy	1.1.3 1.1.4
CK	Conversion from zonal to eddy kinetic energy	1.1.3
λ, ϕ	Longitude and latitude, respectively	
$\overline{(\ )}^{\lambda}$	Longitudinal averaging operator	1.1.5
$(\ )'$	Deviation from the longitudinal average, i.e., $(\ )' = (\ ) - \overline{(\ )}^{\lambda}$	1.1.6
$\{(\ )\}^{\phi}$	Latitudinal averaging operator	1.1.7

ϕ_1, ϕ_2	The southern and northern latitudes bounding the areal domain	1.1.7
$(\ )''$	Deviation from the latitudinal average, i.e., $$(\ )'' = (\ ) - \{(\ )\}^{\phi}$$	1.1.8
$(\ )^{*}$	Deviation from the areal average, i.e., $$(\ )^{*} = (\ ) - \{\overline{(\ )}^{\lambda}\}^{\phi}$$	3.1.7
u	Eastward velocity component	
v	Northward velocity component	
ω	Vertical velocity in the p-coordinate system, i.e., $$\omega = dp/dt$$	
$\mathbb{V}$	Horizontal wind vector	
h	Radiative heating rate	2.3.1
R	Gas constant for dry air	2.1.1
$\mathbb{F}$	Frictional dissipative forces	
X, Y	Components of $\mathbb{F}$	
$\mathbb{V}_g$	Geostrophic horizontal wind vector	2.3.1
$-\sigma$	Stability in the adiabatic-thermodynamic omega equation	2.3.2
J	Jacobian operator	2.3.3
f	Coriolis parameter	
n	Longitudinal wave number throughout except in Section 4.3 where it stands for the degree of a spherical harmonic function	
θ	Potential temperature except in Section 4.3 where it stands for the co-latitude	4.3.1

Fourier Transform Pairs

Variable	u	v	ω	T	Z	θ	h	X	Y
Spectral function	U	V	Ω	t^{o}	z	Q	$\mathcal{H}$	P_x	R_y

$(\ )_y$	Partial derivative with respect to y	
M	Mass of the atmosphere	3.1.1
dm	Differential mass element	3.1.1
Λ	Stability factor	3.1.2
u	Ratio R/c_p	3.1.2
a	Earth's radius	
$\hat{K}(n)$	Wave number "n" kinetic energy at some given latitude, i.e., $\hat{K}(n) = \lvert U(n)\rvert^2 + \lvert V(n)\rvert^2$	3.1.22
$\widehat{KZ}$	Zonal kinetic energy at some given latitude, i.e., $\widehat{KZ} = \hat{K}(0)/2$	3.1.22
$\Psi_{fg}(m,n)$	Function defined by equation C-10 in Appendix C	3.1.24
$\Phi_{fg}(n)$	Function defined by equation C-4 in Appendix C	3.1.24
$F(\theta, \lambda)$	Scalar field representing height or temperature and where θ is the co-latitude	4.3.1
A_n^m , B_n^m	Real Fourier coefficients in the spherical harmonic specification of $F(\theta, \lambda)$	4.3.1
m, n	Longitudinal wave number (rank) and degree of the harmonic, respectively	4.3.1
P_n^m	Normalised associated Legendre function	4.3.1
	Cosine of the co-latitude in Section 4.3	4.3.2
Z_n^m	Amplitude of the harmonics, i.e., $Z_n^m = A_n^m + B_n^m$	4.3.4
$\overline{E}^{\theta,\lambda}$	Mean horizontal kinetic energy	4.3.5

ψ_n^m	Amplitude of the stream function associated with the amplitude of the geopotential height Z_n^m	4.3.5
δ_0^m	Kronecker delta	
$\widetilde{KE}_n^m$	Pseudo-kinetic energy indicator	4.3.6
$\Delta_m^m, \mathcal{E}_m^m$	Errors in KE_n^m and Z_n^m, respectively	4.3.7
χ	Divergence coefficient	4.3.9
$\omega_{R-H}, \omega_{OBS}$	Rossby-Haurwitz and observed angular velocities of atmospheric waves	4.3.9
CE^*, CZ^*	Equivalent to the CE and CZ-terms but computed from the adiabatic-thermodynamic omega equation	5.4.4 5.4.5
BAL	Residual in the budgets of the energy reservoirs at single levels	5.4.4
$r_{fg}, R_{fg}(m)$	Coefficient of linear correlation between variables f and g and its corresponding spectral function	5.3.1 5.3.6
σ_{fg}	Covariance of f and g	5.3.3
σ_f^2	Variance of f	5.3.2

LIST OF APPENDICES

ABSTRACT

The energetics of January 1959 are assessed through a set of spectral energy equations developed for an open atmospheric system. The investigation considers two sets of data: a mid-January five-day set with a high vertical resolution of 10 levels (100 to 10 mb) and the full month's data at three levels (500, 100 and 25 mb).

The diagnostic omega-equation is solved in Fourier spectral form and diabatic radiative effects are included for the stratosphere.

Strong dynamical interactions between the troposphere and the stratosphere are found in wave numbers 1, 2 and 4; this is associated with geopotential flux, whose convergence is mainly responsible for increases in stratospheric activity. The major 25-mb eddy changes are related to wave one and two oscillations in the 500-mb block. Non-linear wave interactions also yield significant modifications in the eddy energies.

The daily spectral energetics are discussed systematically to explain the observed energy fluctuations.

CHAPTER 1

INTRODUCTION

1.1 Brief Historical Summary and Methods

Perverse weather has been one of man's chief irritants, creating a vast array of problems, from the simple need for shelter to the migration of races following climatic change. At the same time it has stimulated his curiosity and great attempts have been mounted to unravel the atmospheric puzzle.

In 1903, Margules provided a dynamical key when he showed that rearranging air masses of different temperatures lowers their centre of gravity and releases potential energy: the gross hydrostatic nature of the fluid binding internal and potential energy together as a temperature function $\overline{(c_v T + gZ)}^p = \overline{(c_p T)}^p$. With the advent of world-wide observational networks it became meaningful to treat the atmosphere as a complete (closed) system and the diagnostic techniques of spectral analysis in terms of available energy were set forth by Van Mieghem (1952) and Lorenz (1955).

In his analysis Lorenz showed that most of the atmosphere's potential energy is tied up in its mean state and only the small part associated with temperature variance on pressure surfaces is "available" for adiabatic redistribution and conversion into kinetic energy so that this rather complex heat engine can continue to run against friction.

In this study the tool of spectral analysis will be applied to hemispheric data to consider, in particular, the vertical structure and coupling of the heat engine from troposphere to stratosphere and the consequences of boundary fluxes in thermodynamically open systems.

The potential energy which is available to be converted into the kinetic energy of motion will be called available energy henceforth and will be designated by A. K will stand for the kinetic energy. Then following Lorenz (1955), A and K are partitioned into their zonal mean values, AZ and KZ, respectively, while the departures of each zonal field from its corresponding A and K, is called AE and KE, respectively. Each of the four equations, resulting from the time derivatives of the four above-mentioned quantities, share common terms with opposite signs between each other, marking the existence of transfers from one mode of energy into another. The resulting four equations are represented symbolically by:

$$\frac{\partial AZ}{\partial t} = -CA - CZ + GZ \qquad (1.1.1)$$

$$\frac{\partial AE}{\partial t} = CA - CE + GE \qquad (1.1.2)$$

$$\frac{\partial KZ}{\partial t} = CZ - CK - DZ \qquad (1.1.3)$$

$$\frac{\partial KE}{\partial t} = CE + CK - DE \qquad (1.1.4)$$

The definition of the terms in Eqns. (1.1.1) to (1.1.4) will be given in the text below.

Define a (λ, ϕ, p)-coordinate system and let u, v and ω be the three components of motion, T the temperature, $\mathbb{V}$ the wind vector, $\mathcal{h}$ the diabatic heating and $\mathbb{F}$ the frictional force per unit thickness. Also we define the longitudinal averaging operator as:

$$\overline{(\ )}^{\lambda} = \frac{1}{2\pi}\int_0^{2\pi} (\ )\, d\lambda \qquad (1.1.5)$$

while the deviation from this average is:

$$(\ )' = (\ ) - \overline{(\ )}^{\lambda} \tag{1.1.6}$$

The latitudinal averaging operator is given by:

$$\left\{(\ )\right\}^{\phi} = \frac{1}{(\sin\phi_2 - \sin\phi_1)} \int_{\phi_1}^{\phi_2} (\ ) \cos\phi \, d\phi \tag{1.1.7}$$

where ϕ_2 and ϕ_1 are the northern and southern latitude circles bounding the region. For the present purpose ϕ_2 and ϕ_1 stand for the north and south pole, respectively. The deviation from the latitudinal average is given by:

$$(\ )'' = (\ ) - \left\{(\ )\right\}^{\phi} \tag{1.1.8}$$

The superscripts λ and ϕ associated with the "bar" and the curly brackets will be omitted when they are not required for clarity. With this in mind the C's, D's and G's can be shown to be proportional to the following quantities:

$$CA \propto -\left\{ \overline{T'v'}^{\lambda} \frac{\partial \overline{T}^{\lambda}}{\partial \phi} \right\}^{\phi} \qquad CZ \propto -\left\{ \overline{\omega}^{\lambda} \overline{T}^{\lambda} \right\}^{\phi}$$

$$CE \propto -\left\{ \overline{\omega' T'}^{\lambda} \right\}^{\phi} \qquad GZ \propto \left\{ \overline{h}^{\lambda} \overline{T}^{\lambda} \right\}^{\phi}$$

$$GE \propto \left\{ \overline{h' T'}^{\lambda} \right\}^{\phi} \qquad CK \propto -\left\{ \cos\phi \, \overline{u'v'}^{\lambda} \frac{\partial}{\partial \phi} \left(\frac{\overline{u}^{\lambda}}{\cos\phi} \right) \right\}^{\phi}$$

$$DE \propto \left\{ \overline{\mathbb{V}' \cdot \mathbb{F}'}^{\lambda} \right\}^{\phi} \qquad DZ \propto \left\{ \overline{\mathbb{V}}^{\lambda} \cdot \overline{\mathbb{F}}^{\lambda} \right\}^{\phi}$$

Since the C's appear alternately with different signs in two equations, they are called conversion or transfer terms. CA represents the conversion of zonal to eddy available potential energy. It is proportional to the covariance of the eddy heat transport and the meridional gradient of the mean zonal temperature. Physically, when heat is transported northward by eddy motions, ($\overline{v'T'}^{\lambda} > 0$, cold northerly winds and warm southerly winds) where $\overline{T}^{\lambda}$ decreases with latitude (the normal state in the troposphere) the energy in AZ is transformed into that of AE.

CK represents the positive conversion from the zonal mode to the eddy mode of kinetic energy. Physically, the mean zonal kinetic energy (averaged over the area of interest), will tend to increase when relative eastward momentum is transported northward by the eddy meridional flow in a field of increasing mean zonal eastward momentum with latitude. Synoptically, southwest to northeast tilts of troughs and ridges imbedded in a mean zonal flow whose strength increases northward indicate visually a conversion of eddy to zonal kinetic energy, i.e., a negative CK.

CE measures the rate at which AE is transformed into KE by the action of the rising warm air and subsiding colder air in zonal planes, while CZ indicates the conversion from AZ to KZ, when the vertical motion versus temperature correlation is limited to circulation in meridional planes.

The G's represent the influence of exterior diabatic sources on the existing thermal field, tending to change the available potential energy reservoir. Heating the warmer areas and/or cooling the cooler regions tends to increase the temperature variance, hence also the available potential energy.

The D's represent the dissipation of kinetic energy in either mode by friction. Velocity profiles are usually flattened by the action of small scale eddy viscosity thus reducing the kinetic energy. On larger scales such a formulation is not generally possible as it may require negative diffusion coefficients (Gilman, 1964).

The energy flow diagram proposed by Phillips (1956) has found acceptance in the literature and a similar format will be used in this study. In Fig. 1.1.1, the direction of the flow represents positive transfer (C's), generation (G's) or dissipation (D's).

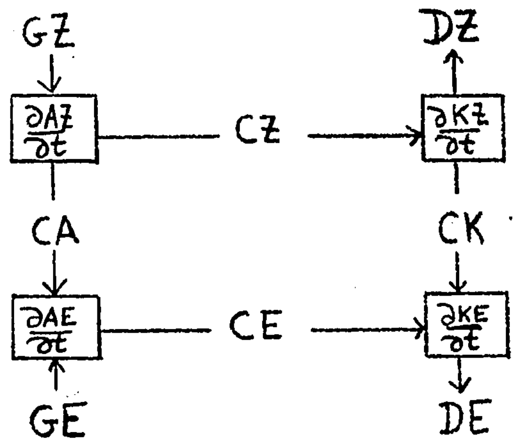

Fig. 1.1.1 Energy flow diagram showing positive direction in conversions, generation or dissipation

Phillips' original diagram represented energy studies for the whole atmosphere, but recently modifications have been added to study the energetics of a truncated volume, by computing the boundary effects.

The numerous studies that followed Lorenz's important paper dealt mainly with tropospheric data as upper level observations were sparse. Oort (1964) and Muench (1965) have listed various energy computations pertaining to the troposphere considered as a closed system. Muench's values for tropospheric average midwinter conditions are reproduced in Fig. 1.1.2.

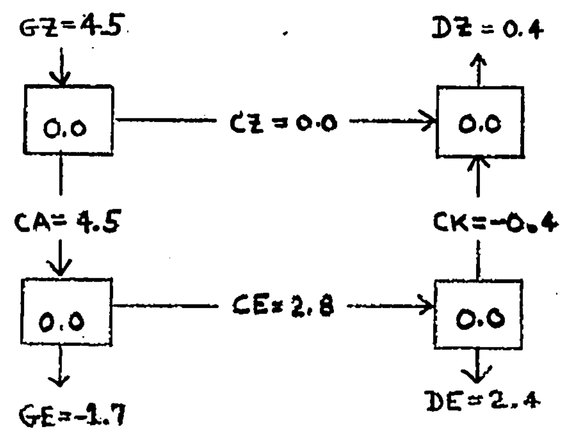

Fig. 1.1.2. Tropospheric energy diagram for mid-winter conditions after Muench (1965). Units: Ergs/cm^2 sec mb.

This shows that the normal tropospheric energy flow provides a zonal temperature field, created and maintained by solar input at a rate of 4.5 ergs/cm^2 sec mb. Portions of this field are transformed into an eddy temperature field by the action of the atmospheric eddies at an equivalent rate of 4.5 units. This eddy field loses energy by radiative and turbulent heat transfer between the earth's surface and the overlying air at a rate of 1.7 ergs/cm^2 sec mb. The eddy available potential energy is transformed into eddy kinetic energy as circulation is established in zonal planes with warm air rising and cold air subsiding. The average rate of transfer is given as 2.8 ergs/cm^2 mb sec. The balance of the eddy kinetic energy is achieved mostly through frictional dissipation. The troposphere rides on a relatively rough surface and suffers large dissipation through a relatively shallow boundary layer. This sink of energy almost cancels the baroclinic CE-transfer, being 2.4 ergs/cm^2 sec mb. The KE balance for the steady case is attained through a barotropic wave to zonal flow interaction at a relatively low rate of 0.4 units. Practically all of the energy transformed into the zonal form is lost in zonal energy dissipation.

Many people have contributed to the diagnostic tools required to compute tropospheric energetics. To name a few, White and Saltzman (1956) computed a CE$>$0 and obtained eddy dissipation of about 5 ergs/cm^2 mb sec. Saltzman (1957) derived the energy equation in the Fourier spectral domain for the closed system. Saltzman alone and conjointly with others produced a series of papers between 1958 to 1964 dealing with the statistics resulting from the spectral method. (Saltzman 1958, 1959; Saltzman and Teweles, 1964). Wiin-Nielsen and his group (Wiin-Nielsen, 1959, 1964, Wiin-Nielsen and Brown,1960, Wiin-Nielsen and Drake,1963) amplified the diagnostic tools in studies of the tropospheric interchanges in spectral, annual and seasonal partitions. Systematic effects of tropospheric diabatic heating are also introduced by the group. Murakami has also studied the long term (yearly) spectral statistics of the troposphere (500 mb in particular) (Murakami and Tomatsu, 1964; Murakami, 1963).

Next endeavours were directed at the stratosphere, as observations reached higher altitudes more frequently. The efforts in this new domain were generally two-fold; the study of seasonal and annual statistics, and the search for the causes explaining the surprising stratospheric behaviour during a sudden warming epoch. Boville (1961), Oort (1963) belong to the first category, while Craig and Hering (1959), Reed and his school (Reed, Wolfe and Nishimoto, 1963; Muench 1965; Perry 1966), Miyakoda (1963), Lateef (1964), Julian and Labitzke (1965), Murakami (1965) belong to the latter.

1.2 Purpose

The present paper is a logical extension of Miyakoda (1963), Muench (1965), Julian and Labitzke (1965) and Perry (1966). It stems out of some of their common suggestions, as their work in turn was more or less suggested by the work of Saltzman (1957) and

Teweles (1963). Some further refinements to the diagnostic methods have been added by Perry (1966). Muench patterned his derivation along Lorenz (1955) but as applied to an open system, (the stratosphere) being careful to preserve all the boundary flux terms. Perry used the spectral approach of Saltzman (1957), Reed et al (1963) and extended it to include the boundary fluxes, as in Muench's case. Perry separated the atmosphere into three layers, two of which overlapped in the stratosphere.

This study considers in detail the spectral and total atmospheric energetics over a short period (5 days) where data are dense (ten levels from 1000 mb to 10 mb) and a longer period (daily, one month) but where data are sparsely distributed in the vertical (three levels: 500 mb, 100 mb and 25 mb). The purpose of the study is to clarify the processes occurring in a more or less normal winter in contrast to previous studies of anomalous winters characterized by major warmings in the upper levels.

Although the general approach and methodology follows previous studies, some original methods were used in the details. A spectral solution of the diagnostic omega-equation has been performed using the 10 levels of information. Radiative transfer in the long-wave terrestrial spectrum and the short-wave solar spectrum has been computed in the stratosphere using a mixture of empirical and fully physical approaches. The diabatic output was inserted into the diagnostic omega-equation and also used to compute eddy and zonal generation processes.

CHAPTER 2

DATA PROCESSING AND MODELLING

2.1 Compilation and Manipulation of Data

Various types of data have been accumulated at McGill through the years. Daily synoptic maps have been analysed and the grid point values at the latitude-longitude intersections extracted. A three-year series of maps, analysed every five days at 500, 100 and 25 mb has been completed but was not used in this study. A second series exists for the same levels but with daily frequency for January 1959. A third set of a shorter time sequence, but for many levels, has been completed for this study. It spans the period from January 12, 1959 to January 16, 1959. It contains ten levels (1000, 850, 700, 500, 300, 200, 100, 50, 25 and 10 mb) of height and temperature fields, excluding only the 1000 mb temperature. Of importance, the 50 mb and 10 mb data were read from the Berlin map series (1962). The hydrostatic test between the McGill 25 mb and the Berlin 10 mb data did not prove consistent over Asia. The maps at 10 mb were reanalyzed and drawn to be more consistent with the sparsely distributed temperature data.

This study uses the 31 daily maps for January 1959 at three levels, and the 12 to 16 January 1959 data for ten levels. The latitude-longitude grid has an interval of 10 degrees in the eastward direction and 5 degrees in the meridional direction, and extends from 80°N to 30°N. Each set of 36 longitudinal grid values was transformed into equivalent Fourier coefficients spanning 15 wave numbers, the computed coefficients were stored on magnetic tapes for further use.

An error check on the data was performed by assigning an upper limit to the Fourier coefficients of wave number higher than 9. The values above the limits were checked against the original maps and corrected when necessary. Table 2.1.1 shows the distribution of the two data sets with time and pressure.

Table 2.1.1. Height (Z) and Temperature (T) fields in this study. P stands for the mean sea-level pressure fields.

P(mb)	MSL	850	700	500	300	200	100	50	25	10
Date Jan/59										
1				Z, T			Z, T		Z, T	
2				"			"		"	
to										
11				"			"		"	
12	P	Z, T	Z, T	Z, T	Z, T	Z, T	Z, T	Z, T	Z, T	Z, T
to										
16	"	"	"	"	"	"	"	"	"	"
17				Z, T			Z, T		Z, T	
18				"			"		"	
to										
31				"			"		"	

The defects in the data and the map analyses have been discussed by Boville (1961). The accuracy of radiosonde instruments, at the time the data were taken, was given as about $\pm$ 3 mb for the barograph and $\pm$ 0.5°C for the thermograph. The geopotential height is obtained as the dependent variable through the integrated hydrostatic approximation of the form:

$$Z = \frac{R}{g} \int_{p}^{p_0} T \, d \ln p \qquad (2.1.1)$$

The height accuracy is given in Table 2.1.2 taken from Boville (1961) and Orvig (1962).

Table 2. 1. 2. Standard error of the computed geopotential height from radiosonde instruments in 1959.

Standard pressure level (mb)	500	300	100	50	25	10
Standard error (ft)	± 50	± 115	± 125	± 200	± 300	± 500

The error due to direct solar heating on the instruments at 25 mb has been discussed by Boville (1961) and will not be repeated here. Suffice to say that the sunlit areas averaged about 3°K warmer than the areas in the dark. Both types of errors have been reduced. Some variations about this mean is due to systematically different instrument characteristics. The mean temperature error has been corrected while the variable instrument characteristic has been reduced from given instrumented corrections, but the corrections were not always sufficient.

2. 2 Methodology in the 5-day Data Set

The study uses Fourier coefficients of the geopotential height, Z, and the temperature, T, as the independent variables. A vertical motion (ω) model has been developed in the Fourier spectral domain using the diagnostic omega-equation approach. The model is fully described in Appendix A. It has nine layers and used the ten levels of data available from January 12 to 16, 1959.

The geostrophic spectral wind components u and v were computed directly from the height field Fourier components. Since the zonal mean of the meridional wind, $\overline{v}^{\lambda}$, is identically equal to zero in such a scheme, its value has been computed by solving for $\overline{v}^{\lambda}$ using a computed mean zonal $\overline{\omega}^{\lambda}$ and the zonally-averaged continuity equation, as shown in Appendix A. Using a mixture of empirical and complete radiation formulae, monthly zonally averaged ozone data and given temperature fields, the field of radiative heating, h, was computed in the stratosphere during January 12 to 16, 1959. Full details on the method are given in Appendix B. All the results were stored in Fourier-coefficient form.

The 5-day energy conversions were based on the input fields of Z and T, on the derived fields of motion (u, v, ω) and on stratospheric heating (h). The vertical motion was computed adiabatically in the troposphere and diabatically in the stratosphere. The frictional dissipative forces, $\mathbb{F}$, are inferred from a budget approach in the kinetic energy results.

2.3 Methodology in the 29-day Data Set

The height and temperature fields at 500, 100 and 25 mb from January 2 to 30, 1959 formed the input data in the one-month study. Because of the poor vertical resolution, the adiabatic-thermodynamic method was used to compute vertical motion. After the thermodynamic equation is retained in time-dependent form, ~~differentiated with respect to time~~, the resulting equation, when solved for ω , leads to the relation:

$$\omega = \frac{\partial T/\partial t + \mathbb{V}_g \cdot \nabla_p T - h/c_p}{-\sigma} \tag{2.3.1}$$

where the stability "$-\sigma$ " is given by:

$$-\sigma = \frac{RT}{p\,c_p} - \frac{\partial T}{\partial p} \tag{2.3.2}$$

h is the heating rate,

c_p is the specific heat of dry air at constant pressure,

$\mathbb{V}_g \cdot \nabla_p T$ is the temperature advection on constant pressure surfaces by the horizontal geostrophic wind $\mathbb{V}_g$.

In the adiabatic case: $h = 0$. Using geostrophy, the temperature advection is given by:

$$\mathbb{V}_g \cdot \nabla_p T = \frac{g}{f} J(Z, T) \tag{2.3.3}$$

where f is the Coriolis parameter and J is the Jacobian operator applied to the (x, y)-plane at constant pressure. Eqn. (2.3.1) may be rewritten as:

$$\omega = \frac{\frac{\partial T}{\partial t} + \left(\frac{g}{f}\right) J(Z, T)}{-\sigma} \tag{2.3.4}$$

Eqn. (2.3.4) has been transformed into the complex Fourier domain using a method developed in Appendix A. The results when $\sigma = \sigma(p)$ only are:

$$\Omega(n) = -\frac{1}{\sigma(p)}\left[\frac{\partial t^{\circ}(n)}{\partial t} - \frac{g}{f a^2 \cos\phi}\left(\sum_{m=-\infty}^{\infty} i\, m\, t^{\circ}(m) \frac{\partial z(n-m)}{\partial \phi} - i\, m\, z(m) \frac{\partial t^{\circ}(n-m)}{\partial \phi}\right)\right] \tag{2.3.5}$$

where $\Omega(n)$, $t^{\circ}(n)$, $z(n)$ are the spectral functions corresponding to the ω, T, Z fields, ϕ is the latitude, a, the earth's radius, m and n are wave numbers.

The 48-hour centered time-difference when applied to the temperature spectral function t°(n), explains the lack of computations for January 1st and 31st.

The low vertical resolution constrains us to accept the stability "$-\sigma$" as a function of pressure only. Then the vertical motion may be computed at any level, given a good set of temperature data in time. The stability had been computed for the 9-layer diagnostic model described in Appendix A, for the five days from January 12 to 16, 1959. The 5-day mean values of this stability at 500, 100 and 25 mb were accepted as representative for the whole month of January 1959. Comparison with stability computations for

January by other investigators supports this approximation (Gates, 1961).

2.4 Comparison between Vertical Motion Models

In view of the conflicting results among statistics using different types of vertical motion, it is necessary to discuss the basic assumptions inherent in each method.

Inspection of the results of both methods when integrated over wave number shows good agreement on the whole, the resemblance being better at 25 mb than at 100 mb. At 500 mb the horizontal maps of the vertical motion are similar but the adiabatic-thermodynamic method shows larger magnitudes than the diagnostic (also adiabatic at 500 mb) method. This difference also exists at 25 mb and 100 mb, but is much smaller than at 500 mb. The difference in magnitude is not unique to this study, but seems to be intrinsic to the two different methods. More specifically, it is due to the different numerical procedures and the physical simplification made in each case. Miyakoda (1963), in a similar study using both types (not spectrally, but on a numerical grid), found that the magnitude of stratospheric ω's resulting from an adiabatic-thermodynamic omega method is larger than the diagnostic ω's by a factor of 1.5, when both computations are performed without a heating field. When heating is introduced in the diagnostic omega equation only, the computed vertical motion fields showed better agreement. Inspection of Miyakoda's graph reveals a reduced factor from 1.5 to about 1.2. The latter factor is found in the present study at 25 mb. When adiabatic computations at 500 mb are compared, both Miyakoda (1963) and this study arrive at large magnitudes in the adiabatic-thermodynamic case, the factor being about 2, but rising occasionally to 3. The larger factor is usually found in the vertical motion maxima.

The anomalous difference between the two methods may be assigned numerically to the analogs for derivatives and physically, to the systematically varying influence imposed by the atmospheric scale changes with height.

The effective grid from which the spectrally independent variables $\zeta(n)$ and $t^{o}(n)$ were obtained remained fixed at all pressure levels. The diagnostic method contains up to the 4th order derivative while the other method requires only first order differentiation. Because of the decreasing significance of the shorter waves (in the synoptic scale) with height, the 25-mb level will be smoothed the least while the 500 mb will be grossly smoothed. The diagnostic model will be more faithfull in the large scale while the adiabatic-thermodynamic method will preserve the shorter scale more effectively. To remedy this, a smaller scale grid would be necessary in the troposphere to preserve the significant synoptic scale effect there, but no change would be necessary in the stratosphere, as far as the grid size is concerned.

The physical assumptions required by the adiabatic-thermodynamic method will lead to some trouble in computing energy statistics. This will be dealt with later when this type of computed vertical motion is applied to the problem of the energetics.

CHAPTER 3

THE ENERGY BUDGET IN THE FOURIER SPECTRAL DOMAIN

3.1 The Spectral Energy Equations for an Open System

This paper adopts the general methodology of Saltzman (1957), Reed et al (1963), Muench (1965) as combined by Perry (1966). The spectral equations are fully derived in Perry's doctoral thesis (Perry, 1966). An abridged form of the derivation is given here so that the physical concepts implied may be clearly underlined.

The (λ, ϕ, p)-coordinate system is adopted with Θ, the potential temperature as our basic parameter. Following Lorenz (1955) the available potential energy of a closed system is defined as the difference between the total potential energy (potential plus internal) and that which would exist if the mass were redistributed to a horizontally stratified state under adiabatic frictionless conditions. Lorenz (1955) has shown that following this definition and conditions, the available potential energy A of the system depends on the variance of potential temperature on isobaric surfaces. In spherical coordinates, the equation becomes

$$\int_M A\, dm = \int_0^{p_0}\int_{-\pi/2}^{\pi/2}\int_0^{2\pi} \Lambda\, \frac{\Theta^{*2}}{2}\, a^2 \cos\phi\, d\lambda\, d\phi\, \frac{dp}{g} \qquad (3.1.1)$$

where

$$\Lambda = -\left(\frac{p}{p_0}\right)^{\mu} \frac{R}{p} \left(\frac{\partial}{\partial p}\left\{\overline{\Theta}^{\lambda}\right\} \right)^{-1} \qquad (3.1.2)$$

In a similar manner the atmosphere kinetic energy is defined as

$$\int_M K \, dm = \int_0^{p_0} \int_{-\pi/2}^{\pi/2} \int_0^{2\pi} \frac{\mathbb{V}^2}{2} a^2 \cos\phi \, d\lambda \, d\phi \, \frac{dp}{g} \tag{3.1.3}$$

The integrand A of Eqn. (3.1.1) represents the contribution of one unit of mass to the available potential energy of the whole atmosphere. In particular the concept of available energy may be applied to any finite air volume when the normal components of the air velocity across the boundaries vanish everywhere since any interaction or contribution to the exterior by any mass elements is nil. As a first approximation, since the interaction between the two hemispheres is rather small, each hemisphere may be practically taken as a closed system. Van Meighem (1961) in deriving the equation for A, obtains the same results as Lorentz except for a small added term due to the atmospheric compressibility which he evaluated to be two orders of magnitude smaller than the main term shown above. As is specifically stressed by Muench and Perry the available energy computed in a truncated open atmospheric volume may be justified by considering it as a contribution to the whole atmosphere, or at least to the whole northern hemisphere. Muench (1965) has computed the relative temperature variance difference between a horizontally truncated volume extending from North Pole to 15°N and the pole-to-pole value. He obtained a difference of 8 percent which lies within the uncertainties inherent in the computational methods. Since our lateral truncations coincide with the 30°N and 80°N latitude circles, larger differences are to be expected. Rough computations indicate stratospheric differences of less than 15 percent, which can be tolerated in the light of other errors. The stratosphere-troposphere demarcation was arbitrarily assigned to the 150 mb pressure surface. Thus p_1 and p_2, the pressures of the upper and lower boundaries, respectively, become 150 mb and 1000 mb for the troposphere and 0 mb and 150 mb for the stratosphere. Letting $\Delta p = p_2 - p_1$, the above two layers are 850 mb and 150 mb thick.

To conform with general usages, the C.G.S. unit per mb has been adopted. In this system, energy exchanges will appear in erg/cm^2 mb sec while the energies will carry the erg/cm^2 mb unit. The longitude λ varies as:

$$0 \leq \lambda \leq 2\pi \tag{3.1.4}$$

and the latitude ϕ,

$$\phi_1 \leq \phi \leq \phi_2 \tag{3.1.5}$$

where ϕ_1 and ϕ_2 are fixed to 30N and 80N, respectively. The kinetic energy averaged over this latitude-longitude grid becomes:

$$K = \left\{ \overline{\frac{\mathbb{V}^2}{2}}^{\lambda} \right\}^{\phi} \tag{3.1.6}$$

Similarly the contribution A of the arbitrarily thick atmospheric layer centered at pressure "p" to the available potential energy of the whole atmosphere is given as:

$$A = \Lambda \left\{ \overline{\frac{\Theta^{*2}}{2}}^{\lambda} \right\}^{\phi} \tag{3.1.7}$$

The integration in the vertical of both K and A when normalized to a stratospheric or tropospheric column of 1 cm^2 cross-section yields the two relationships

$$\int_{p_1}^{p_2} K \frac{dp}{g} = \int_{p_1}^{p_2} \left\{ \overline{\frac{\mathbb{V}^2}{2}}^{\lambda} \right\}^{\phi} \frac{dp}{g} \tag{3.1.8}$$

and

$$\int_{p_1}^{p_2} A \frac{dp}{g} = \int_{p_1}^{p_2} \Lambda \left\{ \overline{\frac{\Theta^{*2}}{2}}^{\lambda} \right\}^{\phi} \frac{dp}{g} \tag{3.1.9}$$

The main development consists in taking the local rates of changes of K and A and expanding the right-hand-side terms by the use of the equations of motion, the thermodynamic equation, the continuity equation and the equation of state for dry air. Formally, it consists in performing the following operations:

$$\frac{\partial K}{\partial t} = \frac{\partial}{\partial t}\left\{\overline{\frac{\mathbb{V}^2}{2}}^{\lambda}\right\}^{\phi} \tag{3.1.10}$$

$$\frac{\partial A}{\partial t} = \Lambda \frac{\partial}{\partial t}\left\{\overline{\frac{\theta^{*2}}{2}}^{\lambda}\right\}^{\phi} \tag{3.1.11}$$

Supplementary application of complex Fourier zonal harmonics is included in Appendix C. Use will be made of i) the equations of motion in spherical and p-coordinates:

$$\frac{\partial u}{\partial t} = -\frac{1}{a\cos\phi} u \frac{\partial u}{\partial \lambda} - \frac{v}{a}\frac{\partial u}{\partial \phi} - \omega\frac{\partial u}{\partial p} + fv + \frac{uv}{a}\tan\phi - \frac{g}{a\cos\phi}\frac{\partial z}{\partial \lambda} - X \tag{3.1.12}$$

$$\frac{\partial v}{\partial t} = -\frac{1}{a\cos\phi} u \frac{\partial v}{\partial \lambda} - \frac{v}{a}\frac{\partial v}{\partial \phi} - \omega\frac{\partial v}{\partial p} - fu - \frac{u^2}{a}\tan\phi - \frac{g}{a}\frac{\partial z}{\partial \phi} - Y \tag{3.1.13}$$

ii) the hydrostatic equation:

$$\frac{\partial p}{\partial z} = -\rho g \tag{3.1.14}$$

iii) the continuity equation:

$$-\frac{\partial \omega}{\partial p} = \frac{1}{a\cos\phi}\left[\frac{\partial u}{\partial \lambda} + \frac{\partial}{\partial \phi}(v\cos\phi)\right] \tag{3.1.15}$$

iv) the thermodynamic equation:

$$\frac{\partial \theta}{\partial t} = \frac{-1}{a\cos\phi} u \frac{\partial \theta}{\partial \lambda} - \frac{v}{a}\frac{\partial \theta}{\partial \phi} - \omega\frac{\partial \theta}{\partial p} + \frac{\alpha h}{c_p} \tag{3.1.16}$$

and v) the equation of state for dry air:

$$\rho = p / RT \tag{3.1.17}$$

Since we will be working in the complex Fourier domain it will be useful to list at this point the notation for the Fourier transform pairs that will be used explicitly in the energy equations. These are listed in Table (3.1.1).

Table (3.1.1) Fourier transform pairs used in the energy equations

Variable	u	v	ω	z	θ	h	X	Y
Spectral function	U	V	Ω	$\mathfrak{z}$	Q	$\mathcal{H}$	P_x	P_y

Following Lorenz (1955) the average kinetic energy is partitioned into its zonal and eddy modes:

$$K = \left\{ \frac{\overline{\mathbb{V}}^{\lambda^2}}{2} \right\}^{\phi} + \sum_{n=1}^{\infty} KE(n) \tag{3.1.18}$$

where

$$KE(n) = \left\{ |U(n)|^2 + |V(n)|^2 \right\}^{\phi} \tag{3.1.19}$$

Following Lorenz's notation:

$$K = KZ + KE, \quad KZ = \left\{ \overline{\mathbb{V}}^{\lambda^2} \right\}^{\phi} \quad \text{and} \quad KE = \sum_{n=1}^{\infty} KE(n) \tag{3.1.20}$$

Noting that KE(n) is the areal average of the kinetic energy of wave number n, we introduce a component of this average, i.e., $\hat{K}(n)$, the zonal average kinetic energy of wave number n at some latitude ϕ. This yields the relationship:

$$KE(n) = \left\{ \widehat{K}(n) \right\}^{\phi} \tag{3.1.21}$$

and

$$\left.\begin{aligned} \widehat{K}(n) &= |U(n)|^2 + |V(n)|^2 \\ \widehat{K}(0) &= |U(0)|^2 + |V(0)|^2 = \overline{u}^{\lambda 2} + \overline{v}^{\lambda 2} = \overline{\mathbb{V}}^{\lambda 2} = 2\widehat{KZ} \end{aligned}\right\} \tag{3.1.22}$$

Noting that, for complex arguments like J(n),

$$\frac{\partial}{\partial t}\left[|J(n)|^2\right] = \frac{\partial}{\partial t}\left[J(n)J(-n)\right] = J(n)\frac{\partial}{\partial t}J(-n) + J(-n)\frac{\partial}{\partial t}\left[J(n)\right] \tag{3.1.23}$$

the rates of change of $\widehat{K}(n)$ are obtained by applying the above rule to U(n) and V(n) once the equations of motion (3.1.12) and (3.1.13) have been expanded and transformed into their complex Fourier spectral forms. Similarly, the equation of continuity (3.1.15) is transformed into its spectral specification. The last result is then used in the expansion of $\partial\left[|U(n)|^2\right]/\partial t$ and $\partial\left[|V(n)|^2\right]/\partial t$ yielding the expression:

$$\begin{aligned} \frac{\partial}{\partial t}\left[|\widehat{K}(n)|\right] = &-\sum_{m=-\infty}^{\infty}\left[\frac{\partial}{\partial p}\left[U(n)\Psi_{\omega u}(m,n) + V(n)\Psi_{\omega v}(m,n)\right] + \frac{1}{a\cos\phi}\frac{\partial}{\partial\phi}\left[\cos\phi\left[U(n)\Psi_{vu}(m,n) + V(n)\Psi_{vv}(m,n)\right]\right]\right] \\ &+\sum_{m=-\infty}^{\infty}\left[U(n)\left[\frac{1}{a\cos\phi}\Psi_{uu_\lambda}(m,n) + \frac{1}{a}\Psi_{vu_\phi}(m,n) + \Psi_{\omega u_p}(m,n) - \frac{\tan\phi}{a}\Psi_{uv}(m,n)\right]\right. \\ &\left.+V(n)\left[\frac{1}{a\cos\phi}\Psi_{uv_\lambda}(m,n) + \frac{1}{a}\Psi_{vv_\phi}(m,n) + \Psi_{\omega v_p}(m,n) + \frac{\tan\phi}{a}\Psi_{uu}(m,n)\right]\right] \\ &- g\left[\frac{1}{a\cos\phi}\Phi_{uz_\lambda}(n) + \frac{1}{a}\Phi_{vz_\phi}(n)\right] - \left[\Phi_{uX}(n) + \Phi_{vY}(n)\right] \end{aligned} \tag{3.1.24}$$

where $\Psi_{fg}^{(m,n)}$ represents wave interaction of f on g, and $\Phi_{fg}^{(n)}$ represents a correlation between f and g at wave number n (see Appendix A and C). Eqn. (3.1.24) relates the time rate of change of the zonal kinetic energy in wave number "n" to four different mechanisms. The first one, given by the first summation over wave number m", is the boundary contribution to the rate of change in the kinetic energy of wave number "n". This is achieved by vertical ($\partial/\partial p$) and horizontal ($\partial/\partial\phi$) convergence in the energy fluxes across those boundaries. This mechanism couples the chosen volume not only with the neighoring activities at wave number "n" but also interacts with energy fluxes at all scales originating in the exterior region. The second summation on "m" exists "in situ" and represents the non-linear wave interaction of all other waves contributing to the kinetic energy of wave number "n". The third term stands for the work done by the ageostrophic part of the wind when acting against the pressure force. This is referred to synoptically as the cross-isobaric flow on a constant height surface, or cross-contour flow on a constant pressure surface. This mechanism will be elaborated later. Finally, the fourth and last mechanism influencing the time rate of change in $\widehat{K}(n)$ is the sink in frictional dissipation.

The interaction of wave number "n" zonal harmonics with those of wave number m = 0 are separated out from the two first summations on "m" in Eqn. (3.1.24). The resulting expansion, upon application of the continuity equation, yields the interaction between the mean zonal (m = 0) kinetic energy and the kinetic energy at the scale of wave number "n":

$$\left.\begin{aligned} -\Big[\, &\Phi_{uv}^{(n)} \frac{\cos\phi}{a} \frac{\partial}{\partial\phi}\left(\frac{\overline{u}^{\lambda}}{\cos\phi}\right) + \Phi_{vv}^{(n)} \frac{1}{a} \frac{\partial \overline{v}^{\lambda}}{\partial\phi} + \Phi_{\omega u}^{(n)} \frac{\partial \overline{u}^{\lambda}}{\partial p} \\ &+ \Phi_{\omega v}^{(n)} \frac{\partial \overline{v}^{\lambda}}{\partial p} - \Phi_{uu}^{(n)} \frac{\tan\phi}{a} \overline{v}^{\lambda} \Big] \end{aligned}\right\} \qquad (3.1.25)$$

It is to be noted that in most other studies, the first term of Eqn. (3.1.25) is retained, while the others are usually neglected; the reasons being that they are usually smaller and that the vertical motion "ω" may not be available. This first term is proportional to the barotropic exchange between wave number "n" and the zonal kinetic energy by the "u-v" correlation, implying northward eddy transport of relative westerly momentum in the zonal flow.

The component of the work term inside the volume, described as the cross-isobaric or cross-contour flow in Eqn. (3.1.24), is transformed using the equation of continuity, the equation of state and the hydrostatic equation, and is thereby related to correlations between vertical velocity and temperature within the volume and to horizontal and vertical convergences of the geopotential at the boundaries. For n $\neq$ 0, the work term which converts potential to kinetic energy, either "in situ" or from the outside, in wave number "n", is given by:

$$\frac{\partial}{\partial p}\left[g\,\Phi^{(n)}_{\omega z}\right]+\frac{1}{a\cos\phi}\frac{\partial}{\partial\phi}\left[g\,\Phi^{(n)}_{vz}\cos\phi\right]-\Lambda\frac{\partial\{\overline{\theta}^{\lambda}\}^{\phi}}{\partial p}\Phi^{(n)}_{\omega\theta} \qquad (3.1.26)$$

Similarly, for n = 0, the "work" term is given by:

$$\frac{\partial}{\partial p}\left[2g\,\overline{\omega}^{\lambda}\,\overline{Z}^{\lambda}\right]+\frac{1}{a\cos\phi}\frac{\partial}{\partial\phi}\left[2g\,\overline{v}^{\lambda}\,\overline{Z}^{\lambda}\cos\phi\right]-2\Lambda\frac{\partial\{\overline{\theta}^{\lambda}\}^{\phi}}{\partial p}\overline{\omega}^{\lambda}\,\overline{\theta}^{\lambda} \qquad (3.1.27)$$

Separating the cases: n $\neq$ 0 from n = 0, using the expansion of Eqn. (3.1.24), the budget equations for $\widehat{K}(n)$ and $\widehat{K}(0)$ result:

$$\frac{\partial}{\partial t}\left[\widehat{K(n)}\right] = -\frac{\partial}{\partial p}\left[\sum_{\substack{m=-\infty\\ \neq 0}}^{\infty}\left[U(m)\,\Psi_{\omega u}^{(m,n)} + V(m)\,\Psi_{\omega v}^{(m,n)}\right]\right]$$

$$-\frac{1}{a\cos\phi}\frac{\partial}{\partial\phi}\left[\cos\phi\sum_{\substack{m=-\infty\\ \neq 0}}^{\infty}\left[U(m)\,\Psi_{vu}^{(m,n)} + V(m)\,\Psi_{vv}^{(m,n)}\right]\right]$$

$$-\left[\Phi_{uv}^{(n)}\frac{\cos\phi}{a}\frac{\partial}{\partial\phi}\left(\frac{\overline{u}^{\lambda}}{\cos\phi}\right) + \Phi_{vv}^{(n)}\frac{\partial\overline{v}^{\lambda}}{a\,\partial\phi} + \Phi_{\omega u}^{(n)}\frac{\partial\overline{u}^{\lambda}}{\partial p} + \Phi_{\omega v}^{(n)}\frac{\partial\overline{v}^{\lambda}}{\partial p}\right.$$

$$\left.-\frac{\tan\phi}{a}\Phi_{uu}^{(n)}\,\overline{v}^{\lambda}\right] + \sum_{\substack{m=-\infty\\ \neq 0}}^{\infty}\left[U(m)\left[\frac{1}{a\cos\phi}\Psi_{uu_\lambda}^{(m,n)} + \frac{1}{a}\Psi_{vu_\phi}^{(m,n)}\right.\right.$$

$$\left.+\Psi_{\omega u_p}^{(m,n)} - \frac{\tan\phi}{a}\Psi_{uv}^{(m,n)}\right] + V(m)\left[\frac{1}{a\cos\phi}\Psi_{uv_\lambda}^{(m,n)}\right. \tag{3.1.28}$$

$$\left.\left.+\frac{1}{a}\Psi_{vv_\phi}^{(m,n)} + \Psi_{\omega v_p}^{(m,n)} + \frac{\tan\phi}{a}\Psi_{uu}^{(m,n)}\right]\right] + \Lambda\frac{\partial\{\overline{\theta}^{\lambda}\}^{\phi}}{\partial p}\Phi_{\omega\theta}^{(n)}\cdot$$

$$-\frac{\partial}{\partial p}\left[g\,\Phi_{\omega z}^{(n)}\right] - \frac{1}{a\cos\phi}\frac{\partial}{\partial\phi}\left[g\,\Phi_{vz}^{(n)}\right] - \left[\Phi_{uX}^{(n)} + \Phi_{vY}^{(n)}\right]$$

Since $\widehat{K(0)} = \overline{\mathbb{V}}^{\lambda^2}$ and $\widehat{KZ} = \overline{\mathbb{V}}^{\lambda^2}/2$, we will write the following equation as the balance for $\widehat{K(0)}/2$, equivalent to KZ, as shown by Eqn. (3.1.22).

$$\frac{\partial}{\partial t}\left[\frac{\overline{\mathbb{V}}^{\lambda 2}}{2}\right] = -\frac{\partial}{\partial p}\left[\overline{\omega}^{\lambda}\frac{(\overline{u}^{\lambda 2}+\overline{v}^{\lambda 2})}{2} + \sum_{m=1}^{\infty}\left[\overline{u}^{\lambda}\Phi_{\omega u}(m) + \overline{v}^{\lambda}\Phi_{\omega v}(m)\right]\right]$$

$$-\frac{1}{a\cos\phi}\frac{\partial}{\partial\phi}\left[\cos\phi\left[\overline{v}^{\lambda}\frac{(\overline{u}^{\lambda 2}+\overline{v}^{\lambda 2})}{2} + \sum_{m=1}^{\infty}\left[\overline{u}^{\lambda}\Phi_{uv}(m) + \overline{v}^{\lambda}\Phi_{vv}(m)\right]\right]\right]$$

$$+\sum_{m=1}^{\infty}\left[\Phi_{uv}(m)\frac{\cos\phi}{a}\frac{\partial}{\partial\phi}\left(\frac{\overline{u}^{\lambda}}{\cos\phi}\right) + \frac{1}{a}\Phi_{vv}(m)\frac{\partial\overline{v}^{\lambda}}{\partial\phi} + \Phi_{\omega u}(m)\frac{\partial\overline{u}^{\lambda}}{\partial p}\right. \tag{3.1.29}$$

$$\left. + \Phi_{\omega v}(m)\frac{\partial\overline{v}^{\lambda}}{\partial p} - \frac{\tan\phi}{a}\overline{v}^{\lambda}\Phi_{uu}(m)\right] - \frac{\partial}{\partial p}\left[g\,\overline{\omega}^{\lambda}\overline{Z}^{\lambda}\right]$$

$$-\frac{1}{a\cos\phi}\frac{\partial}{\partial\phi}\left[g\cos\phi\,\overline{v}^{\lambda}\overline{Z}''\right] + \Lambda\frac{\partial\{\overline{\Theta}^{\lambda}\}^{\phi}}{\partial p}\overline{\omega}^{\lambda}\overline{\Theta}^{\lambda} - \left[\overline{u}^{\lambda}\overline{X}^{\lambda} + \overline{v}^{\lambda}\overline{Y}^{\lambda}\right]$$

Eqn. (3.1.28) and (3.1.29) are the two basic equations dealing with the kinetic energy budget. The next step will lead to equivalent equations but related to the budget of the available energy.

Eqn. (3.1.11) is first partitioned into its zonal and eddy form:

$$\frac{\partial A}{\partial t} = \Lambda\frac{\partial}{\partial t}\left\{\frac{\overline{\Theta^{*2}}^{\lambda}}{2}\right\}^{\phi} = \frac{\partial AZ}{\partial t} + \frac{\partial AE}{\partial t} \tag{3.1.30}$$

$$\frac{\partial A}{\partial t} = \Lambda\frac{\partial}{\partial t}\left\{\frac{\overline{\Theta}''^{2}}{2}\right\}^{\phi} + \sum_{m=1}^{\infty}\Lambda\frac{\partial}{\partial t}\left\{|Q(m)|^{2}\right\}^{\phi} \tag{3.1.31}$$

Hence:

$$\frac{\partial AZ}{\partial t} = \Lambda\frac{\partial}{\partial t}\left\{\frac{\overline{\Theta}''^{2}}{2}\right\}^{\phi} \tag{3.1.32}$$

$$\frac{\partial AE}{\partial t} = \sum_{m=1}^{\infty}\Lambda\frac{\partial}{\partial t}\left\{|Q(m)|^{2}\right\}^{\phi} \tag{3.1.33}$$

The spectral equivalent to the thermodynamic equation (3.1.6) takes the form:

$$\frac{\partial}{\partial t}\left[Q(n)\right] = -\sum_{m=-\infty}^{\infty}\left[\frac{im}{a\cos\phi}Q(m)\,U(n-m) + \frac{1}{a}Q_{\phi}(m)\,V(n-m) + Q_{p}(m)\,\Omega(n-m)\right] + \frac{\alpha}{c_p}\mathcal{H}(n) \tag{3.1.34}$$

Using the same algebraic method as for the kinetic energy equation, making use of the continuity equation, separating the wave interactions to m = 0 from the case where m ≠ 0, yields the budget for the variance of the complex component Q(n) of the eddy potential temperature:

$$\frac{\partial}{\partial t}\left[\left|Q(n)\right|^2\right] = -\frac{\partial}{\partial p}\left[\sum_{\substack{m=-\infty\\ \neq 0}}^{\infty} Q(m)\,\Psi_{\omega\theta}(m,n)\right] - \frac{1}{a\cos\phi}\frac{\partial}{\partial\phi}\left[\cos\phi\sum_{\substack{m=-\infty\\ \neq 0}}^{\infty} Q(m)\,\Psi_{v\theta}(m,n)\right]$$
$$-\left[\frac{1}{a}\frac{\partial\overline{\theta}''}{\partial\phi}\Phi_{v\theta}(n) + \frac{\partial\overline{\theta}''}{\partial p}\Phi_{\omega\theta}(n)\right] + \sum_{\substack{m=-\infty\\ \neq 0}}^{\infty} Q(m)\left[\frac{1}{a\cos\phi}\Psi_{u\theta_\lambda}(m,n) + \frac{1}{a}\Psi_{v\theta_\phi}(m,n) + \Psi_{\omega\theta_p}(m,n)\right] - \frac{\partial\{\overline{\theta}^{\lambda}\}^{\phi}}{\partial p}\Phi_{\omega\theta}(n) + \frac{\alpha}{c_p}\Phi_{h\theta}(n) \tag{3.1.35}$$

The balance of the zonal temperature variance is obtained by letting n = 0, and substituting the zonally averaged continuity equation in Eqn. (3.1.35), yielding:

$$\frac{\partial}{\partial t}\left[\frac{\overline{\theta}''^2}{2}\right] = -\frac{\partial}{\partial p}\left[\overline{\omega}^{\lambda}\frac{\overline{\theta}''^2}{2} + \overline{\theta}''\sum_{m=1}^{\infty}\Phi_{\omega\theta}(m)\right] - \frac{1}{a\cos\phi}\frac{\partial}{\partial\phi}\left[\cos\phi\left[\overline{v}^{\lambda}\frac{\overline{\theta}''^2}{2} + \overline{\theta}''\sum_{m=1}^{\infty}\Phi_{v\theta}(m)\right]\right]$$
$$+\sum_{m=1}^{\infty}\left[\frac{1}{a}\frac{\partial\overline{\theta}''}{\partial\phi}\Phi_{v\theta}(m) + \frac{\partial\overline{\theta}''}{\partial p}\Phi_{\omega\theta}(m)\right] - \frac{\partial\{\overline{\theta}^{\lambda}\}^{\phi}}{\partial p}\overline{\omega}^{\lambda}\overline{\theta}'' + \frac{\alpha}{c_p}\overline{h}^{\lambda}\overline{\theta}'' \tag{3.1.36}$$

According to Eqns. (3.1.1), (3.1.32) and (3.1.33) the balance for both eddy and zonal available energies may be approximated by multiplying Eqns. (3.1.35) and (3.1.36) by Λ .

3.2 Formal Description of the Energy Terms

The energy equations for A and K once integrated over the chosen volume are averaged over a unit volume of one square centimeter in horizontal area and one millibar thick. The results can be formalized as follows:

a) The balance for the zonal kinetic energy:

$$\frac{1}{\Delta p}\int_{p_1}^{p_2}\frac{\partial KZ}{\partial t}\frac{dp}{g} = BKZP + BKZFI - \sum_{m=1}^{\infty} CK(m) + BGZP + BGZFI + CZ - DZ \tag{3.2.1}$$

b) The balance for the eddy kinetic energy:

$$\frac{1}{\Delta p}\int_{p_1}^{p_2}\frac{\partial KE(m)}{\partial t}\frac{dp}{g} = BKEP(m) + BKEFI(m) + LK(m) + CK(m) + BGEP(m) + BGEFI(m) + CE(m) - DE(m) \tag{3.2.2}$$

c) The balance for the zonal available potential energy:

$$\frac{1}{\Delta p}\int_{p_1}^{p_2}\frac{\partial AZ}{\partial t}\frac{dp}{g} = BAZP + BAZFI - \sum_{m=1}^{\infty} CA(m) - CZ + GZ \tag{3.2.3}$$

d) The eddy available potential energy:

$$\frac{1}{\Delta p}\int_{p_1}^{p_2}\frac{\partial AE(m)}{\partial t}\frac{dp}{g} = BAEP(m) + BAEFI(m) + LA(m) + CA(m) - CE(m) + GE(m) \tag{3.2.4}$$

The mathematical expansion and physical description of the formal terms on the right-hand side of Eqns. (3.2.1) to (3.2.4) will be given next. The physical interpretations of many of the terms have been given earlier and will only be summarized. The first group will be the transfers or conversion terms, i.e., the rates at which energy shuttles between its various modes.

a) The conversion CK(n) from the zonal kinetic energy to the eddy kinetic energy of wave number n:

$$CK(n) = -\frac{1}{\Delta p}\int_{p_1}^{p_2}\left\{\Phi_{uv}(n)\,\frac{\cos\phi}{a}\,\frac{\partial}{\partial\phi}\left(\frac{\overline{u}^{\lambda}}{\cos\phi}\right) + \Phi_{vv}(n)\,\frac{1}{a}\,\frac{\partial\overline{v}^{\lambda}}{\partial\phi} - \frac{\tan\phi}{a}\,\overline{v}^{\lambda}\,\Phi_{uu}(n) + \Phi_{\omega u}(n)\,\frac{\partial\overline{u}^{\lambda}}{\partial p} + \Phi_{\omega v}(n)\,\frac{\partial\overline{v}^{\lambda}}{\partial p}\right\}^{\phi}\frac{dp}{g} \qquad (3.2.5)$$

The CK(n)-term measures the barotropic process in which momentum transport of wave number-n interacts with the corresponding horizontal and vertical shears of the zonally averaged zonal and meridional flow components $\overline{u}^{\lambda}$ and $\overline{v}^{\lambda}$.

b) The conversion CE(n) from eddy available energy of wave number n to eddy kinetic energy of the same wave number n:

$$CE(n) = \frac{1}{\Delta p}\int_{p_1}^{p_2}\Lambda\,\frac{\partial\{\overline{\theta}^{\lambda}\}^{\phi}}{\partial p}\,\left\{\Phi_{\omega\theta}(n)\right\}^{\phi}\frac{dp}{g} \qquad (3.2.6)$$

In a relatively stable normal atmosphere, the rising of the warm air and subsidence of the cold air in zonal planes relax the horizontal zonal temperature contrasts and wave number-n kinetic energy is produced by the ensuing eddy motion of the air. In other words, the mass redistribution has decreased the part of the potential plus internal energy which was available at wave number n, and increased the flow at this scale. An inverse correlation between ω and Θ would produce the reverse transfer.

c) The conversion of zonal available energy to zonal kinetic energy:

$$CZ = \frac{1}{\Delta p}\int_{p_1}^{p_2} \Lambda \frac{\partial\{\bar{\Theta}^{\lambda}\}}{\partial p} \left\{\overline{\omega''\Theta''}\right\}^{\phi} \frac{dp}{g} \qquad (3.2.7)$$

This conversion is similar to the preceding case, but the circulation takes place in a meridional plane.

d) The conversion from zonal to eddy available energy of wave number n:

$$CA(n) = -\frac{1}{\Delta p}\int_{p_1}^{p_2} \Lambda \left\{\frac{1}{a}\frac{\partial\bar{\Theta}''}{\partial\phi}\Phi_{v\Theta}(n) + \frac{\partial\bar{\Theta}''}{\partial p}\Phi_{\omega\Theta}(n)\right\}^{\phi} \frac{dp}{g} \qquad (3.2.8)$$

CA(n) measures the exchanges from zonal to wave-n available energy reservoirs. A positive transfer is obtained when wave number-n flow interacts with the zonally average temperature field so that heat at this scale flows northwards relaxing the existing northward zonal temperature gradient. The well known synoptic pattern leading to this positive transfer occurs when the stream function wave leads the temperature wave.

The conversion-terms may be characterized by their appearance with opposite signs, in two of the energy equations. On the other hand, other terms appear only once. They are the energy sink and source terms, called generations or dissipations when they apply to the available or kinetic energy modes, respectively.

e) The generation of eddy available potential energy at wave number n:

$$GE(n) = \frac{1}{\Delta p}\int_{p_1}^{p_2} \frac{\Delta}{c_p}\left(\frac{p_0}{p}\right)^{R/c_p} \left\{\Phi_{(n)} \atop h\theta\right\}^{\phi} \frac{dp}{g} \qquad (3.2.9)$$

A positive correlation between a heating spectral component and the temperature field at the same scale will lead to an increase in the temperature amplitude at that wave number, and hence of the associated spectral available energy. Because of the lack of radiative data, this term has usually been inferred as the residual in balancing the AE(n)-budget. Lately, however, it has been obtained approximately from inconsistencies in adiabatic vertical motion computations as shown by Wiin-Nielsen (1964b) and applied by Brown (1965), Muench (1965), Julian and Labitzke (1965) and Perry (1966). One part of the present study will attempt to find generation-terms from radiative computations as explained in Appendix B.

f) The generation of zonal available potential energy:

$$GZ = \frac{1}{\Delta p}\int_{p_1}^{p_2} \frac{\Delta}{c_p}\left(\frac{p_0}{p}\right)^{R/c_p} \left\{\overline{h}'' \, \overline{\theta}''\right\}^{\phi} \frac{dp}{g} \qquad (3.2.10)$$

Similarly, a positive correlation between the mean zonal diabatic heating and the mean zonal potential temperature contributes to a rise in the zonal temperature variance, indicating a corresponding variation in the zonal available energy. The same considerations as listed in the GE(n)-term description apply to the GZ-term.

g) The dissipation of wave kinetic energy into the smaller scales of motion in the part of the spectrum beyond the resolution of this study:

$$DE(m) = \frac{1}{\Delta p}\int_{p_1}^{p_2} \left\{ \underset{uX}{\Phi(m)} + \underset{vY}{\Phi(m)} \right\}^{\phi} \frac{dp}{g} \tag{3.2.11}$$

h) The dissipation of the zonal kinetic energy to the same smaller scales of motion mentioned above:

$$DZ = \frac{1}{\Delta p}\int_{p_1}^{p_2} \left\{ \overline{u}^{\lambda}\overline{X}^{\lambda} + \overline{v}^{\lambda}\overline{Y}^{\lambda} \right\}^{\phi} \frac{dp}{g} \tag{3.2.12}$$

The second grouping consists of the terms describing the effects of the cross-contour flow, i.e., "$-\mathbb{V}\cdot\nabla gZ$" acting on the boundaries of an open system. It is to be noted that when simple geostrophy is used, this term becomes identically zero. The effect of this term inside the volume has been shown to generate the CE and CZ-terms. The term "$-\mathbb{V}\cdot\nabla gZ$", when applied to the boundaries of our volume, contributes to the local rate of change of the volume kinetic energy by performing work on those boundaries. Since the effects of the pressure force which is transmitted inside the volume is lost integrally from outside the volume, the phenomenon may be called a flux of energy in the form of geopotential. The convergence of this flux across the volume will be a measure of the energy transferred in unit time into the volume at the expense of the neighbouring region. The phenomenon has been partitioned into a zonal and eddy form, and also into a vertical or horizontal character depending on whether the affected boundaries were horizontal or vertical. Following Nitta (1967), these terms may be called inter-volume redistribution terms.

i) The vertical convergence of the flux of geopotential at wave number n across the horizontal boundaries:

$$BGEP(n) = \frac{1}{\Delta p}\left\{\Phi_{\omega Z}(n)\right\}^{\phi}\Big|_{p_2}^{p_1} \qquad (3.2.13)$$

j) The vertical convergence of the zonal flux of geopotential across the horizontal boundaries:

$$BGZP = \frac{1}{\Delta p}\left\{\overline{\omega}''\,\overline{Z}''\right\}^{\phi}\Big|_{p_2}^{p_1} \qquad (3.2.14)$$

k) The horizontal convergence of eddy flux of geopotential at wave number n across the lateral boundaries:

$$BGEFI(n) = \frac{1}{\Delta p}\int_{p_1}^{p_2}\frac{\cos\phi}{a(\sin\phi_2-\sin\phi_2)}\,\Phi_{vZ}(n)\Big|_{\phi_2}^{\phi_1}\,dp \qquad (3.2.15)$$

l) The horizontal convergence of zonal flux of geopotential across the lateral boundaries:

$$BGZFI = \frac{1}{\Delta p}\int_{p_1}^{p_2}\frac{\cos\phi}{a(\sin\phi_2-\sin\phi_1)}\,\overline{v}^{\lambda}\,\overline{Z}''\Big|_{\phi_2}^{\phi_1}\,dp \qquad (3.2.16)$$

The next group of terms is the set of kinetic energy horizontal and vertical flux convergences affecting the KE(n) and KZ reservoirs in the volume:

m)

$$BKEP(m) = \frac{1}{g\,\Delta p}\left\{\sum_{\substack{m=-\infty \\ \neq 0}}^{\infty}\left[U(m)\Psi_{\omega u}(m,m) + V(m)\Psi_{\omega v}(m,m)\right]\right\}^{\phi}\Bigg|_{p_2}^{p_1} \tag{3.2.17}$$

n)

$$BKZP = \frac{1}{g\,\Delta p}\left\{\overline{\omega}^{\lambda}\frac{(\overline{u}^{\lambda 2}+\overline{v}^{\lambda 2})}{2} + \sum_{m=1}^{\infty}\left[\overline{u}^{\lambda}\,\Phi_{\omega u}(m) + \overline{v}^{\lambda}\,\Phi_{\omega v}(m)\right]\right\}^{\phi}\Bigg|_{p_2}^{p_1} \tag{3.2.18}$$

for the flux convergence across the pressure surfaces, and

o)

$$BKEFI(m) = \frac{1}{\Delta p}\int_{p_1}^{p_2} \frac{\cos\phi}{a(\sin\phi_2 - \sin\phi_1)} \sum_{\substack{m=-\infty \\ \neq 0}}^{\infty}\left[U(m)\Psi_{vu}(m) + V(m)\Psi_{vv}(m,m)\right]\Bigg|_{\phi_2}^{\phi_1}\frac{dp}{g} \tag{3.2.19}$$

p)

$$BKZFI = \frac{1}{\Delta p}\int_{p_1}^{p_2} \frac{\cos\phi}{a(\sin\phi_2 - \sin\phi_1)}\left[\overline{v}^{\lambda}\frac{(\overline{u}^{\lambda 2}+\overline{v}^{\lambda 2})}{2} + \sum_{m=1}^{\infty}\left[\overline{u}^{\lambda}\,\Phi_{uv}(m) + \overline{v}^{\lambda}\,\Phi_{vv}(m)\right]\right]\Bigg|_{\phi_2}^{\phi_1}\frac{dp}{g} \tag{3.2.20}$$

for the flux convergence of kinetic energy across the lateral boundaries.

The following set of terms is composed of the corresponding flux convergence associated with the available energy:

q)

$$BAEP(m) = \frac{1}{g\,\Delta p}\;\Lambda\left\{\sum_{\substack{m=-\infty \\ \neq 0}}^{\infty} Q(m)\,\Psi_{\omega\theta}(m,m)\right\}^{\phi}\Bigg|_{p_2}^{p_1} \tag{3.2.21}$$

r)

$$BAZP = \frac{1}{g\Delta p} \Lambda \left\{ \overline{\omega}^{\lambda} \frac{\overline{\Theta}''^{2}}{2} + \overline{\Theta}'' \sum_{m=1}^{\infty} \Phi_{\omega\Theta}(m) \right\}^{\phi} \Bigg|_{p_2}^{p_1} \qquad (3.2.22)$$

s)

$$BAEFI(m) = \frac{1}{\Delta p} \int_{p_1}^{p_2} \frac{\cos\phi \cdot \Lambda}{a(\sin\phi_2 - \sin\phi_1)} \sum_{\substack{m=-\infty \\ \neq 0}}^{\infty} Q(m) \Psi_{v\Theta}(m,n) \Bigg|_{\phi_2}^{\phi_1} \frac{dp}{g} \qquad (3.2.23)$$

t)

$$BAZFI = \frac{1}{\Delta p} \int_{p_1}^{p_2} \frac{\cos\phi \cdot \Lambda}{a(\sin\phi_2 - \sin\phi_1)} \left[\overline{v}^{\lambda} \frac{\overline{\Theta}''^{2}}{2} + \overline{\Theta}'' \sum_{m=1}^{\infty} \Phi_{v\Theta}(m) \right] \Bigg|_{\phi_2}^{\phi_1} \qquad (3.2.24)$$

The next group of terms is related to the spectral partitioning of the energy budgets. The terms represent the interaction of all scales (except m = 0) with wave number n to produce available or kinetic energy. Theoretically, the integration of the terms over the whole spectrum and over a closed system would balance identically to zero. In an open system, the terms need not balance when integrated over "n" since the waves outside the volume may interact with those inside. Logically the result of the integration over wave number, if not zero, may be considered as a boundary flux. The homogeneity of this last group is subdivided into two sub-classes depending on whether it affects the kinetic or available spectrum:

u) The non-linear redistribution of kinetic energy to the kinetic energy of wave number n from all other wave numbers:

$$LK(n)=\frac{1}{\Delta p}\int_{p_1}^{p_2}\Bigg\{\sum_{\substack{m=-\infty\\ \neq 0}}^{\infty} U(m)\left[\frac{1}{a\cos\phi}\Psi_{uu_\lambda}(m,n)+\frac{1}{a}\Psi_{vu_\phi}(m,n)+\Psi_{\omega u_p}(m,n)-\frac{\tan\phi}{a}\Psi_{uv}(m,n)\right]$$

$$+V(m)\left[\frac{1}{a\cos\phi}\Psi_{uv_\lambda}(m,n)+\frac{1}{a}\Psi_{vv_\phi}(m,n)+\Psi_{\omega v_p}(m,n)+\frac{\tan\phi}{a}\Psi_{uu}(m,n)\right]\Bigg\}^{\phi}\frac{dp}{g} \qquad (3.2.25)$$

v) The non-linear redistribution of spectral available potential energy to wave number n from all other wave numbers:

$$LA(n)=\frac{1}{\Delta p}\int_{p_1}^{p_2}\Lambda\Bigg\{\sum_{\substack{m=-\infty\\ \neq 0}}^{\infty} Q(m)\left[\frac{1}{a\cos\phi}\Psi_{u\theta_\lambda}(m,n)+\frac{1}{a}\Psi_{v\theta_\phi}(m,n)+\Psi_{\omega\theta_p}(m,n)\right]\Bigg\}^{\phi}\frac{dp}{g} \qquad (3.2.26)$$

As can be seen in the expansions of LK(n) and LA(n), a triple correlation of Fourier components is involved. This means that because of the atmospheric variability and/or the quality of the data, the results could be fairly noisy, as has been noted by Saltzman and Fleisher (1960b). However, this will be taken into account in the results, and the confidence in the values will only be ascertained by the longer of the two (5 days versus 30 days) time series associated with this report.

CHAPTER 4

ENERGETICS IN THE PERIOD OF JANUARY 12th TO 16th, 1959

4.1 General Remarks Pertaining to the 5-day Study

Since our thermodynamic system cannot be closed in either a geometric or computational sense, it is necessary to carry boundary fluxes and balance terms in the energy cycles. The balance terms, in so far as they rise above the inherent errors, also represent specific processes not formally computed.

In the kinetic energy modes, the balances, BAL_{KE} and BAL_{KZ}, are identified with frictional dissipation by all eddies from wave 13 down to molecular scale. How much of this will reappear as thermal energy is not known, but some clarification of the vertical frictional selectivity will be presented later in this chapter.

The balance terms BAL_{AZ} and BAL_{AE} will measure processes which differ from stratosphere to troposphere. In the stratosphere, they will represent the accuracy of the computed available energy generations, GZ and GE, since the computed diabatic heating can only approximate the real heating because of the unavoidable simplifications in the radiative transfer solutions. In the troposphere, because of the missing generation terms GZ and GE, BAL_{AZ} and BAL_{AE} may be taken as their respective inferred magnitudes.

In view of their complexity the shorthand notation for the energy cycles is employed and for convenience is specified below:

$$\partial KZ/\partial t = BKZ - CK + BGZ + CZ + BAL_{KZ} \tag{4.1.1}$$

$$\partial KE/\partial t = BKE + CK + BGE + CE + BAL_{KE} \tag{4.1.2}$$

$$\partial AZ/\partial t = BAZ - CA - CZ + GZ + BAL_{AZ} \tag{4.1.3}$$

$$\partial AE/\partial t = BAE + CA - CE + GE + BAL_{AE} \tag{4.1.4}$$

where

$$\text{BKZ} = \text{BKZP} + \text{BKZFI}, \tag{4.1.5}$$

$$\text{BGZ} = \text{BGZP} + \text{BGZFI}, \tag{4.1.6}$$

$$\text{BKE} = \text{BKEP} + \text{BKEFI} + \text{LK}, \tag{4.1.7}$$

$$\text{BGE} = \text{BGEP} + \text{BGEFI}\ (\cong 0.0), \tag{4.1.8}$$

$$\text{BAZ} = \text{BAZP} + \text{BAZFI}\ (\cong 0.0), \tag{4.1.9}$$

$$\text{BAE} = \text{BAEP} + \text{BAEFI}\ (\ncong 0.0), \tag{4.1.10}$$

and the previous BAL_{XY} are the values needed to balance the various budgets.

4.2 Energetics During the 12-16 January 1959 Period

Here we look specifically into the events in the chosen 5-day period; a fuller description of the month's events are in Chapter 5. This diagnostic study with high density data in a rather normal warming period should lead to a better understanding of the dynamical interactions involved. Also when compared with results computed for the major warming periods, it should shed more light on the underlying processes or causes.

A. Stratosphere

Synoptics

January 1959 was a more or less normal month with vacillations in the temperature and height fields (Labitzke, 1965). Three large-scale and large-amplitude oscillations were observed and the one in the 12-16 January period is classified as a "minor" warming following the terminology advanced by Julian (1967): that is, a case where the stratospheric polar vortex is displaced significantly by a strong anti-cyclonic circulation appearing at northern latitudes, but the effects do not reach such catastrophic proportions that the stratospheric flow collapses and the meridional temperature gradient reverses.

The 1959 winter stratosphere featured a series of warm waves which moved rapidly eastward around an oscillating cold polar vortex. From the main source region in the Siberian-Aleutian area, the waves travelled eastward to die out over eastern Canada and Greenland (Godson and Wilson, 1963). The striking differences between a mild warming winter (58-59) and a spectacular one (57-58) are shown by the North Pole 10-mb temperatures on Fig. 4.2.1 (after Finger, Mason and Corzine, 1963). The wave in question appears on their figure as the relative maximum on January 15-20, 1959. Boville, Wilson and Hare (1961) studied wave propagation at 25 mb from the 8th to 18th of January and postulated baroclinic instability with a conversion from available to kinetic energy.

However, it will be shown that the energetics will follow a more complex pattern than the one which may be visualized from weather maps.

Energies

The daily fluctuations of the stratospheric energies in their zonal and eddy modes are presented in Fig. 4.2.2 where the subscripts "s" and "t" attached to the energy reservoirs indicate the stratospheric or tropospheric cases, respectively. In the following paragraphs, any unqualified reference to energy will automatically designate the stratospheric case.

Both zonal energies AZ_s and KZ_s suffer a net decrease during the period, the decrease is marked from the 12th to the 13th, when the eddy modes AE_s and KE_s are increasing rapidly. The sharp rise of AE_s in response to the AZ_s fall is borne out by the large CA-exchange process computed on those days. The sharp increase of KE_s is of short duration and then KE_s falls steadily back to near the initial level. The zonal kinetic energy KZ_s is negatively correlated to the changes in KE_s until the 14th, then it goes into a larger decline than its eddy counterpart on the 14th. Of special interest is that the strong KE_s increase on the 12th-13th period is well correlated with maximum eddy pressure interaction on the 12th, and also, as will be shown later, KE_s is found to be negatively correlated to the corresponding tropospheric KE_t, presumably indicating a flux of energy from below.

Energetics

The daily energy flow diagrams arrived at for both stratosphere and troposphere are given as Fig. 4.2.3 to 4.2.7, while the 5-day averaged energy flow diagram is depicted in Fig. 4.2.8. The equivalent information has been listed in a tabular form based on the formalism given by Eqns. 4.1.1 through 4.1.10, and identified as Tables 4.2.1 and 4.2.2. Throughout this treatise the units of the conversions, rates of energy change, are ergs/cm^2 mb sec and the energy unit is 10^4 ergs/cm^2 mb. The number in the energy boxes, under the energy mode identification, is the time rate of change of this energy, computed as the 48-hour centered time difference, except on the first and last day where forward and backward 24-hour time difference schemes have been applied, reducing the reliability of the time derivatives for those days.

Before comparing the results with other studies, especially those of Muench (1965), Miyakoda (1963), Julian and Labitzke (1965) and Perry (1966), a few words of caution are necessary. Most of the above investigators had data extending to the 20°N latitude circle whereas the present study, like Miyakoda's stops at 30°N, so that the cross-boundary fluxes will tend to be more intense in our case. Although Julian and Labitzke (1965) and Miyakoda (1963) solved the diagnostic equation, they did not use the Fourier spectral approach. Muench (1965) used the so-called adiabatic-thermodynamic omega method but added the mean monthly heating as a diabatic correction. Perry (1966) integrated the vorticity equation in the vertical to arrive at a vertical motion profile; this method has the advantage of completeness in the sense that no diabatic heating had to be computed. Further, the study of a minor stratospheric warming is somewhat more difficult since it uses the same diagnostic tools, with all their inherent errors, to resolve weaker signals.

The results of this study are compared first with computations

Table 4. 2. 1. Daily and time averaged energy conversions for January 12 to 16, 1959. Units: $Ergs/cm^2$ mb sec.

Layer	Date	$\frac{\partial KZ}{\partial t}$	BKZ	-CK	BGZ	CZ	BAL
	Jan/59						
Strat.	12	-1. 16	2. 62	2. 23	-3. 60	-1. 15	-1. 26
	13	0. 06	1. 04	1. 18	-2. 80	-0. 49	1. 13
	14	-0. 98	3. 95	1. 44	-3. 75	-1. 42	-1. 20
	15	-1. 97	0. 80	4. 29	-4. 58**	-1. 19**	-1. 29
	16	- . 69	1. 09	4. 84	-5. 40	-0. 95	- . 27
	Mean	- . 96*	1. 90	2. 80	-3. 65	-1. 04	- . 58
Trop.	12	2. 89	3. 38	- . 87	. 74	- . 34	- . 02
	13	. 93	3. 48	- . 99	. 04	- . 37	-1. 23
	14	- . 64	3. 96	-1. 03	. 16	- . 03	-3. 70
	15	1. 39	3. 83	-1. 27	. 48**	- . 26**	-1. 49
	16	. 81	4. 78	-2. 13	. 79	- . 49	-2. 14
	Mean	. 85*	3. 89	-1. 26	. 44	- . 30	-1. 72

* Net rate during period
** Interpolated from results on 14th and 16th

Layer	Date	$\frac{\partial KE}{\partial t}$	BKE	CK	BGE	CE	BAL
	Jan/59						
Strat.	12	3. 59	1. 08	-2. 23	5. 77	-1. 49	. 46
	13	. 81	. 77	-1. 18	3. 29	-1. 28	- . 79
	14	-1. 16	. 62	-1. 44	3. 26	- . 71	-2. 89
	15	- . 41	. 29	-4. 29	4. 41	-2. 61	1. 79
	16	- . 46	1. 20	-4. 84	2. 86	-3. 76	4. 08
	Mean	. 42*	. 79	-2. 80	3. 92	-1. 97	. 53
Trop.	12	-1. 27	1. 29	. 87	-1. 02	1. 40	-3. 81
	13	- . 35	1. 79	. 99	- . 58	1. 11	-3. 66
	14	. 81	1. 15	1. 03	- . 58	1. 51	-2. 30
	15	- . 89	. 20	1. 27	- . 78	1. 84	-3. 42
	16	. 69	1. 03	2. 13	- . 51	1. 81	-3. 77
	Mean	. 32*	1. 09	1. 26	- . 69	1. 53	-3. 39

Table 4. 2. 2. Daily and time averaged energy conversions for January 12 to 16, 1959.
Units: Ergs/cm^2 mb sec.

Layer	Date	$\frac{\partial AZ}{\partial t}$	BAZ	-CA	-CZ	GZ	BAL
	Jan/59						
Strat.	12	-1.97	0.02	-7.76	1.15	0.19	4.43
	13	-1.04	0.01	-4.01	.49	0.08	2.39
	14	- .17	- .07	-4.50	1.42	- .00	2.98
	15	- .12	- .05	-3.81	1.19**	- .00	2.55
	16	0.00	- .15	-2.38	0.95	- .06	1.64
	Mean	- .51*	- .03	-4.49	1.04	0.04	2.80
Trop.	12	.23	.08	-5.06	.34		4.89
	13	1.91	.08	-3.68	.37		5.14
	14	1.33	.06	-6.75	.03		7.97
	15	-1.85	.08	-9.92	.26**		7.73
	16	-2.78	.15	-8.71	.49		5.29
	Mean	.03*	.09	-6.82	.30		6.20

* Net rate during period
** Interpolated from results on 14th and 16th

Layer	Date	$\frac{\partial AE}{\partial t}$	BAE	CA	-CE	GE	BAL
	Jan/59						
Strat.	12	1.39	.04	7.76	1.49	- .82	-7.08
	13	.75	.34	4.01	1.28	- .89	-3.99
	14	.46	.04	4.50	.71	- .91	-3.88
	15	.75	.24	3.81	2.61	- .91	-5.00
	16	.69	.73	2.38	3.76	- .92	-5.26
	Mean	.76*	.28	4.49	1.97	- .89	-5.04
Trop.	12	.93	- .68	5.06	-1.40		-2.05
	13	.17	.55	3.68	-1.11		-2.95
	14	.23	- .26	6.75	-1.51		-4.75
	15	.23	- .06	9.92	-1.84		-7.79
	16	- .58	- .61	8.71	-1.81		-6.87
	Mean	.23*	- .21	6.82	-1.53		-4.88

Table 4.2.3. Comparison with other stratospheric studies after Muench (1965) and Perry (1966). Units: ergs/cm^2 mb sec.

Source	Layer (mb)	CE	CZ	CK	CA	BGE	BGZ	GE	GZ	Period
Paulin	150-0	-1.97	- .49	- 2.80	4.49	3.92	-3.02	- .89	.04	12-16 Jan/59
Perry (1966)	200-0 40-0	1.40 .33	-2.14 -1.42	- 2.36 -10.48	2.74 6.36	0.88 7.15	1.53 -1.65	-1.45 -3.73	-.37 1.06	2-19 Jan/63
Julian and Labitzke(1965)	100-10	3.49	-5.02	- 3.95	3.95	7.56	-2.37	- .36	-1.59	2-27 Jan/63
Kennedy (1964)	200-10 40-10								-.82 .61	Jan (mean)
Muench (1965)	100-10	1.58	-2.34	-1.14	2.02	1.15	1.76		.36	Jan 1958
Miyakoda (1963)	189-.9	-.38	-1.03	1.29	1.22	1.62				Jan 1958
Reed et al (1963)	50	2.20	-3.20	-5.15	1.30	16.80	-9.20			Jan 1957
Oort (1963)	100-30	-.08		- .26	-.21				-.45	Oct-Dec/57
Teweles (1963)	100-50			- .19						Jan 1958
Boville (1961)	25	.42		.27	.88					Jan 1959
Jensen (1960)	100-50	-.83	- .10			2.95				Jan 1958
Sekiguchi (1963)**	50	3.0		- .6	4.0					15-25 Jan/58
Perry (1966)	40-0	-3.79	-1.93	-3.79	.37	5.86	-3.81	-11.28	2.16	23-29 Jan/63
Paulin	25	-1.92	-1.96	-3.74				- .74	0.29	12-16 Jan/59

** Taken from Julian and Labitzke (1965) tabulated by Muench (1965) and Perry (1966).

It is clear from Table 4.2.3 that most of our terms agree in relative magnitude and sign with previous studies. CZ seems to be smaller than most others, but it is close to Jensen's (1961) value. Oort (1963) computed the only negative value for the CA-conversion between zonal to eddy available energy. His statistics for the 30-100 mb layer may be even more biased towards the lower stratosphere. Also Oort's study period is a less active one in which the stratosphere tends to be forced by the more energetic troposphere. As pointed out by Boville (1961) and Perry (1966), this is probably the state of the stratosphere for most of the year when the meridional temperature gradient is reversed. The CE-term differs in sign from those of Perry (1966), Julian and Labitzke (1965) and Muench (1965), but agrees with the values computed by Miyakoda (1963), Oort (1963) and Jensen (1960). Of interest are the relatively large values of the BGE and BGZ terms. The vertical convergence of the eddy geopotential flux seems to check with other results having comparable vertical resolution. On the other hand, BGZ contains two terms: BGZP, or the vertical convergence of the zonal flux of geopotential, and BGZFI, the horizontal convergence of the same parameter. The latter term is the largest in absolute value but stands negative. This term would likely be more negative than Perry's or Muench's since the vertical wall along the 30°N latitude circle is the seat of more activity than is the case further south. If the energy transfers due to the BGE and BGZ processes were used to heat the stratosphere, temperature changes of 0.48 and -0.36°C per day would follow, respectively.

The 5-day averaged energy flow in the strat. sphere will be described next with reference to Fig. 4.2.8. A significant amount of energy from the troposphere is found to enter the stratosphere by the eddy pressure interaction-term BGE averaging 3.92 ergs/cm^2 mb sec. In contrast to BGE, the positive cross-boundary transport of eddy kinetic energy, BKE, contributes only 0.79 erg/cm^2 mb sec to the eddy kinetic energy budget. Part of the energy gain is converted by the CE-process at a rate of 1.97 units to the eddy available energy reservoir through the action of the overturnings in zonal planes. Eddy kinetic energy is transformed into the zonal mode at a rate of 2.80 units. On the average, 0.53 units are needed to balance the eddy kinetic energy budget; this balance implies a negative eddy frictional dissipation, which is at first sight anomalous. Jensen (1961), Kung (1967) have computed negative frictional dissipation above the jet stream region in January 1958. As pointed out by Muench (1965), since the stratosphere is characterized on the whole by small vertical wind shear and large static stability, small dissipation values may be acceptable in reference to the vertical integration of this phenomenon over the stratospheric layer. He goes on to assume possible negative dissipation values for the winter stratospheric layer included between both tropospheric jet stream level and polar night jet level. A vertical profile of the eddy frictional dissipation will be given in a later section of this chapter. Some rather large imbalances in the KE-budget are found to mark the 14th and the 16th. The rather large observed negative rate of change of KE on the 14th (-1.16 unit) is not very well balanced because small absolute values of both the CE and CK processes are inadequate to explain this drop against the positive influences of the BGE and BKE processes. The opposite occurs on the 16th where the CE and CK mechanisms are large, and a large imbalance, of opposite sign, prevails. Inspection of some of the CE magnitudes at data levels reveals that on the 14th, the relatively small CE-conversions at the 100 and 50 mb levels offset those at 25 and 10 mb when the integration in the vertical is performed, while on the 16th the abnormally large magnitudes of the CE transfers at 50 and 100 mb require a large residual of opposite sign. Similarly, CK has a small negative magnitude on the 14th mainly due to its large positive value (2.0 units) at 100 mb while it is negative and large above. The positive sign in CK at 100 mb will be interpreted later when the tropospheric energetics are dealt with. On the other hand, on the 16th, CK is negative, and eddy kinetic energy is transformed into the zonal mode at a relatively large rate contributing further to a large imbalance in the budget, but in a direction opposite to that of the 16th. Both imbalances of the eddy kinetic energy budget could be reduced by 30 to 50% by assigning different weights to the various stratospheric layers, as Muench (1965) did, for example.

The daily variations in the eddy kinetic energy budget are shown in the time-amplitude graph of Fig. 4. 2. 9 and the exchanges in and out of KE will be summarized. On the 12th, under the strong forcing action of the eddy flux of geopotential emanating from the troposphere when the import across the boundaries cancels the transfer to the eddy available energy mode, the eddy kinetic reservoir increases at a large rate, even when CK is moderately negative. There is little change on the 13th, except that the reduced eddy pressure interaction is accompanied by a reduced rate of increase in KE. The sharp negative changes in CE and CK after the 14th force the residual term BAL to change sign and to become large on the 16th. BGE remains large throughout the period due to the contribution of its vertical component BGEP only.

Let us now consider the daily spectral distribution of this component as shown on Table 4. 2. 4.

We see that wave numbers 2 and 4 dominate the flux convergence with a noticeable exception on the 15th, when the pressure interaction at wave number 7 appears to be significant. This latter anomaly has been traced to the computation scheme; the geopotential flux at 150 mb was interpolated from the 200 and 100 mb computed values and the upward flux of geopotential is very significant at 200 mb, but it is practically non-existent at 100 mb.

A daily spectral distribution of the CE-transfer in the stratosphere is given in Table 4. 2. 5.

Table 4. 2. 4 Spectral convergence in the vertical flux of geopotential in the stratosphere and the troposphere during the period January 12 to 16, 1959.

Units: $\mathrm{Ergs/cm^2\ mb\ sec}$

Date (Jan/59)	STRATOSPHERE						TROPOSPHERE					
	12	13	14	15	16	Mean	12	13	14	15	16	Mean
BGZP	-1.76	-.51	-.80	-1.72*	-2.64	-1.48	.31	.09	.14	.30*	.47	.26
$\sum_{n=1}^{12}$ BGEP(n)	5.77	3.29	3.26	4.41	2.86	3.92	-1.02	-.58	-.58	-.78	-.51	-.69
BGEP(1)	1.14	.53	.78	.56	.37	.68	-.20	-.09	-.14	-.10	-.07	-.12
BGEP(2)	1.08	.20	2.05	2.32	.88	1.30	-.19	-.04	-.36	-.41	-.15	-.23
BGEP(3)	.54	.15	-.31	-.09	-.43	-.03	-.10	-.03	.06	.02	.08	.01
BGEP(4)	2.12	1.45	.14	.55	.73	1.00	-.37	-.26	-.02	-.10	-.13	-.18
BGEP(5)	.49	.06	-.07	-.26	.47	.14	-.09	-.01	.01	.05	-.08	-.02
BGEP(6)	.12	.77	.57	.15	.33	.39	-.02	-.14	-.10	-.03	-.06	-.07
BGEP(7)	.22	.05	.19	1.10	.41	.40	-.04	-.01	-.03	-.19	-.07	-.07
BGEP(8)	.01	.03	-.11	.02	.08	.01	-.00	-.01	.02	-.00	-.01	-.00
BGEP(9)	.03	.08	.01	.06	.00	.04	-.01	-.01	-.00	-.01	-.00	-.01
BGEP(10)	.01	-.05	-.00	.01	.03	.00	-.00	.01	.00	-.00	.01	-.00
BGEP(11)	.00	.02	.02	.01	-.01	.01	-.00	-.00	-.00	-.00	-.00	-.00
BGEP(12)	.00	.01	.00	.00	.00	.00	-.00	-.00	-.00	.00	-.00	-.00

* Interpolated between 14th and 16th due to data trouble

Table 4. 2. 5 Daily stratospheric variations of the CE(n) transfer for the first five wave numbers for January 12 to 16, 1959

Units: Ergs/cm^2 mb sec

Date Jan/59	Wave Number				
	1	2	3	4	5
12	-1. 26	-. 27	. 50	0. 47	-. 76
13	- . 01	-. 41	-. 64	0. 74	-. 59
14	- . 22	-. 25	-. 67	0. 69	0. 03
15	- . 50	-. 53	-. 58	-. 38	0. 02
16	-1. 75	-. 68	-. 38	-. 11	-. 09
Mean	-0. 75	-. 43	-. 35	0. 30	-. 38

Table 4. 2. 5 reveals that CE(1), at least on the average, transfers more eddy kinetic energy to eddy available energy than CE(n) for the other waves and that CE(4) acts in reverse by feeding into KE(4) at the expense of AE(4).

A comparison with the spectral barotropic CK(n) term shows that CK(2) dominates in a more definitive manner than CE(1) does. This is clearly shown by Table 4. 2. 6.

Table 4. 2. 6 Spectral decomposition of CK in the stratosphere for January 12 to 16, 1959

Units: Ergs/cm^2 mb sec

Date Jan/59	Wave Number			
	1	2	3	4
12	. 04	-2. 07	. 06	-. 01
13	-. 29	-1. 89	-. 19	. 19
14	-0. 29	-1. 80	. 21	. 17
15	-1. 00	-2. 48	-. 24	-. 21
16	-. 89	-2. 09	-. 81	-. 44
Mean	-. 49	-2. 07	-. 19	-. 06

The zonal kinetic budget is shown graphically in Fig. 4.2.10 where the 5-day mean values may be seen at the extreme right of the graph. On the average, the stratospheric zonal energy of motion is maintained by a significant barotropic transfer at a rate of 2.80 ergs/cm^2 mb sec and by a cross boundary flux of zonal energy at a rate of 1.90 units while it loses to the exterior volume through zonal pressure interactions at a rate of 3.65 units and by a transfer to the zonal available form at a rate of 1.04 units. When the net balance is used to represent the frictional dissipation, the missing link in the budget, a residual of -0.58 ergs/cm^2 mb sec is obtained. To overcome an unsolved computational error in the mean zonal vertical wind for January 15th, BGZ and CZ have been approximated from the values computed the day before and after. A numerical model elaborated by Smagorinsky, Manabe and Halloway (1965) has yielded zonal wind patterns and magnitudes of the order of those found in this study. Cross-sections of the actual mean zonal winds computed geostrophically on January 12 to 16, 1959 are presented on Fig. 4.2.11. and 4.2.12. In the numerical model, the dissipation was computed as being proportional to the square of the velocity. They obtained dissipation of 1.2 erg/cm^2 mb sec in the vicinity of the tropospheric mean zonal jet. Taking the mean stratospheric zonal winds to be on the average slightly more than half the mean tropospheric zonal winds in the jet stream layers, the stratospheric zonal dissipation may be approximated as 30 to 40 percent of the computed one, i.e., in the order of 0.4 to 0.5 erg/cm^2 mb sec. The choices of Muench (1965) and Perry (1966) of 0.4 and 0.7 (Perry had stronger zonal winds to contend with) ergs/cm^2 mb sec, respectively, seem reasonable. The daily energy flows about KZ are fairly well approximated by the 5-day mean description. Of importance is the increase in magnitude with time of both the barotropic transfer (-CK) and the zonal pressure interaction to the exterior (BGZ). The daily and 5-day mean magnitudes of the vertical component of BGZ, i.e., BGZP, are also listed in Table 4.2.4. BGZP amounts to about 40 percent of the stratospheric zonal pressure interaction so that 60 percent is lost through the lateral boundaries.

In the troposphere, the proportions are reversed as the lateral boundaries contribute 40 percent of the zonal pressure interactions on our lower volume. It has been shown earlier that most of the barotropic transfer -CK is explained by the conversion of the energy from wave number 2 flow to the zonal flow.

To summarize, the gradual decrease of KZ is due in a large part to the loss of energy by zonal pressure interaction with the exterior volume accompanied by a small transfer to the AZ-reservoir, while an increasing barotropic transfer from the eddy flow and additional cross-boundary flux of zonal kinetic energy does not quite bring the budget out of the red. Frictional dissipation is identified with the net loss.

The budget of the zonal available energy is exhibited graphically on Fig. 4.2.13. The most striking feature of this budget is the rate at which zonal available energy is transformed into the eddy mode at the beginning of the period. A strong pulse of northward eddy heat transport must have affected the whole stratosphere on the 12th. This pulse diminishes rapidly to reach one third of its initial value on the 16th. The imbalance is found to be large on the 12th, decreasing with time, paralleling the behaviour of CA. The imbalance on the 12th may be partially due to errors in the rate of change of AZ resulting from the forward time-difference scheme. Also, the large values of CA are due to the large values computed at 10 and 50 mb, while those at 25 mb and especially at 100 mb are smaller. There may be some inhomogeneity between the two data analyses employed, i.e., Berlin Free University maps for the first set and McGill's for the second set. When the CA-terms at 25 mb and 100 mb are used to obtain the stratospheric value, the computation yields 1.98 ergs/cm^2 mb sec as the 5-day average. This has the effect of reducing both imbalances in the AZ and AE budget significantly. A third possibility is larger zonal generation (GZ) values for the whole stratosphere. This could be possible on a given day but would not likely last very long, since most studies report small negative values on the average (refer to

Table 4.2.3), for a similar layer. As mentioned earlier, most other studies extended further south to about 20°N to 15°N, adding about 50 percent to our area. The net effect on the zonal generation of available energy would be negative since the stronger solar heating at those latitudes and altitudes would coincide with colder temperatures.

The zonal generations of available energy at the four stratospheric levels are given on Table 4.2.7 below.

Table 4.2.7. Daily and 5-day mean generation of zonal available energy at stratospheric levels for January 12 to 16, 1959.
Units: $\mathrm{Ergs/cm^2\ mb\ sec}$

Level (mb)	10	25	50	100
12 Jan/59	1.90	.29	.41	-.35
13 Jan/59	1.74	.35	.16	-.41
14 Jan/59	1.53	.30	-.07	-.40
15 Jan/59	1.55	.24	-.09	-.16
16 Jan/59	1.53	.29	-.16	-.47
Mean	1.65	.29	.05	-.40

When the 100, 50, and 25-mb results in Table 4.2.7 are given the weights 3:2:1, respectively, the mean GZ becomes -0.15 $\mathrm{erg/cm^2}$ mb sec which is directly comparable to Oort's (1963) results of -0.95 $\mathrm{erg/cm^2}$ mb sec for the 100-30 mb layer. Since this result applies to the whole hemisphere and uses the mean monthly heating rates of Davis (1963), the larger negative value is not surprising. This comparison points to the significant differences in the generations between the lower and the middle stratosphere. The daily changes in GZ at 50 mb are interesting, for Table 4.2.7 shows that GZ changes sign from positive to negative on the 14th. Inspection of the daily zonal vertical temperature profiles reveals a gradual and systematic change in the curvature of those profiles near 50 mb at the lower latitudes (from 45°N to 30°N). The change in curvature with time is shown schematically in Fig. 4. 2. 14.

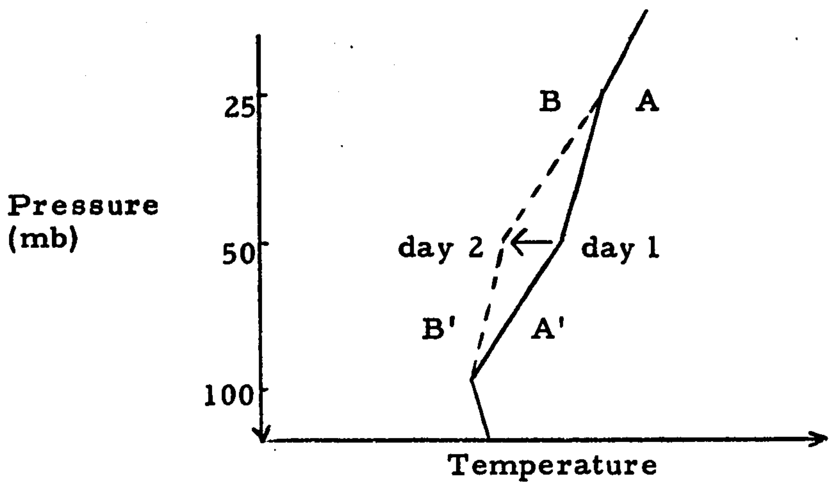

Fig. 4. 2. 14. Schematic change of the vertical temperature profile from day 1 (curve AA') to day 2 (curve BB').

This change of curvature favours a decrease in the cooling action of the 15-micron band of carbon dioxide. This reduced cooling occurs in a relatively colder region (40°N to 30°N), and contributes to a decrease of GZ in time. The stratosphere zonal heating rates due to carbon dioxide are shown in Table 4. 2. 8.

Table 4. 2. 8. The 50 mb zonal heating rates due to radiative transfers in the carbon dioxide 15-micron absorption band. January 12 to 16, 1959.

Units: Degrees centigrade per day

Latitude (°N)	30	35	40	45	50
Date (Jan. 1959)					
12	-.72	-.72	-.73	-.76	-.77
13	-.69	-.69	-.70	-.72	-.72
14	-.66	-.69	-.75	-.79	-.79
15	-.63	-.65	-.68	-.74	-.77
16	-.60	-.66	-.73	-.77	-.77

In summary, AZ assumes a net loss during the chosen period as CA transfers available energy into the eddy mode, while the gain from the meridional overturnings and radiative interactions does not compensate for this drain.

The daily budget of the eddy available energy reservoir is fully depicted in Fig. 4.2.15. AE is characterized by being the terminal for the energies transferred from AZ and KE. Under the impact AE rises continuously and some of its energy is lost due to the effects of the radiation-temperature covariances. The cross-boundary fluxes of eddy available energy are rather small throughout the period. Most of the small cross-boundary fluxes of available energy are due to the non-linear transfer of energy from the temperature waves outside our volume. A large imbalance is found with magnitudes in the order of the CA-term. Sources of this imbalance may lie in the inhomogeneous data and possibly in the systematic underestimation of the carbon dioxide cooling, due to the smoothed vertical temperature field. During the period preceding the stratospheric vortex collapse and major warming in January 1963, Perry (1966) computed net eddy generation in the order of -3 ergs/cm^2 mb sec. In order to clarify the processes in action, the eddy generation results at each stratospheric level are presented in Table 4.2.9.

Table 4.2.9 Vertical distribution of the generation of eddy available energy in the stratosphere for January 12 to 16, 1959.
Units: ergs/cm^2 mb sec

Level (mb)	10	25	50	100
12 Jan. 1959	-1.49	-.61	-1.43	-.41
13 Jan. 1959	-1.68	-.77	-1.44	-.47
14 Jan. 1959	-1.86	-.75	-1.55	-.40
15 Jan. 1959	-2.19	-.86	-1.26	-.45
16 Jan. 1959	-1.67	-.70	-1.43	-.55

It has been shown earlier that the significant eddy generation process is not due to ozone (notwithstanding the minor eddy effect of the absorption of terrestrial radiation in the 9.6-micron band), but is mainly due to the effect of carbon dioxide 15-micron band radiative transfer. A striking result emerges from Table 4.2.9 in that the negative generations at 50 mb and 25 mb appear to be out of step every day when compared to values above and below. Further, this apparent anomaly is explained mostly by wave number 1 spatial generation. Since this is systematic, it is pertinent to determine the causes. To do that, the mean zonal vertical temperature profiles from 30°N to 80°N on the 12th of January 1959 have been drafted on Fig. 4.2.16. The warm belt is centered near 50°N and extends in depth from 200 to about 20 mb. North of 50°N, the coldest temperature is shown to be near 25 mb, while further south the minimum temperature is found between 100 and 200 mb. Re-writing and simplifying the GE-term for level 'p' yields:

$$GE(m) \propto -\left[\frac{1}{p \frac{\partial \{\overline{\theta}^{\lambda}\}^{\phi}}{\partial p}}\right] \left\{ \Phi_{h\theta}^{(m)} \right\}^{\phi} \tag{4.2.1}$$

The areal stability parameter $\partial\{\overline{\theta}^{\lambda}\}^{\phi}/\partial p$ is listed in Table 4.2.10.

Table 4.2.10. Vertical derivative of the area mean potential temperature $\partial\{\overline{\theta}^{\lambda}\}^{\phi}/\partial p$, on January 12, 1959. Units: Degrees Kelvin per mb.

Level (mb)	10	25	50	100
(°K/mb)	-15.1	-10.7	-1.9	-1.0

Tables 4.2.9 and 4.2.10 are used to evaluate the ratio:

$$\frac{GE(m)_{25\text{ mb}}}{GE(m)_{50\text{ mb}}} \cong 0.35 \left\{ \Phi_{h\theta}^{(m)} \right\}^{\phi}_{25\text{ mb}} \Big/ \left\{ \Phi_{h\theta}^{(m)} \right\}^{\phi}_{50\text{ mb}} \tag{4.2.2}$$

Hence, stability contributes partially to decrease the 25 mb "h-Θ" correlation relative to the one at 50 mb. When the same argument is applied between 50 and 100 mb, the coefficient of the covariance ratio increases to about unity. Hence, the stability does not affect the generations in a different manner between those two levels. The next step will show how wave 1 causes the anomalous generations at 50 mb. First, the potential temperature-total heating rate covariances are listed in relative units in Table 4.2.11, valid for January 12, 1959.

Table 4.2.11 Potential temperature-heating rate covariances at various latitudes and eddy generation of available energy for wave numbers 1 and 2, at 25 mb and 50 mb, on 12 January, 1959.
Units: relative, except ergs/cm^2 mb sec for the GE(n)-term

Wave Number	1		2	
Level (mb) / Lat. (^{o}N)	25	50	25	50
80	- .19	- 6.54	- .05	- .57
75	-1.29	- 9.27	-0.28	-1.07
70	-2.73	-11.3	- .44	-1.49
65	-3.78	-12.0	-1.74	-1.06
60	-3.93	-7.52	-2.70	-1.32
55	-2.41	-3.03	-4.76	- .95
50	- .72	-1.15	-5.90	- .44
45	- .35	- .50	-5.55	- .41
40	- .48	- .35	-3.51	- .91
35	- .14	- .44	-2.81	- .33
30	- .18	- .26	-1.72	- .29
GE(n)	- .18	-1.01	- .34	- .19

Table 4.2.11 reveals that the latitudinal covariances of wave number 1 are fairly similar at 50 mb and 25 mb from 30^{o}N to 55^{o}N, but

farther north the 50-mb values clearly predominate. The difference is accentuated when the stability ratio of "0.35" is applied at 25 mb. Further analysis shows that the anomaly results from the difference in heating rates rather than temperature (see Figs. B-2 and B-3 in Appendix B).

The anomaly in the vertical profile of the generation of eddy available energy has been analysed and explained diagnostically, on the one hand by a stability effect, and on the other hand by the predominance of the heating rate field at wave number 1. Now, the 15-micron carbon dioxide radiative transfer may be subdivided into two components: i) the Newtonian cooling, or cooling to space, which is a direct function of the temperature of the emitter, and ii) the radiative transfer between nearby atmospheric layers. The first case may be rejected right away, since both 25 and 50 mb have similar wave number 1 temperature amplitudes. Case ii) must then explain the anomaly. This is explained qualitatively with reference to Fig. 4.2.16. It is noted that colder temperatures at 25 mb cause a kink in the vertical profile, while a weaker kink in the other direction is apparent at 50 mb. According to the well-known tendency of the radiative transfer to smooth any vertical temperature irregularities, less cooling will be found at 25 mb while a tendency for enhanced cooling will exist at 50 mb. A well-known example of this phenomenon is found at the tropopause (Paulin, 1966).

Hence, it has been shown that a significant sink of eddy available energy is due to both horizontal and vertical temperature structure leading to a negative generation of available energy at wave number 1 at 50 mb, and that indirectly, some of this energy is trapped by the 25 mb level, causing interesting interactions, insofar as these changes in curvature in the vertical correspond to the real atmosphere. It is presumed that given a marked eccentric circulation at 25 and 50 mb, this radiative effect would be a persistent phenomenon accentuating the sink of eddy available energy at 50 mb while diminishing the one at 25 mb, and thus causing some radiative inter-level couplings.

The tropospheric-stratospheric interaction via the absorption of terrestrial radiation in the 9.6-micron band of ozone is now considered. The particulars of the process and numerical methods are given in Appendix B. The lower boundary, it is recalled, was chosen as the 850-mb level for clear skies and the 500-mb level for cloudy conditions. This lower boundary, by its characteristic temperature, has a strong influence on the ensuing heating rates in the 50-mb region. Because of latitudinal characteristics of both the temperature and the ozone vertical profiles, the influence of the lower emitter becomes insignificant north of 50°N, in winter. The cloud patterns have then been read only at, and south of, 50°N. A latitudinal phase diagram pairing both temperature and heating rate components due to the 9.6-micron absorption band for wave numbers 1 and 2, at 50 mb and 25 mb, on January 12, 1959 has been drawn as Fig. 4.2.17. A common characteristic emerges from the pairing: all correlations at all latitudes for both 25 mb and 50 mb and for both waves 1 and 2 are negative leading to an overall sink of eddy available energy. Negative heating rates prevail north of 35°N and at 25 mb, since the maximum in the ozone density profile usually lies at or below this level and Newtonian cooling of the ozone at this level would contribute to a net negative generation. Wave number 2 emerges as the largest spectral contributor of the negative eddy generation of available energy at 25 mb. The radiative problem of the 50 mb level is quite different. Lying below the level of the maximum in the ozone vertical profile, positive heating rates would be encountered modulated by the temperatures of the lower boundary. This heating leads again to a negative generation process, as shown by the negative correlation of the pairs at 50 mb on Fig. 4.2.17. The correlations at wave number 2 yield larger negative values than those of wave number 1. Inspection of the heating rates at the scales of wave numbers 3 and 4 yields values in the order of those in wave numbers 1 and 2, but the temperature vectors are much smaller than those in the first two wave numbers, and further, their phase differences are much more randomly distributed, leading to an insignificant contribution to the generation of eddy available energy. The radiative signals at 50 mb engendered by the lower boundary via the 9.6-micron band of ozone contribute about 15 percent to the negative generation of eddy available energy in wave number 1 and about 20 percent in wave number 2. These two waves, it is recalled, explain most of the eddy generation process. The synoptic patterns leading to the above results are now given. The strong warm Aleutian high pressure area, and to some extent the weaker Atlantic anticyclone, are found above the highly perturbed and cyclonically active regions in the troposphere. The extensive cloud area formed by the upward vertical motion (especially over the northern Pacific ocean) are counteracted by the Dines compensation effect yielding downward vertical motion aloft. The locally cold cloud tops reduce the heating influence of the net radiative (9.6-micron) flux convergence in the horizontally warmer regions of the 50-mb level. On the other hand, larger heating is found in the clear sky areas, corresponding to the horizontally colder 50-mb regions; the net effect being the destruction of existing eddy available energy. In a similar fashion, since the Aleutian high is a wave number 1 or eccentric phenomenon, reinforced by wave number 2, the heating rate signals originating in the large-scale lower boundary temperature variations systematically destroy the existing available eddy energy at 50 mb.

Summary of the stratospheric energetics

The energy flow during this 5-day period shows that significant eddy kinetic energy is transmitted from below through the eddy pressure interaction process. This eddy kinetic energy is transformed by barotropic processes into the energy of the zonal flow, while a smaller part is converted into eddy available energy. In opposition to the net increase in the eddy kinetic energy KE, the zonal kinetic energy KZ suffers a net decrease; as it receives energy from KE and from the boundary fluxes, it loses by the zonal pressure interaction to the outside volume, by conversion to the zonal available energy and by frictional dissipation. The zonal available energy AZ also decreases due to the exchanges into the eddy available mode and to an insufficient contribution from the zonal radiative generative processes and the meridional overturnings. The eddy available energy is found to be the main terminal for the dynamical processes (CA, CE); the expected increases are counteracted partially by the radiative-temperature correlations. The computed magnitudes of the negative generation of eddy available energy have been found insufficient to explain all the loss. Inspection of vertical eddy generation processes reveals some anomalous values at 50 mb and 25 mb, i.e., the 50 mb eddy generations are more of the order of those at 10 mb while the 25-mb generations approach those at 100 mb. This anomaly exists in the scales of wave number 1 only and is due to the 15-micron carbon dioxide inter-level radiative transfers. The transfers are particularly effective between the 25-mb and the 50-mb levels. It is found that large-scale dynamical features (cyclonic activity and clouds in the troposphere and anticyclone in the stratosphere) tend to be radiatively coupled through the 9.6-micron absorption band of ozone leading to a systematic destruction of eddy available energy in wave numbers 1 and 2, at or near 50 mb.

B. Troposphere

Synoptics

A synoptic description of the tropospheric events during the period of January 12th to 16th, 1959 has been given by Hill (1963), and will be reviewed here briefly. The period was characterized by a high degree of mid-latitude cyclonic activity. Relatively moderate and decaying cyclones marked the 12th of January, leaving the 13th as the most quiescent day of the series. The mid-latitude synoptics for the last three days of the series, that is, the 14th, 15th and the 16th, are marked by the development of a number of cyclones over the eastern and western Pacific, and also over the western Atlantic. The time series of the tropospheric eddy kinetic energy KE, as shown earlier on Fig. 4.2.2, reveals a minimum on the 13th with a steadying rise thereafter agreeing with the local synoptics. The locus of the minimum at individual data levels appears to propagate upwards at a rate of about 4.5 km/day. This locus of the minimum eddy kinetic energy coincides with a minimum in the northward heat transport found by Hill (1963). A study of actual vertical energy propagation will be made later in this chapter.

In order to anticipate the study covering the whole of January 1959, the mean 500 mb zonal winds are described in Fig. 4.2.18. Some periodic variations in the zonal wind intensities at the latitudes south of 60°N appear with 8 to 10-day cycles. The minima in the fluctuations are shown near the 9th, the 17th to 19th and about the 29th. The cyclic pulsations in the zonal flow are associated with blocking action, and the strongest case falls in the chosen 5-day period. Each block, and especially the one in mid-January, is associated with a characteristic southward shift of the mean zonal jet stream. On the 13th, the jet was moving northeastward across Japan in the established trough-ridge complex. On the 14th, it broke through the ridge with a more easterly course off the Asiatic continent, becoming isolated from the trough-ridge system.

The tropospheric temperature patterns are investigated on Fig. 4.2.19 and 4.2.20, where the -40°C and the -25°C isotherms are mapped for a few days in January 1959. The eccentricity (wave number 1) of the temperature field is clearly indicated by the distribution of the -40°C isotherm. A wave number 2 pattern can be seen on Fig. 4.2.20 but is somewhat masked by other harmonics. Superposition of the two isotherm patterns reveals very large temperature gradients over the Pacific Ocean sector which are not duplicated over the Atlantic counterpart, indicating a high storage of available energy at the scale of wave number 1. The timing of the maximum in the temperature oscillation agrees well with the occurrence of a minimum in mid-latitude zonal winds, i.e. 18th-vs.-19th, and pronounced large scale blocking circulation in the troposphere. The study of blocks is particularly interesting because of the added possibility of interaction with the stratospheric circulation.

The interrelationship between tropospheric blocks and stratospheric warmings has been demonstrated by the early work of Teweles (1958, 1963a), Craig and Hering (1959), and lately by Miyakoda (1963), Labitzke (1965) and Perry (1966). As early as 1958, Teweles advanced the possibility of interaction between both jet streams and polar night jets resulting in a stratospheric warming. Miyakoda has related the January 1958 tropospheric blocking and stratospheric warming in a causal one-to-one correspondence. He stressed especially the almost simultaneous occurrence of the 1958 stratospheric warming and tropospheric cold air southward intrusion in a blocking situation.

The strength of a blocking circulation may be inferred from the persistence of its meridional flow. Strong blocks may persist from 10 to 30 days. The moderate blocking effect of mid-January 1959 lasted from about the 13th to the 21st over both the Atlantic and Pacific.

Energies

The daily changes in the various energy modes in the troposphere may be recovered from Fig. 4. 2. 2. The tropospheric eddy available energy mode shows an increasing trend, while its zonal counterpart exhibits a sharp maximum on the 14th. It was commented earlier that the eddy kinetic energy had one minimum on the 13th; its zonal equivalent suffers a net decrease after being a maximum on the 14th. Abnormal barotropic transfers from KZ to KE are indicated by their negative time correlations after the 14th. The total available energies A_s and A_t, and the total kinetic energies K_s and K_t for the stratosphere and troposphere, respectively, appear on Fig. 4. 2. 21 for our chosen 5-day period. As noted also by others, the normal predominance of the available energy A_t over the kinetic energy K_t in the troposphere reverses in the stratosphere, where K_s is found to be more than twice A_s. A_t and K_t are found negatively correlated after the 13th, indicating possible transfers between the two energy modes. A weaker correlation is found between the stratosphere energy modes but is lasts for the whole 5-day period.

Energetics

The results pertaining to the troposphere will be considered next. First, the energy conversions of this study will be compared to those listed by Perry (1966). Table 4.2.12 exhibits the various results.

Inspection of the above table reveals that all the terms computed in the present report are of the same order of magnitude as those of other tropospheric investigations. An abnormally positive CK-term, i.e., transfer from zonal to eddy kinetic energy, is found during the chosen 5-day period. Most other studies have obtained a negative value. January 1963 yielded positive values, as computed by Wiin-Nielsen, Brown and Drake (1964), Julian and Labitzke (1965) and Perry (1966), but they were about 60 percent of the magnitudes of the present study. Recently, Brown (1967) has recomputed the January 1963 CK-term using the National Meteorological Center and Air Force analyses, and reaffirmed the previous results of Wiin-Nielsen "et al". Let us diagnose the special situation culminating in the abnormal exchange of zonal to eddy kinetic energy.

It is recalled formally that:

$$CK \propto -\overline{u'v'}^{\lambda}\ \partial\overline{u}^{\lambda}/\partial\phi \tag{4.2.3}$$

Hence the sign of CK depends on both $\frac{\partial\overline{u}^{\lambda}}{\partial\phi}$ and $\overline{u'v'}^{\lambda}$. The latter is positive when troughs and ridges have a northeast to southwest orientation. The vertical profiles of the CK-term appear on Fig. 4.2.22 while cross-sections of the mean zonal winds on the 12th and the 16th of January 1959 were presented earlier as Figs. 4.2.11 and 4.2.12, respectively. The 500-100 mb layer coincides with large positive CK-transfers, the maximum being situated in the vicinity of the jet stream level. $\partial\overline{u}^{\lambda}/\partial\phi$ is negative north of 30°N and positive south of this latitude as the maximum westerlies coincide with this latitude in the zonal wind cross-sections. The inclusion of more southern latitudes will lead to a decrease in the positive areal

Table 4.2.12. Tropospheric energy conversion computations. Units: erg/cm^2 mb sec.

(After Perry, 1966)

Conversion term	Oort (range)	Miyakoda (range)	Miyakoda (mean)	Brown (1964)	Julian and Labitzke	Perry	Paulin (5-day mean)
CK	-1.48 to .08	-1.60 to 0.30	-.3		0.71	0.72	1.26
CA	1.88 to 4.08	4.40 to 8.00	6.0		7.4	6.80	6.82
CE	1.10 to 3.47	0.10 to 1.60	1.0		6.25	0.93	1.53
CZ	-.79 to 0.35		.13		-2.00	-.14	-.30
GZ	1.07 to 3.30			5.0	4.70 (from balance)	4.00	6.20 (from balance)
GE	-1.57 to 0.58			-4.6	-.91 (from balance)	-4.33	-4.88 (from balance)
BGZ					0.24	-.03	.44
BGE					-.76	-.33	-.69

Results apply to:
Oort - whole atmosphere, various years
Miyakoda - 189 to 811 mb, January 1958
Brown - 200 to 1000 mb, January 1959
Julian and Labitzke - 100 to 1000 mb, January 1963
Perry - 200 to 1000 mb, January 1963
Paulin - 150 to 1000 mb, 12 to 16 January 1959

integrated CK-term as $\overline{u'v'}^{\lambda}$ is likely positive over most of the region. The effect of this addition may be approximated by considering the transport of zonal kinetic energy across the vertical boundaries, as given by the computed BKZFI-term in Table 4.2.13.

Table 4.2.13. Horizontal convergence of the flux of zonal kinetic energy BKZFI and CK-transfer in the troposphere on January 12 to 16, 1959.
Unit : erg/cm^{2}mb sec.

DATE (Jan. 1959)	12	13	14	15	16
BKZFI	3.05	3.45	4.10	3.84	4.17
CK	0.87	0.99	1.03	1.27	2.13

Referring to Eqn. 3.2.20, the meridional convergence of $\sum_{m=1}^{\infty} \overline{u}^{\lambda} \Phi_{uv}(m)$ emerges as being the main contributor to BKZFI. The changes in CK when the southern boundary is shifted to about 20°N may be approximated from Table 4.2.13. Both $\overline{u}^{\lambda}$ and $\overline{u'v'}^{\lambda}$ would likely suffer a 50 to 80 percent decrease, and BKZFI could easily be reduced by 50 percent: the lost flux convergence appearing as an integral part of the CK-process. Hence according to this rough analysis, the barotropic transfer CK may become normally negative each day except perhaps on the 16th.

The spectral distribution of the interaction between the eddy and the zonal flow at the levels where the anomaly originates, i.e. 200 and 300 mb, are now investigated. This special distribution of CK (n) is found in Table 4.2.14.

The results in Table 4.2.14 are transformed to a pictorial form in Fig. 4.2.23. It is seen that contrary to Wiin-Nielsen (1964, a) and Perry (1966), the predominating conversion from the kinetic energy of zonal flow to wave number 3 flow which they found has not materialized here. The zonal to eddy transfer is shared by most other spectral transfers but predominantly by wave numbers 2, 5 and 6 at 200 mb and 2, 5, 6 and 7 at 300 mb, this effect being more striking on the last day of the series.

Table 4.2.14. Daily and spectral distribution of the CK (n) - term at 200 and 300 mb, on January 12th to 16th, 1959. Unit: erg/cm^2 mb sec.

Date	Pressure	Wave Number							
Jan. 1959	Level (mb)	1	2	3	4	5	6	7	8
12	200	.30	.83	-.62	1.73	.69	.18	.16	.01
	300	-.61	.51	-.02	1.56	1.48	.36	.50	-.40
13	200	.13	1.24	-.06	.80	.62	1.07	.49	-.14
	300	.79	.56	.01	.20	.45	.78	-.00	-.11
14	200	.23	.44	.53	.41	-.09	.21	.13	-.05
	300	.53	.66	.33	.56	-.23	.28	.81	.01
15	200	.01	1.13	-.11	-.38	.63	.43	.21	.40
	300	.38	1.19	.68	.19	.08	.49	.82	1.00
16	200	.52	3.10	-1.12	-.82	2.23	2.56	-1.19	.10
	300	.65	1.56	.89	-.16	2.30	.95	1.30	1.48

All in all, it has been shown that the positive tropospheric CK-conversions were mainly due to the jet stream layer interactions between the zonal and eddy flow, that this anomalous transfer may be somewhat artificial, considering the location of the chosen vertical boundaries at 30^{o}N, and that this effect could not be pinned down to a single wave number as was the case in January 1963, but was shared by most wave numbers, especially wave numbers 2, 5 and 6 for the combined 200 mb - 300 mb layers.

The computed CA-transfers obtained in this study agree almost exactly with the other investigations, although Oort's (1963) values were taken from various previous studies and are either valid for the whole of winter, or for the whole year, and as such should be lower than the corresponding January (1958, 1959 and 1963) results.

Similarities and differences in the CE and CZ processes are all shown on Table 4.2.12. This will shed light on the validity of one of the most important and also the most difficult parameters to obtain: the vertical motion. This study, as well as those of Perry and Miyakoda found CE and CZ magnitudes significantly smaller than those of Julian and Labitzke. It is felt that our vertical motion model gives highly smoothed results, affecting the synoptic scale through the use of a grid which is effectively almost twice as large as the standard 1977-National Meteorological Centre grid used by Julian and Labitzke. A study by O'Neil (1964) has shown that by shortening the grid size by a factor of 2, the vertical motion resulting from the solution of the diagnostic omega-equation in the troposphere increases by a factor between 2 and 3. Perry's vertical motion although computed from the vorticity equation, used the same basic grid as in the present study. In fact, he commented on the effect of the numerical smoothing of the model and concludes that the vertical motion is more reliable in the long waves. The agreement in magnitudes between Perry's CE and CZ computations and those of this study are not too surprising. Another smoothing influence in the diagnostic omega-equation consists in the existence of high order derivatives (3rd and 4th order). At 500 mb, the adiabatic (thermodynamic) method involving first order derivatives only, yields vertical velocities two or three times larger than the velocities from the higher order analog.

The generation terms GE and GZ agree in magnitude and sign. The most recent computation of generation of zonal available energy was done by Vernekar (1967). His results were about 50 percent of those computed by Brown (1964) for January 1963, but when the vertical integrations are made comparable, Vernekar's values become about 70 percent of Brown's results. For the 1000-200 mb layer, Vernekar (1967) computed a mean January 1963 generation of zonal available energy of 3.8 erg/cm^{2}mb sec. Assuming that the January 1959 values from Brown (1964) were 30 percent too large, then our balance-inferred GZ is too large by a factor of 2, which is rather good, considering the crudeness and the errors in its computation.

The boundary pressure interaction terms BGZ and BGE generally agree in magnitude and sign with those of the other investigation and their magnitudes are characteristically small.

The daily and 5-day mean tropospheric energy flow has been presented earlier conjointly with its stratospheric counterpart as Fig. 4.2.3 to 4.2.8, while the equivalent information was tabulated in

Tables 4.2.1 and 4.2.2. With reference to Fig. 4.2.8, the 5-day mean tropospheric flow will be described next. From balance requirements, zonal available energy is produced at a rate of 6.2 ergs/cm^2 mb sec, due to the correlation of temperature with solar zonal heat input, zonal latent heat released and zonally averaged turbulent heat transfer. The zonal available energy thus produced will interact with the tropospheric motion system and be deformed into eddies, the rate of deformation showing as a transfer to the eddy available energy at a rate of 6.82 ergs/cm^2 mb sec. The boundary fluxes are rather negligible when compared to the processes affecting both AZ and AE. The eddy available mode transfers some of its energy baroclinically to the eddy kinetic energy counterpart at a rate of 1.53 ergs/cm^2 mb sec. AE shows a net gain throughout the period which is approximately 0.23 ergs/cm^2 mb sec in the rate units used. The generation of eddy available energy is inferred from the residual of the AE-budget. Radiative and earth surface-air exchanges would then degenerate eddy available energy at a rate of 4.88 ergs/cm^2 mb sec. The reality of this value is vouched for by the dynamically inferred studies of Brown (1964) and Perry (1966). Brown's result is the mean for January 1959, and as such seems to verify ours. Since the GE-value depends critically on the CE-term, it is important to recall some of the assumptions used in deriving it. It has been shown earlier that the vertical motion is smoothed on the synoptic scale due to some numerical considerations. The adiabatic computation of the vertical motion in the troposphere neglects two opposing phenomena: the weakening effect of the long wave radiative cooling due to clouds in the mid-troposphere (Katayama, 1967) and the strengthening influence of the latent heat released, which is probably larger in absolute magnitude than the first process (Danard, 1963). It is thought that because of these various physical omissions and numerical characteristics, the baroclinic transfers may be slightly larger and the generation of eddy available potential energy might be somewhat less.

Following the energy flow, the eddy kinetic energy reservoir stands at the intersection of an active energy cycle. Not only does it receive energy baroclinically at a rate of 1.53 units and barotropically at 1.26 units, it also receives a net influx of this energy mode by cross-boundary processes. Notwithstanding the small net rise in eddy kinetic energy during the period and the small loss to the outside by pressure interaction, the budget is balanced by assuming frictional dissipation at a rate of 3.39 ergs/cm^2 mb sec. This balance-inferred frictional dissipation DE is fairly well representative of the values used by various investigators although it is a bit larger than the most recent results. One of the earlier estimates of dissipation is that of Brunt (1941) who computed an average loss of 5 ergs/cm^2 mb sec for the whole atmosphere. Jensen (1961) reported 4.5 ergs/cm^2 mb sec for January 1958. White and Saltzman (1956) inferred a value of 5 ergs/cm^2 mb sec. Very recently, Kung (1966, 1967) made a systematic study of the total (eddy and zonal) dissipation of the kinetic energy by computing it as the residual between the generation of kinetic energy within the volume (cross-isobaric flow), the outflow of kinetic energy across the volume boundaries and the local rate of change of kinetic energy. The volume comprised North America only, and the latest of the two studies (1967) used 5 year winter data twice daily (0000 and 1200 G.M.T.) in order to make the mean statistics applicable to the hemisphere. Real winds were used and the dissipation is obtained as a residual "without employing specific theories" in the author's words. Kung's (1967) 5-year mean free atmosphere frictional dissipation study yields a value of 3.36 ergs/cm^2 mb sec, which in passing is very close to our computed dissipation of 3.39 ergs/cm^2 mb sec. In the domain of atmospheric general circulation models, Smagorinsky, Manabe and Holloway (1965) computed zonal and eddy frictional dissipation of kinetic energy at rates of 0.6 and 2.2 ergs/cm^2 mb sec, respectively. Smagorinsky et al (1965) and Kung (1967) have published their computed vertical profiles of the frictional dissipation. The dissipation of the eddy kinetic energy at the data levels of this study have been gathered from the residuals in the following expansion of the eddy kinetic energy budget at level "p":

$$DE_p = CE_p + CK_p + BGEP_p + BKEFI_p + BKEP_p - \left.\frac{\partial KE}{\partial t}\right|_p \qquad (4.2.4)$$

All the terms of Eqn. (4.2.4) have been computed except $BKEP_p$, since this divergence was computed for the whole stratosphere and troposphere only. Over the troposphere it averaged only 0.24 erg/cm^2 mb sec while a negative value with larger magnitude (-0.79 unit) was computed for the stratosphere. The results of Eqn. 4.2.4 are given in Fig. 4.2.24 where the equivalent computations of Smagorinsky et al (1965) and Kung (1967) were added for easy reference. The three curves show the characteristic maximum dissipation at jet stream levels. Very striking negative values are noticed above and below the jet stream level in Kung (1967). The negative signs are probably quite real, considering the long time period used in the statistics. It is interesting to note that a small negative value is also computed in this report at 700 mb. The eddy frictional dissipation of this report is found to decrease with height above 300 mb and to be negative at 25 mb. This decrease with height is shared by Smagorinsky et al (1965) although he does not compute negative values. In Kung (1967), negative values are found between 200 and 100 mb. The rapid increase in the dissipation above 100 mb is somewhat surprising. Notwithstanding errors, the larger amplitude of the dissipation forces at jet stream levels may indicate that on the chosen 5-day period, the atmosphere was more active than a winter mean case, and as such was losing more energy to the frictional influences. A return to higher dissipation is felt at 850 mb, anticipating the large sink of eddy kinetic energy by friction in the boundary layer.

The zonal kinetic energy mode empties itself anomalously towards the eddy kinetic energy reservoir at a rate of 1.26 erg/cm^2 mb sec and towards the zonal available energy by the action of the overturnings in meridional planes at the small rate of 0.30 erg/cm^2 mb sec. On the other hand, its net increase in time (0.85 erg/cm^2

mb sec) is mainly explained by the strong influx of this energy across the boundary at a rate of 3.89 ergs/cm^2 mb sec. It has been shown above that this large import is due to the location of the southern boundary and explains partially the anomalous exchange to the eddy kinetic energy mode. The production of zonal kinetic energy by the action of the pressure forces at the boundaries, energy which has originated mainly in the stratosphere, is of little significance to the bulky lower layer (0.44 erg/cm^2 mb sec), but it was a rather heavy loss in the stratosphere (3.65 ergs/cm^2 mb sec). When the zonal frictional dissipation is inferred from the balance, it becomes a rate of 1.72 ergs/cm mb sec, or about 1/3 of the latest total (zonal plus eddy) dissipation values, as originally advocated by Kuo (1951) from the early work of Brunt (1941) and White (1950). Our zonal frictional dissipation rate is larger than the latest approximations which range from 0.5 to 1.0 erg/cm^2 mb sec.

Although the period included between January 12 and 16, 1959 was a fairly homogeneous one, the essential characteristics of the daily budgets will be given in the next few paragraphs. The daily fluctuations of the tropospheric components of each of the four energy modes will be given in appropriate time diagrams while some added time-wave number diagrams will describe the daily spectral distribution of the significant transfers.

The daily budget of the tropospheric zonal available energy is depicted on Fig. 4.2.25. The changes of AZ are found to be fairly well correlated to the magnitudes of the rate of transfer to AE by the CA-process. The other computed processes are rather small, i.e., CZ and BAZ. As mentioned earlier, the GZ-process may be approximated by the residual in the balance. Its magnitude is somewhat larger on the 14th and 15th, but on the whole not unreasonable. The spectral and daily CA-conversion is shown on Fig. 4.2.26. The eddy deformation of the temperature field by the tropospheric flow is produced in a fairly selective manner by wave number 2, 4, 7 and 8. Even then, the effects of the various scales are not felt simultaneously.

The post-13th period (the cyclonic activity was minimum on the 13th) had wave number 2 scale predominant first (13th to 16th), then waves 4 and 7 follow suit on the 15th and 16th, while wave 8 had some significance on the 14th and 15th. CA(n) decreased on the 16th in all of these significant scales, as can also be seen in the total CA-process. The establishment of blocking circulation during this period is clearly indicated by the CA(2) transfer magnitude over the period with the added contribution of CA(4), CA(7) and CA(8) on and after the 14th.

The daily budget of the eddy available energy is shown on Fig. 4.2.27. A relatively large destruction of eddy available energy by the GE-process is required to balance the large input from the CA-process and the smaller (although possibly underrated) CE-transfer to KE. The balance-inferred dissipation of eddy available energy is found to vary from 2 to 8 ergs/cm^2 mb sec, with a mean of 4.6 ergs/cm^2 mb sec. Krueger, Winston and Haines (1965) have computed a mean January eddy generation term of about -1.8 erg/cm^2 mb sec from a balancing approach, similar to that used in this report. Brown (1964), from an interplay between the vorticity and thermodynamic equation, obtained generations values near -5 ergs/cm^2 mb sec. Lately, Perry (1966), in a somewhat similar manner, computed eddy generation values ranging from -1.71 to -7.23 ergs/cm^2 mb sec during January 1963. It is felt that our magnitudes, even when they are large, approximate the generation of eddy available energy within tolerable limits.

The baroclinic transfer of eddy available to eddy kinetic energy has been partitioned into its spectral elements on Fig. 4.2.28. Some similarities and differences appear between the CE(n) and the CA(n) distributions. The overturnings in zonal planes are spectrally less significant than the corresponding wave 2 heat transport, although their times of maximum magnitude coincide. CE(4) has about the same significance CA(4) had. The relative significance of CE(7) duplicates the role of CA(7), as shown earlier.

The daily budget of the eddy kinetic energy in the troposphere is presented in Fig. 4.2.29. The residual is characterized by being larger than any given transfer during the period, all conversions and local rate of change being less than 2 units while the residual varies from more than 2 units to less than 4. The influx of eddy kinetic energy BKE is shown to oscillate but has a decreasing trend in time. The eddy kinetic energy rate also oscillates and is the only term changing sign during the period. CE and BGE have opposite sign throughout the period as shown by Fig. 4.2.30 and 4.2.28. Both processes, it is recalled, are due to the cross-isobaric flow at constant level, or equivalently, the cross-contour flow on a constant pressure surface. The BGE-process was produced when we arbitrarily limited the volume, and the CE-process for the whole atmosphere became artificially truncated. The BGE-process then refers to the eddy energy in the lower layer which appears as eddy kinetic energy in the other layer. In this sense, as pointed out by Muench (1965), the stratosphere becomes a sink for some of the tropospheric energy. An important difference resides in the significance of the scales in the CE and BGE processes. While both processes have about the same significance at the scale of wave number 4, the predominance of wave number 7 over wave number 2 in CE has reversed in the BGE-process. Further, it was shown earlier that vertical flux of geopotential of the smaller scales was rapidly absorbed between 200 mb and 100 mb.

It seems to be appropriate here to test some of the theoretical results against real data computations. According to Charney and Drazin (1961), Charney and Pedloski (1963), Murakami (1967), baroclinically unstable wave disturbances do not propagate energy upwards significantly, they are exponentially absorbed or reflected by the strong westerlies in the jet stream layer. A test is set up using the synoptic scale of wave number 7. The daily profiles of flux of geopotential at wave number 7, BGE (7), have been plotted on Fig. 4.2.31. The rapid absorption of this flux is evident in the 100-200 mb layer. The daily variation in the profile is noteworthy. The flux of geopotential is generally upwards on the 12th, and maximum at 300 mb. On the 13th, the flux is directed downward, except maybe near 300 mb. A tremendous surge in the flux appears on the 14th, and reaches the highest strength on the 15th, while it decays on the 16th. As shown by these results, the theories of the above-mentioned authors are verified at this time.

The barotropic transfer is anomalously positive as it feeds the eddy kinetic energy mode at the expense of its zonal counterpart, this being due to the strength of this transfer at jet stream level. The magnitude of this process increases monotonically with time. The spectral barotropic transfers are fairly similar to those described for the whole troposphere and duplicate closely those described earlier for 200 and 300 mb.

The dissipation of eddy kinetic energy by the free atmosphere frictional stresses is fairly similar to the 5-day mean case which has been discussed in detail earlier.

The zonal kinetic energy remains the last budget to balance. The daily components of this budget appear on Fig. 4.2.32. All the components are fairly steady in time except the local rate of change of the zonal kinetic energy itself, so that the balance residual fluctuates in unison with $\partial KZ/\partial t$. Little can be added to what was given earlier when the 5-day mean case was dealt with.

Summary of tropospheric energetics

The results obtained in dealing with the tropospheric energy cycle during the period January 12 to 16, 1959 will now be summarized.

Synoptically, a minor stratospheric warming is in progress at the same time as a tropospheric blocking circulation which is largely defined by wave numbers 1 and 2.

The following energy cycle persists throughout the period:

$$AZ \longrightarrow AE \longrightarrow KE \longleftarrow KZ \dashrightarrow AZ$$

This cycle is the normal baroclinic energy cycle, except that the transfer KZ to KE is somewhat anomalous, most likely because of the southern boundary.

The dissipation of eddy kinetic energy by the free atmosphere frictional stresses has been computed at each data level as the residual in the balance of the eddy kinetic energy mode. The resulting vertical profile had a very realistic shape, although the dissipations at the jet stream level were on the large side.

The spectral decomposition of the tropospheric CA and CE processes led to the dominance of the scales corresponding to waves 2, 4 and 7, and also 8. The BGE-process was shown to be negatively correlated to the CE barotropic transfer, even in the spectral domain. The absorption and/or reflection of synoptic scale baroclinically unstable wave distrubances was demonstrated in the study of the daily vertical profiles of the geopotential flux of wave number 7, hence verifying some theoretical results.

C. Tropospheric-stratospheric interactions

The dynamical processes linking the troposphere and the stratosphere have been computed and here we consider their characteristics in time, totally and spectrally. The fluxes of eddy geopotential and their convergences are shown in Figs. 4. 2. 33 and 4. 2. 34. For easy comparison of the magnitudes of the dynamical exchanges and radiative exchanges, a second scale (^{o}C/day) has been added to Fig. 4. 2. 33. The daily profiles in the first figure suggest the existence of vertical oscillations with wavelengths from 10 to 18 km, whose amplitudes are more noticeable in the lighter stratosphere. The tropospheric and lower stratospheric vertical profiles agree well with a comparable study by Nitta (1967) and with a numerical experiment by Smagorinsky et al (1965). Since these investigators had a crude stratospheric model, little can be deduced from their results in the stratosphere. Smagorinsky et al (1965) computed a maximum vertical divergence of the eddy geopotential flux at 500 mb of about 4 ergs/cm^{2}

mb sec, which is comparable to our 500 mb maximum divergence of 2-3 ergs/cm^2 mb sec, and they also found zero geopotential flux convergence near 300 mb. Flux convergence and upward energy propagation characterize the stratosphere for the period except on the 16th at the highest levels when the geopotential flux is downward and divergent. Vertical coherence in the flux convergence is maximum on the 12th and this coherence weakens gradually after the 14th as a maximum in this field appears to propagate downward. On the 16th, divergence in the geopotential flux originates above 25 mb and indicates a gain of energy at levels at and below 25 mb at the expense of the layer above. Coinciding with the exchanges between the middle and upper stratosphere, a very large flux of geopotential takes place across the 200 mb level creating a large gain of energy in the 200-25 mb layer on the last day. The spectral height-time diagrams in Figs. 4. 2. 35 and 4. 2. 36 describe the scales in which the geopotential fluxes and their convergences take place. The vertical coherence in the geopotential flux convergence on the 12th seems to be associated mostly with wave numbers 4 and 1. Flux divergence at wave number 3 in the stratosphere on and after the 14th is associated with downward flux propagation at the same scale permeating the whole atmosphere. The downward energy propagation appearing at high levels on the 16th can best be explained by the geopotential fluxes of wave number 1 and also wave number 3. Wave number 2 geopotential flux remains directed upwards during the period with maximum strength on the 14th and 15th. The convergence associated with this flux in the stratosphere is also persistent with maximum magnitudes on the 14th and 15th. The maximum temperatures found at 10 mb on the 14th in the stratospheric Aleutian anticyclone seemed to have progressed downward and reached the 50 mb level by the 18th. The downward progression of a warm core from the stratopause to 30 km following increased planetary-scale activity has been duplicated by Byron-Scott (1967) in his recently published comprehensive numerical model on stratospheric photo-chemical processes and their interactions with large-scale dynamics.

The processes which lead to a sustained warming will be categorized next. In face of a continuous energy transfer to the stratosphere from the troposphere, by the pressure interaction process in the eddy mode, stratospheric eddy kinetic energy is transferred into eddy available energy in the same layer via the zonal modes and the negative CE-transfer. At times of maximum transfer, the dissipative action of the radiative processes cannot keep up with the temperature increase, and temperatures above normal values may persist. This characteristic of the mid-January warming period may have been enhanced by the particular behaviour of wave number 1, (and partly wave number 3) which is found to feed energy to the 25-100 mb layer at the expense of the 0-25 mb layer. The vertical motion associated with this scale may be responsible for the warmer temperatures in the Aleutian anticyclone. It is postulated that the weakening of this scale of vertical motion as indicated by the decline of KE(1) at 25 mb (to be shown in next chapter) will bring about the end of this minor warming.

To summarize the stratospheric-tropospheric pressure interactions, it is noted that:

1) The stratosphere acts as a sink of planetary scale kinetic energy as it transforms it into a form that can be radiatively dissipated to space.

2) The energy seems to be carried by pulses in the geopotential flux creating intermittent signals which have reasonable vertical coherence.

3) Some significant energy propagates downward at wave number 1 and also at wave number 3, at a lesser rate but in a more persistent manner. It is suggested that wave number 1 vertical motion involved in the transfers may be the link in explaining the warmer temperature in the Aleutian high pressure area.

4) Wave numbers 2 and 4 together contribute the largest part of the transfer from the troposphere to the stratosphere.

5) Occasionally, the pressure interaction in wave number 3 is such that it connects the upper layers to the surface boundary layers which become a sink for stratospheric energy. This process is rather weak, though.

D. The stratospheric and tropospheric budget in the spectral domain

The mean 5-day spectral energy budget for wave numbers 1 to 7 will be analyzed next.

The results pertaining to the mean spectral kinetic energy budget are given in Fig. 4.2.37. In the stratosphere, the kinetic energy at wave number 1 is being drained off through the exchanges to the other waves, to the zonal flow and through a conversion into the available energy of wave 1. It gains by the pressure interaction with the troposphere and possibly also from the upper stratosphere as shown earlier. Extra additive effects result from advection of kinetic energy at scale of wave number 1 through the horizontal and vertical boundaries, as given by the BK-term, after this term has been redefined formally as applicable to each wave number scale:

$$BK(n) = BKEFI(n) + BKEP(n) \qquad (4.2.6)$$

The net balance is not very good as the actual kinetic energy at wave number 1 shows a net increase during the 5 days, requiring a negative frictional dissipation for balance. The LK(n) daily variations for wave number 1 are quite large and not necessarily in phase with the variations of the other terms, contributing significantly to the poor budget at this scale. In the troposphere wave 1 loses kinetic energy through both pressure interaction to the stratosphere and to other waves. The loss is compensated for mostly by the boundary transport and also in a rather small part by the exchange from the zonal flow and the available energy of wave 1.

A strong stratospheric-tropospheric link is achieved through both the upward progression of the flux of geopotential and the flux of kinetic energy across the vertical and horizontal boundaries at wave 2 scale. The ensuing stratospheric kinetic energy is re-channelled through the dispersive barotropic processes (CK, LK) and through the baroclinic process (CE) into available energy of wave 2. In the troposphere the exported energy is resupplied from the dispersive processes CK and LK, from the baroclinic process CE and from the flux of kinetic energy at the boundaries. The above energy reservoir receives a net gain, which in balancing the budget must imply a loss of about 1 erg/cm^2 mb sec in frictional dissipation from wave number 2 to the scales smaller than those investigated in this study.

In the stratosphere, wave number 3 kinetic energy sits at the receiving end of the non-linear wave interaction process gaining significantly while suffering a net loss through the other three transfers: CK, CE and BGE, the BK-process being nil. In the troposphere, making exceptions for the negative CK(3)-transfer, the three other processes yield transfers in the opposite direction to the corresponding ones in the stratosphere. Of importance is the relatively large loss into the energy of other waves compensating for the additive effect of the boundary BK-process. The pressure interaction is interesting at this scale since the stratospheric energy is transferred directly into the friction layer where it is dissipated. The same process occurred in January 1963 as shown by Perry (1966), but the rates of exchanges were remarkably larger.

The large computed influx of geopotential from the troposphere into the stratosphere characterized wave number 4 stratospheric energy flow, while the other processes were rather small. Slight KE(4) gains through CE(4) and LK(4) are somewhat balanced by the loss through CK(4) and BK(4). In the troposphere, the kinetic energy of wave number 4 behaves in a normal fashion by being more active in its transfers. The significant sink of wave number 4 kinetic energy resides in the loss of geopotential to the layer above and dispersion into the other waves. It is partially compensated for by the exchanges between the zonal flow, the available energy of wave 4 and boundary imports. A decrease in wave 4 kinetic energy is indicated and is verified by the net 5-day change of this component.

The kinetic energy of waves 5 to 7 gains through the LK-process, wave 5 leading. A negative CE-transfer affects those scales, and again wave 5 leads in this domain. The CK-transfers are small and of little importance, except perhaps at wave number 5 which shows a rate of about -.25 erg/cm^2 mb sec. The relatively larger transfers in the positive BGE-terms at wave numbers 6 and 7 are somewhat paradoxical. This effect was shown to result from the vertical integration schemes and remains compatible with the theoretical results of Charney and Drazin (1961) and/or Charney and Pédloski (1963). The tropospheric kinetic energy at waves 5, 6 and 7 are found to be involved in a relatively active cycle of fairly uniform characteristics. They all lose energy by the pressure interaction term at a relatively small rate, and as shown above, this energy is rapidly trapped in the lower stratospheric layers. As a group, they gain energy through interaction with waves 1, 3 and 4. This seems contrary to the findings of Saltzman and Fleisher (1960, a, b), Teweles (1963) and Perry (1966). Our results are more along the lines of Murakami and Tomatsu (1964). The first group of investigators found that for long time averages (seasonally and yearly) the middle synoptic waves (n = 5 to 9) contribute their energy to both sides of the spectrum. Murakami and Tomatsu, in a 500 mb study of the year 1962 found that waves 2 to 6 send their energy to the rest of the spectrum. One must add that the present 5-day results do not carry the weight of those long averages and are extracted from very noisy triple correlation computations.

A similar description of the mean 5-day energy exchanges, but related to the eddy available energy, is shown on Fig. 4.2.38. In the stratosphere, remarkably large conversions of zonal available energy to that of waves 1 and 2 were computed. On the other hand, waves 4, 2 and 7 led, in the order given, for the corresponding transfers in the troposphere. It has been shown that the CA-process is proportional to the "vT" correlation. It has been shown also by Charney and Drazin (1961), Van Mieghem (1963) that the upward flux of geopotential is proportional to the same "ωT" correlation. It is of little surprise to find qualitatively from the CA(n)-distribution what has been noted earlier in this study, i.e., the upward propagation of waves 1 and 2 flux of geopotential across the whole atmosphere. Waves 4 and 7 propagate upwards but wave 7 shows little progression above the tropopause. Wave 4 propagates upward on the 12th of January but the effect weakens very significantly after this date. Kinetic energy is being transformed into available energy at all the wave scales present in the stratosphere, the transfer decreasing with wave number. In the troposphere, this baroclinic exchange is distributed differently, being fairly small at the low wave number side of the spectrum and yielding maximum intensity at wave number 7 followed by wave number 4. The transfer is of course in the opposite direction to that in the stratosphere. Even in the stratosphere, the negatively computed CE-process may not be valid for the whole layer, but more of this will be analysed later in Chapter 5. Very little has been done about the non-linear exchange between the components of available energy spectrum. Murakami (1963, b), in a theoretical study, has derived some possible non-linear exchanges between the planetary scale (n = 1, 2 and 3) and the long wave scale (n = 6) and postulated that probably the long waves feed their available energy into the planetary scale. Yang (1967a), in a 12-month study (February 1963 to January 1964) computed a general downscale cascading of available energy in the troposphere, and seasonally the effect became more vigorous in winter.

This short time study reveals that in the stratosphere wave number 2 feeds some of its available energy to waves 1 and 6, while the other scales showed little interaction. In the troposphere waves 2 and 4 feed their energy to the other waves, but only to waves 3 and 5 in a significant fashion. Of interest, in the troposphere, it appears that the neighbouring scales are related by the non-linear interaction in the domain of available energy: wave 2 feeds wave 3 and possibly wave 1, wave 4 interacts with waves 3 and 5 by sharing some of its energy in the available mode, and also probably extending its action to the lower scales.

The spectral generation of available energy is also depicted in Fig. 4.2.38. The stratospheric results arose from the solution of the equations of radiative transfer. The stratospheric dissipation decreases with wave number, being a strong function of temperature. Wave 1 and 2 scales appear to be the major dissipators. Since the boundary flux of spectral available energy appears to be very small (BA-shafts in Fig. 4.2.38), the budget of each wave may be approximated. It is assumed that the necessary balance, after the net change in AE(n) is included, approximates the full GE-term, since our own radiative solution used a simple climatological absorber distribution. Larger negative radiative generation for the wave numbers 1 and 2 is necessary for the balance. It has been demonstrated earlier that the radiatively computed GE-term was significantly smaller than other dynamically-inferred values, and this discrepancy seems to be concentrated in the scales of wave numbers 1 and 2.

The budgets of waves 3, 4 and 5 are apparently good, while the transfers associated with the budgets of waves 6 and 7 are insignificantly small and little can be said definitely.

The tropospheric eddy generation term GE(n) has been inferred from the spectral balance of the terms, once the net 5-day change of AE(n) has been included (not shown on the graph). It is instructive to comment on the relative size of the results. All the GE(n)-terms are negative, indicating stronger radiative cooling over warmer regions, and vice-versa. It is expected that the radiative and turbulent surface-air heat exchanges would cause a negative generation at all wave lengths, especially in the longer wave end of the spectrum. It would also be expected that on the synoptic scale, the GE(n)-values would be somewhat less negative than shown since the effects of the latent heat released in the warm air regime would tend to increase the CE(n)-terms.

The last item of this 5-day spectral study has been incorporated in Fig. 4.2.39 describing the whole atmospheric spectral flow set-up.

Note that in Fig. 4. 2. 39 K(n) and A(n) are identical to KE(n) and AE(n), respectively. The diagram will have a two-fold purpose: it will permit a "vue d'ensemble" of the major processes in action during the period while it will also conveniently summarize the essential findings of this chapter.

Troposphere

The solar energy absorbed by the ground sets up a field of zonal available energy in the troposphere after it has been redistributed through convection, radiative and turbulent heat transfers, latent heat release, etc. The action of the air in motion is to perturb the zonal temperature field, mainly into the scales of wave number higher than 5, but also in a significant fashion into the scales of wave numbers 2 and 4, due to the air motion eddies associated with the topographic, frictional and heat influences originating at the earth surface. The temperature eddy fields interact with each other, in such a way as to increase the "long" and synoptic scale portion of the spectrum at the expense of the more or less stationary temperature field of waves 2 especially, and also 4. Some of the non-linear interactions feed the available energy spectrum outside our volume of interest, presumably accumulating mostly south of 30°N, but this export is found to be small. Destruction of available energy occurs at all wave lengths, the wave number group larger than 5 losing most followed by wave number 2.

A higher degree of baroclinicity is shown by the "long" and synoptic waves, while a relatively small exchange into the eddy kinetic energy is found in the waves 1 to 4. In all probability, the transfer from available to kinetic energy for the waves 5 to 12 could be larger for reasons mentioned earlier.

Except for wave number 3, zonal kinetic energy transfers its excess in a somewhat anomalous manner to all the other waves, the effect being larger for the group of wave numbers larger than 5. The eddy kinetic energy reservoir, at most scales, resides at the end of the energy flow, and notwithstanding the relatively large frictional dissipation, this coincides with a net increase in the activity of synoptic disturbances in the troposphere. The loss to the stratosphere through the pressure interaction term is a relatively small item for the bottom heavy troposphere, but the effect is more marked at the scales of wave number 2 followed by 4 while wave 3 actually gains energy from the layer above. The dispersive activity between the waves by non-linear interaction is somewhat anomalous for the period. The rather large daily variation makes the mean 5-day results of little statistical significance; besides, any three-parameter correlation would naturally be very noisy. Because of formal similarities between the CK(n) and the LK(n) terms, the cause of the anomaly in the former conversion, i.e., the southern boundary, may also partially explain the anomaly in the latter. In any case, the scales of wave numbers 1, 3 and 4 seem to feed energy into the remainder of the spectrum. Simultaneously, a significant export of energy across the boundaries characterizes the non-linear wave interaction process for the period. This loss is counteracted by the positive effect of the boundary BKE-effect which is mostly effective across the 30°N vertical wall.

The zonal kinetic energy reservoir is being drained off by the barotropic exchanges to the waves as shown above, and also by a weak transfer of kinetic energy to zonal available energy. The zonal kinetic energy is maintained by large transport of the same quantity through the vertical wall along 30°N, and by a smaller but still significant import from the stratosphere through the zonal pressure interaction process BGZ.

Stratosphere

In the stratosphere, the maintenance of wave numbers 1 and 2 kinetic energy is fairly similar but KE(2) is associated with more vigorous processes. Both spectral energy reservoirs lose energy by dispersing it into the other waves and the zonal flow, and by converting it into the eddy available mode (in this process, wave 1 dominates in magnitude). Both KE(1) and KE(2) receive significant energy from the pressure interaction with the troposphere. KE(3), KE(4) and KE(5 to 12) have fairly dissimilar exchanges. The kinetic energy of waves 5 to 12 reflects similar characteristics to those found for waves 1 and 2, except maybe that it sits at the receiving end of the non-linear wave interaction mechanism. The only property common between the kinetic energy of waves 3 and 4 and the above mentioned smaller scale group is a similar gain through the non-linear wave interactions, but all resemblance ends there. Wave 4 is unique in presenting an active tropospheric-like energy cycle, i.e., of the form:

$$AZ \longrightarrow AE(4) \longrightarrow KE(4) \longrightarrow KZ$$

KE(4) is also gaining significantly from its pressure interaction with tropospheric upward flux of geopotential at the same scale. The energy cycle attached to the wave group 5 to 12 duplicates the computation of Oort (1963) for the total yearly indirectly driven stratosphere. The eddy kinetic energy in this group, after being enhanced by tropospheric influences through the BGE-term, is then converted to eddy available energy which in turn is being destroyed by counter-gradient heat transport, while in the barotropic branch of the circuit, the kinetic energy of this wave group is transformed into the zonal mode by the net horizontal convergence of the northward transport of relative westerly momentum. KE(3) is characterized by a loss in all transfers except one: the gain through the non-linear wave interaction. The rate of energy input by the above process coupled with the net lowering of KE(3) magnitudes are sufficient to give a good balance for the budget at this scale. Of interest for our period, the downward transfer of energy at this scale reaches occasionally the tropospheric boundary layer. The similarity of this result with Perry's (1966) has been noted.

It is instructive to note that the mean 5-day non-linear wave interaction in the stratosphere approaches the results of Perry (1966) observed during January 1963. Wave 3 kinetic energy is maintained at the expense of both waves 1 and 2. Waves 5 and 7 energies were also registering a net gain. Although the excess input into wave 3 approximated that found by Perry by this process, the energy interchanges from waves 1 and 2 into waves 4, 5, 6 and 7 were larger than Perry's.

The effects of the boundaries lead to a moderate gain by the flux of eddy kinetic energy, and a small loss to the waves outside the volume by the dispersive non-linear process. The interaction with scales of wave numbers larger than 12, referred to already as the frictional dissipation, is obtained from a residual of the total eddy kinetic energy budget. It is not unreasonable to have negative dissipation for the stratosphere, as shown before, but the magnitude obtained remains too large at -0.53 erg/cm^2 mb sec.

The increase in the eddy available energy as a whole during the period at almost the sole expense of the zonal available energy, has been noted before. This net 5-day increase is shared by each of our wave partitions except wave number 4. AE(1) sustains the largest increase in time, being also the largest eddy. This increase may be qualitatively inferred from the flow diagram, as it accepts at moderate to high rates energy from the zonal available mode, from the other waves of the available reservoir and from the transfer from the kinetic energy of the wave number 1 flow (noting that this last transfer could in all actuality be less, for reasons given before). AE(1)'s unique loss occurs in the radiatively dissipative effect of the GE(1)-process, which acts at moderate rates and represents the largest loss of available energy when compared to the other equivalent spectral radiative dissipators. The net small increase of AE(2) may be thought of as the result of a near balance between input from both the CA(2) and the CE(2) processes on the one hand, and the output from the LA(2) and the GE(2) mechanisms on the other hand. The increase in AE(3) is again due to a near balance between the small input by the CE(3) transfer which stands large enough to slightly overcompensate the energy drain through the other processes. The counter-gradient transport of heat is noticeable at this scale. AE(4) has been shown to reside in the circuit of an active tropospheric-like energy cycle.

It is the only spectral available energy reservoir which decreases in time, and this net loss is due to the spectral baroclinic CE(4)-process which stands about five times larger (although overrated) than any other process at this scale. This can be verified from Fig. 4.2.38.

Non-linearity of the eddy available waves produces a small increase across the boundaries, while internally wave 2 and 3 feed the rest of the spectrum as the spectral quantity AE(2) loses most and AE(1) gains most. Presumably the remarkable increase of AE(1) during the period is due in no small part to the transfer from the available energy concentrated in the variance of the temperature field at wave number 2 scale.

The stratospheric zonal available energy feeds on the zonal radiative influences to maintain itself, this effect increasing with height within the layer. The mean meridional circulation, indirect in character, transfers a small amount of energy from the zonal kinetic to the zonal available energy reservoir. A large net eddy transfer of heat northward down the zonal temperature gradient contributes to a moderate depletion of the zonal available reservoir during the 5-day period.

Comparisons

The spectral energy flow diagram given in Fig. 4.2.39 has been patterned on one given by Perry (1966) which covers the whole month of January 1963, for quick visual comparisons. Little difference in flow direction can be found in the troposphere. One notes the rather small transfer computed for waves above number 3, possibly due to the rather large smoothing introduced by Perry into his data. Both studies arrive at a more or less normal tropospheric energy flow except for the anomalous KZ $\rightarrow$ KE transfer which is explained differently in each study. The January 1963 anomalous barotropic exchange is due solely to the large transfer of zonal kinetic energy to that of wave number 3 flow, this effect surpassing that of other waves and acting in a normal direction. This report finds that on the contrary KE(3) feeds the zonal flow KZ while the other waves are responsible for the anomalous transfer. It has been shown earlier that this result may be artificial as the volume lateral truncation at 30°N could be responsible for the abnormal transfer. The non-linear wave interaction transfer shows limited similarities, centered mostly on the planetary scale. KE(1), KE(2) interactions with the remaining spectrum are similar in both studies, while the individual waves larger than 2 are found to share energy non-linearly in an opposite fashion to that found in Perry's. This tropospheric non-linear wave interaction distribution has been shown to be closer to the one computed by Murakami (1964).

In the stratosphere, one of the main differences resides in the direction of the CE-term. The present report obtains the case: KE $\longrightarrow$ AE. Both sudden warmings of 1957 and of 1963, studied by Reed et al (1963) and by Perry (1966), respectively, had this process flowing in the reverse direction leading to baroclinic instability. The study of the 1958 sudden warming by Miyakoda (1963) and Murakami (1965) did compute baroclinic transfer in the same direction as in our study. As pointed out by Murakami (1965) since the 1957 warming (and also the 1963 warming) was characterized by amplification and eventual stratospheric breakdown at wave number 2, it is likely that warmings (sudden or not) subjected to the development of an eccentric polar vortex such as in 1958 (and also mid-January 1959) can be caused by different partitioning of the spectral energy interactions. The minor warming of mid-January 1959 has been shown earlier to be accompanied by an increase in the kinetic energy of wave number 1 flow while the other eddies were actually decreasing during the period. The actual stratospheric energy in the wave number 1 flow increased until January 18th while the corresponding kinetic energy in wave 2 flow decreased until this date then levelled off for a while.

The stratospheric non-linear wave interaction process agrees generally with Perry's: the larger scales of motion waves 1 and 2 exchange their energy with the smaller scales. Murakami (1965) computed a similar spectral distribution during January 1958 as his larger waves 1 and 2 did feed the remainder of the spectrum, this being especially significant at the early stage of the warming. Thus it seems that a tendency exists such that the non-linear wave interaction acts in such a way as to relax any large amplitude difference between the waves. Murakami (1965) has also computed the non-linear wave interaction of available energy for the period of December 1957 to February 1958, inclusive. It resulted that before and at the initial stage of the warming, waves 1, 2 and 3 were supplied with available energy from the other waves, while the roles reversed during the final stage of the warming. During the 12-month period from January 1963 to January 1964, Yang (1967a) computed as a predominant lower stratospheric mode, the available energy exchange from the smaller to the larger scales (and the reverse was computed in the troposphere), the exchanges being more vigorous in the winter season. It seems, therefore, that the pre-warming non-linear available wave interaction, i.e., the transfer to the very large scales from the smaller scales, is a characteristic of the winter season and the yearly average. The present report approaches Murakami's final warming stage characteristics in that a net exchange from waves 1, 2 and 3 is increasing the available energy of the waves of smaller scales.

In a further effort to rationalize the processes leading to this minor warming, it is postulated that since the eccentric elongation of the flow observed with the warming is not likely barotropic (since CK < 0), nor baroclinic (CE < 0, or at least very small if positive), it must be forced from the exterior. Actual strong fluxes of geopotential at the planetary scale have been computed and shown capable of perturbing the stratospheric flow significantly. It is then concluded that the pressure interaction due to the baroclinicity of the troposphere is the cause of the perturbed stratospheric flow: this has been termed by Boville (1965, 1966) as the non-linear baroclinic interaction process. Further, the planetary geometry in the troposphere responsible for the pressure interaction may be said to be associated with the blocking circulation observed during the period and ultimately to be caused by the stationary influences of the topographical and diabatic heat sources of the northern hemisphere surface.

4.3 Diagnosis from Spherical Specification

A. The method of spherical harmonics

In order to study the meridional as well as the longitudinal scale effects, the height and temperature fields at the nine levels of data were transformed into a set of spherical harmonic coefficients. The height or temperature fields $F(\theta, \lambda)$ may be represented by the following double summation:

$$F(\theta,\lambda) = \sum_{m=0}^{\infty} \sum_{n=m}^{\infty} \left[A_n^m \cos m\lambda + B_n^m \sin m\lambda\right] P_n^m \tag{4.3.1}$$

where A_n^m and B_n^m are the real Fourier coefficients for the longitudinal wave number m (also called rank); n is called the degree of the harmonic, which, when associated with the rank m, i.e., "n-m", is similar to a wave number in the meridional extent ("n-m" is equal to the number of nodes found between the two poles); θ is the co-latitude, λ represents the longitude and P_n^m is the normalized associated Legendre function:

$$P_n^m = \frac{1}{2^n n!}\left[\left(\frac{2n+1}{2}\right)\frac{(n-m)!}{(n+m)!}\right]^{\frac{1}{2}} (1-\mu^2)^{\frac{m}{2}} \frac{d^{n+m}}{d\mu^{n+m}}(\mu^2-1)^n \tag{4.3.2}$$

where

$$\mu = \cos\theta$$

The missing data from 30°N to the equator were added artificially by using computed mean monthly zonal height and temperatures for January. The Fourier coefficients were obtained by extrapolating linearly to zero the 30°N coefficients. Similarly, those at 85°N have been set to be half those at 80°N, while the 85°N mean zonal value was interpolated from the 80°N and the north pole values. The odd "n-m" values were used, so that only the northern hemisphere Fourier coefficients were required, as they implied those over the southern hemisphere by the anti-symmetry rule. This is mathematically necessary but physically without consequence, as advanced by Deland (1965a) and demonstrated by Merilees (1966). The latter investigator had the use of global data and computed co-efficients based either on the global description or the hemisphere (north or south) coupled with the anti-symmetric rule. The amplitude and phase components associated with the global data showed little (if any) coherence in time, but the amplitude and phase components associated with either hemisphere (north or south) data were very coherent as each hemisphere showed quite different behaviour. This effect was shown indirectly in the results using the global description.

The Fourier latitudinal set (A_{θ} (m), B_{θ} (m)) and the spherical harmonic set (A_n^m, B_n^m) are related through the orthogonality in degree between the Legendre functions. The formal relations between the two sets follow:

$$A_m^m = \int_0^{\pi} A_{\theta}(m)\; P_m^m \sin\theta \, d\theta$$
$$B_m^m = \int_0^{\pi} B_{\theta}(m)\; P_m^m \cos\theta \, d\theta \qquad (4.3.3)$$

while the amplitude of the harmonics becomes:

$$Z_m^m = \left({A_m^m}^2 + {B_m^m}^2 \right)^{1/2} \qquad (4.3.4)$$

Nineteen sets of (A_θ (m), B_θ (m)) are available to compute the integral (4.3.3).

B. Vertical structure

The vertical structure for the longitudinal wave 1 to 3 has been analysed for various meridional degrees, more specifically for "m - n" equal to 1, 3 and 5. The 5-day mean phases and amplitudes (hereby defined as stationary) of the height spherical harmonics Z_n^m were computed for the following (m, n) sets: (1, 2), (1, 4), (1, 6), (2, 3), (2, 5), (2, 7), (3, 4), (3, 6) and (3, 8). The results are plotted on Fig. 4.3.1. The Z_n^1 and Z_n^2 height amplitudes are about 5 times the Z_n^3 amplitudes. Z_n^1 and Z_n^2 show a westward tilt with height indicating northward heat transport and associated upward flux of geopotential as indicated in the previous section. Of the three Z_n^1's, Z_2^1 shows the largest westward tilt with height in the stratosphere; Z_4^1 presents the largest stratospheric amplitudes while Z_2^1 dominates in the troposphere. Z_6^1 may be characterized as having the least of all. The general location of the wave number 1 ridge would be about 90°W at 300 mb and tilting to about 170°W at 10 mb. The dominance of Z_4^1 over Z_2^1 in the stratosphere, and the reverse in the troposphere explains the more northern location of the stratospheric high pressure area at wave number 1 when compared with the tropospheric high (wave 1) location.

The longitudinal wave number 2 harmonics have similar characteristics to wave 1, but have somewhat lesser magnitudes. Z_3^2 and Z_5^2 show significant westward tilt with height, but Z_3^2 leads in this field. Their magnitudes are about equal in both stratosphere and troposphere. The magnitudes of Z_7^2 are significant at and above 100 mb only. This harmonic has a negligible tilt with height above 100 mb. Here again, upward flux of geopotential may be inferred from the two harmonics Z_3^2 and Z_5^2, so that the large flux measured at longitudinal wave number 2 is mainly explained by the two largest meridional wave numbers.

The Z_n^3 harmonics present quite different characteristics. One striking feature is the general eastward stratospheric tilt found in all three harmonics: Z_4^3, Z_6^3 and Z_8^3. Note the change in scale in Fig. 4.3.1 for m = 3. Except for Z_4^3 which is plagued with erratic and insignificantly small tropospheric amplitudes, both Z_6^3 and Z_8^3 show near neutral tilt below the tropopause. The eastward tilt with height in the stratosphere at longitudinal wave number 3 fits the earlier results of downward geopotential flux and counter-gradient eddy heat transport at this wave number. This phenomenon seems to be shared by all three Z_n^3 harmonics except maybe for Z_4^3 in the 25-10 mb layer. An item of significance is the decrease in the amplitudes of Z_6^3 and Z_8^3 above 300 mb, although Z_6^3 recuperates at and above 50 mb. This is related to the low kinetic energy of the flow associated with those harmonics. This will be shown later.

C. The kinetic energy spectral distribution for the lowest harmonics

Merilees (1966) has expanded the mean horizontal kinetic energy $\overline{E}^{\theta,\lambda}$ for harmonic of degree n:

$$\overline{E}^{\theta,\lambda} = \frac{1}{8}\left(\frac{g}{2\Omega a}\right)^2 \sum_{n=1}^{\infty} \sum_{m=0}^{\infty} n(n+1)\left(\psi_n^m\right)^2 (1+\delta_0^m) \tag{4.3.5}$$

where ψ_n^m is the amplitude of the stream function associated with the (m, n)-pair, $\delta_0^m = 1$ if m = 0, and $\delta_0^m = 0$ otherwise. Ω is the rate of rotation of the earth and "a", its radius. Not having computed the stream function harmonic amplitudes, we define a pseudo-mean kinetic energy indicator $\widetilde{KE}_n^m$:

$$\widetilde{KE}_n^m = n(n+1)\ (Z_n^m)^2 \tag{4.3.6}$$

Before going into kinetic energy computations, it may be convenient to assess the error involved in the data and its implication for the results. The instrumental errors accepted in the height data were listed earlier in Chapter 2, Table 2.1.2. The calculation of the effects of these errors on the spherical harmonic coefficients will follow.

Let Δ_n^m and $\mathcal{E}_n^m$ stand for the errors in the pseudo-kinetic energy $\widetilde{KE}_n^m$ and the height component Z_n^m, respectively. From Eqn. (4.3.6), it follows that:

$$\widetilde{KE}_n^m + \Delta_n^m = n(n+1)\left(Z_n^m + \mathcal{E}_n^m\right)^2$$

and after simplification:

$$\Delta_n^m \cong 2n(n+1)\, Z_n^m\, \mathcal{E}_n^m$$

The relative error becomes then:

$$\frac{\Delta_n^m}{\widetilde{KE}_n^m} \cong 2\,\frac{\mathcal{E}_n^m}{Z_n^m} \qquad (4.3.7)$$

Hence, grossly, the relative error in the pseudo-kinetic energy is twice the corresponding error in the spectral height field.

The next problem is to assume or infer some distribution of the error field in the spectral height components. In order to assess the portion of the spectral components due to instrument (or other) errors, some of Merilees (1966) results are used. He transposed into the spherical harmonic domain a result that Godson (1959) has shown to be valid in the Fourier analysis of data, namely that the variance may be equally distributed into all independent wave components, after it has been divided by the number of degrees of freedom in the system. As far as the variance is concerned, it may be produced by 17 waves (from 36 longitudes), at each of 11 latitudes used for the field specification. Adding to this 18 independent means of each latitude, there result 17 x 11 + 18 = 205 degrees of freedom. The standard error of each Z_n^m component may be given by the relationship:

$$\varepsilon_m^m = \frac{\text{standard error of instrument}}{(205)^{1/2}} \tag{4.3.8}$$

Table 4. 3. 1 gives the accepted standard error of the height field with the associated ε_n^m as a function of pressure.

Table 4. 3. 1 Accepted radiosonde errors in the height with the corresponding standard errors in the spherical harmonic components.

Unit: meter

Level (mb)	500	300	100	25	10
Instrument error	± 15	± 35	± 38	± 91	± 150
S.H. component error ε_n^m	± 1.09	± 2.43	± 2.64	± 6.3	± 11

It is of interest to find the range of the relative errors of the height components at stratospheric levels, using the mean 5-day data. This is shown in Table 4. 3. 2.

Table 4. 3. 2 Five-day average relative error (%) in the stratospheric spherical harmonic component Z_n^m

Z_n^m / Level(mb)	Z_2^1	Z_4^1	Z_6^1	Z_3^2	Z_5^2	Z_7^2	Z_4^3	Z_6^3	Z_8^3
100	1.9	2.9	5.9	2.1	2.3	8.8	9.1	4.4	6.0
25	2.5	2.3	4.2	3.3	3.1	7.0	12	17	24
10	3.3	2.7	4.8	3.3	3.9	9.2	14	18	37

It is then inferred that components associated with zonal wave numbers larger than 3 would have a rather large portion of their amplitudes within the error domain. This is more so for the pseudo-kinetic energy since its relative error is twice that of the height components. Further, for this last parameter, the results for degree 3 and rank 8 or above may be mostly included in the error spectrum.

Time-vertical cross-sections of KE(m) and $\widetilde{KE}_n^m$ are given in Figs. 4.3.2 to 4.3.4 for m = 1 to 3, respectively.

The spectral partition at longitudinal wave number 1 will be tackled first. The daily variation and vertical coherence of KE(1) are shown to be closely related to those of $\widetilde{KE}_6^1$ and $\widetilde{KE}_4^1$ in the stratosphere. Because the kinetic energy is proportioned to the product "n(n+1)", the relative magnitudes of the kinetic energy component are not the same as the height amplitudes Z_n^m. The magnitudes of the $\widetilde{KE}_n^1$ decrease in the following order: $\widetilde{KE}_4^1$, $\widetilde{KE}_6^1$ and $\widetilde{KE}_2^1$ in the stratosphere, and $\widetilde{KE}_6^1$, $\widetilde{KE}_4^1$ and $\widetilde{KE}_2^1$ in the troposphere, notwithstanding the amplification of the error portion by the n(n+1)-factor.

The relative distribution of the components and of total kinetic energy of wave 2 are illustrated in Fig. 4.3.3. We find the following relationships upon inspection of the graphs. KE(2) is most appropriately related to $\widetilde{KE}_3^2$ and $\widetilde{KE}_7^2$ in the stratosphere, while $\widetilde{KE}_5^2$ explains it better in the troposphere. $\widetilde{KE}_3^2$ is slightly larger than $\widetilde{KE}_7^2$ in the stratosphere, while $\widetilde{KE}_5^2$ is at least twice as large as any of the two other spectral energies in the troposphere.

Fig. 4.3.4 reveals that changes in $\widetilde{KE}_6^3$ and $\widetilde{KE}_8^3$ closely approximate the changes in KE(3). $\widetilde{KE}_4^3$ seems to be divorced from KE(3) except possibly at 25 and 10 mb near the end of the 5-day period. In the stratosphere, the spectral kinetic energy dominance follows in the given order: $\widetilde{KE}_6^3$, $\widetilde{KE}_8^3$ and $\widetilde{KE}_4^3$, while in the troposphere the order changes to : $\widetilde{KE}_8^3$, $\widetilde{KE}_6^3$ and $\widetilde{KE}_4^3$, notwithstanding the n(n+1) error amplification factor.

D. Transient waves in the atmosphere

Following a method of analysis introduced by Deland (1964), the planetary scale spherical harmonics of January 12 to 16, 1959, have been separated into a stationary (5-day mean amplitude and phase) and a transient wave (the deviation of the daily from the 5-day mean vector). Although the mean was computed from only 5 days of data, it may be used to approximate the "forced" mode of Bradley

(1967) while the time deviation should approach his "free" mode.

It was found rather quickly that our 5-day averaging period was not to be recommended for most waves in the planetary scale. Bradley (1967) did verify from tropospheric data that an averaging time of 5.5 days was satisfactory for zonal wave numbers 3 and larger, while 10.5 days proved necessary for zonal wave numbers 0, 1 and 2 because of their longer period of rotation.

Boville (1966) has computed the transient waves of January 1959 at 500, 100 and 25 mb, taking the whole month as averaging period. He found that the largest component, Z_2^1, showed excellent vertical coherence, as the transient waves were closely correlated in their rotation at the three levels of analysis. Boville (1966) also analysed the behaviour of Z_5^2 and Z_6^3 yielding vertical coherence similar to that of Z_2^1, but their horizontal motions, contrary to Z_2^1 (which was retrogressive or moving westward) were progressive. Deland (1967, b) also reported good vertical phase coherence between travelling planetary-scale waves in both troposphere and stratosphere. The behaviours of the harmonics Z_2^1, Z_5^2 and Z_6^3 are reproduced from Boville (1966) in Figs. 4.3.5, 4.3.6 and 4.3.7, respectively. The phase-amplitude relationship of the three above mentioned harmonics, but computed from our data, are depicted in the harmonic dials of Fig. 4.3.8, 4.3.9 and 4.3.10, respectively. They are associated with the 500, 100 and 25 mb levels. The progressive phase motion of Z_2^1 at 25 and 100 mb seems at first sight to contradict the results of Boville (1966). Similarly, at the same levels, during the first half of the period, Z_5^2 moves retrogressively, also contradicting Boville. This anomaly may be traced back to the time span over which the 5-day mean is applied. With reference to daily computations during January 1959 by Boville (unpublished), it is found that the actual stationary waves were in the process of reforming and/or moving to a new location, so that the actual concept of a stationary wave proved to be meaningless when applied to the wrong time scale. Z_6^3 is shown to be progressive (Fig. 4.3.10) as in Boville (1966). It possesses good vertical coherence between the three levels. Of interest, the eastward tilt with height of the Z_6^3 harmonic between 25 and 100 mb on the 15th and 16th coincides with the downward flux of geopotential and associated southward eddy heat transport noted earlier for longitudinal wave number 3.

Some of the results cited above may be discussed in the light of the recent finding of Bradley (1967). Using the diagnostic method of characteristic patterns (set of three orthogonal modes: zonal, meridional and vertical), he succeeded in isolating significant tropospheric modes from the data. Amongst some of his findings, a few are reproduced here. They may have some direct or indirect bearing on our results.

1) "Vertical mode 2 (associated with the atmospheric divergence) of any zonal wave number moves predominantly <u>eastward</u> unless a time filter is applied".

2) "Vertical modes 1 and 3 of zonal wave number (m) 1 through 5 moves predominantly <u>westward</u> with much vacillation unless a time filter is applied".

3) "The 5.5-day mean of the waves shows no mean significantly different from the zero relative to the earth".

4) "The deviation from the 5.5-day mean has characteristics that all vertical modes of zonal wave numbers greater than 3 move <u>east</u>. For zonal wave number 1, 2 and 3, vertical modes 1 and 3 move <u>west</u> with much vacillation, and vertical mode 2 moves <u>east</u> with much vacillation".

5) "Vertical modes 1 and 3 have phase speeds close to non-divergent Rossby-Haurwitz values assuming a meridional wave number (n-m) of 2, 3 or 4, which is an approximation to the dominant meridional mode".

6) "The divergent modes (vertical mode 2) have zonal speeds absolutely smaller than the relevant Rossby-Haurwitz values, and independent of meridional wave number".

7) "The vertical mean wave has the same characteristic as

vertical modes 1 and 3, but the meridional wave numbers are less closely coupled".

8) "The zonal phase velocities of the total transient, 5.5-day average, and fast moving modes are all independent of the amplitudes of the corresponding waves . . .".

The periods of the surface harmonics have been approximated, when possible, by measuring their partial rotation during the 5-day span. The harmonics of zonal wave numbers 1 through 3 and meridional wave number 1 exhibited periods of 6 to 7 days, while waves with higher meridional wave number (3 and 5) had rotations taking 7 to 11 days, the longer periods being somewhat associated with lower zonal wave number m at higher levels. Item (4) is especially significant here. Since the mean time average in the above case is fairly close to ours (5.5-days versus 5-days), the implications of this item may be compared with our results. The atmosphere as a whole, during our period, is highly baroclinic (recalling that the geopotential flux transport is a baroclinic process at its source). It has been shown that the baroclinic process is closely related to cross-isobaric flow on a constant height surface or cross-contour flow on a constant pressure surface, a phenomenon often associated with the atmospheric divergence index. Thus, due to this atmospheric baroclinic-divergence relationship, the vertical mode 2 would amplify and tend to decrease the mean atmospheric westward motion of the planetary waves, although following items (5) and (7), it would still be westward moving in the troposphere.

Deland (1967, a) has indicated a corrective change to the theoretical wave speed resulting from the Rossby-Haurwitz non-divergent barotropic model. He computed a so-called divergence coefficient χ, which when multiplied by the local rate of geopotential height change in the vorticity equation, approximates the effect of divergence at the level of interest. The coefficient has been given as:

$$\chi = m(m+1)\left(\omega_{R\text{-}H} - \omega_{OBS}\right)\omega_{OBS} \tag{4.3.9}$$

where $\omega_{R\text{-}H}$ and ω_{OBS} are the Rossby-Haurwitz and observed phase speeds, respectively, of degree "n", interpreted in the units of angular velocity. The inclusion of the divergence coefficients reduces the wave speeds from those given by the Rossby-Haurwitz model. Eqn. 4.3.9 admits only ω's of the same sign. Thus any sign difference in the ω's may be explained by the remainder process of the spectral vorticity equation: i.e., the non-linear wave interactions, but this becomes a study of its own.

In order to test items (2), (4) and (7), at least in the troposphere, Table 4.3.3 has been constructed to indicate this particular observed horizontal motion of the various planetary scale harmonic vectors.

Table 4.3.3 Horizontal motion of the transient spherical harmonics at various levels during the period of January 12 to 16, 1959. Legend: P: progressive, R: retrogressive, V: variable, R→P or P→R: when the direction of motion changes significantly during the period, X: unknown, due to relocation of stationary component.

m	1			2			3		
n-m / Level (mb)	1	3	5	1	3	5	1	3	5
10	X	R	V	R	V	R→P	R	P	P
25	X	X	X	R	R→P	R→P	R	P	P
50	X	X	X	V	P	V	P	P	P
100	X	X	X	V	P	P	V	V	P
200	P	V	V	R	P	P	R	V	P
300	R	V	V	R	P	V	R	V	P
500	R	R	V	V	V	V	R	V	P
700	R	P	R	P	P	V	R	V	P
850	R	P	V	V	P	V	R	V	P

General retrogressive motion is shown to exist at the largest scales, notwithstanding the stratospheric Z_n^1 whose rotations are uncertain due to the 5-day computation, but they were shown to be retrogressive in Boville (1966). Z_n^2 is retrogressive at the lowest degree (n-m-1) but tends to become progressive as the meridional scale decreases. It must be noted that Z_5^2 remains progressive for most of the month as shown by Boville (1966).

The Z_n^3 harmonics change from retrogressive (Z_4^3) to progressive (Z_6^3, Z_8^3) as the meridional scale decreases also.

Item (8) has been verified by plotting amplitudes against phase speed of the various harmonics (not shown here) yielding no significant correlations.

The variation of the total (transient + mean mode) kinetic energy density analogue $(Z_2^1)^2$ in time and altitude has been investigated on Fig. 4.3.11.

It may be worth noting that except on the 12th, the atmospheric energy densities have comparable magnitudes in the vertical. Also the large decrease in density near 300 mb from the 12th to the 13th, and the 14th to the 15th are in large part due to non-linear wave interaction, as revealed by some of our computations (not given here) for the 300 mb level.

E. Summary of the spherical harmonics study

The essentials of this section will be summarized next.

a) The 5-day mean spherical harmonic height coefficients of longitudinal wave number 1 and 2 are about five times larger than those of wave 3 when compared to those of same latitudinal wave number.

b) In association with the minor stratospheric warming occurring during the period, longitudinal wave number 1 predominates in the height field. The meridional profile shows latitudinal wave number (n-m) 3 to dominate in the stratosphere while the amplitude of the latitudinal wave number 1 leads in the troposphere, or synoptically, this implies that the stratospheric high pressure centre of the middle latitudes (and in the Pacific) is shifted further north (and also further west) than the corresponding entity in the troposphere. Longitudinal wave number 2 has slightly smaller magnitudes than wave 1, with meridional wave numbers 1 and 3 sharing in about equal parts the geopotential field description. The components of zonal wave 3 have very different characteristics from the above mentioned zonal spectra. Zonal waves 1 and 2 show significant westward tilt with height, while zonal wave 3 exhibits occasional eastward tilts corroborating the finding of downward progression of geopotential flux for this mode. Significant decreases in amplitude were found above the tropopause associated with meridional waves 3 and 5 of zonal wave 3.

From a chosen set of longitudinal wave numbers portraying the planetary waves, the following tentative relationships were found to hold in the mean:

c) For any given atmospheric zonal wave number m, the largest latitudinal scales (n-m = 1) were shown to contribute <u>least</u> to the eddy kinetic energy, excepting perhaps the eddy kinetic energy at m = 2, where $\widetilde{KE}_3^2$ is second in magnitude.

d) At any given zonal wave number m, the <u>largest</u> contribution comes from the middle meridional scale (n-m = 3) in the <u>stratosphere</u>, while the <u>smallest</u> meridional scale (n-m = 5) prevailed in the <u>troposphere</u> (excepting possibly the case for m = 2 where a complete reversal occurs: i. e., $\widetilde{KE}_5^2$ is the largest and $\widetilde{KE}_7^2$ the least).

The characteristics of the "free" waves may be summarized now.

e) The largest scales were found to retrogress in agreement with theory, with a tendency for zonal wave numbers 2 and 3 to have their shorter meridional scales to be progressive.

f) Irrespective of their longitudinal scales (m), the transient modes associated with meridional wave number (n-m) 1 have been tentatively associated with a period of 6 to 7 days, while the shorter latitudinal scales exhibit 7 to 11 day periods, the latter periods being better correlated with the lowest longitudinal wave numbers at higher levels.

g) No significant correlation could be found between the various harmonic amplitudes and their phase speeds.

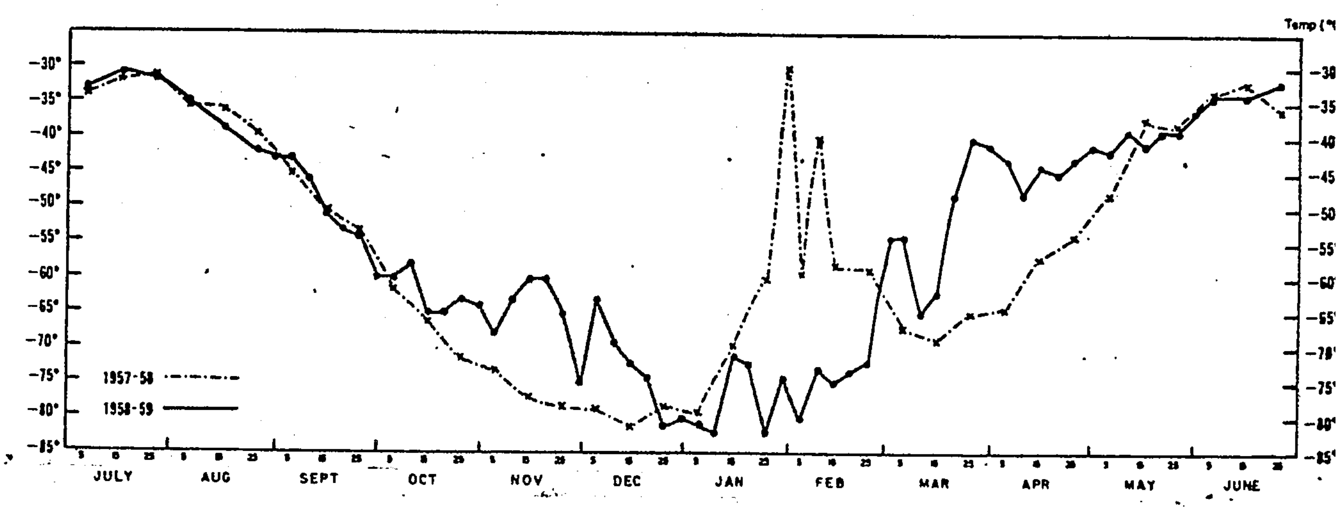

FIG. 4. 2. 1. Comparison of 10-mb. North Pole temperatures during 1957-58 to those extrapolated from charts analysed for 1958-59. (After Finger, Mason and Corzine, 1963)

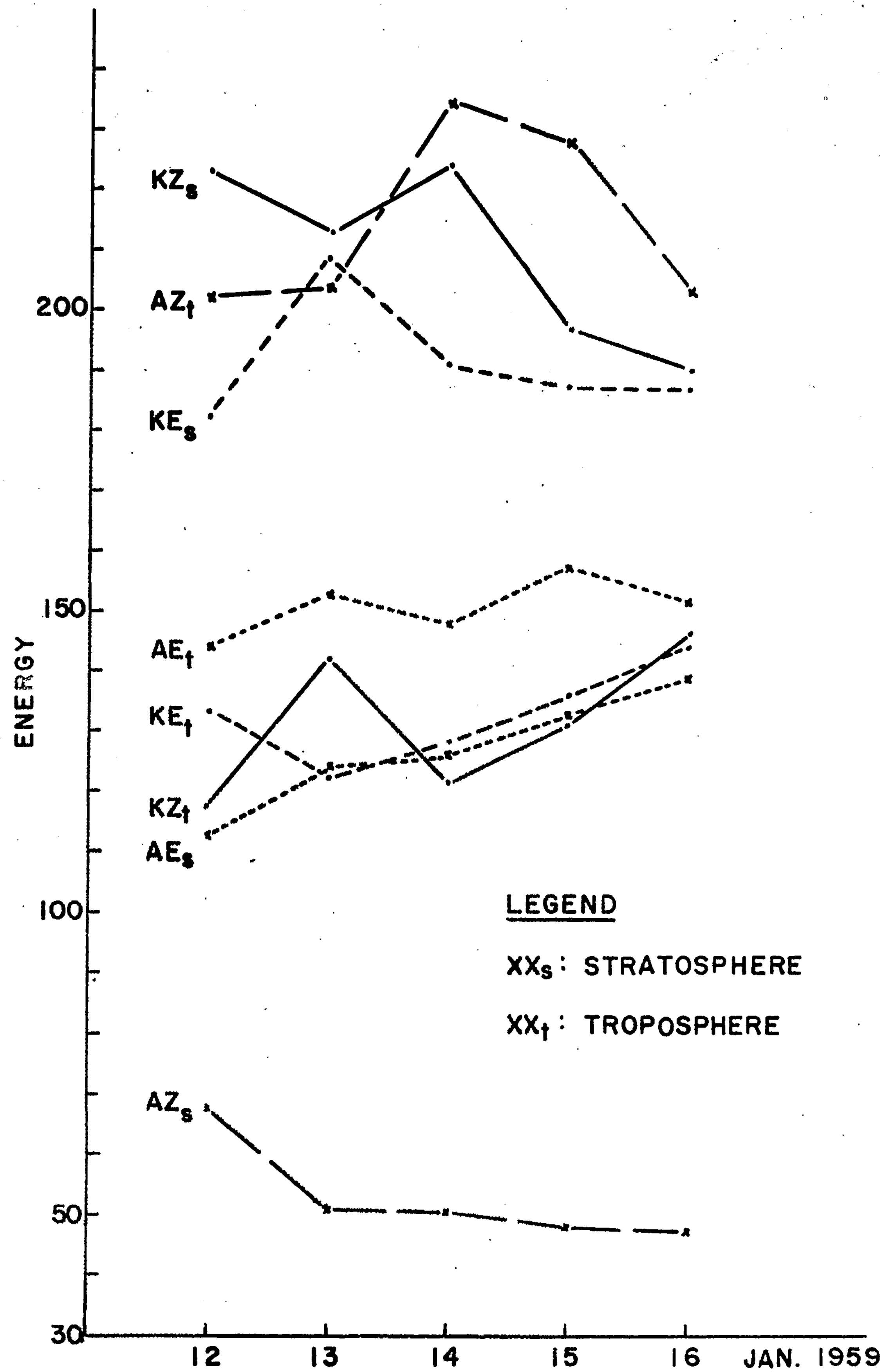

FIG. 4.2.2. Time variations of the various stratospheric and tropospheric energy modes for January 12 to 16, 1959. UNITS: 10^4 ergs/cm^2 mb.

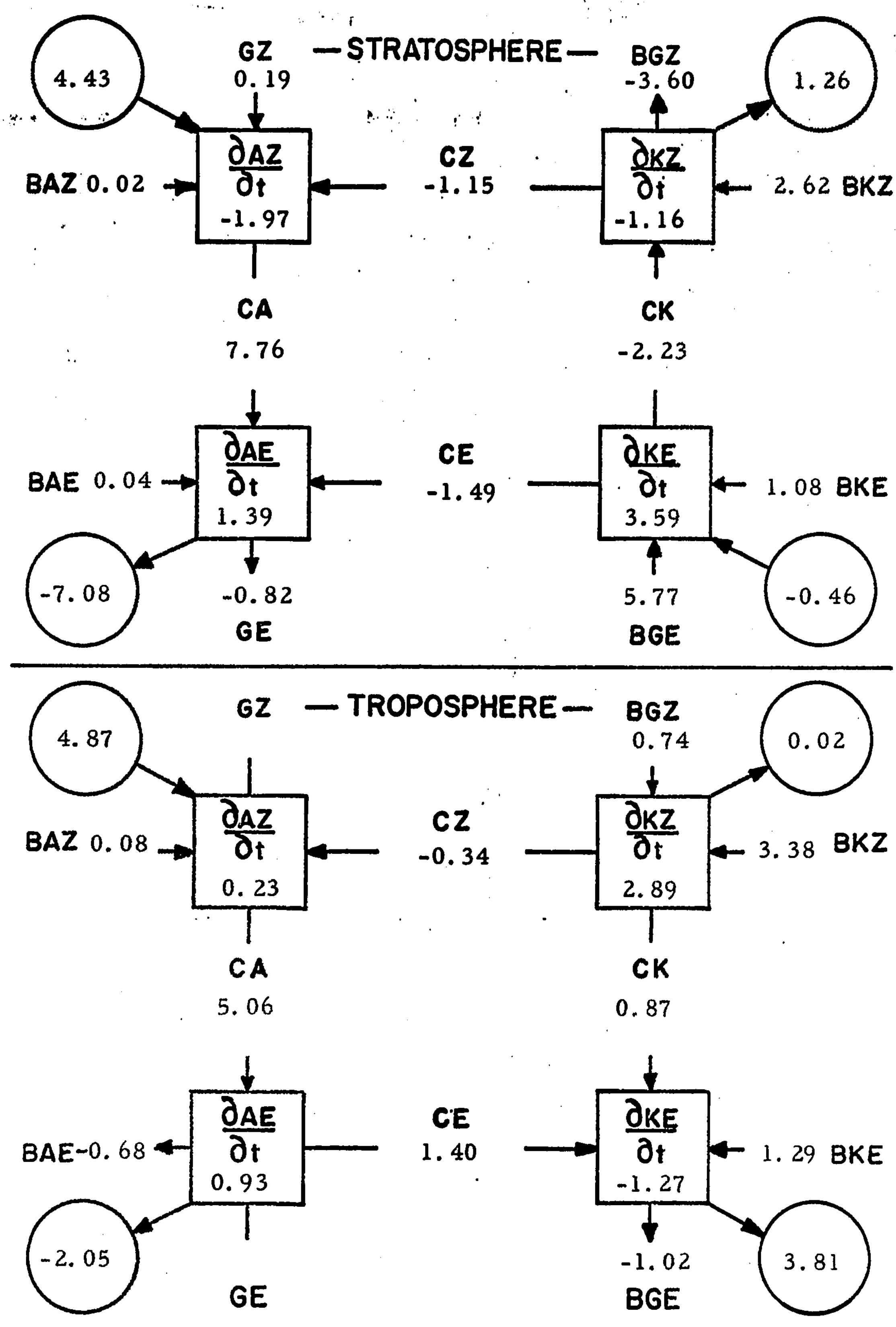

Fig. 4.2.3. Energy flow diagram for January 12, 1959
Units: Ergs/cm^2 mb sec.

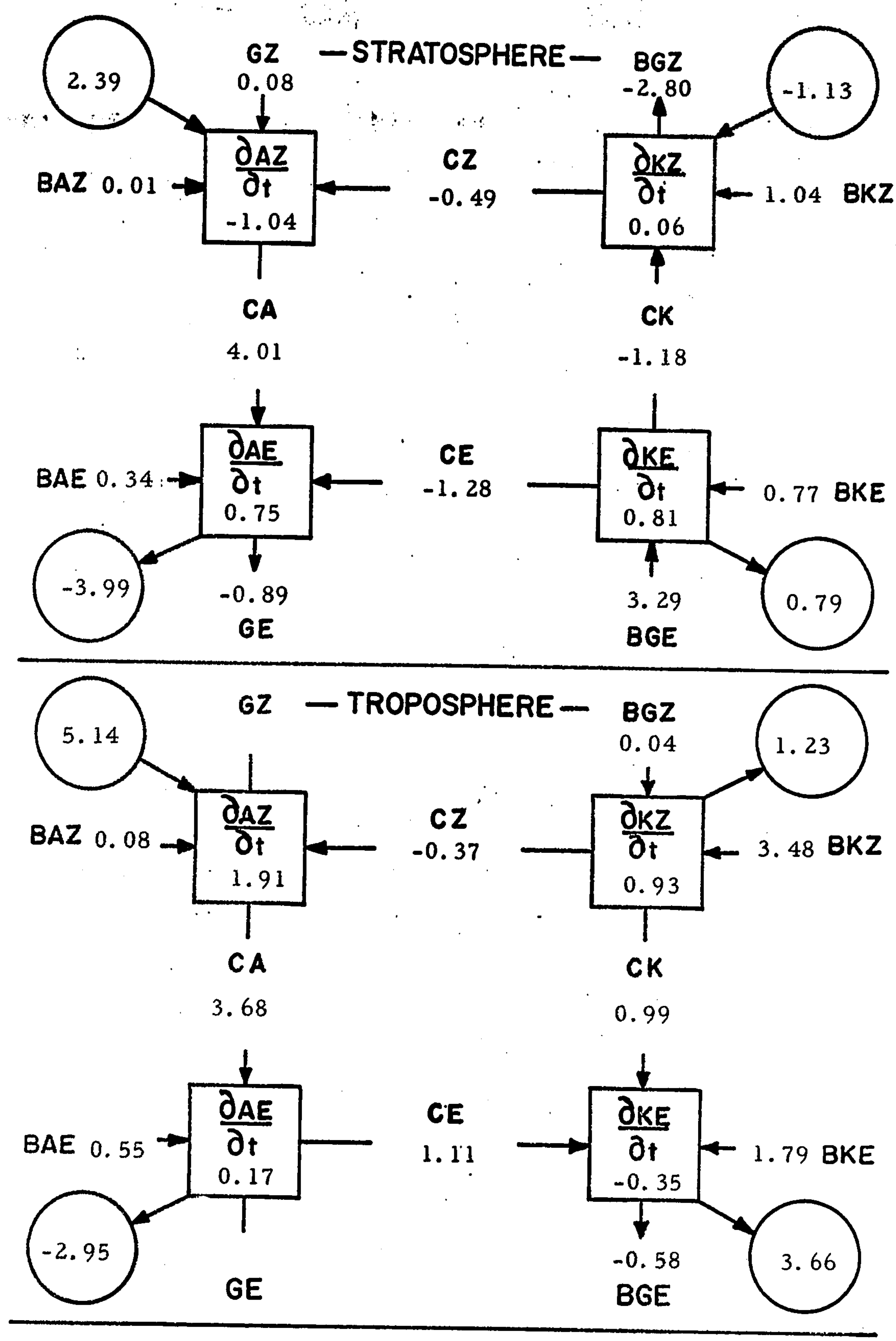

Fig. 4.2.4. Energy flow diagram for January 13, 1959
Units: Ergs/cm^2 mb sec

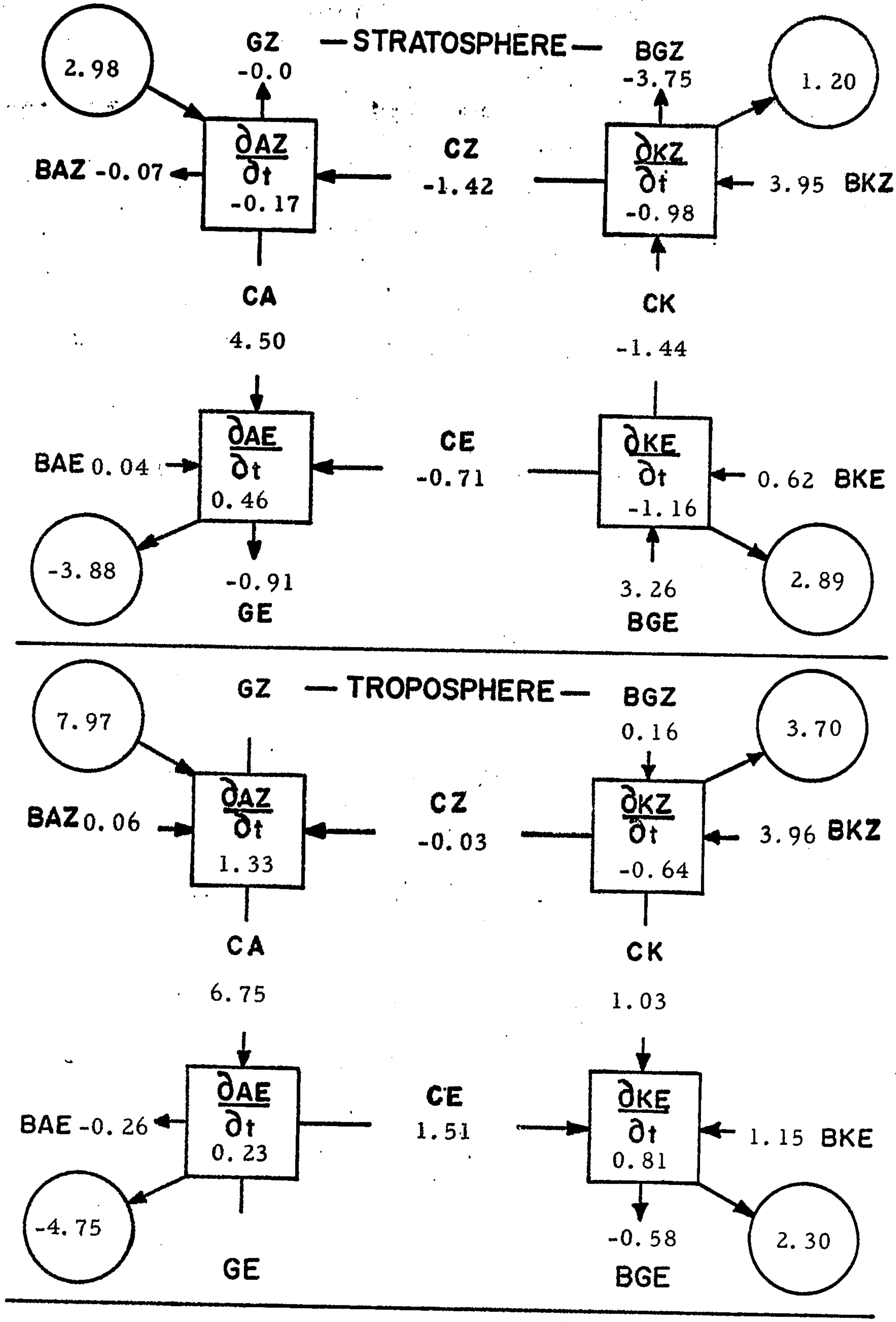

Fig. 4.2.5. Energy flow diagram for January 14, 1959.
Units: Ergs/cm^2 mb sec

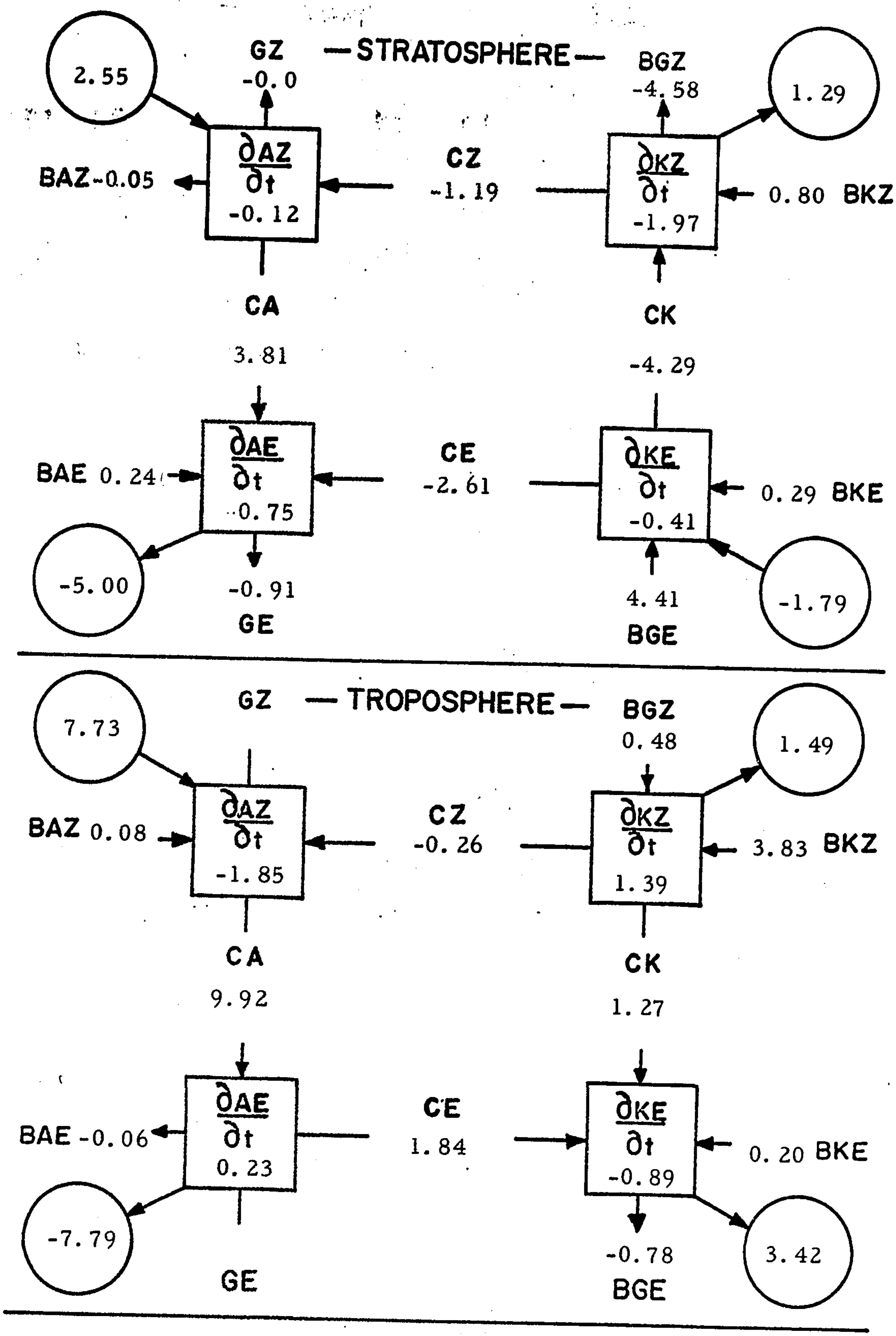

Fig. 4.2.6. Energy flow diagram for January 15, 1959

Units: Ergs/cm^2 mb sec

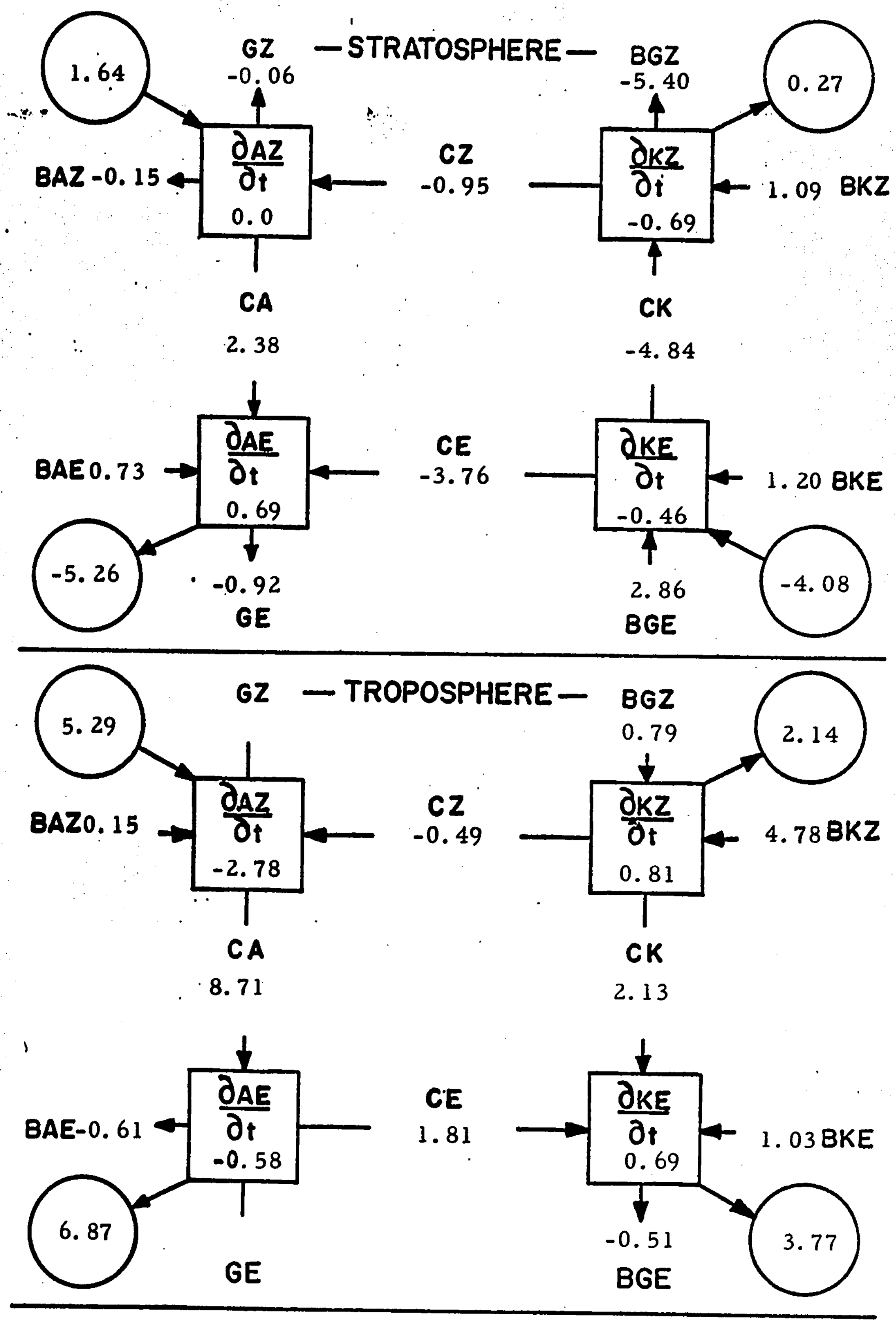

Fig. 4.2.7. Energy flow for January 16, 1959
Units: Ergs/cm^2 mb sec

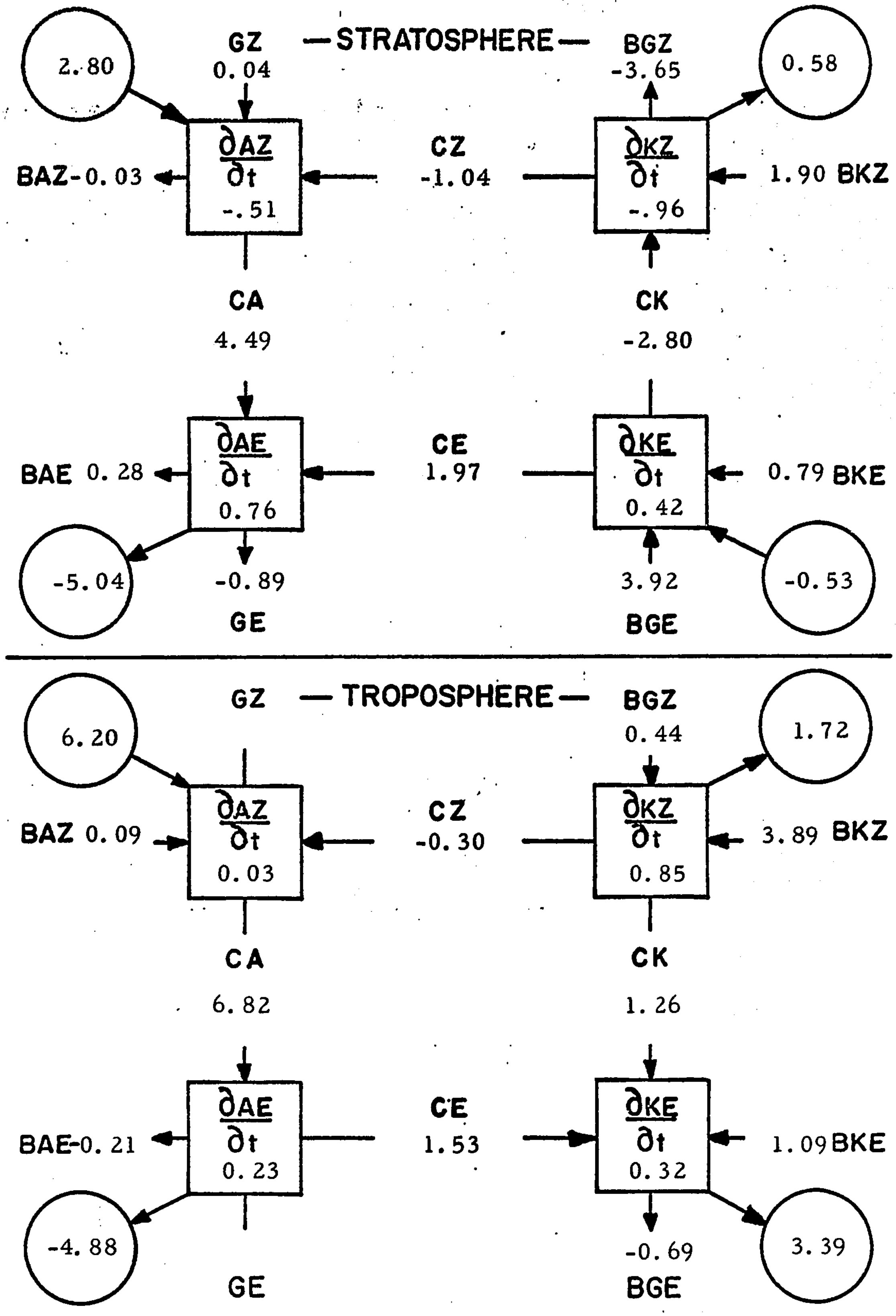

Fig. 4.2.8. 5-day mean energy flow diagram for the period January 12-16, 1959.

Units: Ergs/cm^2 mb sec.

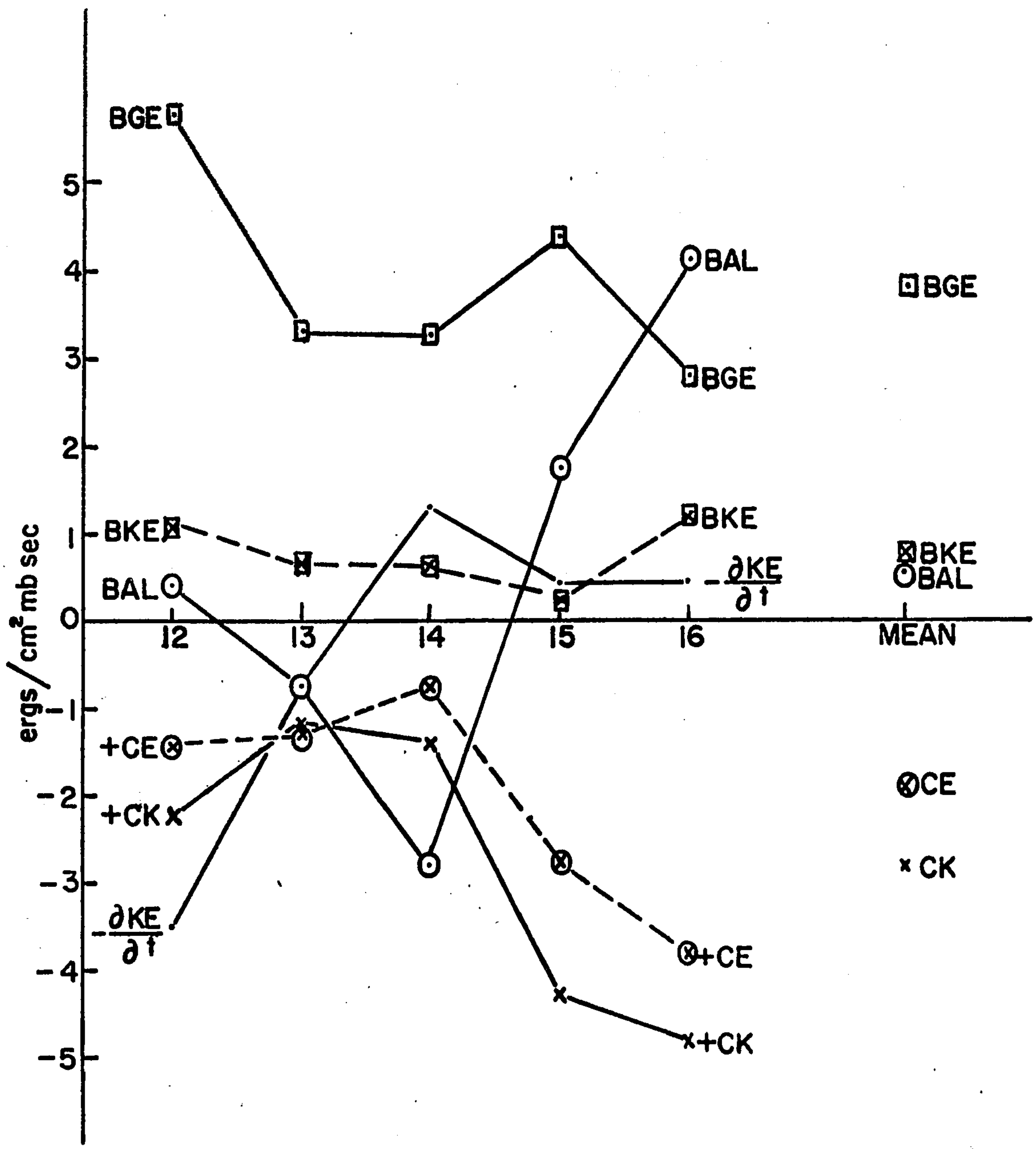

FIG. 4.2.9. Eddy kinetic budget for January 12-16, 1959 in the stratosphere.

Units: ergs/cm^2 mb sec

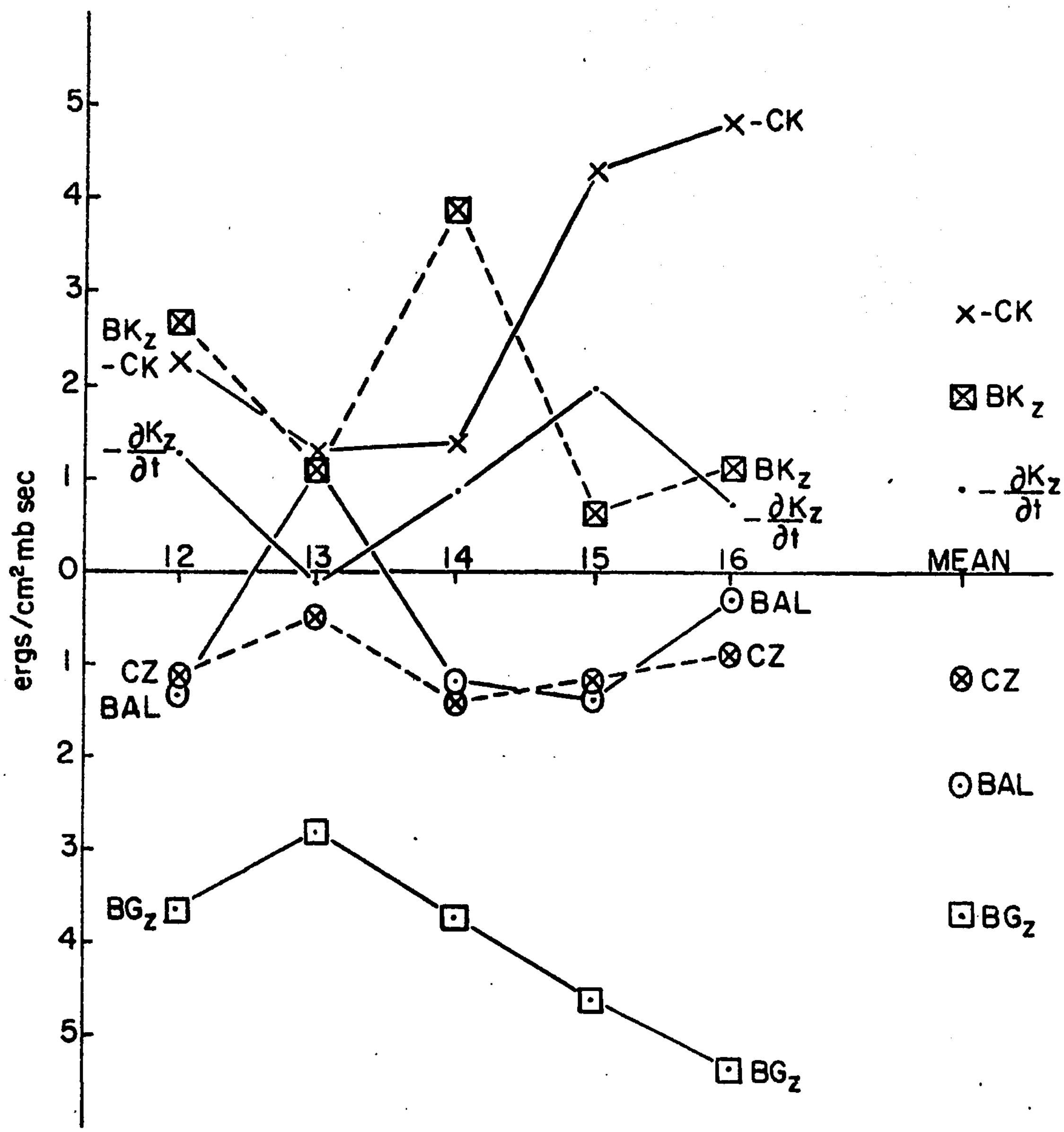

Fig. 4.2.10. Zonal kinetic energy budget (KZ) in the stratosphere for January 12 to 16, 1959. Units: Ergs/cm^2 mb sec.

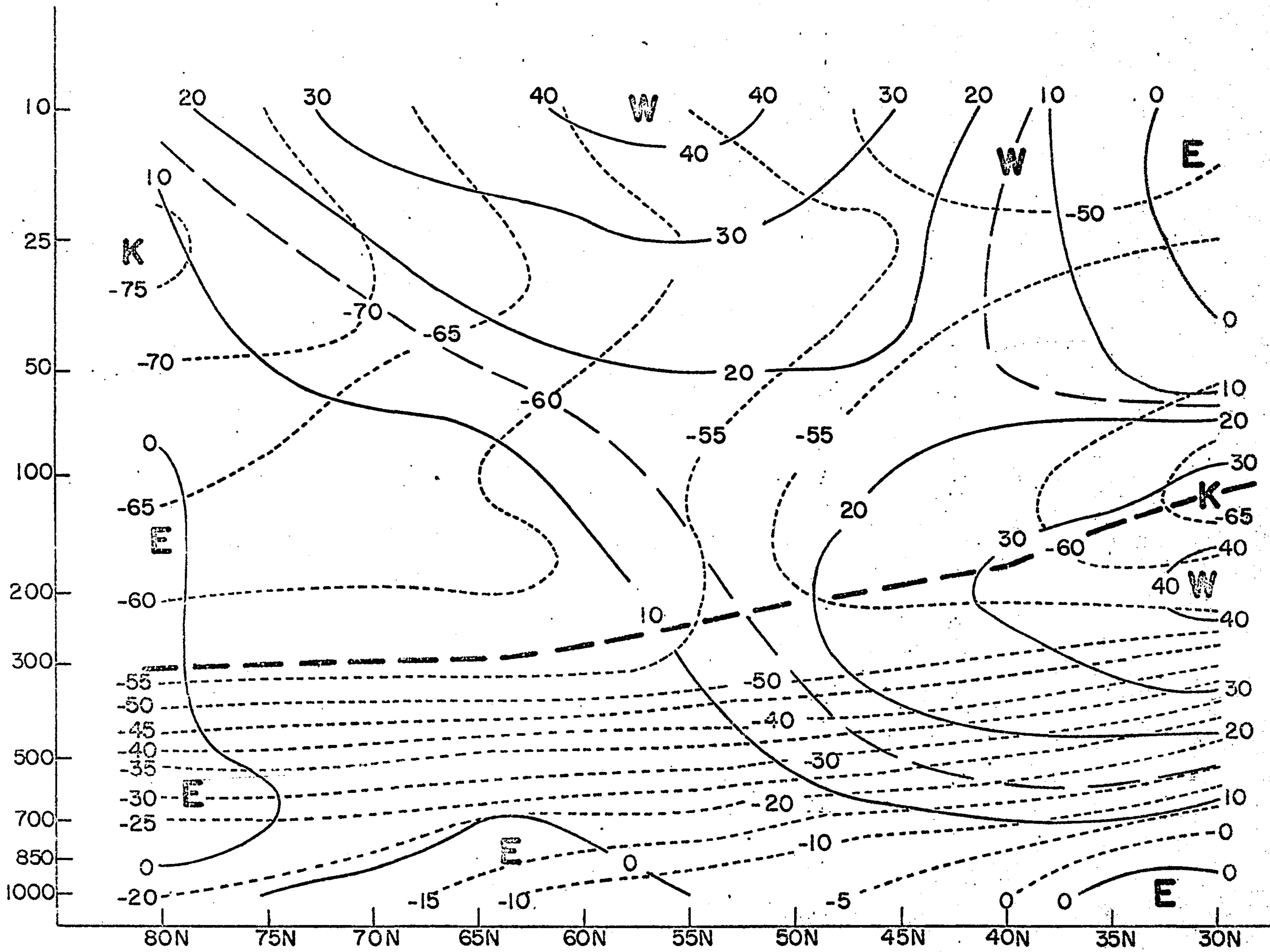

FIG. 4.2.11. MEAN ZONAL WINDS AND MEAN ZONAL TEMPERATURES ON JANUARY 12, 1959.

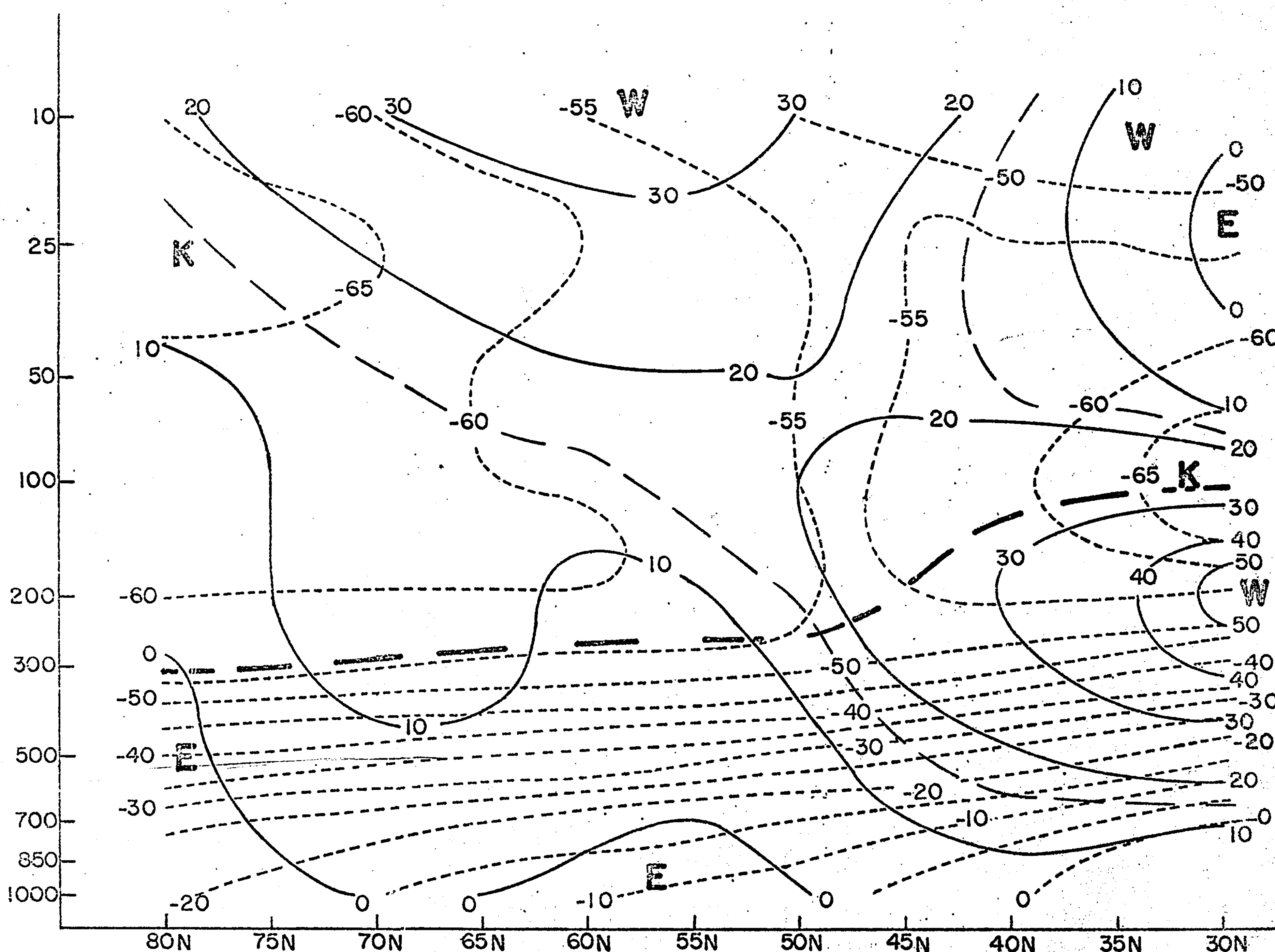

FIG. 4.2.12. MEAN ZONAL WINDS AND MEAN ZONAL TEMPERATURES ON JANUARY 16, 1959.

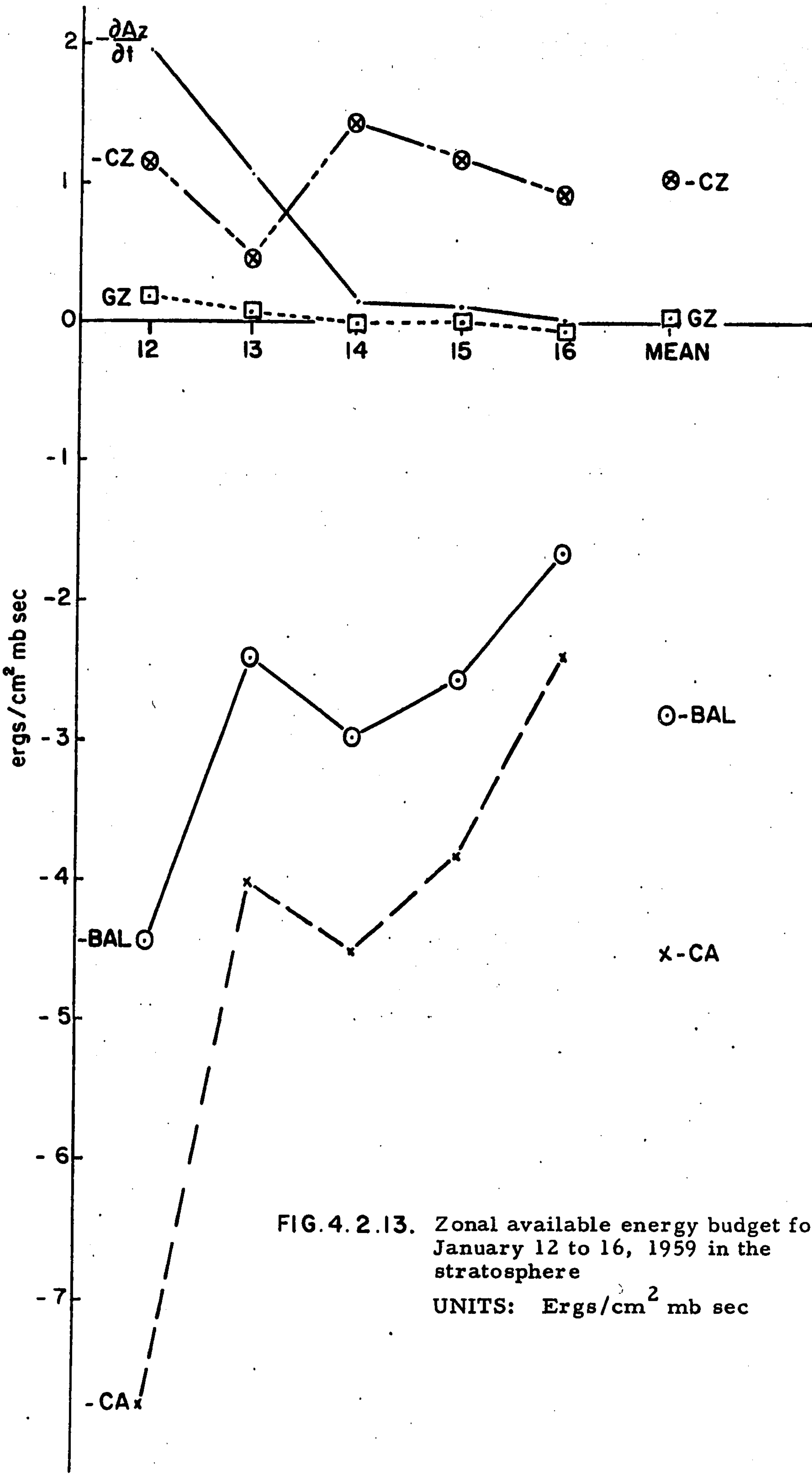

FIG. 4.2.13. Zonal available energy budget for January 12 to 16, 1959 in the stratosphere

UNITS: Ergs/cm^2 mb sec

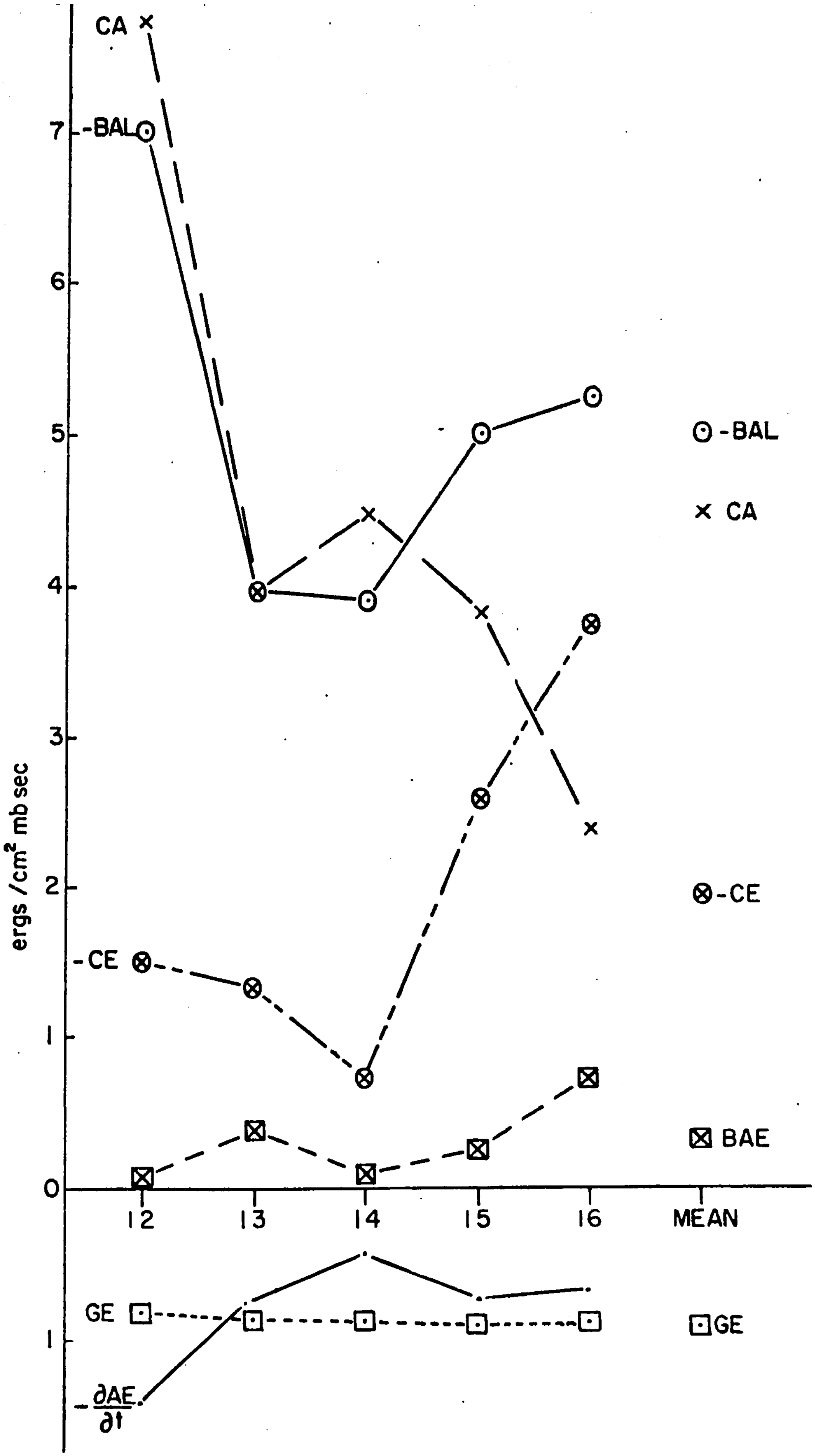

Fig. 4.2.15 Eddy available energy budget (AE) in the stratosphere for January 12 to 16, 1959. Units: Ergs/cm^2 mb sec.

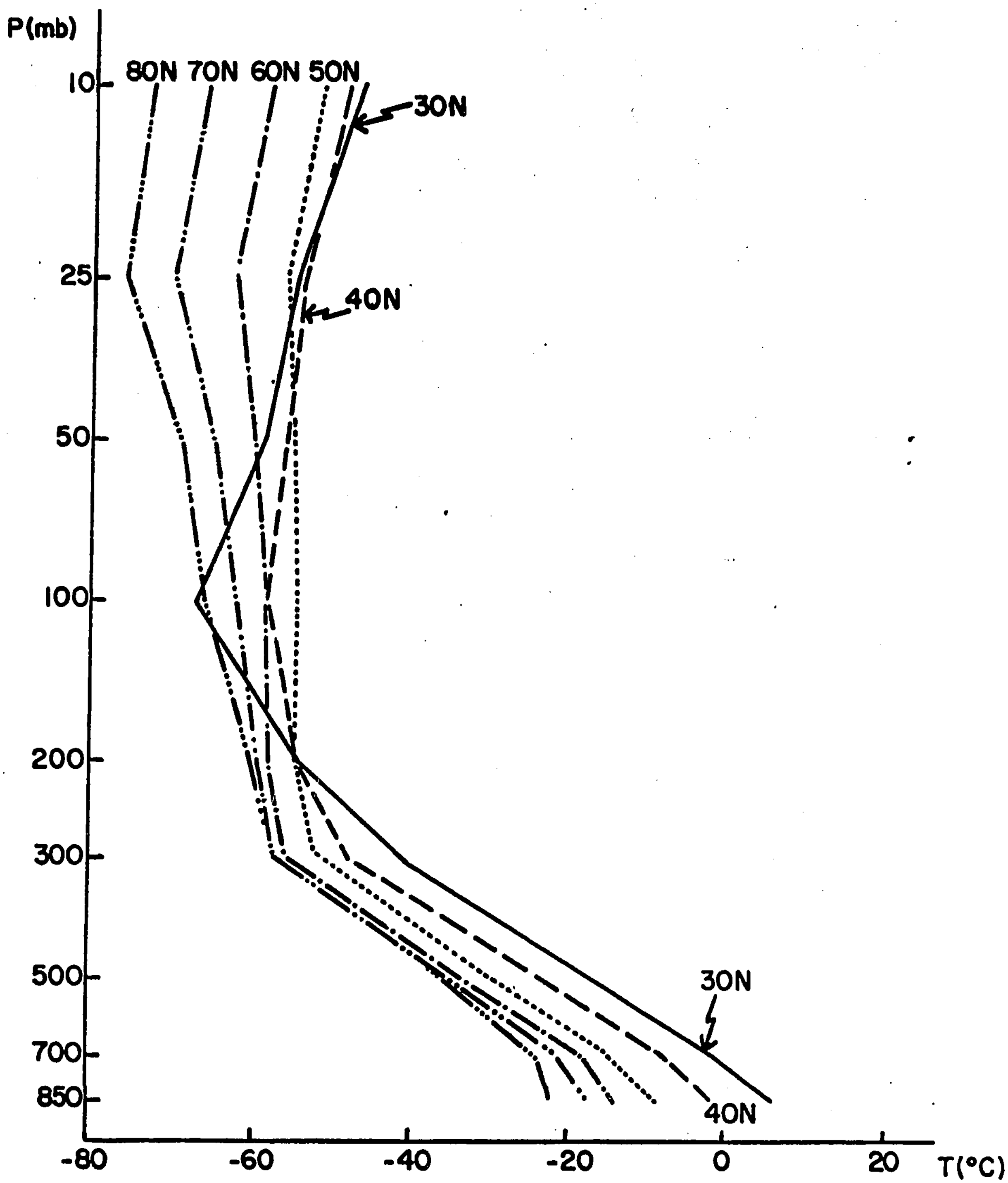

FIG. 4.2.16. Zonal Temperature Vertical Profiles, January 12 1959

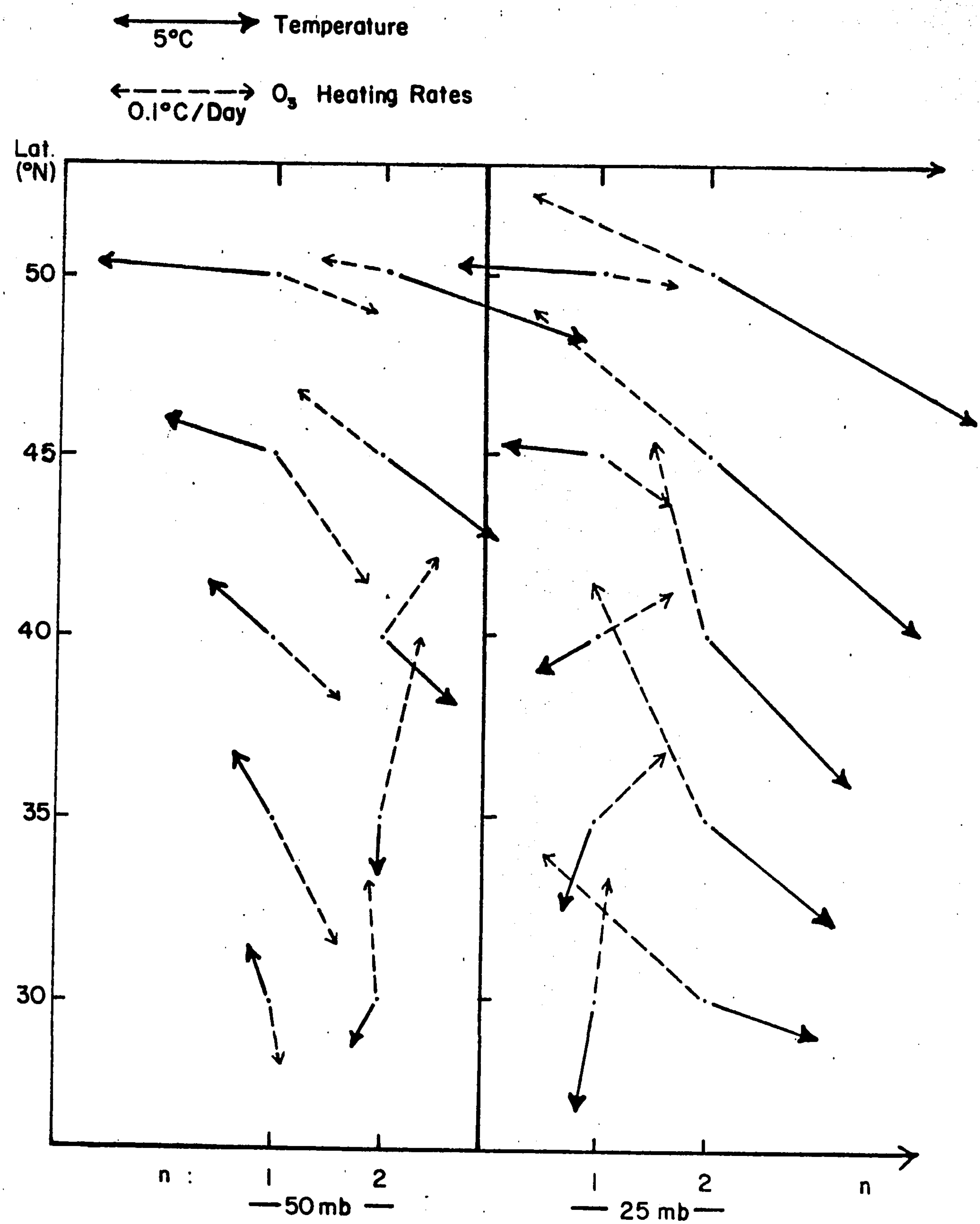

FIG. 4.2.17. Amplitude and phase of temperature and heating rates due to the absorption by ozone in the 9.6-micron band. Wave numbers 1 and 2 at 25 mb and 50 mb on January 12 1959.

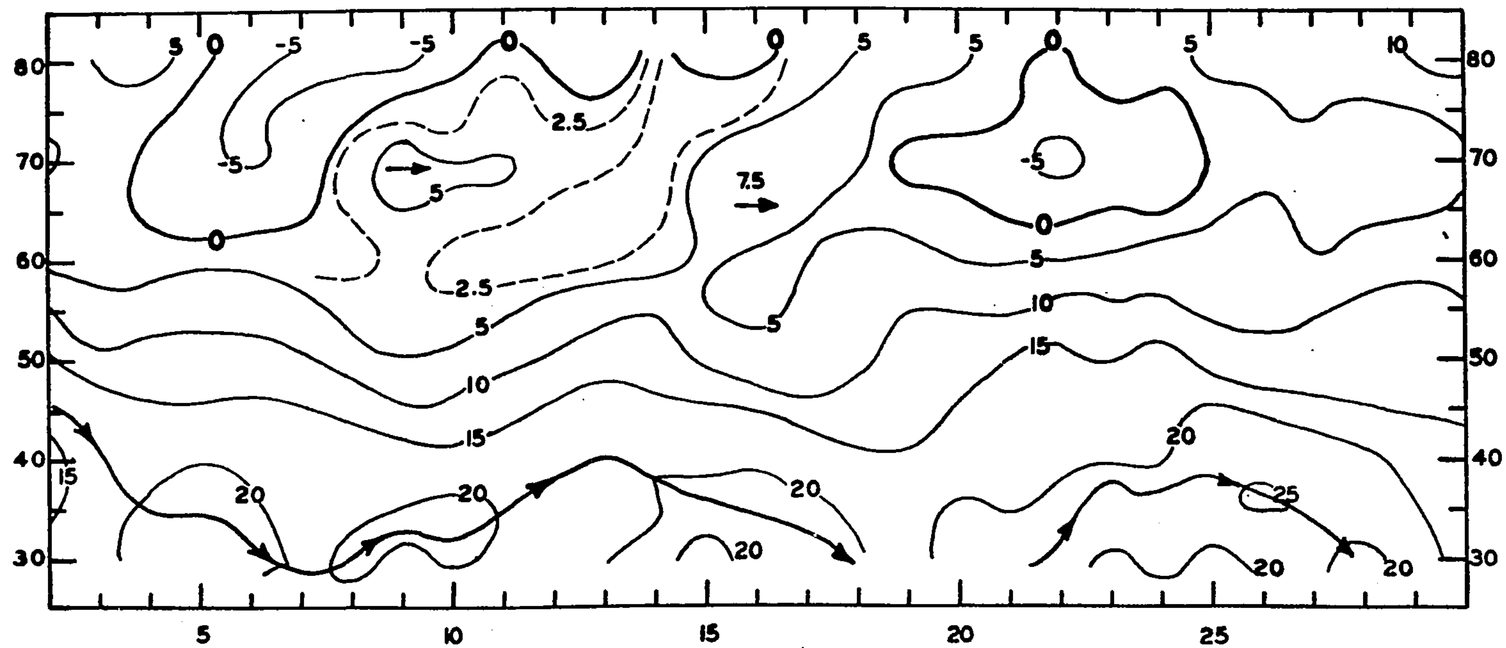

FIG: 4.2.18 MEAN ZONAL WIND U(m/sec) AT 500MB DURING JANUARY 1959

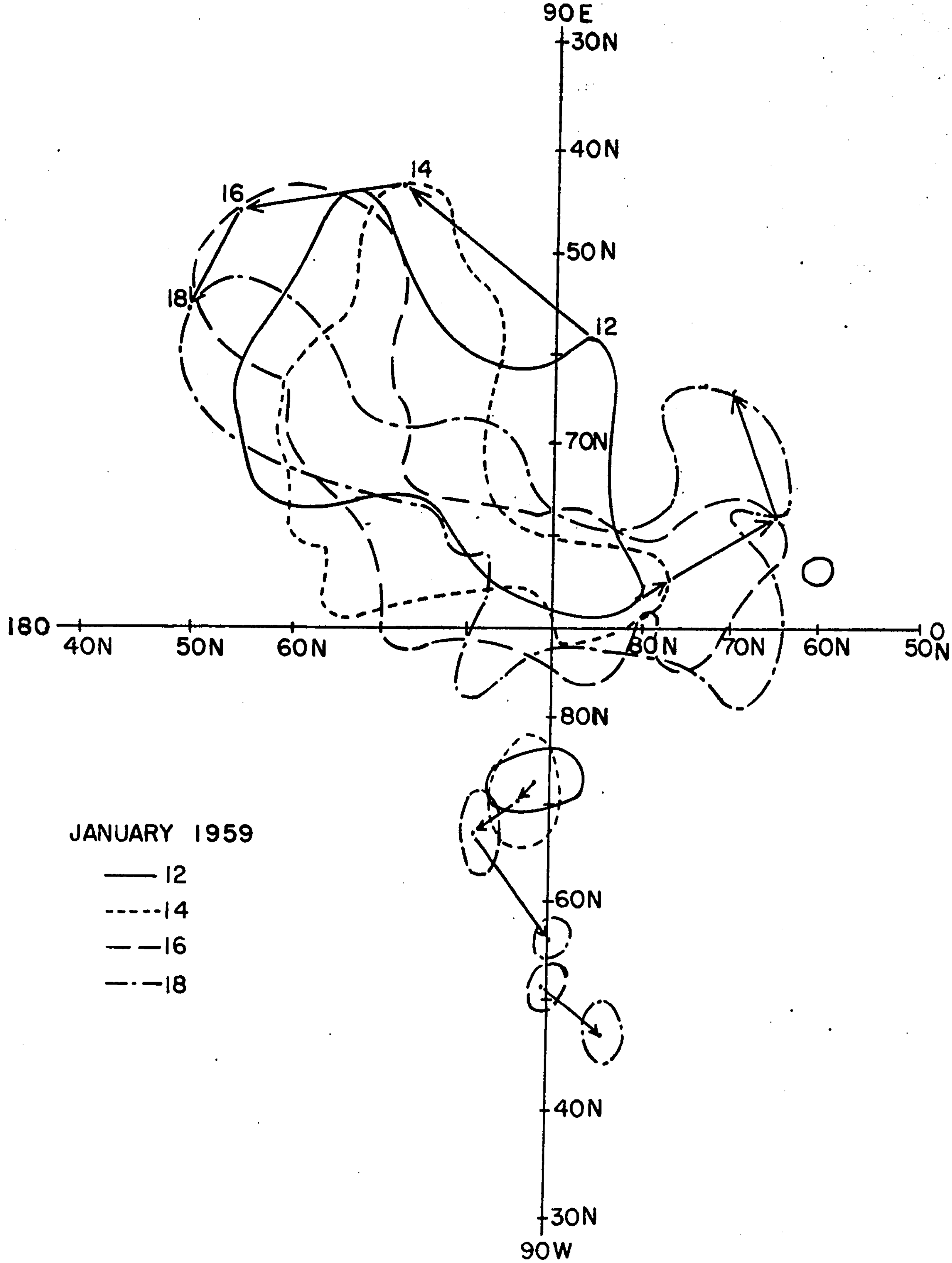

Fig. 4.2.19 Isotherm of -40°C at 500 mb over the northern hemisphere for January 12 to 18, 1959

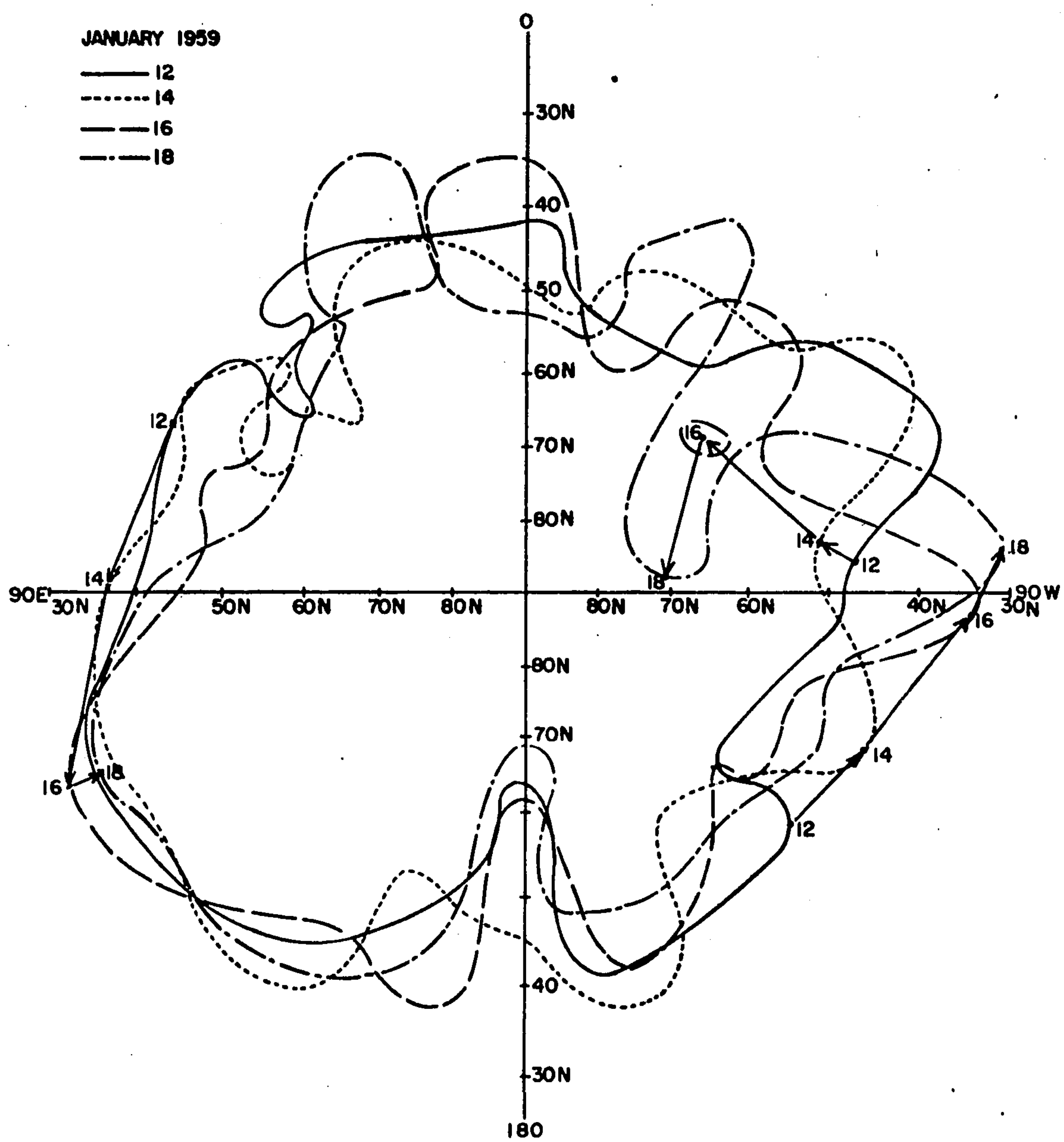

Fig. 4.2.20 500 mb -25°C isotherm for a few days in January over the Northern Hemisphere

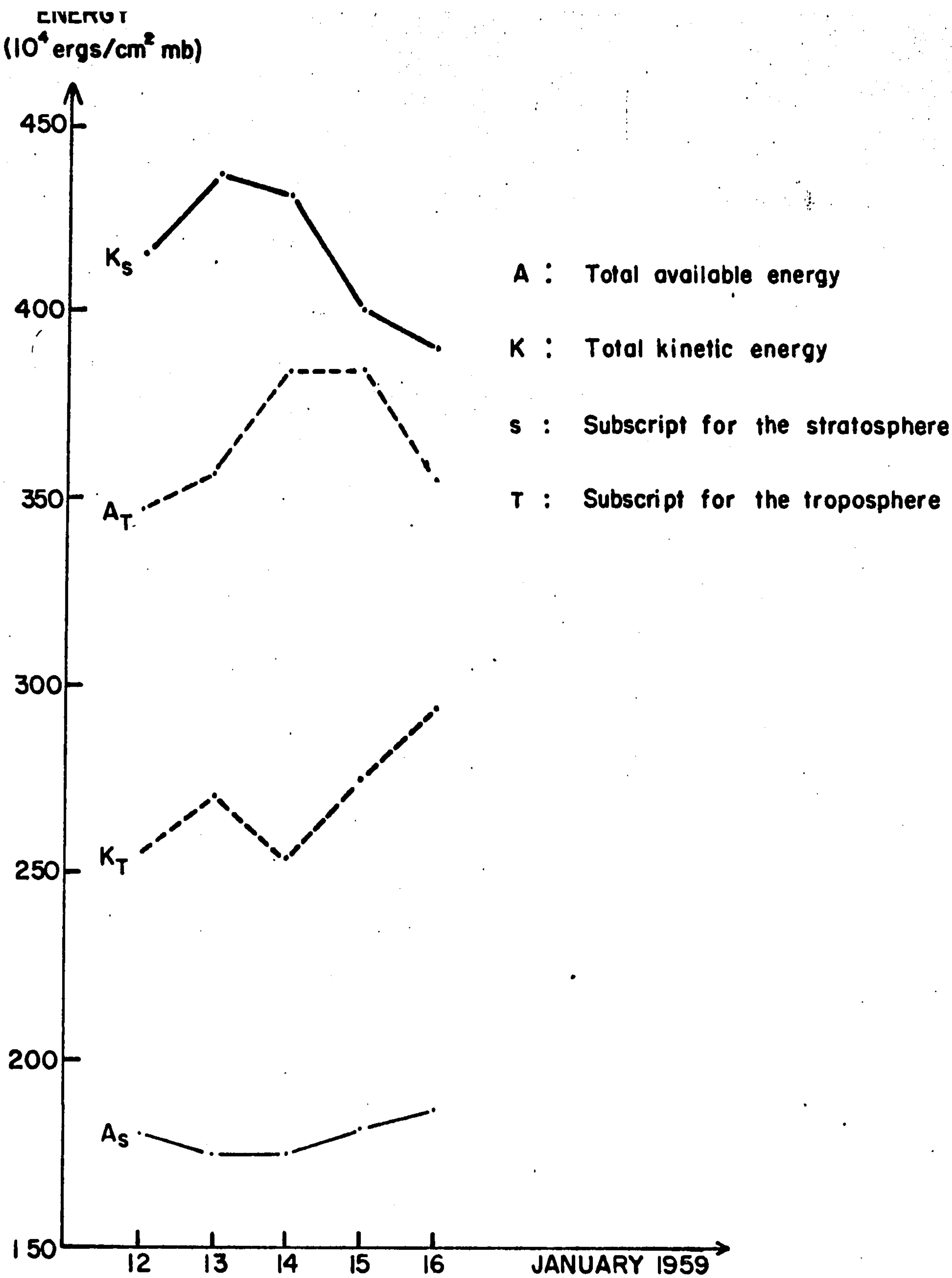

FIG. 4.2.21. Total available and kinetic energy from January 12 to 16, 1959.
UNITS: 10^4 x ergs/cm^2 mb.

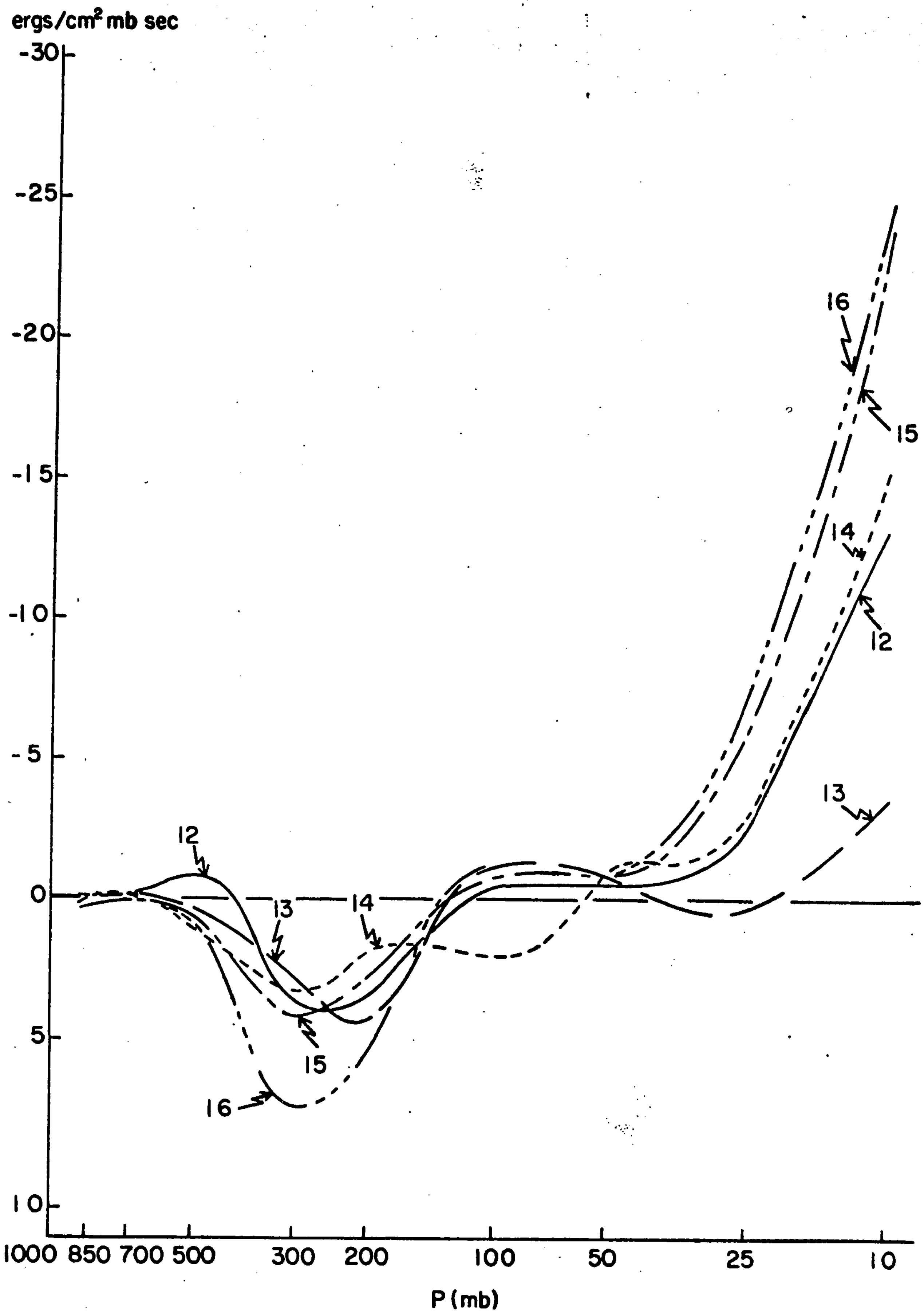

Fig. 4.2.22 Daily vertical profile of the CK-conversion for January 12 to 16, 1959.
Units: Ergs/cm^2 mb sec.

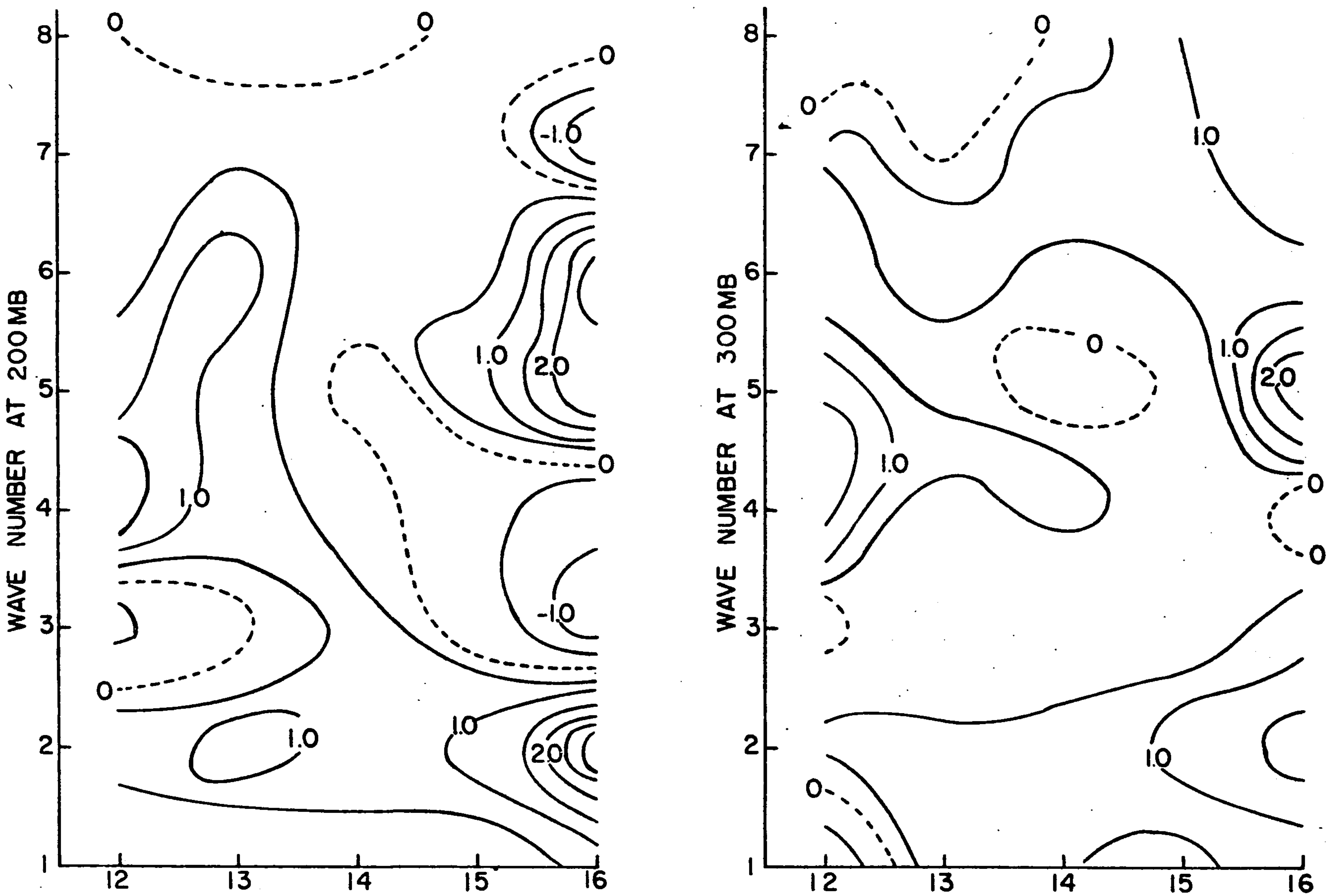

Fig. 4.2.23 Time-wave number diagram for the zonal to eddy kinetic energy conversion term CK (n) at 200 mb and 300 mb for January 12 to 16, 1959. Units: Ergs/cm^2 mb sec.

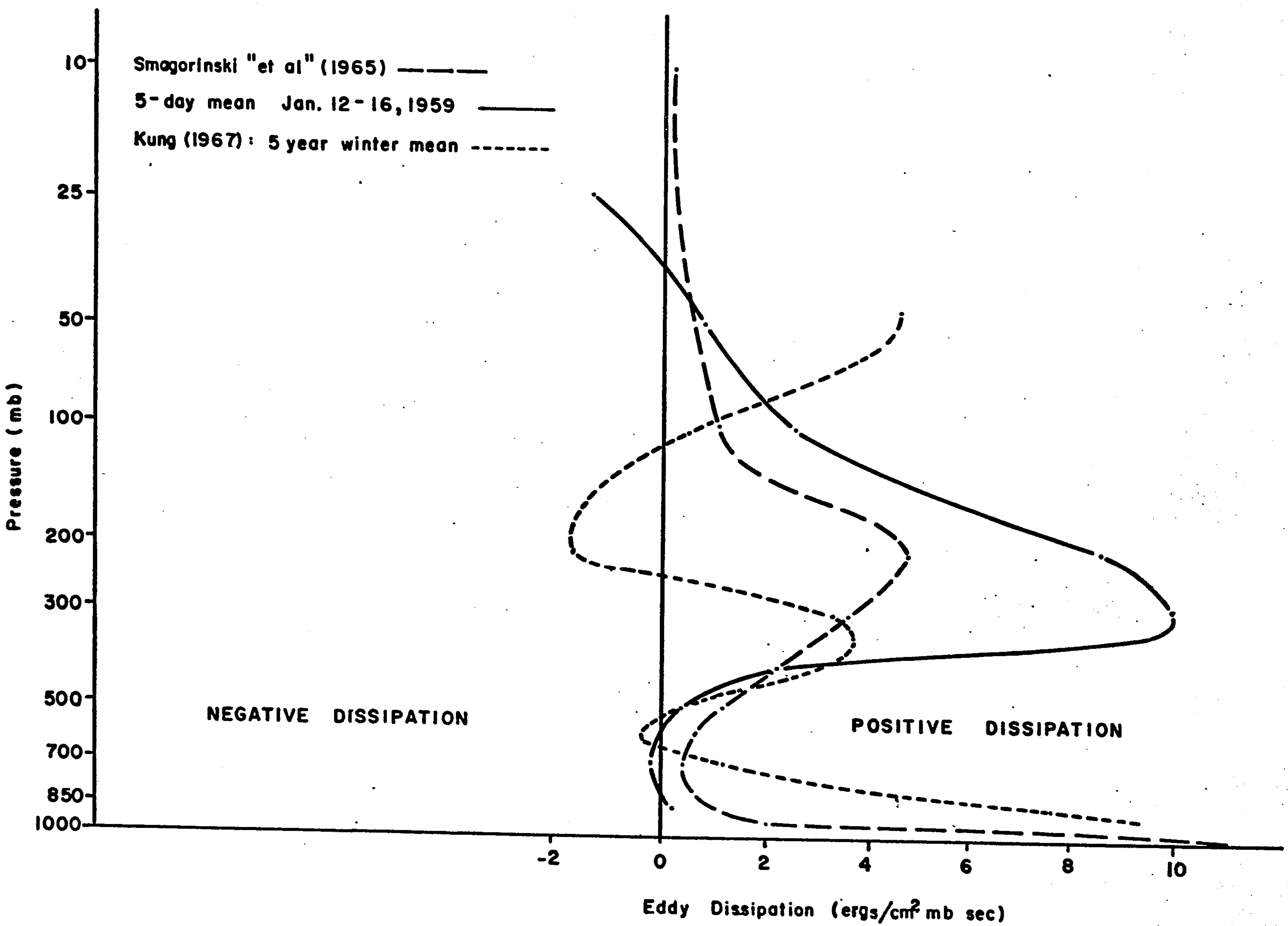
Smagorinski "et al" (1965)
5-day mean Jan. 12-16, 1959
Kung (1967): 5 year winter mean
Pressure (mb)
10
25
50
100
200
300
500
700
850
1000
NEGATIVE DISSIPATION
POSITIVE DISSIPATION
-2
0
2
4
6
8
10
Eddy Dissipation (ergs/cm^2 mb sec)

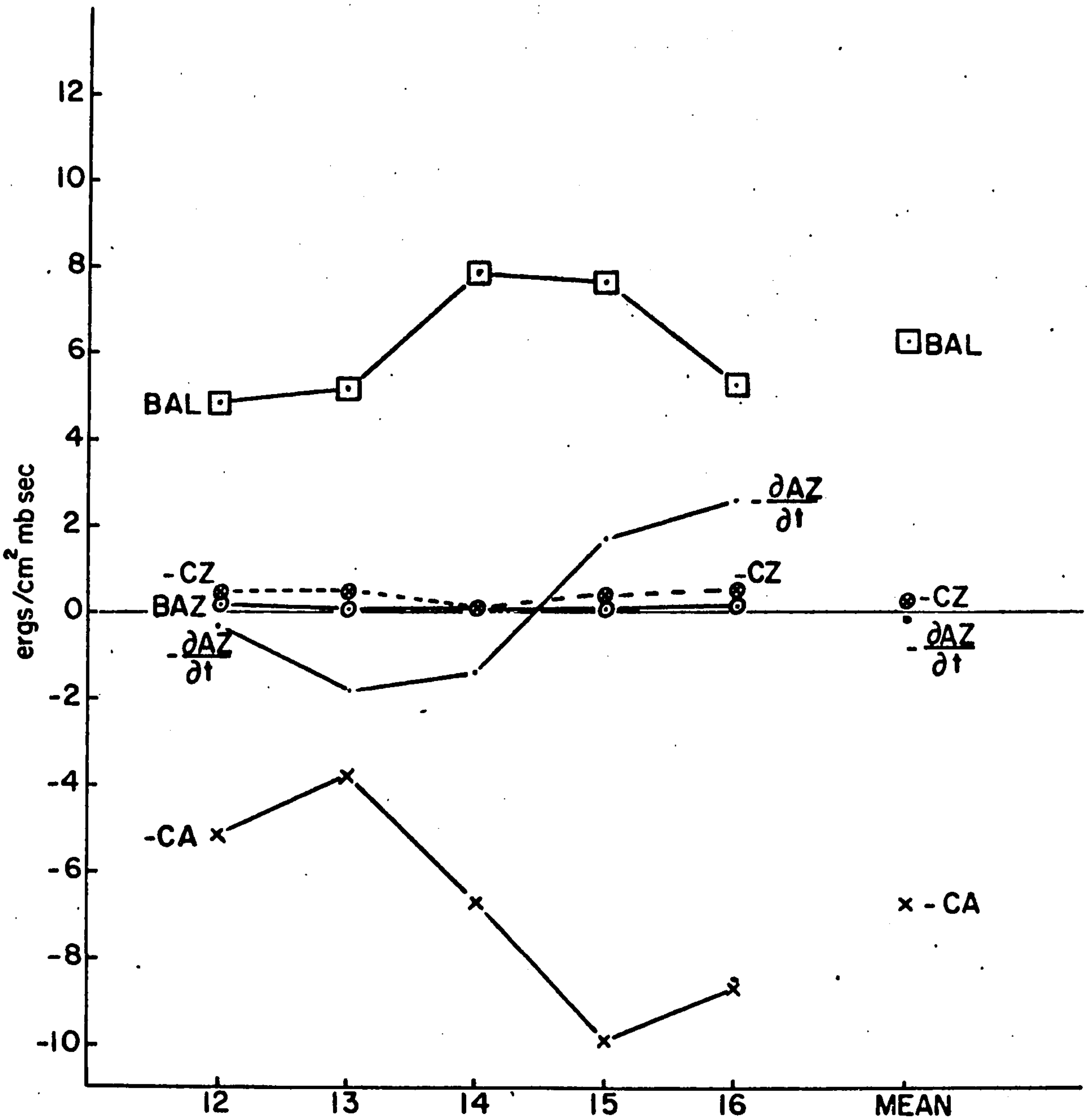

Fig. 4.2.25 Daily budget of the zonal available potential energy (AZ) in the troposphere for January 12 to 16, 1959. Units: Ergs/cm^2 mb sec.

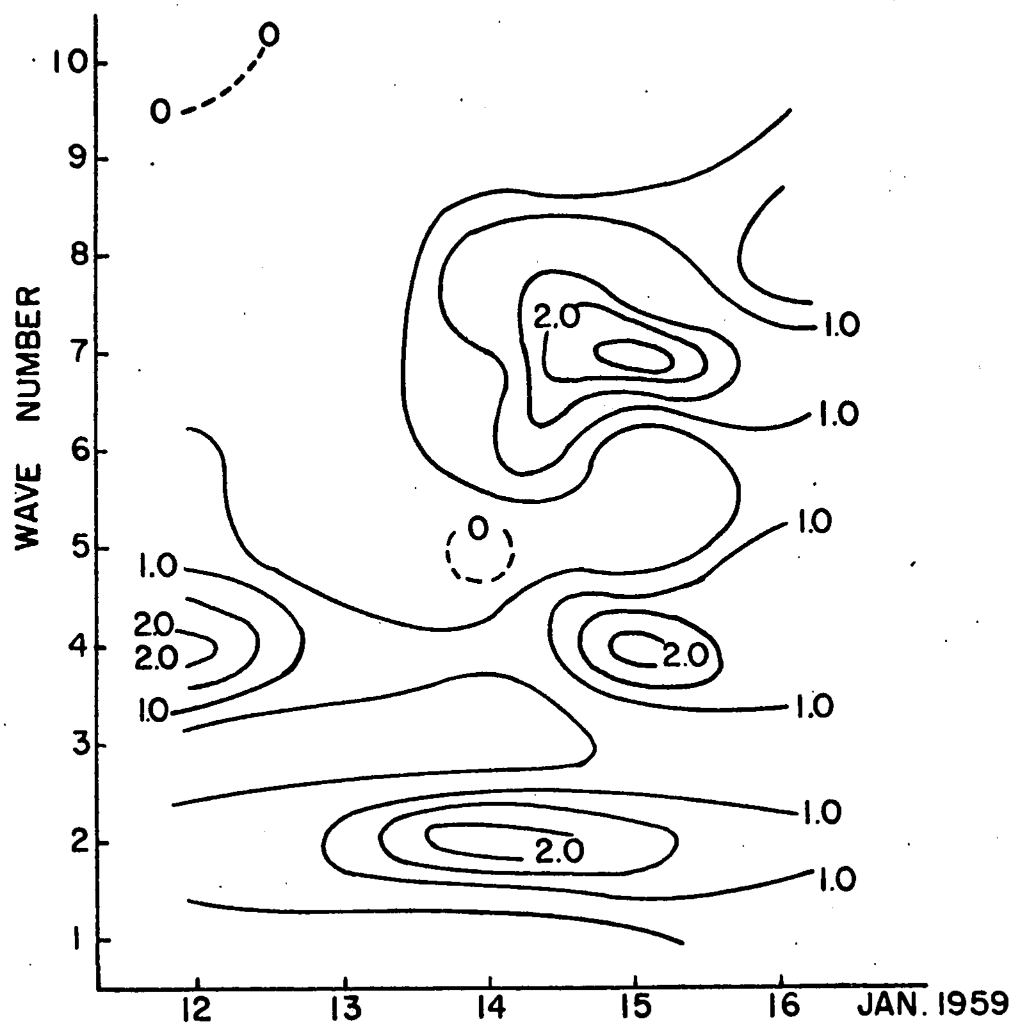

Fig. 4.2.26. Time-wave number diagram of the CA (n)-conversion term in the troposphere for January 12 to 16, 1959. Units: Ergs/cm^2 mb sec.

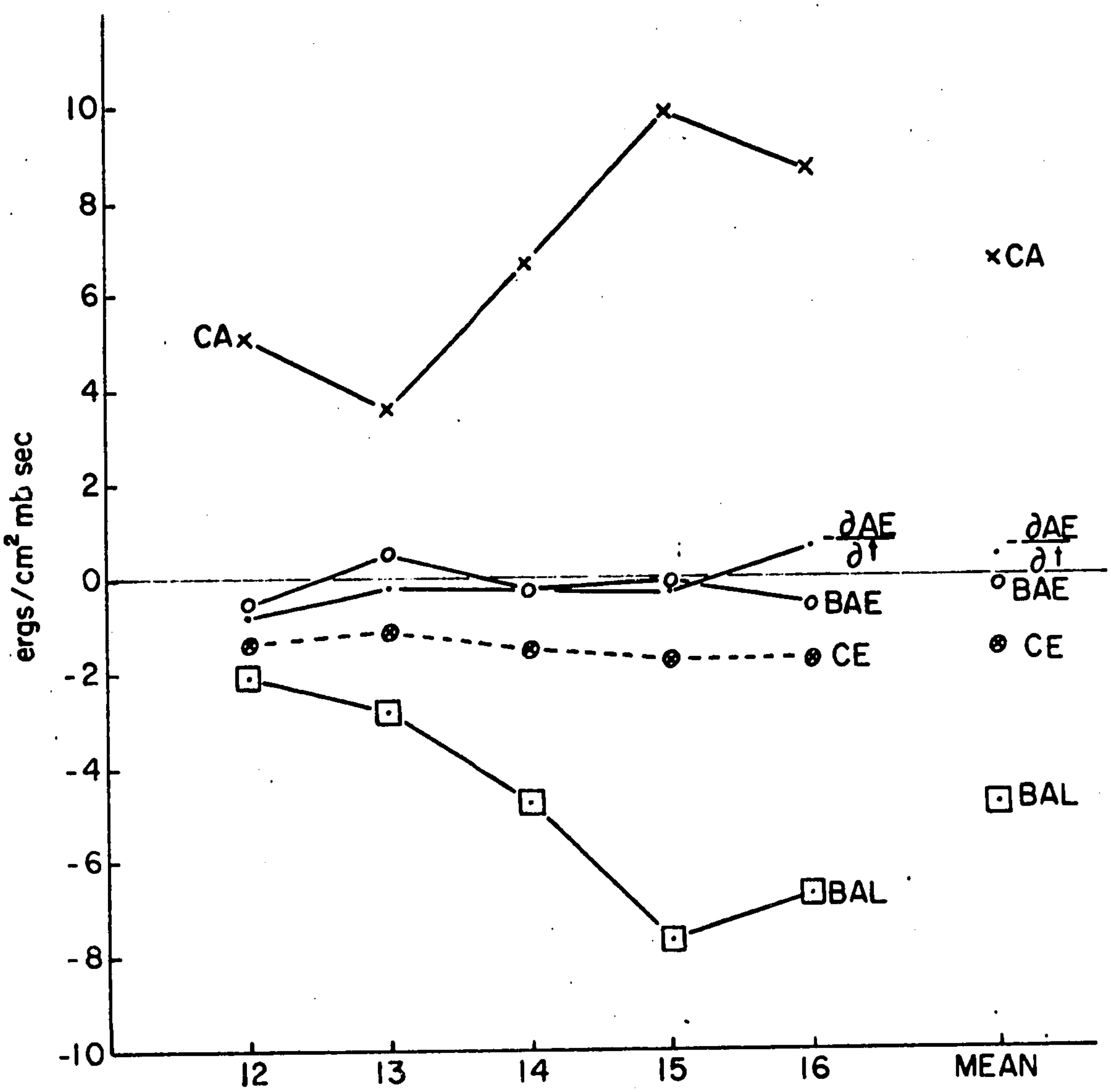

Fig. 4.2.27 Daily budget of the eddy available energy (AE) in the troposphere for January 12 to 16, 1959. Units: Ergs/cm^2 mb sec.

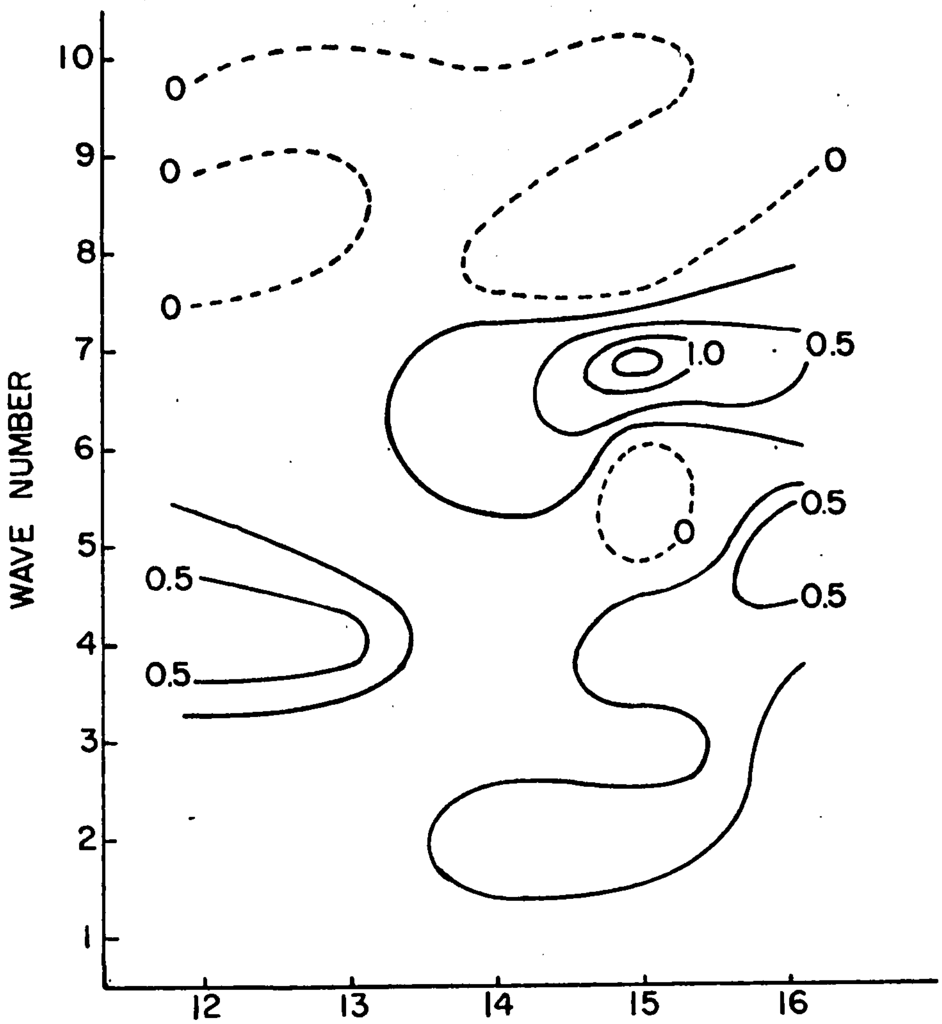

Fig. 4.2.28 Time-wave number diagram of the CE (n)-conversion term in the troposphere for January 12 to 16, 1959. Units: Ergs/cm^2 mb sec.

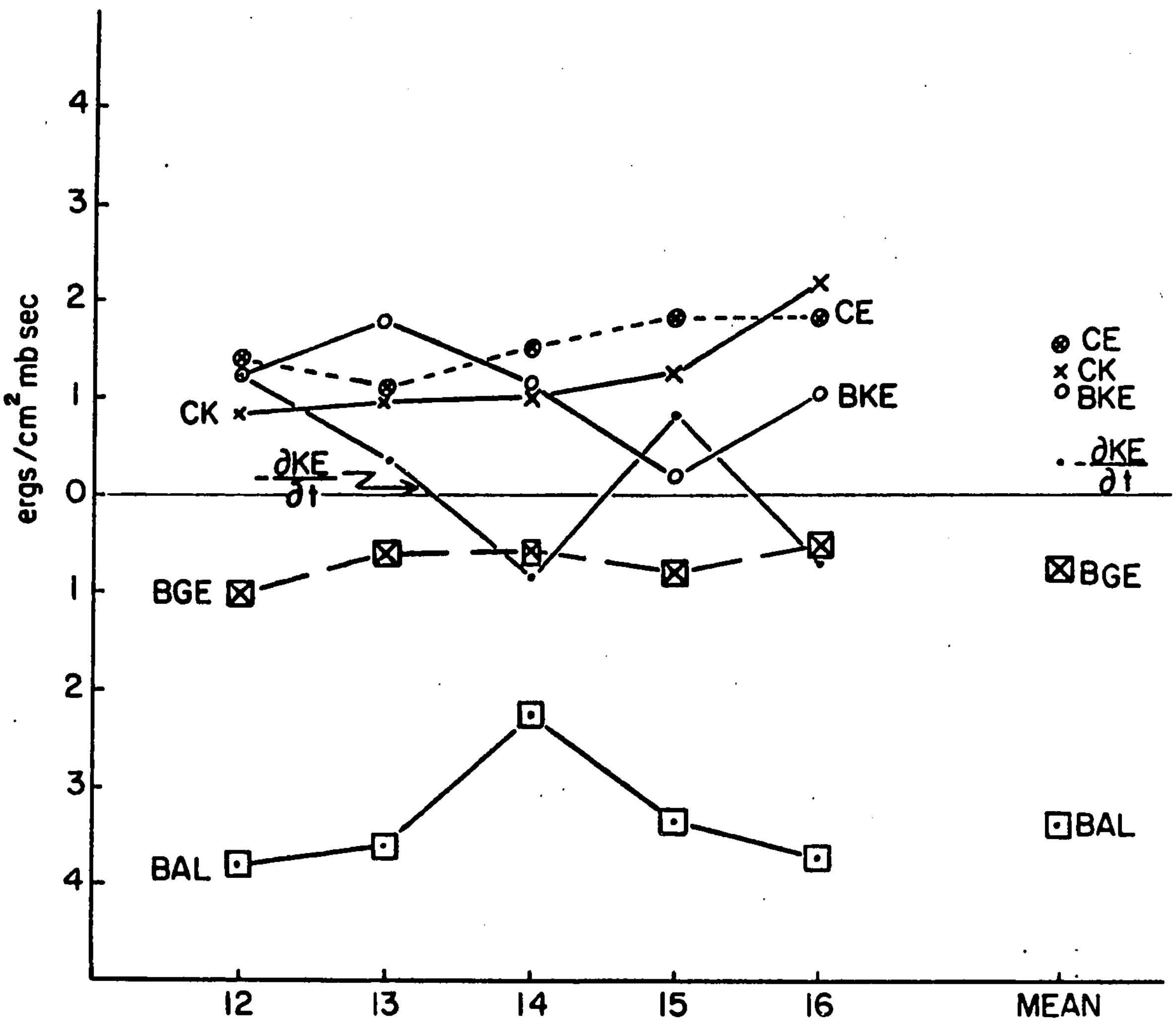

Fig. 4.2.29 Daily budget of the eddy kinetic energy (KE) in the troposphere for January 12 to 16, 1959. Units: Ergs/cm^2 mb sec.

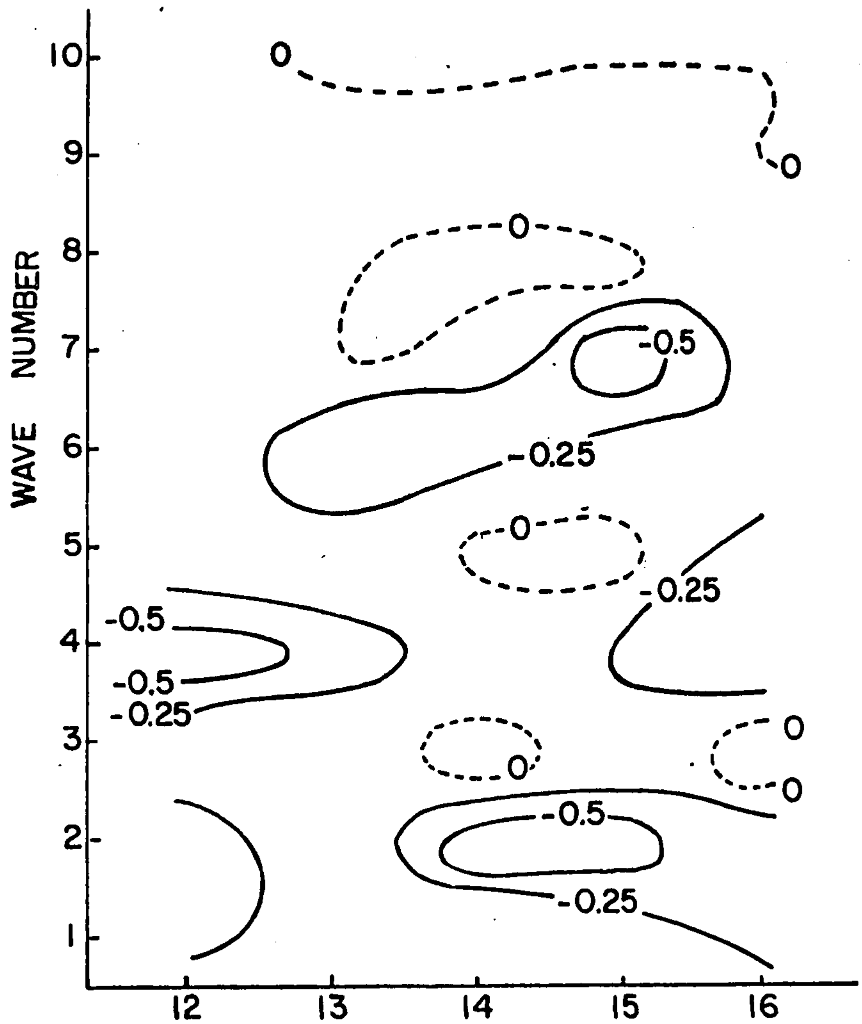

Fig. 4.2.30 Time-wave number diagram of the BGE (n)-term in the troposphere for January 12 to 16, 1959. Units: Ergs/cm^2 mb sec.

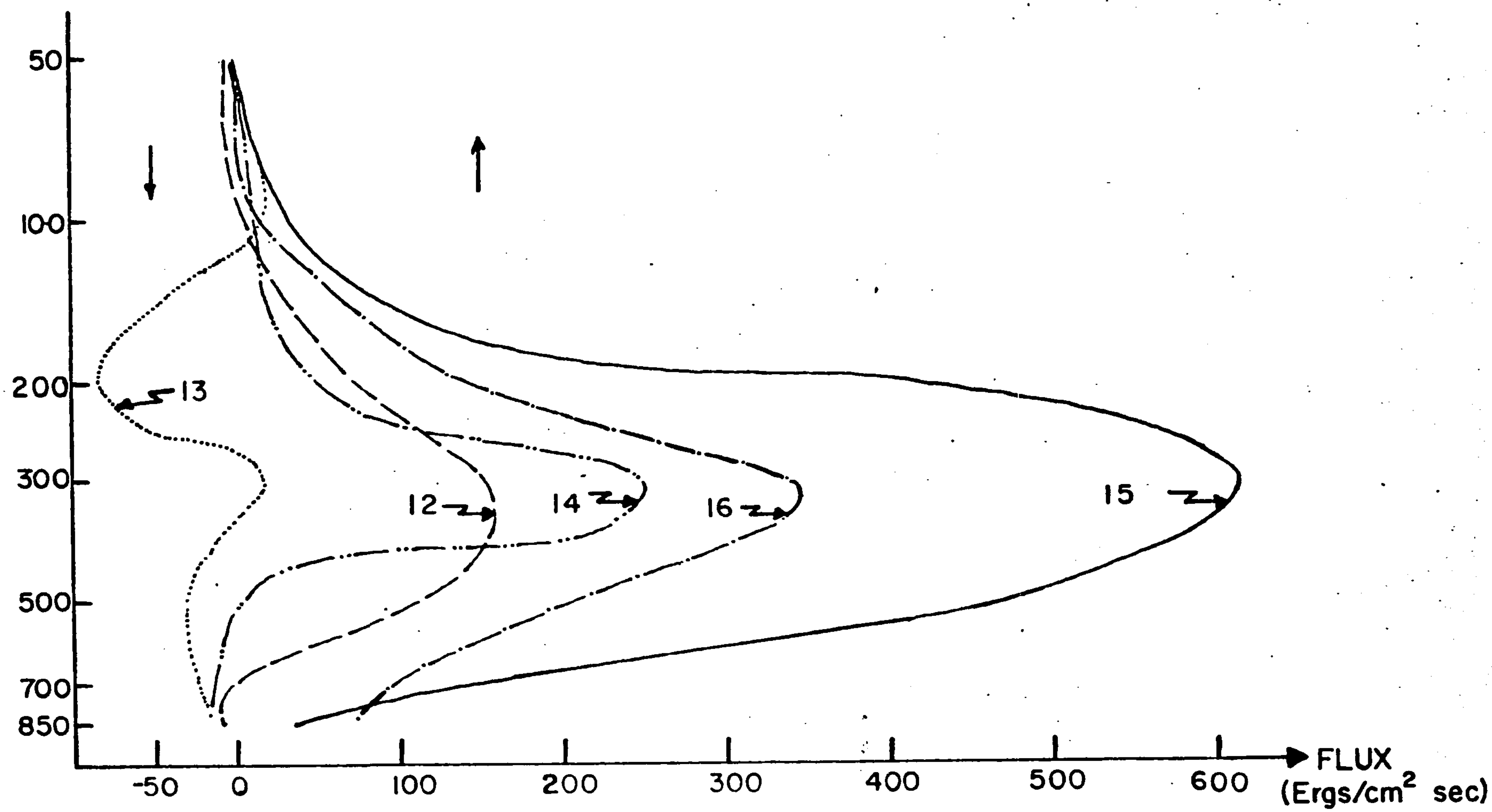

Fig. 4. 2. 31 Vertical distribution of the geopotential flux at wave number 7 during January 12 to 16, 1959. Positive values indicate upward flux. Units: Ergs/cm^2 sec.

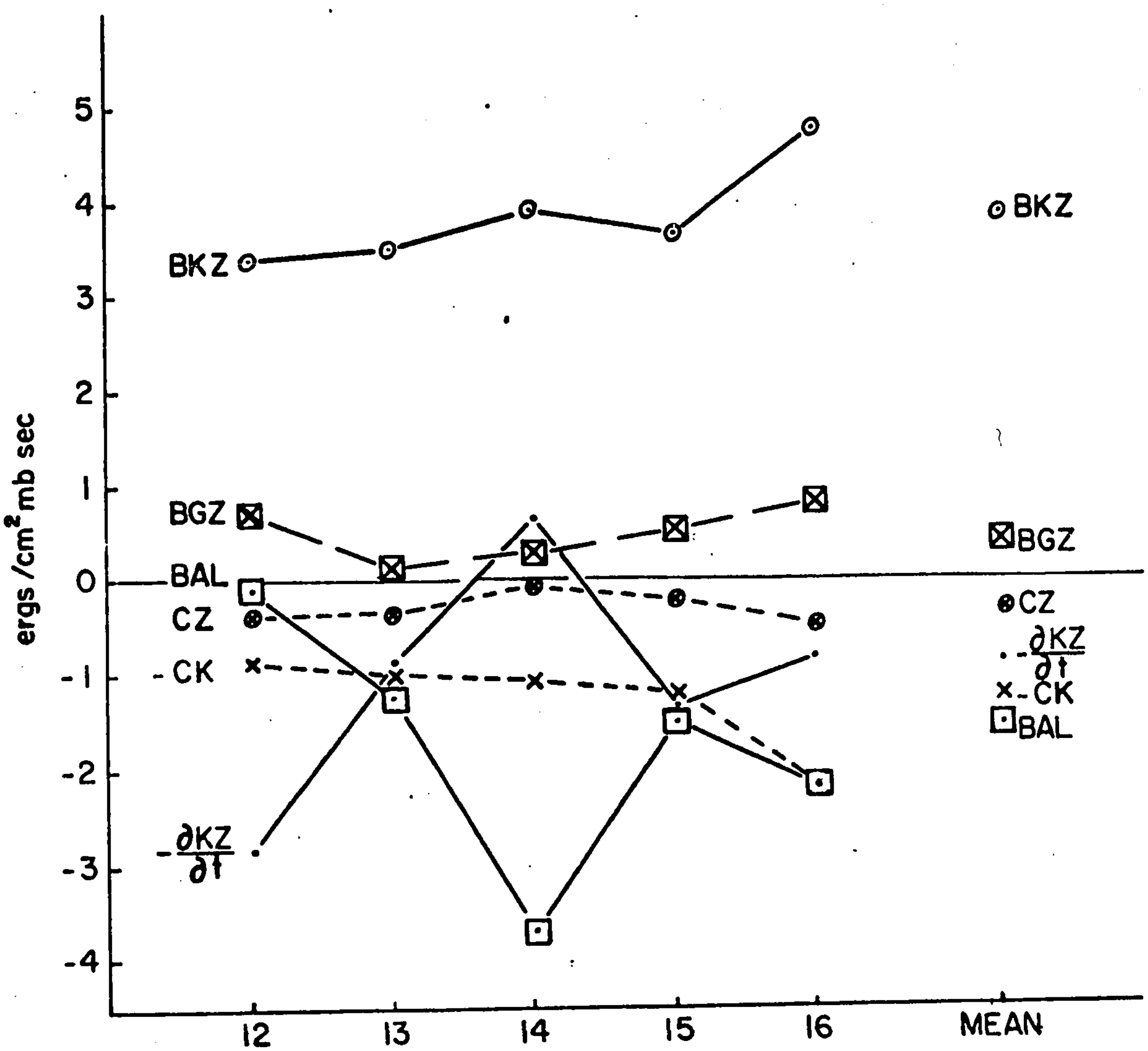

Fig. 4.2.32 Daily budget of the zonal kinetic energy (KZ) in the troposphere for January 12 to 16, 1959. Units: Ergs/cm^2 mb sec.

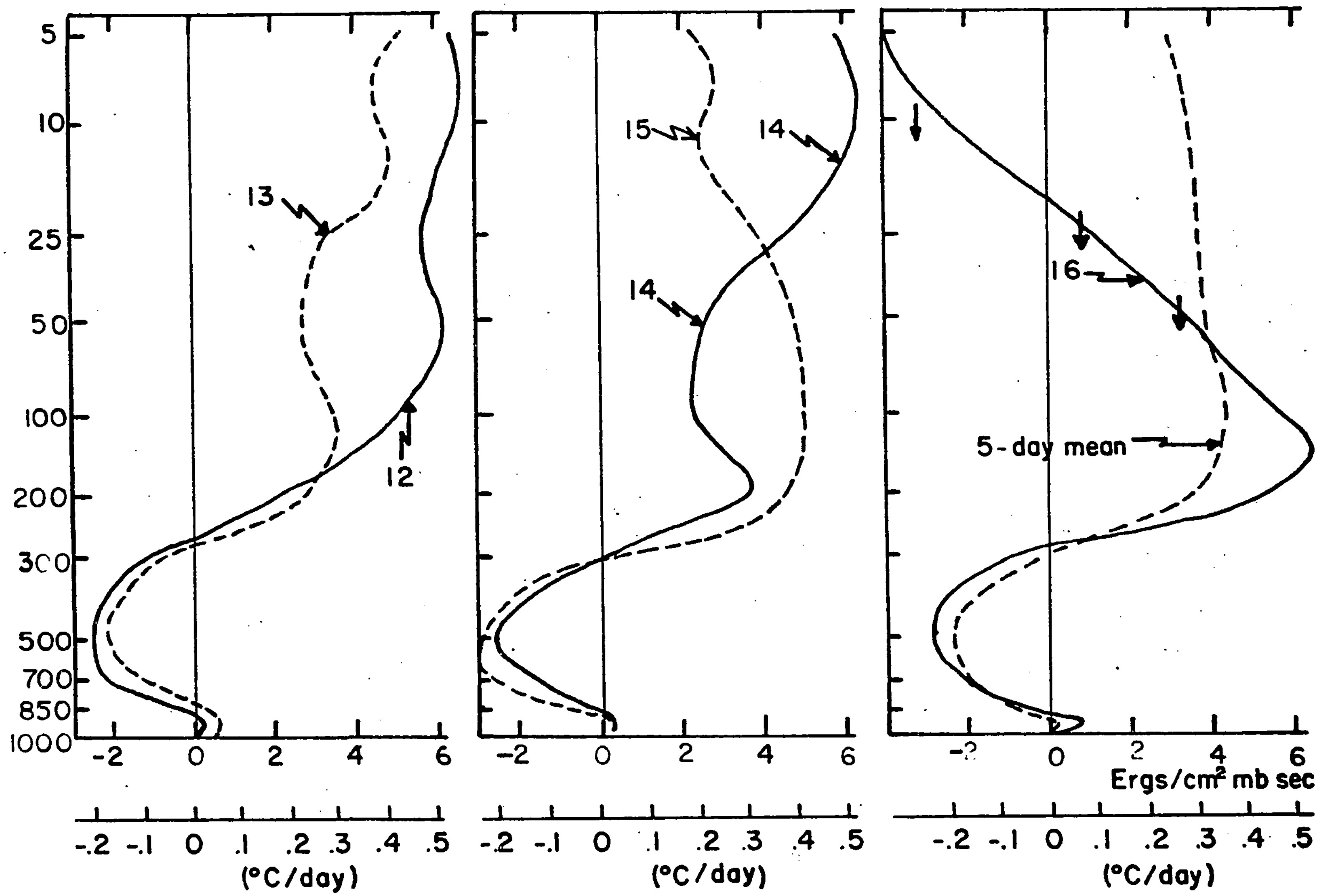

FIG. 4.2.33. Vertical profile of the daily geopotential flux convergence in the atmosphere for January 12 to 16, 1959.
Arrows indicate downward geopotential flux, while it is upward otherwise.
UNITS: Ergs/cm^2 mb sec.

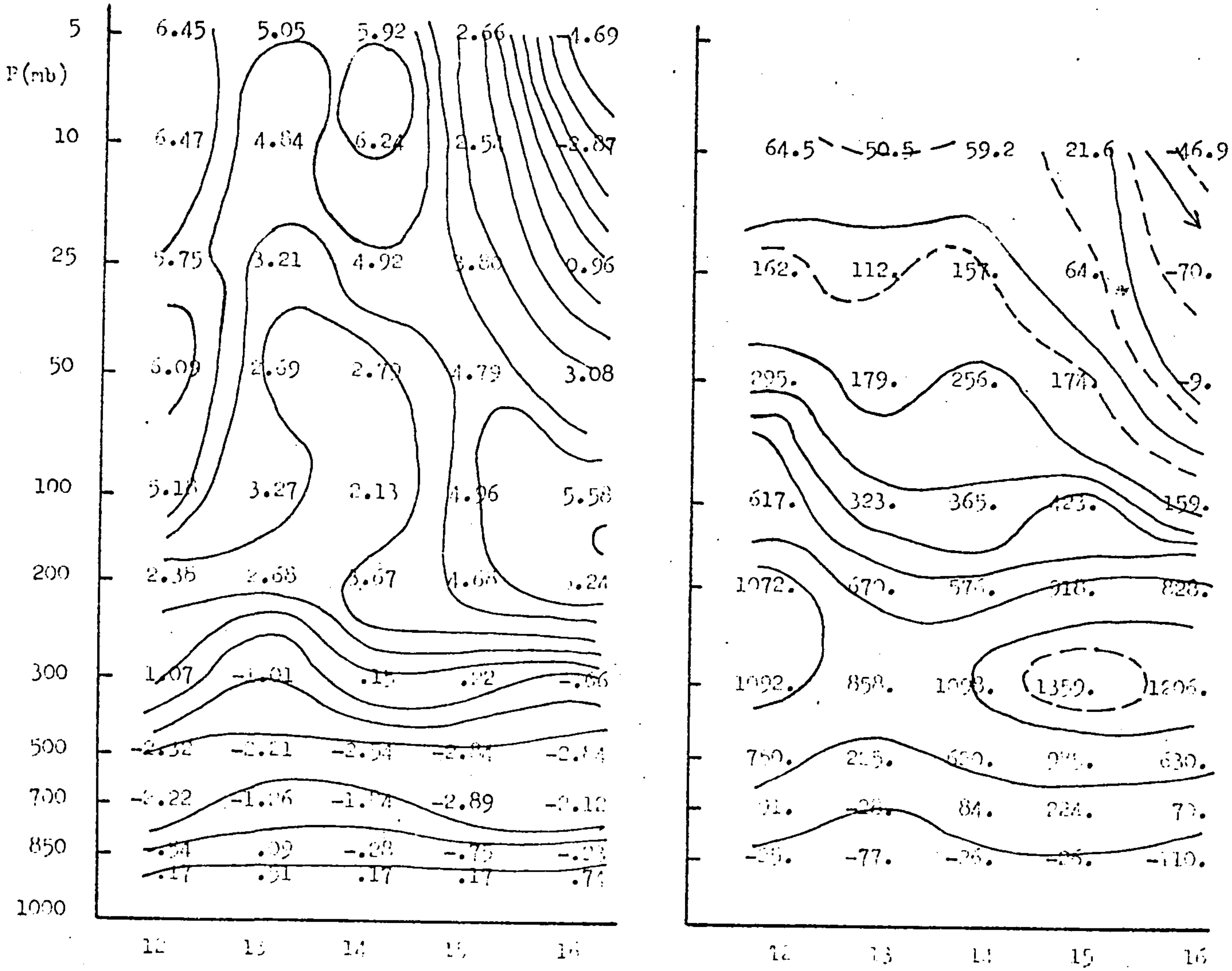

Fig. 4.2.34. A: Time-height diagram of the eddy geopotential flux convergence in the vertical.
UNITS: Ergs/cm^2mb sec.

B: Time-height diagram of the eddy geopotential flux in the vertical.
UNITS: Ergs/cm^2sec.

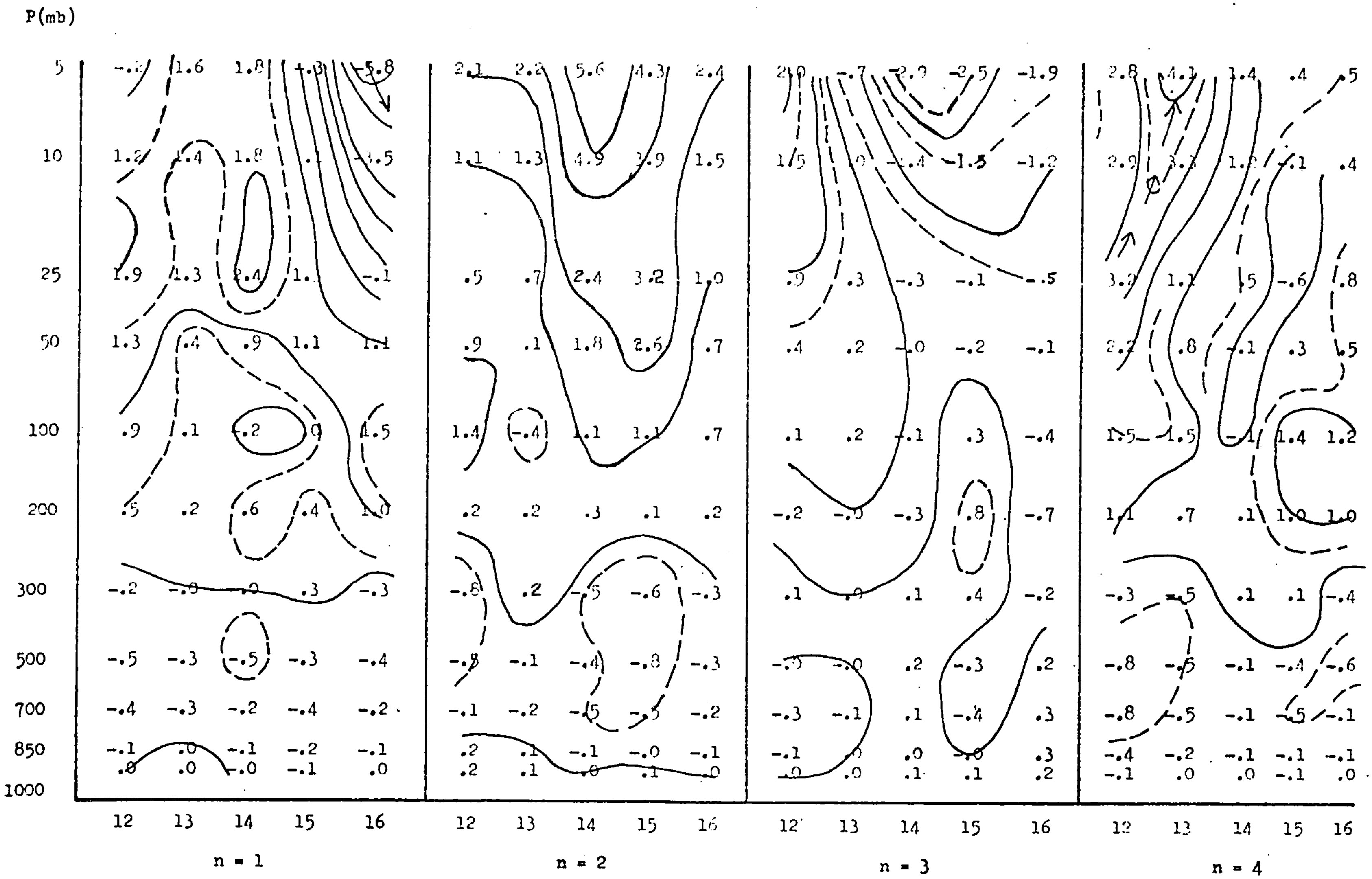

FIG. 4. 2. 35. Daily and spectral vertical flux convergence of geopotential for the period January 12 to 16, 1959.

UNITS: Ergs/cm^2 mb sec.

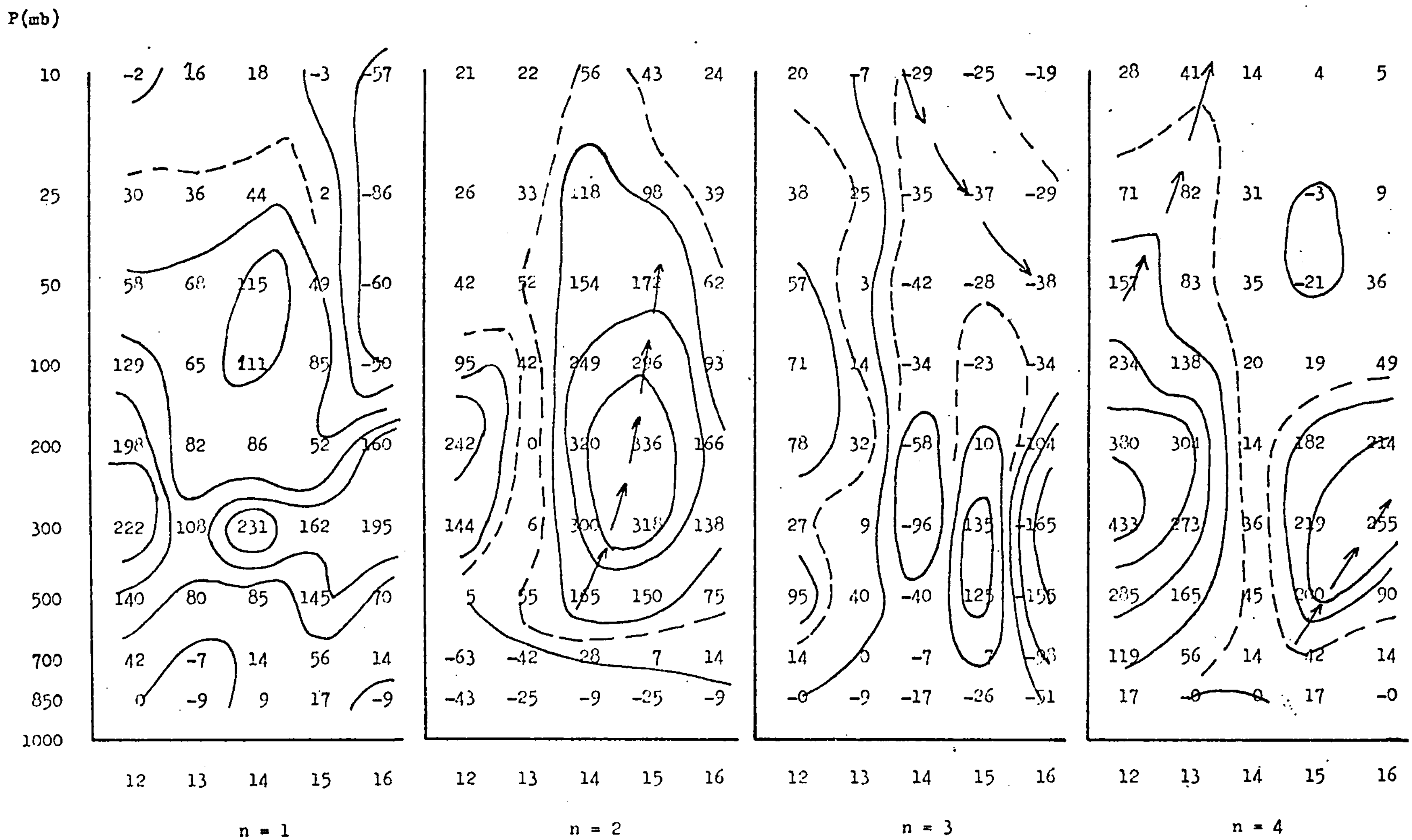

FIG. 4. 2. 36. Daily and spectral vertical geopotential flux for the period January 12 to 16, 1959.
UNITS: Ergs/cm^2 sec.

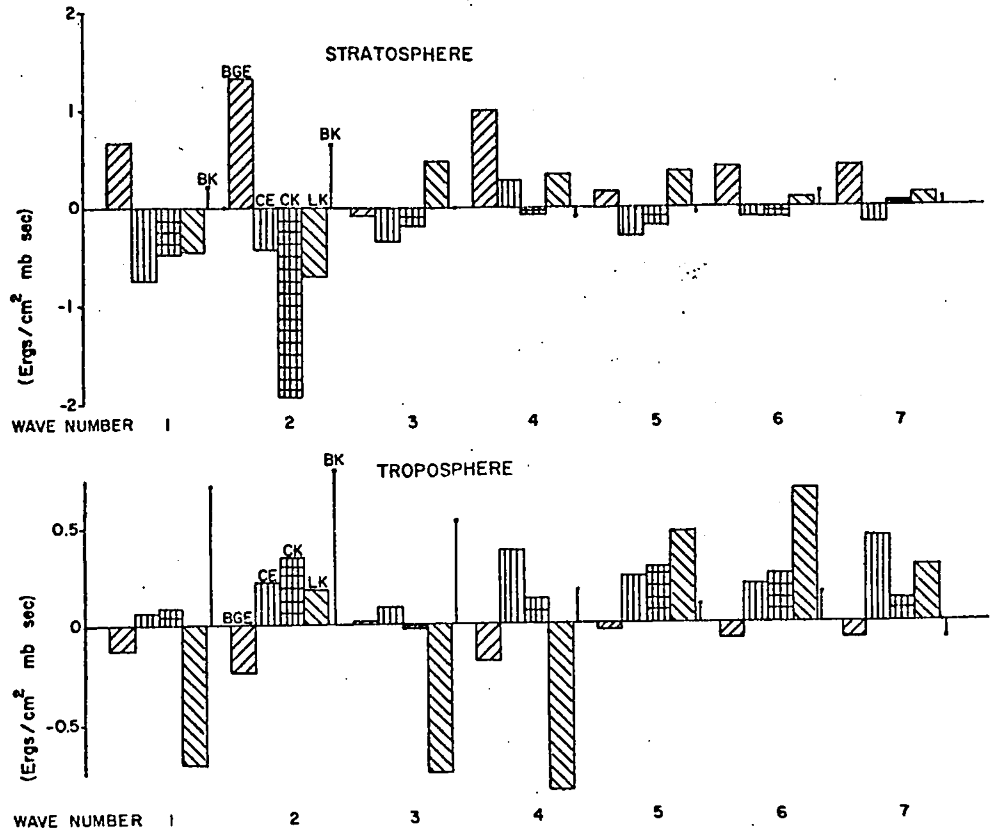

FIG. 4. 2. 37. Five-day mean spectral kinetic energy budget for the 12 to 16 January 1959 period.
Units: Ergs/cm^2 mb sec.

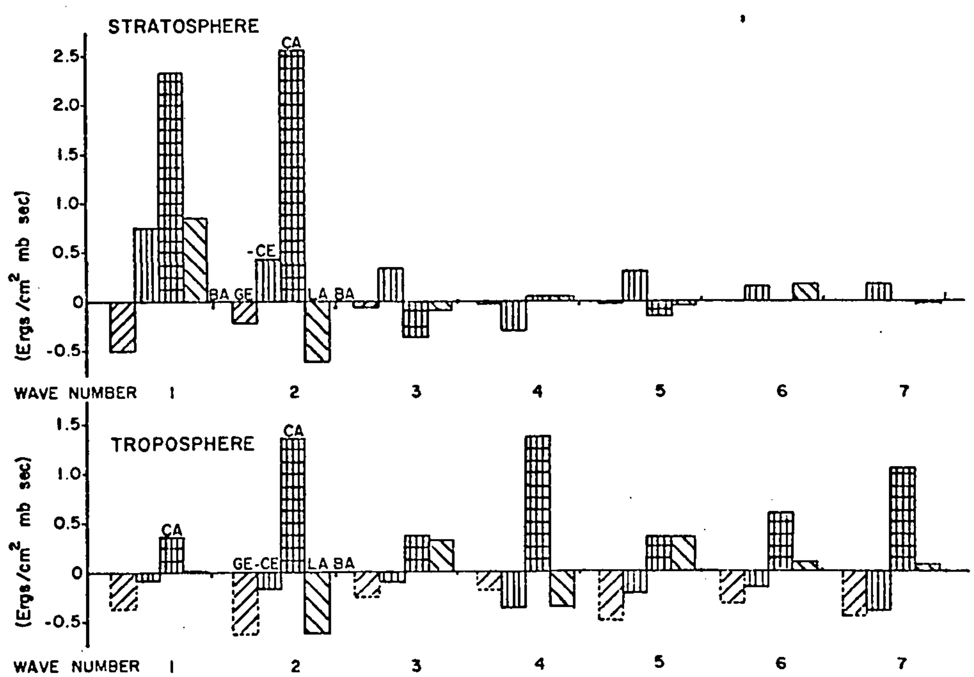

FIG. 4. 2. 38. Five-day mean spectral available energy budget for the 12 to 16 January 1959 period.
Units: Ergs/cm^2 mb sec.

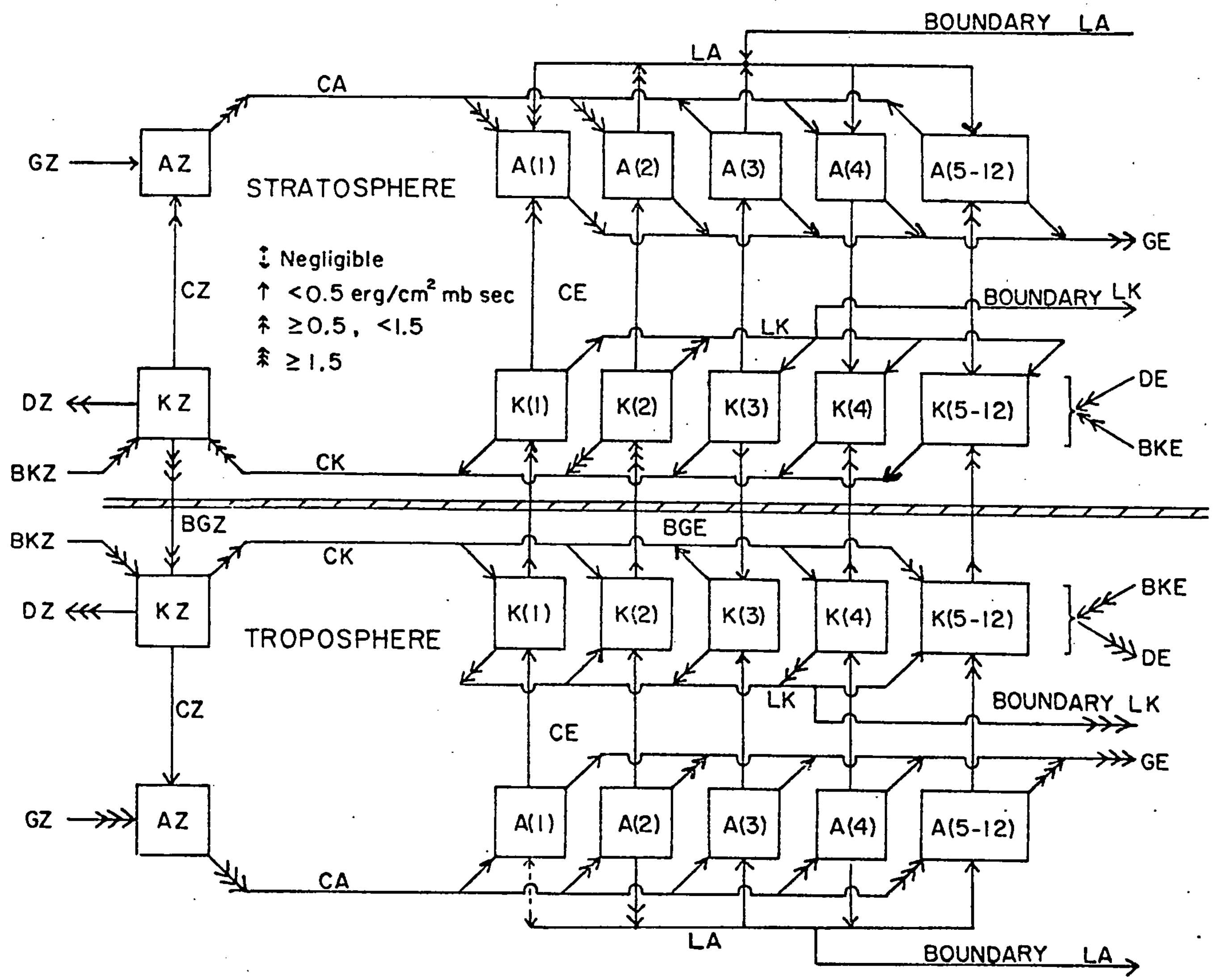

FIG. 4. 2. 39. Spectral energy diagram averaged over the January 12 to 16 1959 period. Intensities of exchanges are proportional to number of arrow heads. Units: Ergs/cm^2 mb sec.

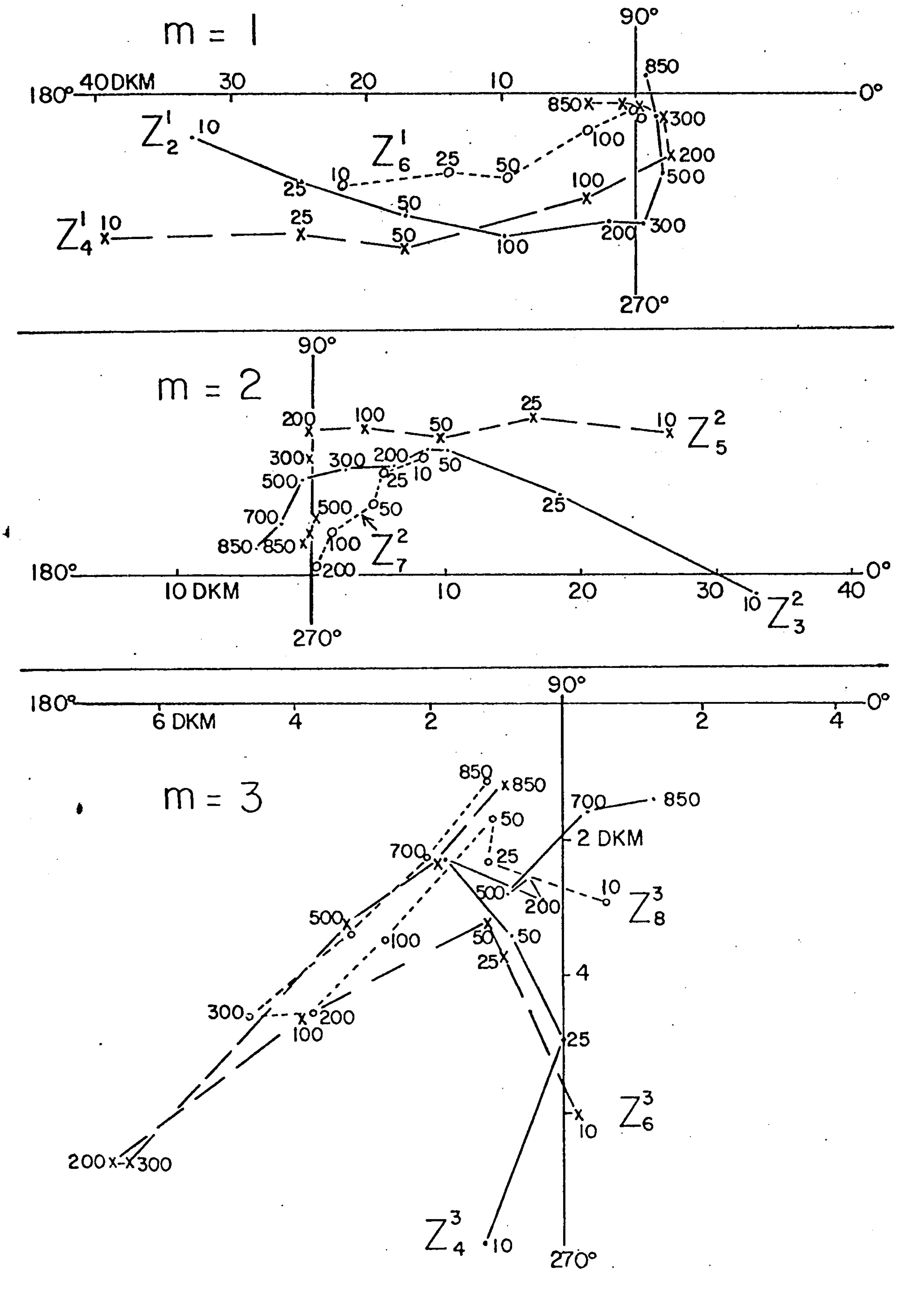

Fig. 4.3.1. Five-day mean vertical structure of planetary harmonics.
Units: Dekameters.

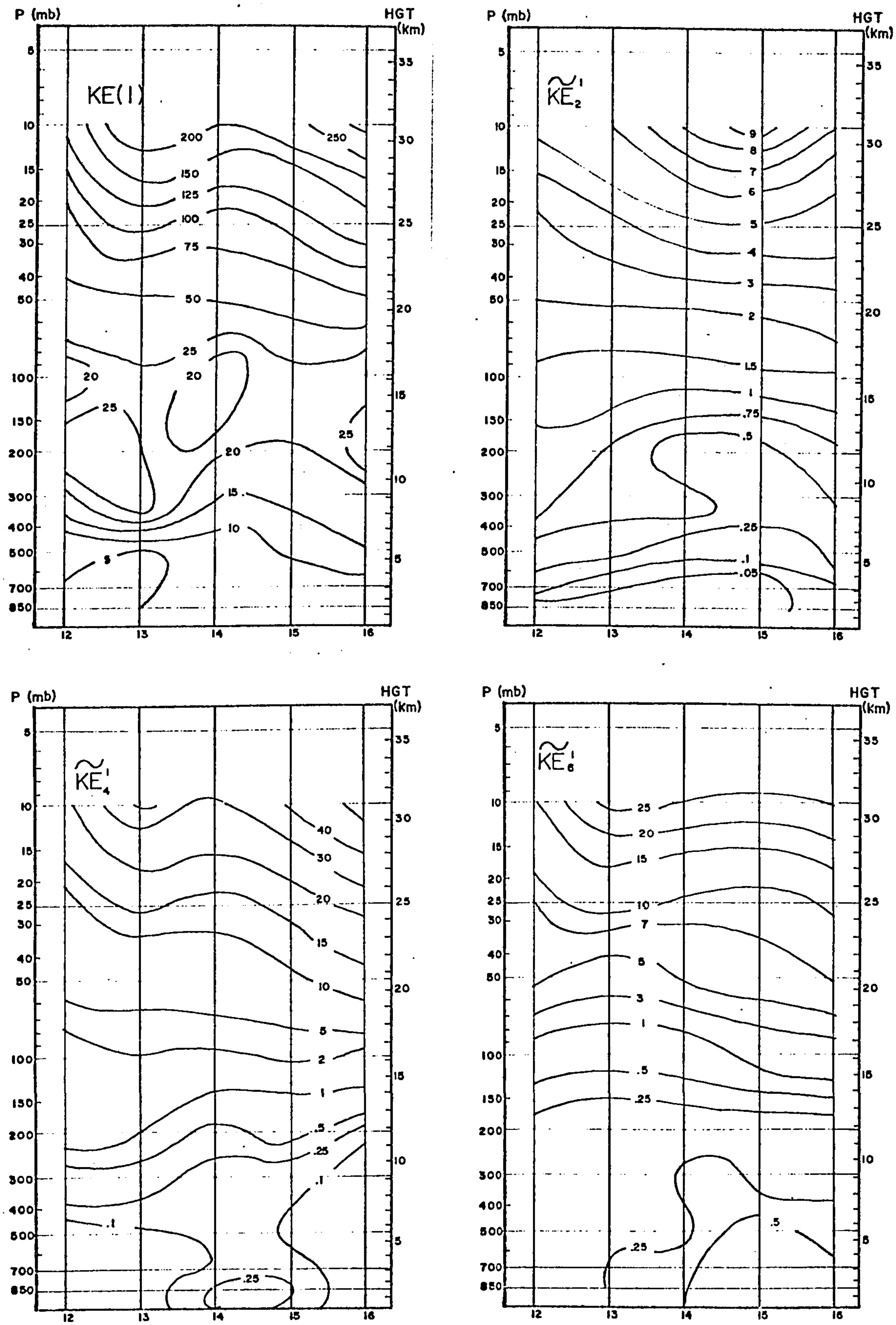

Fig. 4.3.2 Kinetic energy for longitudinal wave number 1, KE(1), and pseudo-kinetic energy of the spherical harmonics $\widetilde{KE}_2^1$, $\widetilde{KE}_4^1$ and $\widetilde{KE}_6^1$ for January 12 to 16, 1959.
Units: 10^4 ergs/cm^2 mb for KE(1) and 10^3 dkm^2 for $\widetilde{KE}_n^m$.

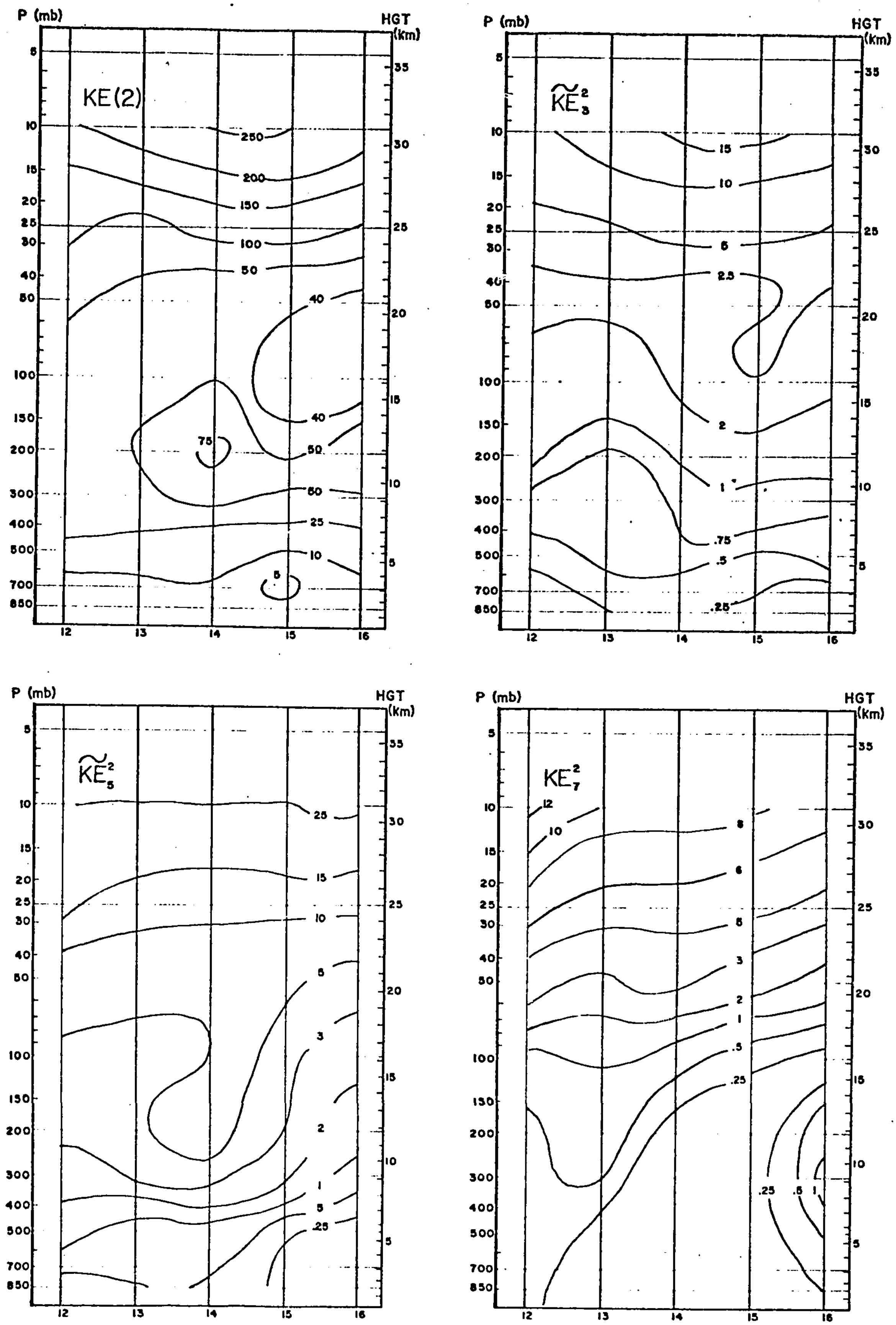

Fig. 4.3.3 Kinetic energy for longitudinal wave number 2, KE(2), and pseudo-kinetic energy of the spherical harmonics $\widetilde{KE}_3^2$, $\widetilde{KE}_5^2$ and $\widetilde{KE}_7^2$ for January 12 to 16, 1959.
Units: 10^4 ergs/cm^2 mb for KE(2) and 10^3 dkm^2 for $\widetilde{KE}_n^m$.

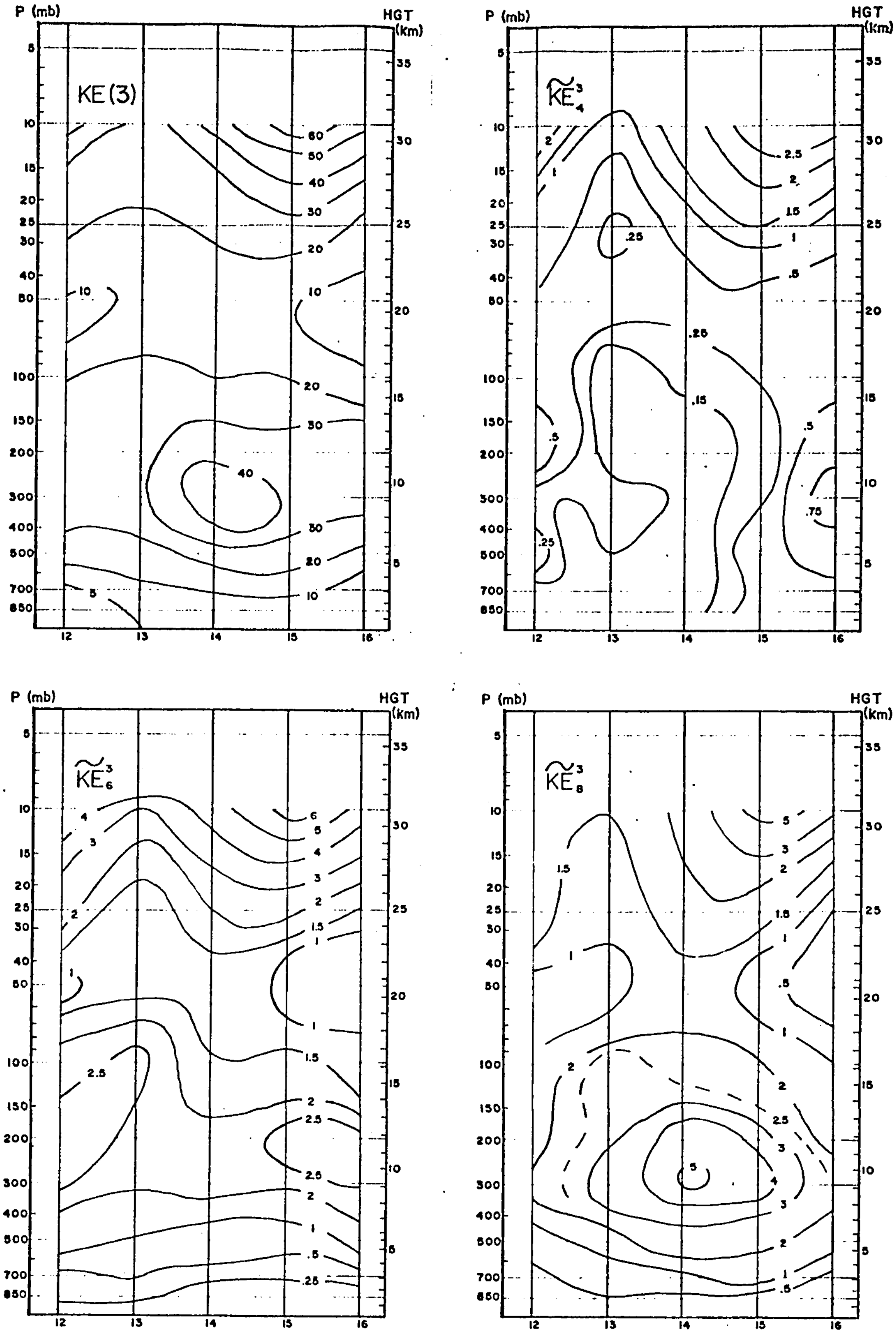

Fig. 4.3.4 Kinetic energy for longitudinal wave number 3, KE(3), and pseudo-kinetic energy of the spherical harmonics $\widetilde{KE}_4^3$, $\widetilde{KE}_6^3$ and $\widetilde{KE}_8^3$ for January 12 to 16, 1959.
Units: 10^4 ergs/cm^2 mb for KE(3) and 10^3 dkm^2 for $\widetilde{KE}_n^m$.

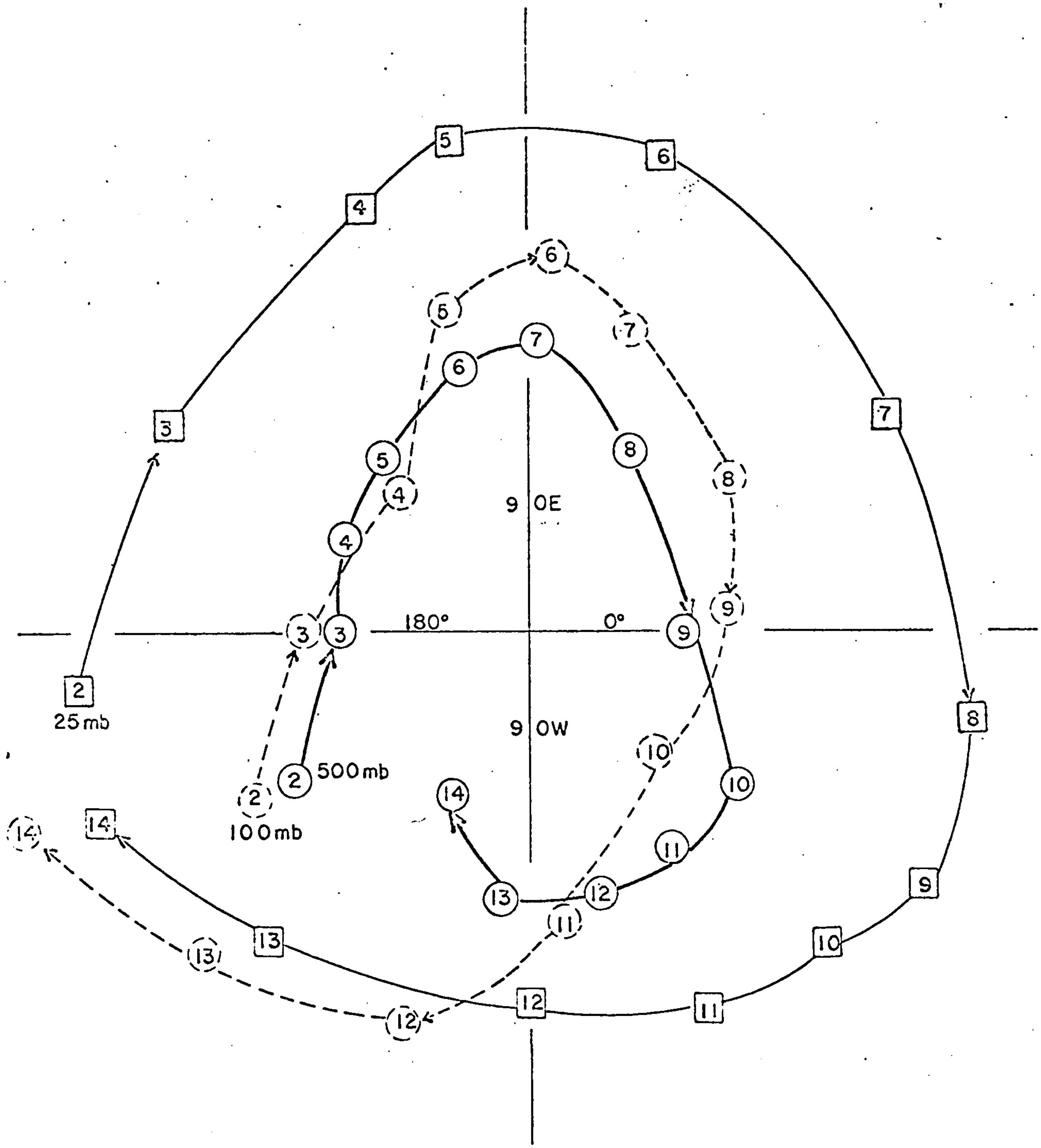

Fig. 4.3.5. Harmonic dial of the separated moving components of planetary wave Z_2^1 taken from daily values of the geopotential height at 500, 100 and 25 mb during January 1959. Enclosed numbers are central dates for 3-day running means showing relative amplitude and position. The waves at the three levels appear to move closely in phase and are retrogressive. (After Boville (1966)).

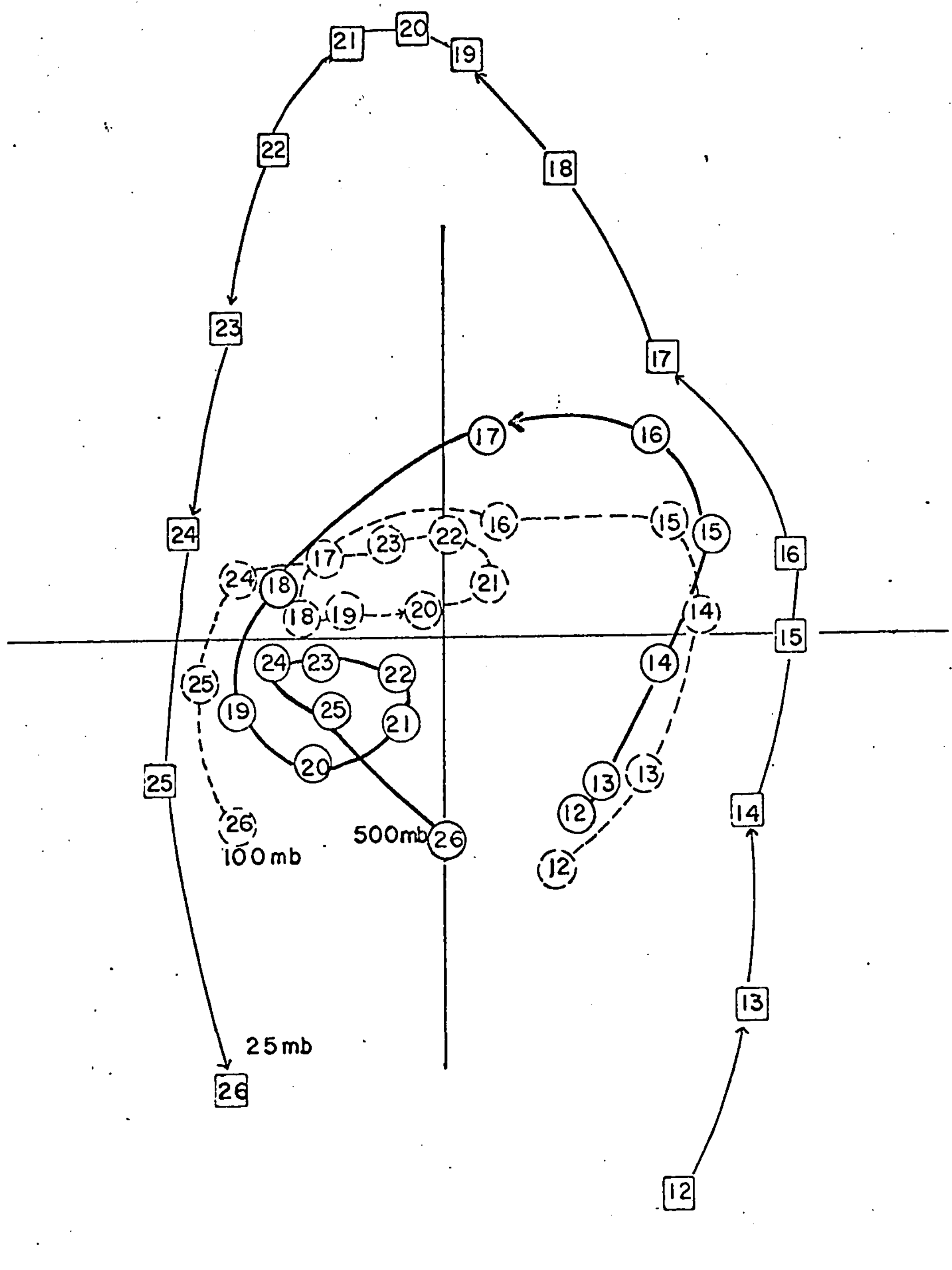

Fig. 4 3.6. Harmonic dial of separated moving components of planetary wave Z_5^2 for January 1959. There is general phase correspondence over the two week period and waves are progressive.(After Boville 1966)

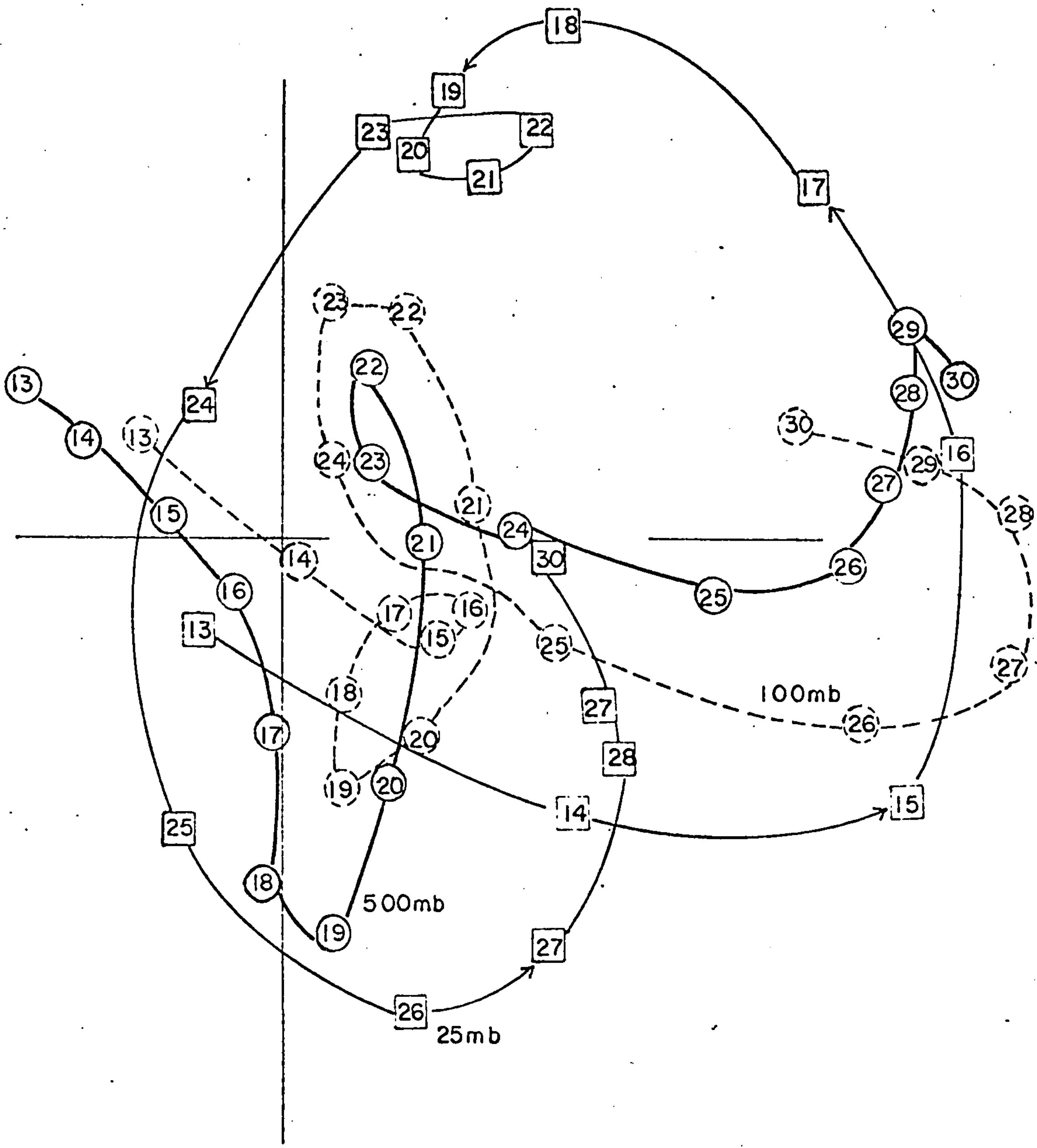

Fig. 4.3.7. Harmonic dial of separated moving components of planetary wave Z_6^3 for January 1959. There is still a general correspondence in phase of this progressive wave. (After Boville (1966)).

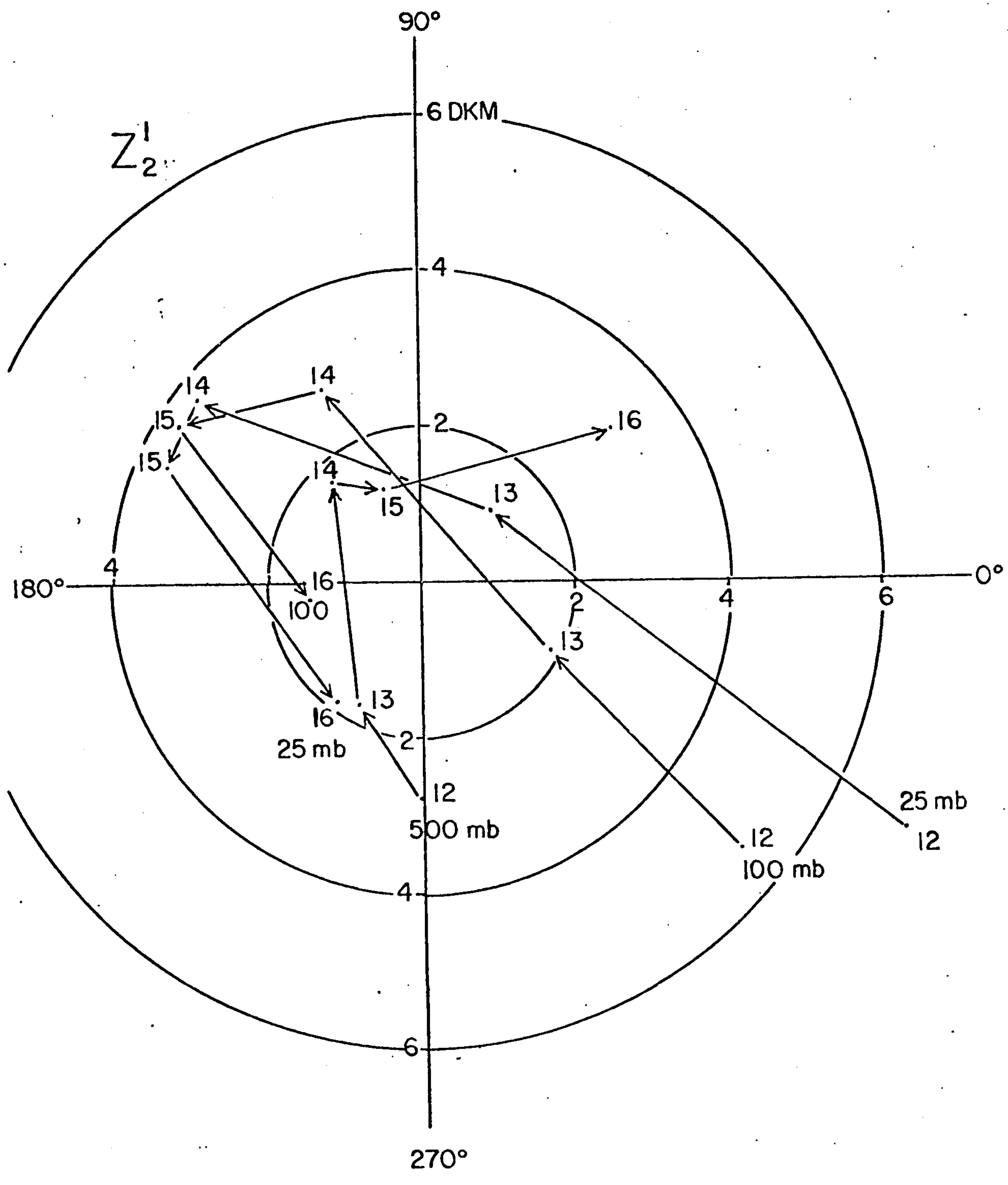

Fig. 4.3.8. Harmonic dial of separated moving components of planetary wave Z_2^1 for January 12 to 16, 1959.
Units: Dekameters.

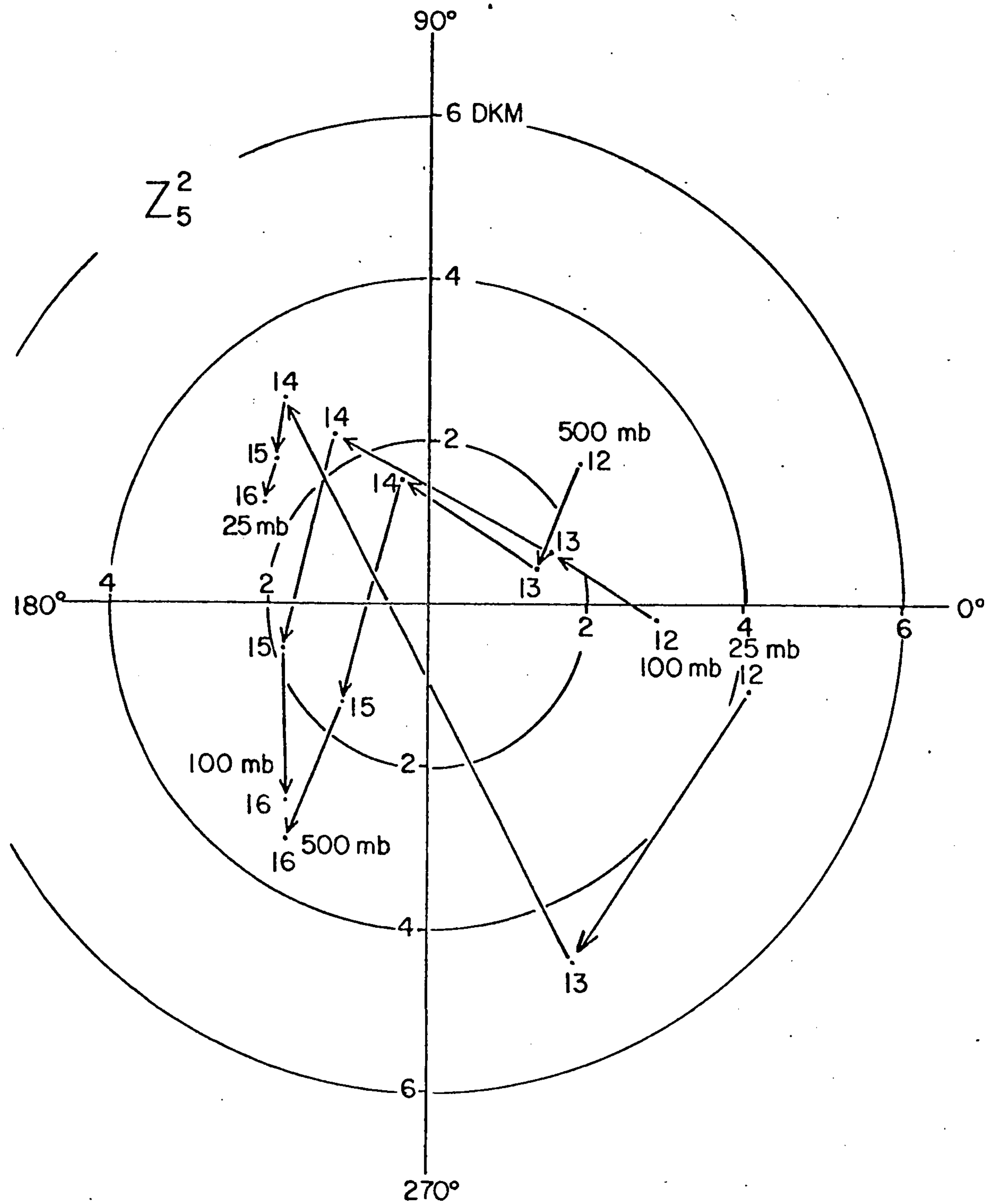

Fig. 4.3.9. Harmonic dial of separated moving components of planetary wave Z_5^2 for January 12 to 16, 1959.
Units: Dekameters.

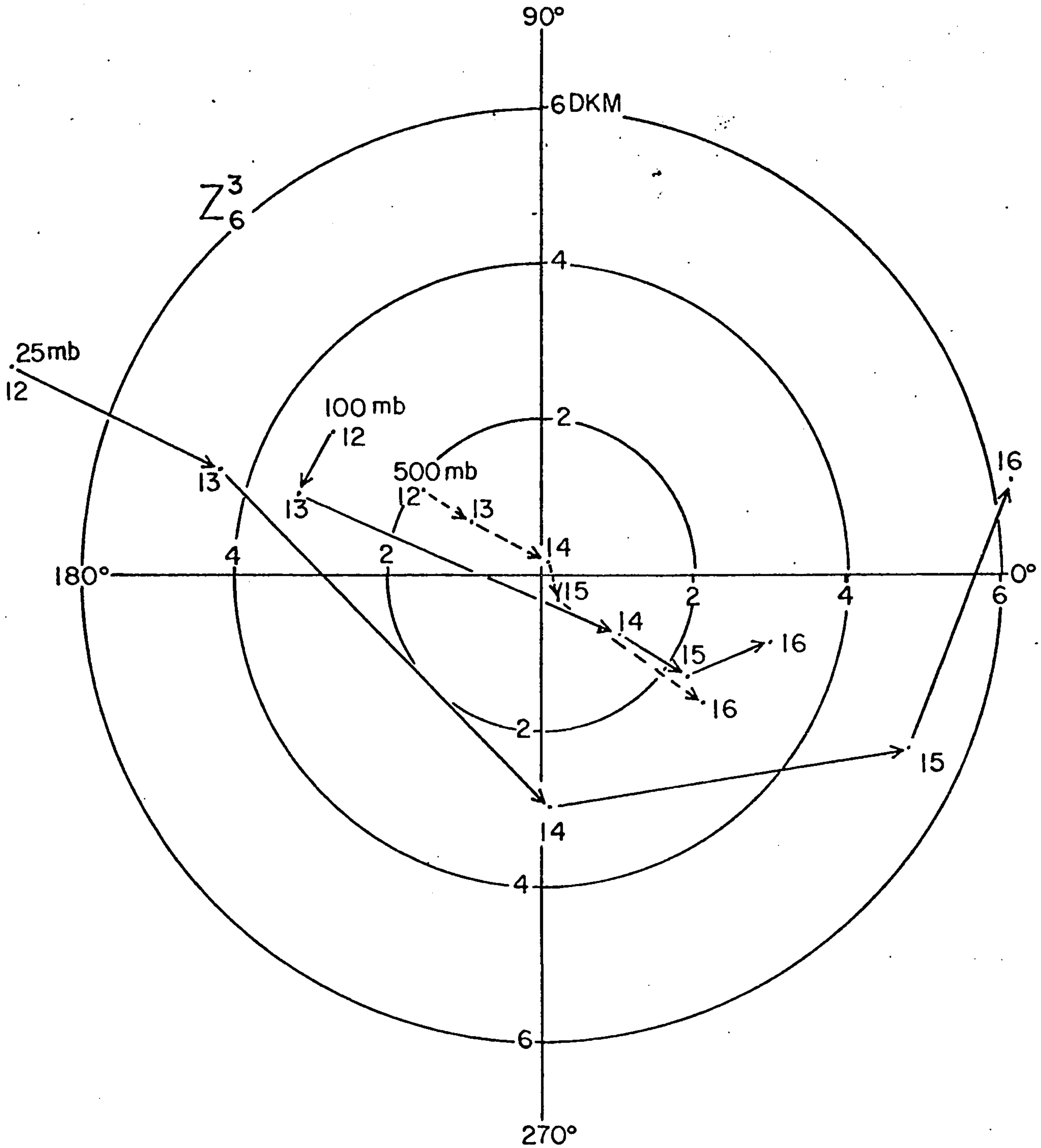

Fig. 4.3.10. Harmonic dial of separated moving components of planetary wave Z
for January 12 to 16, 1959.
Units: Dekameters.

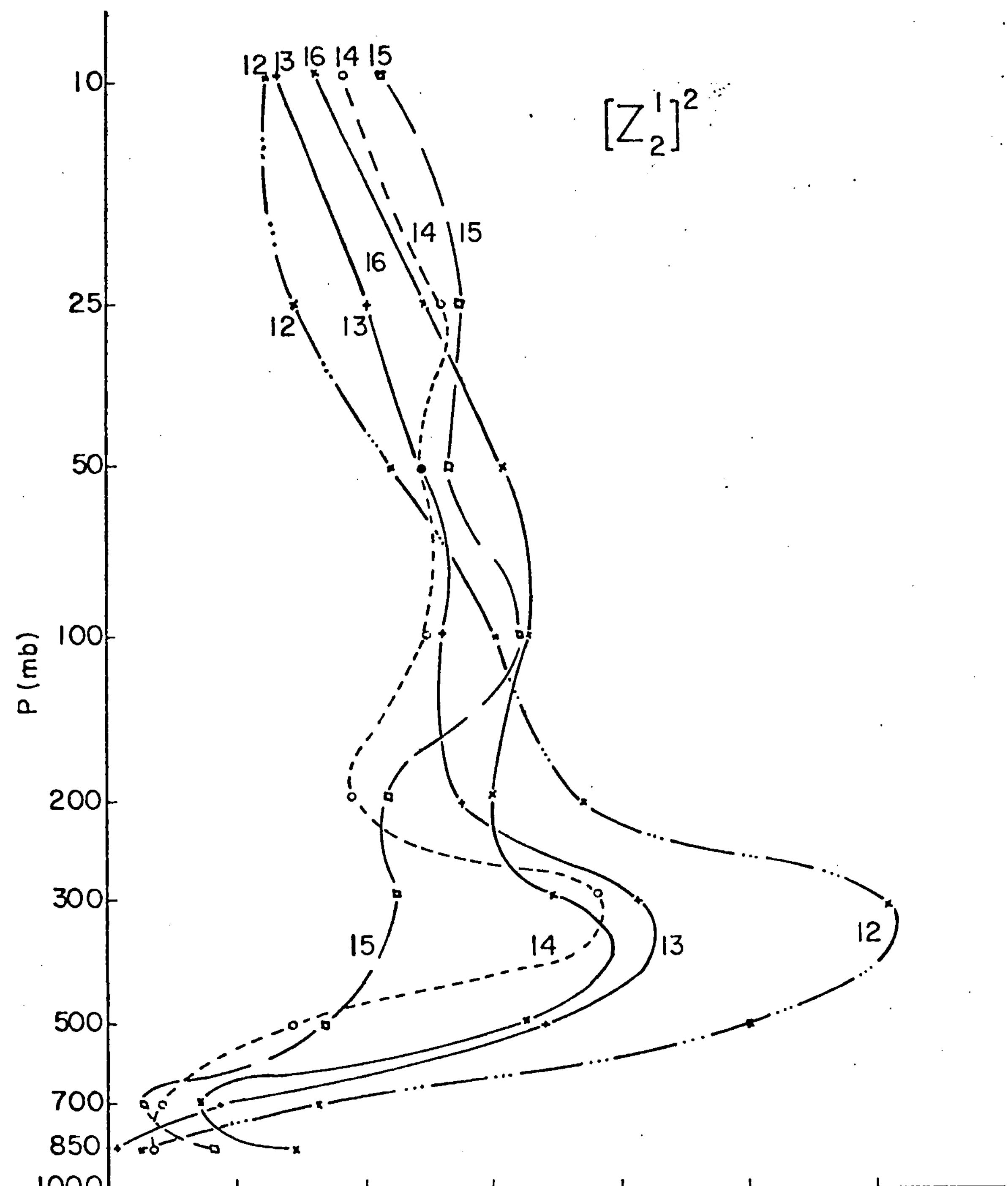

Fig. 4.3.11. Vertical distribution of the kinetic energy density analog for January 12 to 16, 1959. Relative units.

CHAPTER 5

MONTHLY MEAN AND DAILY ENERGETICS OF JANUARY 1959

5.1 Synoptic Description of Events in January 1959

Tropospheric synoptics

January 1959 showed a very stable and persistent weather pattern. It was very similar to the December 1958 pattern and had the lowest January zonal index of the decade (Stark, 1959). A pulsating blocking regime persisted through the mouth in the troposphere. This pulse had a period of about 10 to 12 days.

Three maxima in the 500-mb block are found in mid-latitude during this month. The maxima in the blocking circulation, as inferred from Fig. 4.2.18 which depicts the daily and latitudinal distribution of the 500-mb mean zonal winds, may be localized in mid latitudes in the periods: 7th to 9th, 16th to 19th, and near the end of the month. The daily height variance at 50°N and 500 mb, as portrayed on Fig. 5.1.1, yields results which are in phase with the zonal winds variations: the maxima of this variance occur on the 9th, the 18th to 20th and the 27th.

The peaks in the 500-mb temperature variance coincide fairly well with those of the heights fields. A significant difference is found in that the trend of the height variance is to increase throughout the month whereas the temperature variance shows the reverse trend, indicating a gradual decrease in the total available energy in the troposphere during this month.

Stratospheric synoptics

The sequence of events in the stratosphere in January 1959 will be depicted with reference to the 25-mb height and temperature maps. The description given by Boville, Wilson and Hare (1961), Steiner (1961) and Godson and Wilson (1963) is summarized here. The end of December 1958 presented a circumpolar vortex with temperatures below -80°C and a contrasting maximum temperature of -45°C near Japan. By the 3rd of January, local deepening was in progress with three large troughs over North America, western Europe and eastern Asia. A widespread high covered the whole north Pacific as the -45°C isotherm spread from the area north of Japan to the whole of Kamchatka. The progress of a warm wave and its associated trough across North America from the 8th to the 18th has been described by Godson and Wilson (1963) and Boville "et al" (1961). During this period, the eccentricity of the flow increased as the centre of the polar vortex shifted towards Europe. From the 18th to the end of the month, the polar vortex retrogressed over the Canadian Archipellago with a very specific reorganization in the contour structure. The strong warm high which had covered the north Pacific and western Canada on the 18th collapsed as the North American trough retrogressed to a central Canada-midwestern U.S. line near the end of the month. The western European trough collapsed while the eastern Siberian trough strengthened somewhat. Visually, the 25-mb flow pattern near the end of the month was remarkably bipolar and symmetric about the pole.

5.2. Behaviour of the Various Energy Modes during January 1959

The activity occurring in the troposphere, lower stratosphere and middle stratosphere is interpreted through the computed energetics of the 500-mb, 100-mb and 25-mb pressure levels, respectively.

A gross description of the events in the three layers is presented by the daily variations in the zonal and eddy modes of available and kinetic energy in Figs. 5.2.1, 5.2.2 and 5.2.3. Associated with the warmings of January 1959, the atmosphere shows three main changes in the energies which are more or less coherent in the vertical. Fig. 5.2.1 shows that early in the month, at 500-mb, a sharp decrease in AZ coincides with a large increase in AE. The AZ curves flattens from the 4th to the 5th, while AE reaches a maximum on the 4th. As

AE decreases rapidly from the 4th to the 7th, KE reaches a maximum on the 7th. The variation in AZ is somewhat incoherent, except that as KE decreases monotonically to a minimum on the 13th-14th, AZ reaches a relative maximum on those dates, while a net maximum in KZ is shown on the 16th. To re-start the cycle, AZ, after being at its lowest value on the 10th, increased gradually to a maximum on the 17th and 19th, while AE, a minimum on the 12th, increases more or less with AZ to reach a general maximum on the 18th and 20th. There is a difference in KE in this cycle, since it shows a maximum simultaneously with AE on the 18th. As KE decreases rapidly afterwards until the 22nd, KZ goes in the reverse direction to reach a maximum on the same day. From the 22nd on, KZ does not show a trend, but oscillates about a mean value. AZ reaches a local minimum on the 21st and increases more or less monotonically to a plateau on the 26th and 27th, falling rapidly thereafter. AE decreases at a fair rate in the 20-25th period, in opposition to the rates shown in AZ, but reaches a maximum one to two days later than AZ, i.e., on the 28th. Hence to summarize the series of events during January 1959, we present the following approximate cycle, noting dates on which the maxima in the various modes coincide:

AZ (about 1 January)→AE(5 January)→KE(7th)→KZ(13th-14th and 16th)→AZ (17th)→AE(18th and 20th)↔KE(18th)→KZ(22nd)→AZ(26th-27th)→AE(28th)↔KE(28th). The 500-mb level shows a more or less normal tropospheric cycle between the various energy modes. A period of about 11 days appears in the energy cycle. Winston and Krueger (1961) have noted similar energy pulses in the exchanges for the period of mid-December 1958 to mid-January 1959. The so-called normal tropospheric cycle of AZ→AE→KE→KZ has been found by most studies in winter. It may be noted that the pulses in the eddy kinetic energy coincide with the pulses in the 500 mb blocking patterns described earlier. The existence of another energy cycle of about twice the frequency but of lower amplitude will be presented later in this chapter. For the purpose of later comparisons with upper events, the 500-mb data show maxima in the eddy kinetic energy on the 7th, 18th and 28th.

Fig. 5.2.2 depicts the daily variations in the various energy modes at 100 mb during the month. The zonal available energy, AZ, is flat most of the month with higher values towards the end of the period. The eddy available energy shows a monotonic climb after the 8th, a flat maximum from the 17th to the 19th, and then subsides steadily to its lowest value on the 26th. AE and KE show rather low negative correlation for the month; during the 14th-17th period a significant increase in AE occurs at the same time as a large decrease in KE, suggesting dominance of the negative baroclinic process KE$\rightarrow$AE as shown earlier in the 5-day mid-January study. The KE reservoir seems to be affected by two oscillations superposed over each other. During the first half of the month, the eddy kinetic energy is slightly larger than during the second half. A second cycle, having a 5-day period, emerges in a striking manner; peaks are found on the 3rd, 8th, 13th, 18th-19th, 23rd and 28th of January 1959. The zonal kinetic energy variations do not seem to be too well organized with respect to the KE variations.

Fig. 5.2.3 depicts the daily fluctuations in the energy reservoirs at 25 mb during the month in question. The available energies AE and AZ show a good negative correlation with one period of about three weeks. From the 10th to the 15th, we have the energy flow AZ$\rightarrow$AE in progress, while it reverses its direction in the next part of the period. The eddy kinetic energy fluctuations have remarkably large amplitudes throughout the month. Many different time scales are involved. The main maxima are found on the 3rd, 9th, 17th and 28th. Of significance to the previous 5-day study is the large increase in eddy kinetic energy which starts on the 10th and reaches its maximum value on the 17th. It has been shown earlier that wave number 1 was the largest contributor to the eddy kinetic energy in the stratosphere. It is instructive to compare the scales involved in the large fluctuations during January 1959. Fig. 5.2.4 depicts the spectral behaviour in the eddy kinetic energy for waves 1, 2, and 3. It is interesting to note that whereas the eddy kinetic energy at wave number 1 was dominant during the 15th-18th period, wave 2 played the main role in the peaks on the 9th and 28th. Wave 3 explains a minor fluctuation on the 5th and is shadowed in the total case on the 25th by the rapid drop of KE(1). All in all, the net changes in the total eddy kinetic energy seem to be composed of three main time fluctuations with periods of about 20 days. It is of course difficult to give any weight to these large time scale processes because of our limited time series, but it is thought that they may be referenced and tested with subsequent data. In any case, had the kinetic energy at wave number 2 been in phase with wave 1, the eddy kinetic energy would have been within 50×10^4 ergs/cm^2 mb of the eddy kinetic energy computed by Perry (1966) on January 25, 1963 for the 30 mb to 10 mb layer, coinciding with the January 1963 major sudden warming in the stratosphere. Notwithstanding non-linear interactions, assuming a) a 20-day period in all the waves fluctuations, b) taking the three large scales, i.e. n = 1, 2 and 3, as the only significant ones, c) accepting a tolerance of $\pm \pi/6$ of a cycle, i.e., accepting only 6 in/out phase positions, and d) assuming that the waves are randomly distributed with respect to each other in time, then the probability for the waves to become in phase simultaneously over the six winter months is:

$$(1 \times 1/6 \times 1/6) \quad (6 \times 30)/20 = 1/4,$$

or once every 4 years. The observed frequency of a major warming once every 4 years seems to support this crude statistical computation, and may serve to show that major warmings need strong wave phasings, whether they are random or interrelated.

5.3. Total, Eddy and Spectral Correlations in January 1959

The 30-day data do not possess the high vertical resolution of the earlier 5-day study. In order to get the most of the available information in the vertical, Boville (1961) has correlated spectral kinetic energies between 500 mb and 25 mb. A relatively high correlation coefficient of 0.68 was found for the kinetic energy values (5 days apart) of wave number two. Teweles (1963) also used the correlation method in an effort to find significant inter-level, interwave and interlatitude relationships. Perry (1966) has investigated the spectral and interlevel relationships of the height and temperature fields. Following his notation, the average correlation coefficient of two arbitrary fields "f" and "g" may be written as:

$$r_{fg} = \frac{\sigma_{fg}}{\sigma_f \, \sigma_g} \tag{5.3.1}$$

where the average variance σ_f^2 or σ_g^2 on a spherical grid between latitudes ϕ_1 and ϕ_2 is given by:

$$\sigma_f^2 = \frac{1}{2\pi(\sin\phi_1 - \sin\phi_2)} \int_{\phi_1}^{\phi_2} \int_0^{2\pi} f^{*2} \cos\phi \, d\lambda \, d\phi \tag{5.3.2}$$

and the covariance σ_{fg} of the two given fields "f" and "g" is:

$$\sigma_{fg} = \frac{1}{2\pi(\sin\phi_1 - \sin\phi_2)} \int_{\phi_1}^{\phi_2} \int_0^{2\pi} f^* g^* \cos\phi \, d\lambda \, d\phi \tag{5.3.3}$$

Expanding "f" and "g" into their area mean, latitudinal and zonal deviations, the following two relationships emerge:

$$\sigma_f^2 = \left\{ \overline{f}''^2 \right\}^{\phi} + \sum_{m=1}^{\infty} \left\{ \Phi_{ff}(m) \right\}^{\phi} \tag{5.3.4}$$

$$\sigma_{fg} = \left\{ \overline{f}'' \, \overline{g}'' \right\}^{\phi} + \sum_{m=1}^{\infty} \left\{ \Phi_{fg}(m) \right\}^{\phi} \tag{5.3.5}$$

We partition the correlation coefficient defined in Eqn. (5.3.1) as:

$$r_{fq} = \overline{r_{fq}}^{\lambda} + \sum_{m=1}^{\infty} R_{fq}(m) \tag{5.3.6}$$

The first term on the right-hand side of Eqn. (5.3.6) is the part of the areal correlation due to the zonal means, i.e.:

$$\overline{r_{fq}}^{\lambda} = \frac{1}{(\sigma_f^2 \ \sigma_q^2)^{1/2}} \left\{ \overline{f}'' \ \overline{q}'' \right\}^{\phi} \tag{5.3.7}$$

The second term of Eqn. (5.3.6) is the portion of the correlation due to various scales, i.e.,

$$R_{fq}(m) = \frac{1}{(\sigma_f^2 \ \sigma_q^2)^{1/2}} \left\{ \Phi_{fq}(m) \right\}^{\phi} \tag{5.3.8}$$

The total correlation r_{fq}, the eddy contribution to total correlation $\sum_{m=1}^{15} R_{fq}(m)$ and the individual spectral contributions $R_{fq}(m)$, for n = 1, 2 and 3 are depicted in Figs. 5.3.1, 5.3.2 and 5.3.3, as applied to the three possible interlevel combinations of the height data at 500, 100 and 25 mb, when taken two at a time. The total correlation of the 25-500 mb heights on Fig. 5.3.3 appears to be least of the three sets of correlation coefficients, as might have been expected. It is also the most variable during the month and averages about 0.6. Both 100-500 mb and 25-100 mb total correlation coefficients oscillate about the 0.85 mark, but the former set shows larger daily amplitude oscillations during the month. The comparison of the total correlation against the portion explained by the eddies, yields an overall dominance of the latitudinal means in interlevel correlations. This total positive correlation shows that the atmosphere is regulated by a general cold polar vortex at this period of the year. Between January 17th to 20th, the mean zonal correlation part is least between the three pairs, reflecting the least symmetry between the mean zonal heights of the latitudes. This coincides with the strongest tropospheric block and stratospheric warming during the month.

The troposphere (500 mb) and lower stratosphere (100 mb) relationship during January may be seen on Fig. 5. 3. 1. Maxima in the eddy contribution to the total correlation are shown to occur on the 4th, 10th, 20th and 28th-29th. These maxima may be explained in order of magnitude mostly by wave 3 for the first maximum, then by waves 2, 3 and 1 for the second peak, then by waves 1 and 2 for the third maximum and by waves 2 and 1 in the last case.

The lower stratosphere (100 mb) and the middle stratosphere (25 mb) height correlations are exhibited in Fig. 5. 3. 2. The total eddy correlation coefficients show two regions of rising values: the first one between the 2nd and the 20th of January, and the second from the 25th to the 30th. They differ from the 500-100 mb coefficients in that the early January maximum is non-existent in the stratosphere. The breakdown into the wave number domain is diagnostically rewarding. The month can be partitioned into four regimes. In early January, the wave number 1 contribution to the 25-100 mb set decreases rapidly so that wave 3 explains about 50 percent of the total eddy portion. By the 20th, when the total eddy contribution has attained its peak (0. 27), 80 percent is explained by wave 1. The decreasing role of wave 2 in the post-14th period reverses again after the 26th in such a way that it contributes about 2/3 of the eddy portion by the 30th of January. In order to inspect a possible vertical structure, Table 5. 3. 1 has been constructed showing the date of various maxima in the spectral contribution to the eddy correlation coefficients of the three chosen interlevel sets.

Table 5.3.1. Spectral contribution given as a percentage of the eddy contribution to the total interlevel height correlation coefficients at time of maximum relationship during January 1959.

Layer (mb)	Wave No.	1	2	3
100-25	Date	2 X 20 30	2 19 14 22 30	5 X 26
	% contribution	51 X 80* 24	40 59 40 26 65**	50 X 16
500-100	Date	2 11 21 29	3 10 14 20 27	4 19 26
	% contribution	25 23 32 37	36 28 37 30 43	54 33 23
500-25	Date	X X 21 28	4 10 14 20 30	5 X 26
	% contribution	X X 55 28	44 50 45 47 71	81 X 23

* The largest single wave contribution: 0.3 out of a total correlation coefficient of 0.86.

** The second largest single wave contribution: 0.18 out of a total correlation coefficient of 0.88.

Table 5.3.1 shows good vertical coherence in wave 1 scales about the 21st, in wave 2 on the 2nd, 10th to 14th, 20th to 22nd and 30th, and lastly in wave 3 about the 4th and 5th and also 26th. Referring to the 20-day cycle in eddy kinetic energy of all wave 1, 2 and 3 flows, a variation in time of similar frequency is found to exist in the spectral correlations at the same large scales for the 25-100 mb interrelationship of the height field. The spectral correlation associated with wave 1, 2 and 3 shows a higher harmonic behaviour in time, where the 3 waves appear to have periods near 10 days but with lesser amplitudes. It appears then that in the vertical, periodic time oscillations of the largest space scales have some vertical coherence in time scales of about 20 days, while a superposed period of about 10 days is attached to the spectral correlations between the same scales but to the two lower levels of 500 mb and 100 mb.

The spectral contributions of waves 1, 2 and 3 to the correlation between the 500 and 25-mb levels in the geopotential height field may be seen in Fig. 5.3.3. As mentioned before, the total correlation is smaller than the other two-level combinations, and a large daily variability is found. The eddy contribution is rather small during the first half of the month, contributing less than 0.1 to the total correlation coefficient of 0.6. Some steady rise follows on after the 17th and a first maximum is reached on the 21st (0.12). The highest monthly value of 0.19 is attained on the 30th. The spectral contribution to the correlation exhibits some similarities with the other two cases, but also shows differences. The 20-day cycle is still apparent in all three wave numbers (1, 2 and 3). A superposed cycle of twice this frequency is also present. Referring to Fig. 5.2.4 of the previous section and Fig. 5.3.3 here, it is concluded that the relatively large positive correlations in waves 1, 2 and 3 occur in periods of high kinetic energy activity in those scales at 25 mb.

The daily fluctuations in the spectral correlation will be described next. On the 5th, wave number 3 explains 81 percent of the whole eddy contribution, being the dominant scale during the first week. From the 10th to the 14th, wave 2 leads the spectral 25-500 mb geopotential interrelationship. The gradual take-over by wave number 1 kinetic energy at 25 mb during the third week of the month is reflected in the maximum wave 1 correlation on the 21st. The bi-polarity of the 25 mb flow dominates by the 25th, as shown by both the kinetic energy and the 25-500 mb correlation at this scale.

The gross temperature interlevel correlation has also been computed but has not been reproduced graphically. The temperature covariances between the 500-25 mb and the 100-25 mb layers are positive throughout the month, but the 500-100 mb temperature covariance is on the other hand uniformly negative. The signs of the covariances are vouched for by the mean monthly zonal temperature profiles in the meridional direction. At 25 mb, the warm belt is at about 40°N while it is displaced further north to 50°N at 100 mb. At 500 mb the meridional temperature gradient is uniformly positive. The negative meridional temperature gradient at 100 mb covers a large enough area to make its areal covariance with the 500 mb temperature negative, while it is not large enough to yield a similar negative value for the covariance between the 25 mb and the 100 mb temperatures. On the other hand, the smaller negative temperature gradients south of $40^{o}N$ at 25 mb do not succeed in reversing the sign of the areal covariance between this level and the 500 mb temperature field.

From the preceding discussion, some vertical and time coherence in wave numbers 1, 2 and 3 has been shown, although the results are not conclusive on their own. A further detailed study must be performed in order to assess the indefinite conclusions of the above correlation approach. The needed particulars will be included in the following sections of this chapter.

5.4 Introductory Remarks about the Daily Computed Energetics during January 1959.

The energetics of January 1959 will be described in this section using an approach similar to that of the previous chapter wherein the chosen 5-day period was treated in detail. The present study, in contrast to the 5-day study which had vertical detail but a relatively short time duration, has a crude vertical resolution but a longer duration in time.

Some simplifications have been made in the energy budget equations given in Chapter 3. In general, all terms associated with the vertical motion correlation other than the CE and CZ terms have been omitted. This follows the usual procedure of most earlier studies which either lacked vertical motion or decided not to use it because of the relatively small values yielded by the correlation in question. The results computed for the 5-day period have been used to estimate the order of magnitude of the deleted terms.

The transfer between the zonal to eddy kinetic energy is rewritten here for easy reference:

$$CK(m) = -\frac{1}{\Delta p}\int_{p_1}^{p_2}\Big\{\underset{(A)}{\Phi_{uv}(m)\,\frac{\cos\phi}{a}\,\frac{\partial}{\partial\phi}\Big(\frac{\bar{u}^{\lambda}}{\cos\phi}\Big)} + \underset{(B)}{\Phi_{vv}(m)\,\frac{1}{a}\,\frac{\partial \bar{v}^{\lambda}}{\partial\phi}}$$

$$-\underset{(C)}{\frac{\tan\phi}{a}\,\bar{v}^{\lambda}\,\Phi_{uu}(m)} + \underset{(D)}{\Phi_{\omega u}(m)\,\frac{\partial \bar{u}^{\lambda}}{\partial p}} + \underset{(E)}{\Phi_{\omega v}(m)\,\frac{\partial \bar{v}^{\lambda}}{\partial p}}\Big\}^{\phi}\frac{dp}{g} \qquad (3.2.5)$$

It is found that the terms (D) and (E) in Eqn. (3. 2. 5) above are, on the average, 2 or 3 orders of magnitude smaller than the smallest of (A), (B), and (C). It is recalled that $\bar{v}^{\lambda}$ was obtained from known vertical motion zonal values through the equation of continuity. The vertical resolution in the present chapter prohibits the use of this method, hence it has been necessary to reject terms (B) and (C) of Eqn. (3. 2. 5). This deletion is not as fortunate as the previous simplification.. Although $\bar{v}^{\lambda}$ and $\partial\bar{v}^{\lambda}/\partial\phi$ are small with respect to $\bar{u}^{\lambda}$ and $\partial\bar{u}^{\lambda}/\partial\phi$ respectively, by 1 to 2 orders of magnitude, $\Phi_{uu}(n)$ may be of the order of $\Phi_{uv}(n)$ or even larger, which could make the (C)-term occasionally not significantly smaller than the (A)-term. On occasions, the (C)-term may be numerically larger than a below average (A)-term. This phenomenon appears on the 14th of January 1959, at 100 mb.

The non-linear kinetic wave interaction LK(n)-term has been found to be:

$$LK(m) = \frac{1}{\Delta p}\int_{p_1}^{p_2}\Big\{\sum_{\substack{m=-\infty\\ \neq 0}}^{\infty} U(m)\Big[\underset{(A)}{\frac{1}{a\cos\phi}\Psi_{uu_{\lambda}}(m,n)} + \underset{(B)}{\frac{1}{a}\Psi_{vu_{\phi}}(m,n)} + \underset{(C)}{\Psi_{\omega u_{p}}(m,n)} - \underset{(D)}{\frac{\tan\phi}{a}\Psi_{uv}(m,n)}\Big]$$

$$+V(m)\Big[\underset{(E)}{\frac{1}{a\cos\phi}\Psi_{uv_{\lambda}}(m,n)} + \underset{(F)}{\frac{1}{a}\Psi_{vv_{\phi}}(m,n)} + \underset{(G)}{\Psi_{\omega v_{p}}(m,n)} + \underset{(H)}{\frac{\tan\phi}{a}\Psi_{uu}(m,n)}\Big]\Big\}^{\phi}\frac{dp}{g} \qquad (3.2.25)$$

A frequency test based on the occurrence of magnitudes above an arbitrarily assigned value was made on the eight terms of Eqn. (3.2.25), at different data levels. Terms (A) and (B) appeared most frequently in the given order. They were especially large near 30°N at 300 mb and near 55°N to 65°N at 10 mb, in relation to the jets at those levels. Of interest, the terms (C) and (G) (both involving the vertical motion) were found on the average to be two to three orders of magnitude smaller than their neighbours, but under very specific conditions they rose to within one order of magnitude of the other terms: in the stratosphere (10, 25 and 50 mb), for wave 1 at 60°N. This may be interpreted to imply almost significant exchange of energy into wave 1 from the spectral inter-relation between vertical motion and vertical wind shear locally.

Recalling that:

$$\Lambda = -\left(\frac{p}{p_0}\right)^{\mu} \frac{R}{p} \left(\frac{\partial}{\partial p}\left\{\overline{\theta}^{\lambda}\right\}\right)^{-1} \qquad (3.1.2)$$

it is seen that a stability parameter is needed to compute the available energy and its transfers. Because of the relative scarcity of the data in the vertical, the mean 5-day values of $\partial\{\overline{\theta}^{\lambda}\}^{\phi}/\partial p$ computed in the previous chapter have been used as a daily constant at 25, 100 and 500 mb. The largest relative errors (deviation of the daily values from the 5-day mean in $\partial\{\overline{\theta}^{\lambda}\}^{\phi}/\partial p$) were found to be 2%, 3% and 13% at 25, 100 and 500 mb, respectively. The differences at 25 mb and 100 mb are negligible while they may not be so at 500 mb. The 5-day mean $\hat{\sigma}$, given by:

$$\hat{\sigma} = \widehat{\frac{\partial T}{\partial p} - \frac{RT}{p c_p}} = \widehat{\frac{T}{\theta}\frac{\partial \theta}{\partial p}} \qquad (5.4.1)$$

are compared with the mean January values as given by Gates (1961) on Fig. 5.4.1. The two vertical profiles are shown to be fairly coincident up to 40 mb, the highest level in Gates's paper. According to this, we have concluded that it was fairly safe to use the 5-day computed mean as an approximation to the daily stability values for January 1959. The simplified stability assumption will affect the energy exchanges between kinetic and available energy.

The conversion from zonal to eddy available energy is reproduced again here.

$$CA(m) = -\frac{1}{\Delta p}\int_{p_1}^{p_2} \Lambda \Big\{ \underset{(A)}{\frac{1}{a}\frac{\partial\bar{\Theta}''}{\partial\phi}\Phi(m)_{v\theta}} + \underset{(B)}{\frac{\partial\bar{\Theta}''}{\partial p}\Phi(m)_{\omega\theta}} \Big\}^{\phi} \frac{dp}{g} \qquad (3.2.8)$$

From computations performed in the 5-day study, on the average term (B) above manages to remain one to two orders of magnitude smaller than the (A)-term. It is then deleted, adding little error in a study of this type.

The boundary terms dealing with the available energy modes have been deleted altogether. Table 5.4.1 sums up the order of magnitude of those terms with respect to unit transfer.

Table 5.4.1. Orders of magnitude of some boundary terms of the available energy budget with respect to the transfer unit of 1 erg/cm^2 mb sec, based on results taken during the 12-16 January 1959 period.

Terms	BAZFI	BAEFI(n)	BAZP	BAEP(n)
Orders of magnitude	-3 to -5	-3 to -5	-1 to -2	-1 to -2

The non-linear wave interaction of the eddy available energy is also associated with the stability-term Λ and some vertical motion correlations. Its expansion is recalled here:

$$LA(m) = \frac{1}{\Delta p}\int_{p_1}^{p_2} \Lambda \Big\{ \sum_{\substack{m=-\infty \\ \neq 0}}^{\infty} Q(m) \Big[\underset{(A)}{\frac{1}{a\cos\phi}\Psi(m,m)_{u\theta_\lambda}} + \underset{(B)}{\frac{1}{a}\Psi(m,m)_{v\theta_\phi}} + \underset{(C)}{\Psi(m,m)_{\omega\theta_p}} \Big] \Big\}^{\phi} \frac{dp}{g} \qquad (3.2.26)$$

Term (C) has been deleted. It has not been computed separately earlier, but an idea of its magnitude may be inferred from results using both methods, notwithstanding the slight modification in Λ. For the three levels presently investigated, for wave numbers 1 to 6, the residual indicates that the (C)-term is negative most of the time. The magnitude of the absolute error for the sum over "n" is less than 0.3 erg/cm^2 mb sec at 25 and 100 mb, becoming as large as 1 erg/cm^2 mb sec at 500 mb, where the vertical motion is much larger. The strong wave interaction values are found to be as high as 1 erg/cm^2 mb sec in the stratosphere, making a possible error of 30% associated with the deletion of this term. At 500 mb, strong interactions give exchanges up to 2 ergs/cm^2 mb sec, leading to a possible maximum relative error of 50%. These are, of course, large errors, but they are maxima in the error field, their average may be approximated to half of these values since the deleted term is very noisy, being a triple correlation.

It has been noted earlier, in Chapter 2, that both vertical motion models used in this study gave similar patterns, but when correlated to a common third field, occasionally significantly different results occurred. The numerical, physical and mathematical differences between the two models have been described in Chapter 2, but a further systematic error creeps in when the adiabatic thermodynamic vertical motion method is used as explained by Wiin-Nielsen (1964b) and Muench (1965). The computation of the transfers between the available and kinetic energy using the above vertical motion model, gives the rate of change of the available energy from both the kinetic energy exchanges and the generation from radiative and other diabatic effects. Any other vertical motion model which does not use local temperature changes in time will tend to approximate the kinetic-available energy exchanges only. This phenomenon has been used by Julian and Labitzke (1965) and Perry (1966) to infer the generation of available energy with success. Letting CE* and CZ* be the eddy and zonal conversions between the corresponding modes of available to kinetic energy computed from the adiabatic-thermodynamic equation, we have, following Muench

(1965) and/or Wiin-Nielsen (1964b):

$$CE^* = CE - GE \tag{5.4.2}$$

$$CZ^* = CZ - GZ \tag{5.4.3}$$

where CE and CZ are the approximations to the real kinetic-available transfers occurring in the atmosphere. A comparison of stratospheric conversions between the eddy and zonal modes of available to kinetic energy is given in Fig. 5.4.2 and 5.4.3. The values consist of the vertically integrated results for the 25-100 mb layer in both CE* and CE cases. The spectral equivalents for wave 1 and 2 are also shown in Fig. 5.4.2. The general characteristic is that when GE is found from Eqn. (5.4.2), it is consistently negative, i.e., a negative generation of eddy available energy by diabatic processes. The same goes for GE(1) and GE(2), but not for GZ. It is interesting to compare the dynamically inferred generation terms against the one computed directly from the diabatic diagnostic model. The results are shown in Table 5.4.2.

Table 5.4.2. Comparison of generation terms inferred as a residual, GE_r, $GE(n)_r$, GZ_r, and those computed from the diabatic diagnostic model, GE_d, $GE(n)_d$, GZ_d. Units: Ergs/cm^2 mb sec.

Jan. 1959	GE_r	GE_d	$GE(1)_r$	$GE(1)_d$	$GE(2)_r$	$(GE(2)_d$	GZ_r	GZ_d
12	-3.30	-.47	-1.20	-.18	-1.75	-.23	1.40	-.13
13	-3.40	-.56	-1.20	-.25	-1.45	-.18	.90	-.16
14	-2.20	-.51	- .95	-.30	- .80	-.12	1.15	.05
15	-2.35	-.58	-1.40	-.31	- .60	-.09	1.65*	-.18
16	-2.65	-.59	-2.60	-.31	-1.00	-.13	1.60	-.21

* A subjective correction has been given to the zonal vertical motion on the 15th, as noted earlier in Chapter 4.

Characteristically, the above table demonstrates that both methods produce consistent negative generation of eddy available energy, but the residual method (GE_r) give values 4 to 7 times larger in magnitude than the diagnostic results (GE_d). It is convenient, at this point, to compare some results from Perry (1966) dealing with the GE-term over the warming period of January 17-25, 1963. This term averaged -3 ergs/cm^2 mb sec over his period, compared to about the same value for the January 12-16, 1959, i.e., the GE_r-term in Table 5.4.2. It is thought that this value is too high for our period, since it is somewhat more radiatively quiscent than in 1963, but it permits a valid check on the diagnostically inferred generation GE_d. The physical assumptions about the ozone distribution in the horizontal and vertical plus some necessary smoothing of the vertical temperature profiles limit the computed GE_r-term magnitudes, and it would be conservative to raise their values by a factor of 2 to 3. The amplification in the GE_d-term would improve the stratospheric AE and AE(n) budgets as found in the previous chapter. Further, the net conversion between the eddy from the available and kinetic energies would be made consistent in both vertical motion models, leading to an indirect eddy circulation in the zonal planes in the stratosphere for the 5-day average (at least for the vertically integrated lower plus middle stratosphere).

The uniformly positive magnitude of the GZ_r-term does not seem to fit most previous negative magnitudes brought forth by other investigators, as shown earlier in Table 4.3.1. It is then assumed that the direct computations GZ_d are more realistic.

It is of interest to search deeper into the problem of computing the available energy generation. The latitudinal distribution of the "ω T"-correlation from both vertical motion models at 25 mb on January 12, 1959, has been expanded on Fig. 5.4.4. The phases for both types of vertical motion coefficients are shown to be in good agreement with each other and the agreement is best at wave number 1. Also relatively good coherence exists in the magnitudes of the vectors up to 70°N, but farther north, the adiabatically computed components are much larger, especially for wave number 1. This is likely due to the boundary conditions imposed implicitly in the diagnostic omega model where the components are over-smoothed at and north of 70°N. At the scale of wave number 1, the rather large negative "ω T "-

correlation north of 55^{o}N renders the resulting CE(1)*-term positive and relatively large. The resulting negative CE(1)-term prevailing south of 55^{o}N is responsible for the relatively small negative value when the areal mean is performed. A similar latitudinal distribution of the "ω T"-correlation exists with respect to the sign in wave number 2. In summary, even when the two spectral coefficients of the vertical motion at 25 mb are at first sight relatively similar in magnitude and phase, the systematic non-randomness in both magnitude and phase, makes their spectral correlations with the same temperature field dissimilar. This systematic bias in the results is due to the two numerical models used for the vertical motion problem and also to the adiabatic or non-adiabatic character of the chosen solution. It is convenient to note here that the incomplete diabatic specification in the diagnostic omega model probably leads to lesser negative generation of eddy available energy in the stratosphere.

In the computations which will follow, CE* and CZ* are available only. This should be kept in mind during the discussion.

The approximated budget will be given at each of the three levels according to the following formulae:

$$-\frac{\partial AZ}{\partial t} - CA - CZ^{*} = -BAL \tag{5.4.4}$$

$$-\frac{\partial AE}{\partial t} + CA - CE^{*} = -BAL \tag{5.4.5}$$

$$-\frac{\partial KE}{\partial t} + BGE + CK + CE^{*} = -BAL \tag{5.4.6}$$

$$-\frac{\partial KZ}{\partial t} + BGZ - CK + CZ^{*} = -BAL \tag{5.4.7}$$

The balance terms "BAL" in both Eqns. (5.4.4) and (5.4.5) have been computed. Since CE* and CZ* include the generation terms in addition to the corresponding CE and CZ transformations, BAL should be a small number standing for the boundary transport of available energy. This was found by both Muench (1965) and Perry (1966). This has been reaffirmed in the 5-day study of the previous chapter. The balance terms "BAL" of the last two equations above have not been evaluated because they stand for various missing terms such as the dissipation of kinetic energy to the shorter scales of motion, the boundary advections and also the inaccuracy of the BGE and BGZ terms due to the adiabatic thermodynamic omega equation used here. Since the pressure interaction terms were computed for a layer having the level of interest as its base, then only their daily variations may be of significance.

5.5 25-mb Energetics during January 1959.

The daily variations in the different energy terms at 25 mb are given in both tabular and graphic form. The reader is referred to Tables 5.5.1 to 5.5.4 and to Figs. 5.5.1 to 5.5.4.

The budget of the zonal available energy at 25 mb will be discussed from Figs. 5.2.3 and 5.5.1. AZ, from Fig. 5.2.3, may be characterized by a 20-day oscillation: there is a maximum between the 2nd and the 11th, a minimum plateau follows from the 14th to the 19th and a flat maximum spread over the 21st-27th period. There are rather small changes in AZ as the radiative generation and transfer from the zonal kinetic energy (CZ*) almost compensate the transfer to the eddy available energy (CA). In Fig. 5.5.1, -CA and -CZ* are rather well negatively correlated in time and -CA lags behind -CZ* by about three days, i.e., 8th-11th, 20th-23rd and 26th-27th.

The eddy available energy on Fig. 5.2.3 shows a similar 20-day oscillation which is negatively correlated to AZ. From Fig. 5.5.2, the energy transfers CA and -CE* are well correlated negatively and -CE* shows little lag, with extrema on the 11th, 23rd-24th, 27th-29th. Since -CE* includes the eddy radiative gene-

Table 5.5.1. Energy terms associated with the balance of the zonal available energy at 25 mb in January 1959.

UNITS: ergs/cm^2 mb sec.

DATE JAN. 1959	AZ	−CA	−CZ*	−BAL
2	−2.31	−4.20	6.67	0.16
3	−.87	−2.99	4.87	1.01
4	.35	−2.60	2.79	0.54
5	.41	3.19	3.59	1.35
6	−.69	−2.80	4.22	0.73
7	−.06	−2.73	2.58	−.09
8	−.52	−4.03	5.12	0.57
9	−.64	−2.90	3.93	0.39
10	1.10	−7.07	3.95	−2.02
11	1.68	−7.66	3.17	−2.81
12	2.84	−6.89	2.63	−1.42
13	2.43	−6.65	1.30	−2.92
14	.86	−3.28	2.38	−.04
15	−.23	−3.21	3.17	−.21
16	−.17	−2.14	2.36	0.05
17	−.81	−2.29	2.93	−.17
18	.12	−1.61	0.16	−1.33
19	.12	−2.09	0.81	−1.16
20	−1.62	−2.86	3.93	−.55
21	−.58	−2.14	2.57	−.15
22	.06	−4.46	3.08	−1.32
23	−.35	−5.17	3.04	−2.48
24	−.35	−4.36	3.95	−.76
25	−.17	−2.62	2.13	−.66
26	−1.50	−3.24	3.64	−1.10
27	.29	−4.23	3.17	−.77
28	1.74	−3.85	0.73	−1.38
29	1.04	−2.15	0.99	−.12
30	1.04	−2.65	0.00	−1.61
MEAN	.11	−3.66	2.89	−.63
ST. DEV.	1.16	1.62	1.50	1.10
CONF.	.37	0.52	0.48	0.35

LEGEND: Observation taken at 0000Z each day. CA: Transfer from zonal to eddy available potential energy. CZ*: conversion from zonal available potential energy to zonal kinetic energy computed from the adiabatic (thermodynamic) method.
MEAN: arithmetic mean for the month.
ST. DEV: standard deviation.
CONF: 95% confidence range for mean according to a student-T test.
−BAL: the sum of the terms to the left of the column "−BAL".

Table 5.5.2. Energy terms associated with the balance of the eddy available energy at 25 mb in January 1959.

UNITS: ergs/cm^2 mb sec

DATE JAN. 1959	- AE	CA	$-CE^*$	-BAL.
2	1.16	4.20	-4.80	0.56
3	1.62	2.99	-4.87	-.26
4	.58	2.60	-3.72	-.54
5	.12	3.19	-3.33	-.02
6	1.04	2.80	-4.72	-.88
7	.64	2.73	-3.82	-.45
8	.23	4.03	-4.72	-.92
9	.00	2.90	-2.76	0.14
10	-1.04	7.07	-6.57	-.54
11	-1.16	7.66	-7.54	-1.04
12	-1.45	6.89	-6.21	-.77
13	-1.10	6.65	-5.23	0.32
14	-.29	3.28	-2.42	0.57
15	-.06	3.21	-3.33	-.18
16	.75	2.14	-2.22	0.67
17	.69	2.29	-3.34	-.36
18	.81	1.61	-3.14	-.72
19	.75	2.09	-2.82	0.02
20	.81	2.86	-4.83	-1.16
21	.00	2.14	-5.03	-2.89
22	-.58	4.46	-2.73	1.15
23	-.41	5.17	-4.68	0.08
24	1.56	4.36	-8.66	-2.74
25	.93	2.62	-4.27	-.72
26	.99	3.24	-3.53	0.70
27	-17	4.23	-5.40	-1.34
28	.17	3.85	-4.63	-.61
29	-.29	2.15	-2.68	-.82
30	1.04	2.65	-5.21	-1.52
MEAN	0.25	3.66	-4.39	-.49
ST. DEV.	0.82	1.62	1.53	0.92
CONF.	0.26	0.52	0.49	0.30

LEGEND: (See also Table 5.5.1.). CE^* conversion between the eddy models of available and kinetic energy resulting from the adiabatic (thermodynamic) method.

Table 5.5.3. Energy terms associated with the balance of the eddy kinetic energy at 25 mb in January 1959.

UNITS: ergs/cm^2 mb sec.

DATE JAN. 1959	KE	BGE	CK	CE^*
2	-9.49	13.20	-1.40	4.80
3	.41	10.25	-1.22	4.87
4	3.30	8.57	0.21	3.72
5	-1.10	8.83	-1.01	3.33
6	1.91	10.05	-1.22	4.72
7	-.23	7.29	-1.30	3.82
8	-9.95	7.99	0.33	4.72
9	-.29	6.02	-2.35	2.76
10	2.31	14.25	-2.55	6.57
11	-2.26	15.09	-3.74	7.54
12	-5.15	16.62	-2.91	6.21
13	-2.26	17.22	-.15	5.23
14	-.12	10.61	-3.10	2.42
15	-.35	10.39	-6.35	3.33
16	-1.74	7.46	-7.20	2.22
17	-1.04	8.94	-5.15	3.34
18	2.26	6.29	-2.62	3.14
19	1.85	12.69	-.77	2.82
20	2.55	12.54	-1.14	4.83
21	6.80	16.37	0.15	5.03
22	3.65	16.32	0.09	2.73
23	1.04	13.14	-2.06	4.68
24	2.03	15.32	-1.51	8.66
25	-.64	7.96	0.60	4.27
26	-2.78	7.17	1.64	3.53
27	-5.21	9.04	0.06	5.40
28	-3.36	9.07	-.41	4.63
29	-2.31	7.08	-2.04	2.68
30	-4.98	11.78	-6.20	5.21
MEAN	-.86	10.95	-1.84	4.39
ST. DEV.	3.72	3.46	2.19	1.53
CONF.	1.20	1.11	0.70	0.49

LEGEND: (See also Table 5.5.1 and 5.5.2). BGE: work performed at the boundaries by the eddy pressure forces on 25-0 mb layer, CK: transformation of zonal to eddy kinetic energy.

Table 5.5.4. Energy terms associated with the balance of the zonal kinetic energy at 25 mb in January 1959.

UNITS: ergs/cm^2 mb sec.

DATE JAN. 1959	KZ	BGZ	-CK	-CZ*
2	1.27	-16.78	1.40	-6.67
3	2.72	-11.02	1.22	-4.87
4	1.91	-5.59	-.21	-2.79
5	.17	-7.71	1.01	-3.59
6	1.74	-8.92	1.22	-4.22
7	.52	-4.49	1.30	-2.58
8	-3.47	-9.95	-.33	-5.12
9	.29	-8.71	2.35	-3.93
10	2.89	-6.46	2.55	-3.95
11	.75	-5.29	3.74	-3.17
12	1.85	-5.12	2.91	-2.63
13	2.49	-1.51	0.15	-1.30
14	2.20	-6.09	3.10	-2.38
15	-.35	-12.38	6.35	-3.17
16	-1.10	-8.25	7.20	-2.36
17	-.99	-8.98	5.15	-2.93
18	.75	-0.50	2.62	-.16
19	1.33	-1.33	0.77	-.81
20	-.52	-9.39	1.14	-3.93
21	-1.04	-6.08	-.15	-2.57
22	-1.27	-6.18	-.09	-3.08
23	-1.97	-6.34	2.06	-3.04
24	-2.03	-7.23	1.51	-3.95
25	-.35	-4.64	-.60	-2.13
26	-.69	-6.29	-1.64	-3.64
27	.29	-7.22	-.06	-3.17
28	1.68	-.11	0.41	-.73
29	.93	1.23	2.04	-0.99
30	1.74	-.95	6.20	-.00
MEAN	0.40	-6.29	1.84	-2.89
ST. DEV.	1.58	3.93	2.19	1.50
CONF.	0.51	1.27	0.70	0.48

Legend: (See also Tables 5.5.1.to 5.5.3). BGZ: work performed at the boundaries by the zonal pressure forces on 0-25 mb layer, CZ: transformation from zonal available to zonal kinetic energy.

ration term, one would not expect to find a clearcut lag with CA. It is interesting to note that minimum values in CE* and CA are found in the period 14th to 19th, an indication of small baroclinicity, at this time at 25 mb. Also worth noticing are the large CA and CE* processes operating almost simultaneously on the 11th and during the 23rd-24th period. In the light of previous results, this may be due to the increased eddy heat transport northward where the composite CE* is more effectively reduced by radiative effects.

The eddy kinetic energy budget at 25 mb is shown in both Table 5.5.3 and Fig. 5.5.3. It is noted that the BGE-term denotes the vertical flux convergence between 25 mb and the top of the atmosphere. It is only inferred then that the trend shown is proportional to the energy trapped in the stratospheric layer about the 25-mb level. From previous discussion and recalled by Fig. 5.2.3, the eddy kinetic energy suffers the largest changes in time compared to those of the other energy modes. Of special interest are the four peaks on the 3rd, 12th, 17th and 28th. The peak on the 9th is not well substantiated by the energy transformation terms. The peak on the 3rd is shown to be directly related to the BGE-term. The second peak could be explained mostly by both the BGE and the CE* terms, but one must have some reservation for the last process. Of interest on the 12th-13th period is the near zero value of the CK-term, permitting the flux from below to control the KE-reservoir more effectively. The continuous but less drastic increase from the 14th to the 17th is shown to be due to the BGE-mechanism and possibly some baroclinic transfer, as the eddy kinetic energy reservoir is depleted into its zonal form barotropically. The drop in the eddy kinetic energy after the 17th is difficult to explain from the processes computed at these times. It is inferred that the high state of the kinetic energy reservoir is lowered partly by the frictional dissipative processes and partly by outflux from the layer in question, and probably the computed vertical eddy convergence of the geopotential flux in the 0-25 mb layer is not a good indicator of the actual exchange of the layer about the 25 mb level. It will be shown later that the geopotential flux convergence in the 100-25 mb layer operated at relatively low intensity during this period. Of interest are the time lags of BGE with respect to CE* on the one hand and to CK on the other. The rapid increase of KE in the 10th-13th period and the lesser rise afterwards until the 17th is well correlated with the daily fluctuations of BGE especially and CE*. The KE reservoir is also modulated by the barotropic CK-process which is found to be nil on the 13th while it counteracts a KE increase before and especially afterwards. Assuming that a likely GE-value of -3 ergs/cm^2 mb sec as found by Perry (1966) in the 40-0 mb layer for the month of January 1963 is applicable to the 25 mb level (half of this negative generation has been computed using the radiative transfer method applicable to the same layer from the results of Chapter 4). A net baroclinic process is then inferred at the small rate of 0.9 ergs/cm^2 mb sec. The overall energy flow about KE during this period may be given schematically as:

$$
\begin{tikzcd}
AE \arrow[r, dashed] & KE \arrow[r] & KZ \\
 & BGE \arrow[u] &
\end{tikzcd}
$$

where the eddy pressure interaction explains most of the changes in KE. The final increase in eddy kinetic energy from the 25th to 28th may be explained by the BGE, CK and CE* processes, given in the order of their significance. It should be noted that the barotropic process CK transfers energy from the zonal mode KZ to the eddy mode KE during this period. The eddy kinetic energy stabilization after the 28th would be likely due to an increasing barotropic transfer of eddy to zonal kinetic energy.

The budget of the zonal kinetic energy is shown in Table 5.5.4 and Fig. 5.5.4. The daily variations of KZ are shown on Fig. 5.2.3. KZ is negatively correlated to KE during the month, indicating significant exchanges between these two energy modes by the barotropic mechanism CK. It is interesting to note that AZ and KZ have the same trend during the month being minima around the period January 14 to 19, showing that both meridional temperature gradients and zonal winds are minima at the same time as maxima in eddy temperature field and eddy kinetic energy at 25 mb. Fig. 5.5.4 reveals that of all the energy terms shown, only -CK acts in the direction to balance the KZ budget during the month. The effect of CZ*, BGZ and also DZ, the frictional dissipation, would tend to transfer some energy from KZ into some other form of energy, and only the boundary fluxes (BKZ) can keep the balance by transporting zonal kinetic energy in the layer from the exterior. No significant lag can be noted between -CK, CZ* and/or BGZ. CZ* and BGZ appear to vary simultaneously showing some possible vertical coherence between the variation of the zonal pressure force in the layer around 25 mb and the one acting on the vertical and lateral boundaries. With reference to Fig. 5.2.3, KZ shows a large time scale decrease past mid-January with a gradual ascent afterwards. This may be due to the gradual decrease in magnitudes of both CZ* and BGZ during the first half of the month. In order to assess any possible cycle in the energy transfers at 25 mb during January 1959, a time diagram exhibiting the locus of the dates of the significant maxima in the transfers has been constructed in Fig. 5.5.5. At 25 mb, the results are quite revealing. Within the short time series available, some energy pulses appear to be transferred from one mode to another in a cyclic fashion characterized by a period of about 12 days. It is worth at this point to anticipate later results at 500 mb where an energy cycle of the type:

$$AZ \longrightarrow AE \longrightarrow KE \longrightarrow KZ \longrightarrow AZ$$

is in progress. The largest variations in the transfers at 500 mb appear to have a similar period to the one at 25 mb. It can be seen from Fig. 5.5.5 that a 6-day period in the fluctuations of the energy transfers also appear at 500 mb. From the same figure, one notices that the locus of the 500 mb 12-day period leads the corresponding 25 mb locus by 5 to 9 days. The time lapse between the two loci is minimum in mid-January, this lapse being of the order of theoretically deduced equivalent from vertical energy propagation studies (Charney, 1949; Charney and Drazin, 1961; Muench, 1965).

In summary, it is found that the energy cycle at 25 mb bears a good resemblance to a normal tropospheric cycle, notwithstanding the significant addition of the BGE and BGZ-terms to the cycle. This cycle may be schematically given as:

$$\begin{tikzcd} AZ \arrow[r] & AE \arrow[r] & KE \arrow[r] & KZ \arrow[r] \arrow[d, dash] & AZ \\ & & BGE \arrow[u] & BGZ \arrow[d] & \\ & & \arrow[u, dash] & & \end{tikzcd}$$

A pulse in the energy exchanges can be followed in time along this cycle exhibiting a period of about 12 days. A good correlation is found to exist between a similar energy flow cycle at 500 mb, the relationship being best at mid-month as the 500 mb cycle leads the one at 25 mb by 5 to 9 days.

5.6 The 100 mb Energetics during January 1959

The daily variations of the 100-mb energy terms are depicted in two ways: first by Tables 5.6.1 to 5.6.4 and also by Figs. 5.6.1 to 5.6.4. The 100 mb level is taken to depict the phenomena arising in the lower stratosphere. The transfer terms are found to be characteristically about half the values of their counterparts at 25 mb. Also significant here are the frequent changes in the signs of the transfers CA, CE*, CK, CZ*, BGZ and even BGE occasionally, which at 25 mb were rather infrequent, if occurring at all.

Because of the complexity of the energy cycles at 100 mb, they have been catalogued into five different types, irrespectively of the sign of the BGE mechanism. The types are listed and explained in the next few paragraphs.

Type 1. Case where the ultimate source of energy is the troposphere (through the BGE-term) while the sink would be the radiative loss by the GE and the GZ processes. Schematically:

Table 5.6.1. Energy terms associated with the balance of the zonal available energy at 100 mb in January 1959.
UNITS: ergs/cm^2 mb sec.

DATE JAN. 1959	AZ	-CA	-CZ*	-BAL
2	1.85	-0.07	0.87	2.65
3	.06	0.53	-.76	-.17
4	-.52	-0.58	1.32	0.22
5	-.69	-0.93	0.73	-.89
6	.29	-0.50	0.34	0.13
7	.12	0.64	-.70	0.06
8	.29	-0.46	-.15	-.32
9	.41	-.56	-.05	-.20
10	.64	-2.46	3.01	-.09
11	-.23	-2.83	0.55	-2.51
12	.06	-.98	0.45	-.47
13	-.23	-1.41	1.55	-.09
14	.12	-.66	0.78	.24
15	-.12	-.19	0.44	.13
16	-.52	-.51	0.29	-.74
17	.46	-1.68	-1.09	-2.31
18	.46	0.09	-1.59	-1.04
19	.00	-.20	0.51	0.31
20	.17	-.40	0.38	0.15
21	-.52	0.15	0.40	0.03
22	-1.27	2.04	0.21	0.98
23	-.35	-.75	2.27	1.17
24	-.06	0.02	1.02	0.98
25	-1.10	0.47	1.03	0.40
26	-.81	-.99	2.95	1.15
27	.46	-.82	1.58	1.22
28	1.10	-3.09	0.33	-1.66
29	.81	-2.24	1.25	-.18
30	.69	-.58	0.67	.78
MEAN	0.01	-.65	0.48	-.00
ST. DEV.	0.66	1.08	1.12	1.06
CONF.	0.21	0.35	0.36	0.34

LEGEND: See Tables 5.5.1 to 5.5.4.

Table 5.6.2. Energy terms associated with the balance of the eddy available energy at 100 mb in January 1959.

UNITS: ergs/cm^2 mb sec.

DATE JAN 1959	AE	CA	$-CE^*$	-BAL
2	-.35	0.07	0.58	.30
3	.12	-.53	0.75	.34
4	.29	0.58	0.12	.99
5	-.17	0.93	0.61	1.37
6	-.35	0.50	-.26	-.11
7	.69	-0.64	-.07	-.02
8	.58	0.46	-.07	.97
9	-.93	0.56	1.12	.75
10	-1.22	2.46	-1.34	-.10
11	-1.22	2.83	-1.69	-.08
12	-.81	0.98	0.06	-.23
13	.06	1.41	-.93	0.54
14	-.23	0.66	0.37	0.80
15	-1.62	0.19	2.25	0.82
16	-1.85	0.51	2.62	1.28
17	-.58	1.68	-.03	1.07
18	-.12	-0.09	0.29	0.08
19	.64	0.20	-.80	0.04
20	1.74	0.40	-2.15	-.01
21	1.74	-0.15	-1.96	-.37
22	1.66	-2.04	-.94	-1.32
23	1.16	0.75	-2.29	-.38
24	.86	-0.02	-.24	0.60
25	1.04	-0.47	-.81	-.24
26	1.04	0.99	-1.09	0.94
27	.29	0.82	-.92	0.19
28	-.87	3.09	-1.29	0.93
29	-1.22	2.24	-.62	0.40
30	-1.16	0.58	-.18	-.76
MEAN	-.03	0.65	-.31	0.30
ST. DEV.	1.02	1.08	1.16	0.64
CONF.	0.33	0.35	0.37	0.20

LEGEND: See Tables 5.5.1. to 5.5.4.

Table 5.6.3. Energy terms associated with the balance of the eddy kinetic energy at 100 mb in January 1959.

UNITS: ergs/cm^2 mb sec.

DATE JAN. 1959	KE	BGE	CK	CE*
2	-6.25	4.26	0.53	-.58
3	-2.43	3.91	-.31	-.75
4	1.10	3.08	-.09	-.12
5	.58	1.64	-.57	-.61
6	-.52	1.10	-1.30	0.26
7	-2.89	1.52	0.24	0.07
8	-.87	-.78	-.19	0.07
9	2.61	0.35	1.01	-1.12
10	1.10	3.14	1.16	1.34
11	-.93	4.92	0.43	1.69
12	-1.33	4.46	0.59	-.06
13	.64	4.22	-.61	0.93
14	2.78	3.74	2.18	-.37
15	2.55	3.10	-.37	-2.25
16	.58	2.92	-.62	-2.62
17	-2.37	4.27	-.17	0.03
18	-2.14	8.19	0.05	-.29
19	-.06	-.95	0.23	0.80
20	-.87	.65	-.64	2.15
21	2.14	1.95	-.05	1.96
22	-.99	4.90	-.98	0.94
23	-1.45	0.20	1.70	2.29
24	3.24	-.05	0.41	0.24
25	.06	1.87	-.17	0.81
26	.06	0.77	-.17	1.09
27	-2.49	-1.32	-.25	0.02
28	.12	-2.26	-1.15	1.29
29	3.93	0.00	-.01	0.62
30	1.39	1.26	0.16	0.18
MEAN	-.09	4.32	0.04	0.31
ST. DEV.	2.19	2.11	0.78	1.16
CONF.	0.70	0.68	0.25	0.37

LEGEND: (See Tables 5.5.1. to 5.5.4.) BGE: work performed at the boundaries by the eddy pressure forces on the 25-100 mb layer.

Table 5.6.4. Energy terms associated with the balance of the zonal kinetic energy at 100 mb in January 1959.

UNITS: ergs/cm^2 sec mb

DATE JAN. 1959	KZ	BGZ	-CK	CZ*
2	3.47	-3.50	-.53	-.87
3	.93	-4.41	0.31	0.76
4	-.99	-3.69	0.09	-1.32
5	.23	-6.52	0.57	-.73
6	.17	-1.56	1.30	-.34
7	-2.37	-2.43	-.24	0.70
8	-.29	-4.70	0.19	0.15
9	1.10	-1.97	-1.01	0.05
10	1.16	2.30	-1.16	-3.01
11	.41	-5.41	-.43	-.55
12	-.93	-3.34	-.59	-.45
13	-2.26	-1.28	0.61	-1.55
14	.12	-1.54	-2.18	-.78
15	3.93	2.55	0.37	-.44
16	.64	-1.28	0.62	-.29
17	-.52	-.92	0.17	1.09
18	-.99	-6.45	-.05	1.59
19	-1.80	-1.47	-.23	-.51
20	-.87	1.33	0.64	-.38
21	1.27	-.96	0.05	-.40
22	-.52	-3.59	0.98	-.21
23	-1.97	-7.85	-1.70	-2.27
24	.29	-.52	-.41	-1.02
25	1.50	-.26	0.17	-1.03
26	.64	2.76	0.17	-2.93
27	-3.47	1.32	0.25	-1.58
28	.29	-5.39	1.15	-.33
29	2.61	-5.18	0.01	-1.25
30	-1.74	-3.33	-.16	-.67
MEAN	0.00	-3.31	-.04	-.48
ST. DEV.	1.69	2.09	0.78	1.12
CONF.	0.54	0.67	0.25	0.36

LEGEND: (See Tables 5.5.1. to 5.5.4.) BGZ: work performed at the boundaries by the zonal pressure forces on the 25-100 mb layer.

$$\begin{tikzcd} AZ & AE \arrow[l] & KE \arrow[l] \arrow[r] & KZ \\ & & BGE \arrow[u] & \end{tikzcd}$$

This case is similar to the indirectly driven lower stratosphere as found by Oort (1963) for the yearly mean.

Type 2. This is the normal cycle for a baroclinic troposphere (notwithstanding BGE and BGZ), or schematically:

$$\begin{tikzcd} AZ \arrow[r] & AE \arrow[r] & KE \arrow[r] & KZ \\ & & BGE \arrow[u] & \end{tikzcd}$$

In this case the eddy kinetic energy is both fed by baroclinic processes "in situ" and also transmitted baroclinically from the troposphere. It is to be noted that this mechanism was found to be predominant at 25 mb throughout the whole month. This type of cycle in the stratosphere has been called a mixed baroclinic type by other investigators.

Type 3. This cycle is similar to Type 1 except that CA is positive. In the troposphere CA is normally positive which means that northward eddy heat transport is flowing down the mean zonal temperature gradient. Due to the existence of the zonal warm belt around 50°N at 100 mb, the northward eddy heat transport over the whole area coincides with a northward gradient of the mean zonal temperature south of the warm belt while down gradient conditions exist north of the belt. The CA-term will be positive or negative depending whether the north side of the belt or the south side have more weight in the areal integration. The negative CA process is usually found in summer at 100 mb when warmer temperatures prevail over the northern areas. This energy cycle may be shown schematically:

$$\begin{tikzcd} AZ \arrow[r] & AE & KE \arrow[l] \arrow[r, dashed] & KZ \\ & & BGE \arrow[u] & \end{tikzcd}$$

This type has been presented by Miyakoda (1963) as the lower stratosphere case in early winter when the eddy modes are on the increase.

Type 4. It is referred to by Miyakoda (1963) as causing an elongation of the flow pattern. It is similar to Type 3 but with a positive CK-process, i.e., KZ $\longrightarrow$ KE. Again increases in both KE and AE are indicated. Schematically:

$$\begin{tikzcd} AZ \arrow[r] & AE & KE \arrow[l] & KZ \arrow[l] \\ & & BGE \arrow[u] & \end{tikzcd}$$

Type 5. It is Type 2 with a difference, i.e., CK is positive (KZ $\longrightarrow$ KE), making the eddy kinetic energy at the intersection of all transfer flows: BGE, CE and CK. Miyakoda (1963) attributed the "explosive warming" of January 1958 to this type of energy cycle. Schematically, it becomes:

$$\begin{tikzcd} AZ \arrow[r] & AE \arrow[r] & KE & KZ \arrow[l] \\ & & BGE \arrow[u] & \end{tikzcd}$$

In order to seek interrelationship between levels with respect to the daily energy cycle types, Table 5.6.5 has been constructed. It depicts the daily distribution of the energy flow types at 25 and 100 mb.

Table 5.6.5. Energy flow types as defined above for the 25 and 100 mb levels during January 1959. Undefined Type X stands for other possible flow types

Date (Jan. 1959)	2	3	4	5	6	7	8	9	10	11	12	13	14	15	16
25 mb Type	2	2	5	2	2	2	2	2	2	2	2	2	2	2	2
100 mb Type	4	1	3	3	2	X	2	X	5	5	4	2	4	3	3
Date (Jan. 1959)	17	18	19	20	21	22	23	24	25	26	27	28	29	30	
25 mb Type	2	2	2	2	5	5	2	2	5	5	5	2	2	2	
100 mb Type	2	X	5	2	X	X	5	X	X	2	2	2	2	5	

From Table 5.6.5, and Fig. 5.2.2, it is found that the peaks in the eddy kinetic energy at 100 mb are associated with active energy flows of the Type 2, 4 or 5. Selecting the peaks which seem to be associated in time with those of 25 mb, it may be fruitful to couple them with the eddy pressure interaction affecting the 100-25 mb layer. This association and coupling are given in Table 5.6.6 in an effort to single out the relative strength of the mechanisms in action.

Table 5.6.6. Peaks in the eddy kinetic energy of both 25 and 100 mb levels associated with active energy cycles. Strength of the eddy pressure interaction on the 100-25 mb layer simultaneous to the maxima in eddy kinetic energy. Units of the pressure interaction terms: Ergs/cm^2 mb sec.

Date of Peaks (Jan. 1959)	8-9	13	17	20	23	28
25 mb cycle Type	2	2	2	2	2	2
100 mb cycle Type	2	2	2	2	5	2
BGE	- .21	4.22	4.27	.65	.20	-2.26
BGE(1)	-1.10	2.48	2.83	2.92	1.81	-1.30
BGE(2)	1.78	1.36	1.01	- .55	0.75	0.02
BGE(3)	- .47	0.64	- .07	-1.72	- .62	- .34

Table 5.6.6 tries not only to ascertain the direction of the various flows leading to peaks in the eddy kinetic energy reservoir, but also tries to measure the magnitude of the mechanisms leading to these higher energy states. It is noted first that all peaks are clearly associated with active energy cycles (notwithstanding a numerically decreased CE-value when compared to the CE*-value used). The peaks on the 8th-9th, 20th, 23rd and 28th appeared to be of some minor oscillation riding on a longer time-scale trend. The peaks on the 13th and 17th coincide with maximum impact from energy transmitted from the troposphere through the BGE-process, and as shown previously, and re-verified here, this phenomenon is clearly most significant at the scale of wave number 1. The scale of wave number 2 has about half the significance of the larger scale. The ephemereal peak in eddy kinetic energy on the 28th must be due to a pulse from the southern boundary, the frictional dissipation process being likely small at this level, since all other transfers are contributing to a decrease in KE.

In summary, the energy cycle at 100 mb is characterized by flows in various directions. At first sight, the changes from active to forced cycles seemed randomly distributed in time, but closer inspection reveals that the 100 mb active cycles when associated with those of 25 mb give eddy energy peaks at both levels. A comparison of those peaks revealed the essential influence of the energy imported from below by the BGE-mechanism and to some extent local barotropic-baroclinic activity. Further, the strength and duration of the BGE-process coincides with its own intensity at the scale of wave number 1, with wave 2 helping. A look at the monthly mean BGE(1) and BGE(2) shows that the latter is larger than the former on the average for the 100-25 mb layer. It is concluded that both eccentricity and bi-polarity of the stratospheric flow were transmitted from below during January 1959, and that the period of more intense and lasting eddy kinetic energy was fed by a stronger eccentrical pressure interaction mechanism with the help of its bipolar equivalent. Other eddy energy peaks were found to be caused mostly by the pressure interaction process at the scale of wave number 2.

5.7 500 mb Energetics during January 1959

The energy flow at 500 mb is found to be either Type 2 or 5 as the sign of the CK-process fluctuates. The daily variations of the four energy transfers CA, CE*, -CK and CZ* may be seen on Fig. 5.7.1, where a transfer magnitude above the zero-line indicates that the direction of energy transfer is in the so-called tropospheric energy flow direction:

$$AZ \longrightarrow AE \longrightarrow KE \longrightarrow KZ,$$

i.e., of Type 2. Type 5 prevails when the CK-term is positive, i.e., KZ$\longrightarrow$KE. The information on Fig. 5.7.1 has been listed on Table 5.7.1, where the monthly mean, standard deviation and the 95% confidence range for the mean following a Student-t distribution were added.

The 500 mb energetics of January 1959 are characterized by about five large amplitude pulsations in CA, CE* and CZ*, also shared in a smaller fashion by CK. These pulsations are centered about the 4th, 11th, 16th, 22nd and 27th, showing a period of about 6 days. This cycle may be further developed into a 12-day period indicated by the distribution in time of the largest peaks. The CA major peaks are found on the 3rd, 15th and 27th; those of CE* follow on the 5th, 17th and 29th. Going back to Fig. 5.5.5, the time locations of these pulses have been plotted, taking care to separate the 6-day period from the 12-day period. As was found in Section 5 of this chapter, after the 6-day period has been filtered out from the time series a 12-day period appears to exist in parallel to an earlier cycle at 25 mb. A time difference of about 8 days separates the pulses of the equivalent terms at both levels, although a lesser lapse of 5 to 7 days is found to separate the CE*'s, and the BGE's at their respective levels. Assuming that the BGE-terms are the energy propagators of tropospheric energy into the stratosphere, a time lapse of 5 to 7 days is in the order of theoretical results (Charney, 1949; Charney and Drazin, 1961) and also of some observational results (Muench, 1965).

Table 5.7.1. Energy terms at 500 mb during January 1959.

UNITS: ergs/cm^2 mb sec.

DATE JAN. 1959	CA	CE*	CK	CZ*
2	8.37	3.33	0.22	-.53
3	16.55	6.18	-1.73	-5.16
4	14.05	11.20	0.39	-3.27
5	11.46	14.10	-.54	-6.18
6	11.77	8.01	-.93	-6.62
7	5.80	2.28	-.13	4.28
8	8.16	5.90	-.07	-.27
9	7.16	7.40	-.38	-2.58
10	10.40	7.82	0.89	-8.60
11	11.01	9.02	0.38	-8.75
12	6.90	5.52	-.93	-4.15
13	3.19	3.31	0.25	-1.14
14	13.41	8.83	0.66	-12.80
15	17.30	7.89	0.04	-12.89
16	12.59	8.16	0.34	-12.85
17	16.87	8.81	0.48	-6.09
18	14.15	8.57	1.26	-8.03
19	12.40	8.49	-.65	-5.12
20	9.35	7.49	-.40	-3.37
21	4.48	5.21	-.67	0.90
22	9.12	9.90	0.07	-5.05
23	15.14	9.82	-.99	-9.27
24	10.86	5.73	0.21	-4.82
25	3.08	0.99	0.60	-4.64
26	5.19	3.04	-.46	-3.38
27	9.03	4.83	0.69	-5.27
28	5.00	4.83	0.32	-2.02
29	6.74	7.04	-.27	-.97
30	7.04	5.53	-.08	-4.99
MEAN	9.88	6.87	-.09	-4.95
ST. DEV.	4.10	2.84	0.65	4.07
CONF.	1.32	0.91	0.21	1.31

LEGEND: See Tables 5.5.1 to 5.5.4.

A persistent blocking circulation characterized January 1959. Some pulsation in the circulation index has been observed. Recalling the earlier description of the synoptic events at 500 mb, the three main blocking patterns were observed on the 6th-9th, 15th-19th and near the end of the month. All three blocking dates have characteristic maxima in CA and CE*, and also positive CK values, i. e., KZ$\longrightarrow$KE on the average. The unusual strength of the mid-month block is shown in a striking manner by high peaks in AE and KE in Fig. 5. 2. 1 and in addition the intensity of the CA, CE* and CK processes are spread over a longer time period. It is then concluded that a blocking circulation is produced by a cycle of the type:

$$AZ \longrightarrow AE \longrightarrow KE \longleftarrow KZ$$

its strength being proportional to the individual transfer magnitudes and durations. The energy associated with the three blocks in January 1959 (6-9,15-19, 25-28) seemed to have propagated upwards as maxima in eddy kinetic energy at 25 mb are observed slightly later (9th, 17-20, 28-30).

In summary, during January 1959, the circulation at 500 mb followed an energy flow of this type:

$$AZ \longrightarrow AE \longrightarrow KE \longleftrightarrow KZ$$

It has been found that the transfers KZ$\longrightarrow$KE, when coupled with large positive pulsations in CA and CE* were associated with blocking circulation whose magnitudes were proportional to the size and persistence of the above mentioned pulsations. Further, similar 12-day periods were found to exist in both 25 and 500 mb energy cycles, the 500 mb period being a sub-harmonic of a superposed 6-day cycle. A good correlation, given a few days' lag, was found to exist between the existence of maxima in the 500 mb blocking circulation index and the occurrence or maintenance of eddy kinetic energy in the stratosphere.

5.8 Monthly Mean Energetics of January 1959

The monthly mean energy flows at 25, 100 and 500 mb are presented in Fig. 5.8.1, 5.8.2 and 5.8.3, respectively. The magnitudes of the transfers, their standard deviations and 95% confidence ranges for the mean (from a t-test, assuming the 29-day data to be independent, i.e., 28 degrees of freedom) may be found in Tables 5.5.1 to 5.5.4, 5.6.1 to 5.6.4 and 5.7.1, for the 25 mb, 100 mb and 500 mb results, respectively.

The mean January 1959 25-mb energy flow is of the type:

$$\begin{tikzcd} AZ \arrow[r] & AE \arrow[r] \arrow[d] & KE \arrow[r] & KZ \arrow[r] \arrow[d] & AZ \\ GZ \arrow[u] & GE & BGE \arrow[u] & BGZ & \end{tikzcd}$$

as can be seen on Fig. 5.8.1. AZ has suffered a slight decrease during the month, so that assuming a relatively small BAZ-term, a fairly good balance is achieved in the energy terms affecting the maintenance to AZ. Recalling that: $CZ^* = CZ - GZ$, and that the mean January 1963 GZ-value for the 0-40 mb layer (Perry, 1966) and/or the 5-day mean GZ-value 1.06 and 0.80 ergs/cm^2 mb sec, respectively, it is found that the 25 mb CZ-term must be about -2 ergs/cm^2 mb sec. This value agrees in sign but is a bit larger than the mean 5-day 25 mb CZ-term computed from earlier data using the diagnostic omega-equation (-1.17 erg/cm^2 mb sec). AE has not changed significantly during the month. The cross-boundary non-linear wave interaction in the eddy available energy reservoir shows a slight import of energy (0.21 unit). To balance AE, only a relatively small cross-boundary import of eddy available energy was deemed necessary (0.52 unit). When the CE*-term is separated into its CE and GE components, the results yield significantly different GE-values from those computed radiatively. It is convenient, at this point, to diagnose the cause of the radiatively computed generation terms versus the dynamically inferred equivalent.

Perry (1966), using the dynamical approach, computed a GE-value of -3.75 ergs/cm^2 mb sec for the 0-40 mb layer averaged over January 1963. The present investigation, for the same layer, yields an eddy generation of -1.14 erg/cm^2 mb sec when averaged over the 5-day sequence of mid-January 1959. Although Perry's computations were taken during a period of much larger warming, the difference is too large to be satisfactorily explained by a larger cooling rate, due presumably to the carbon dioxide radiative transfer. This situation presents an occasion to review critically the radiative approach of this study.

Since the long-wave absorption at 25 mb (mainly due to the 15-micron CO_2) has been computed quite completely, one should consider further the treatment of short wave solar absorption. The solar heating rates were based on solar zenith angles and sunlight duration only, which effectively assumes zonal uniformity in absorber concentration (Appendix B). This assumption implicitly involves the distribution of ozone, the main absorber. Let us consider the effect of dynamically induced ozone variations in view of the physical laws involved in the ultra-violet radiative transfer. The effect of vertical motion is demonstrated on Fig. 5.8.4 where upward motion decreases the ozone and downward motion increases the ozone in the 25-mb layer. The diabatic solar heating in the ultra-violet by the absorption of ozone is proportional to both the ozone density and the actual flux of solar photons that can be absorbed at the level of interaction. Since the photon flux varies exponentially along the path, the shorter ozone path length of Curve A in Fig. 5.8.4 compared to Curve B would over-compensate the decrease of ozone density at the level of interest, i.e., near 25 mb. The net effect will be increased absorption, hence increased heating at Curve A near 25 mb compared to Curve B. It has been shown that the motions which create high ozone amounts also create high temperature regions (MacDonald, 1963). It follows that there will then be an additional negative GE which can be grossly allowed for. This diagnosis calls for a simultaneous study of eddy generations using both radiative and dynamical methods. This could be performed over a smaller space domain where ozone data can be gathered on a daily basis, such as has been done over North America for the last few years. In the case of a hemispheric study, some crude correction to the vertical advection could be applied to the zonal vertical profile of ozone.

In view of the above discussion, the GE-process has been raised to a rate of -2.5 ergs/cm^2 mb sec.

The budget of the eddy kinetic energy, showing a net increase during the month, needs a large loss through frictional dissipation. A net export of eddy kinetic energy across the boundaries has been postulated in face of a slight positive cross-boundary flux of eddy kinetic energy from the non-linear wave interaction mechanism at an average rate of 0.34 erg/cm^2 mb sec.

Following a net decrease in KZ during the month, its budget requires positive cross-boundary flux of this energy mode over the month in order to counteract the loss to the zonal available energy mode and to the exterior by the zonal pressure interaction process and possibly by the zonal frictional dissipation mechanism.

The 100 mb energy flow in January 1959 is characterized by the non-significance or at least the near non-significance of the sign of the averaged transfers at the 95% confidence level. Notwithstanding the statistical test on the variability of the 100 mb energy flow, its monthly averaged distribution will be given. The CZ* and the CE* terms have been corrected by extracting the mean 100 mb 5-day GZ (-.42 unit) and GE (-.44 unit) from our earlier study. The resulting mean monthly energy flow at 100 mb may be schematically given as:

$$
\begin{tikzcd}
AZ \arrow[r] \arrow[d, dash] & AE \arrow[d, dash] & KE \arrow[l] & KZ \arrow[l, dashed] \arrow[r] \arrow[d, dash] & AZ \arrow[d, dash] \\
GZ \arrow[d] & GE \arrow[d] & BGE \arrow[u] & BGZ \arrow[d] & GZ \arrow[d] \\
{} & {} & {} \arrow[u, dash] & {} & {}
\end{tikzcd}
$$

It is to be noted that the BGE and the BGZ are applicable to the 25-100 mb layer strictly speaking. Also here, the BGZ denotes the vertical pressure interaction as the meridional mean zonal velocity $\overline{v}^{\lambda}$ was not available.

The slight rise in AZ at 100 mb during January 1959 can be explained by assuming a very small positive contribution of the BAZ-term (0.17 unit). AE receives a significant amount of energy from AZ during January 1959. A very small amount of energy is needed to balance this energy mode, this positive contribution could be conveniently given by the BAE-term at a rate of 0.34 erg/cm^2 mb sec. Part of this boundary flux may be explained by the cross-boundary non-linear wave interaction term $\sum_{m=1}^{15}$ LA(n) which averaged 0.18 erg/cm^2 mb sec over the month.

Assuming that the 100 mb 5-day averaged GE-term approximates the mean monthly value, a small negative yield for the CE-process results at -0.13 erg/cm^2 mb sec. It must be added that the mean is not statistically significant at the 95% confidence level.

The slight increase in KE during the month is less than one expects from the geopotential eddy flux convergence BGE of the 100-25 mb layer. Since the CK and CE processes are practically negligible, and assuming from the results of the 5-day study that the frictional dissipation is also very small, it is concluded that eddy kinetic energy is lost through the flux of this energy mode across the boundaries, presumably the lateral ones.

KZ underwent little change during January 1959. After the CZ-term has been approximated to about -0.90 erg/cm^2 mb sec, the balance of the zonal kinetic energy budget requires a significant cross-boundary import, assuming again that the zonal frictional dissipative process is small.

The 500 mb mean January energy flow is similar to the so-called tropospheric cycle, i.e., of the type: AZ$\longrightarrow$AE$\longrightarrow$KE$\longrightarrow$KZ, as may be seen on Fig. 5.8.3. A difference is noted, however. Although the CK barotropic process is normally negative on the average, the sign is not statistically significant at the 95% confidence level. This fact could have been expected from its daily fluctuations in an earlier section of the present chapter.

A rather large imbalance is found to exist at the zonal available energy reservoir. The 9.88 ergs/cm^2 mb sec transfer through the northward heat transport is not adequately explained by the adiabatically computed CZ*-term and the relatively large but still insufficient average drop in zonal available energy AZ (about 0.70 erg/cm^2 mb sec) during the month. A net import of zonal available energy across the boundaries of the order of 4 to 5 ergs/cm^2 mb sec would be required to balance the budget. This is at first sight quite unlikely as actual computations of this boundary transfer in the 5-day study yielded rather negligible values. One possible explanation of this anomaly may reside in the adiabatic character of the vertical motion whereby the upward motion is increased zonally by latent heat released mainly in colder mid-latitudes and whereby the downward component is unchanged. This process would cause a more negative over-all CZ transfer. For unchanged GZ process, this would tend to relax the imbalance. A second possibility resides in incompatibility between the CA and GZ values used. The value of the CA-process has a usual maximum at 500 mb. The GZ term used is applicable to the whole troposphere. It is difficult to reconcile the existence of a large positive GZ process over a layer centered about the 500 mb level. It may be that the vertical convergence of the $\left\{\overline{\omega}^{\lambda}\overline{\theta}''^{2}/2\right\}^{\phi}$ – term, in the BAZP-term in Eqn. (3.2.22) is very significant as a vertical flux of zonal available energy across the layer about the 500 mb level. This term was negligible in the 5-day case since the mean zonal vertical motion was either nil or very small at the boundaries of the stratospheric or tropospheric layer. Similar remarks may be applied to the eddy available energy budget, except that maybe the BAEP-term (Eqn. (3.2.21)) must be negative, although it is conceivable that the 500 mb eddy generation of available energy could be larger than the mean tropospheric value. A third possibility is the limited meaning of the concept of available energy, as applied to a thin atmospheric layer. The direction of CE and CZ have been inferred from the computed CE* and CZ*, using mean January tropospheric GE and GZ values computed by other investigators. The readily computed tropospheric generation values from Brown (1964) for January 1959, when applied to the region from 30^{o}N to 80^{o}N yield GZ and GE rates of about 5 and -4 ergs/cm^2 mb sec, respectively. More recent results from Krueger et al (1965) and Vernekar (1967) tend to lower slightly the monthly mean GZ and GE for some other Januaries. In the mean, these new results would encourage more negative CZ's and more positive CE's.

Assuming 500 mb eddy kinetic energy dissipation of the order of about 0.75 erg/cm^2 mb sec (see Fig. 4.2.7 in the 5-day study), and eddy geopotential flux divergence across the 700-300 mb layer of about 2.5 ergs/cm^2 mb sec (from the 5-day study), the balance of KE may be achieved by a small boundary influx of eddy kinetic energy given mostly by the component of this cross-boundary transport included in the non-linear wave interaction at a rate of 0.68 erg/cm^2 mb sec.

Assuming with Kuo (1951) that DZ is about half of DE, namely about 0.40 erg/cm^2 mb sec, the slight net increase in KZ during the month can be explained by a net cross-boundary influx of this energy mode at a rate of about 1 erg/cm^2 mb sec.

The mean 25, 100 and 500 mb energetics during January 1959 may be summarized at this point.

The 25 mb energy transfers follow the well-known tropospheric energy cycle having an additive influence in the pressure interaction mechanisms BGE and BGZ. The BGE-term was the main source of eddy kinetic energy, and the main sinks were in the strong frictional influences and in energy flux export to the exterior. The zonal radiative heating is acting as a small source of available energy, while the strong sink of this energy was due to eddy radiation-temperature correlations. A part of this energy loss has been explained by the dynamic vertical coupling between the vertical motion and the associated (eddy) change in the ozone vertical profile. A method of improving the parametric equation used with respect to solar heating at 25 mb has been advanced.

The 100 mb energy flows are characteristically small and for most of them, variable in direction. The 100 mb energy flow showed a general trend for forced inert layer, where warm air is subsiding and cold air is rising, although the CA-term is still positive in the areal average. The sink of available energy is shared in equal parts by both zonal and eddy radiative-temperature correlations GZ and GE, respectively. A net gain of kinetic energy is inferred in the layer by the pressure interaction mechanism.

The 500 mb level has the characteristic tropospheric energy flow: AZ⟶AE⟶KE⟶KZ⇠⇢AZ, with moderate baroclinic exchanges and insignificant barotropic processes. A strong heat transport term is found to exist in the mean. The source of available energy, the GZ-term is counterbalanced by the loss due to the GE-term. A large imbalance in the AZ and AE budget has been partially explained by the intrinsic adiabatic character of the vertical motion, by somewhat incompatible CA, GZ and GE-terms as applicable to different layers, and also to possible inaccuracy of the computed available energies when applied to a thin atmospheric layer. The possible significance of previously negligible terms such as BAZP and BAEP was also demonstrated when applied to the layer about the 500 mb level.

Both the KE and the KZ budgets are satisfactorily explained by the import of these respective energies across the boundaries by the BKE and the BKZ processes, respectively. Non-linear wave interactions across the boundaries were found sufficient to explain the BKE intensity needed.

5.9 Spectral Kinetic Energy during January 1959

In this section the monthly mean energy transfers pertaining to the kinetic energy budget are presented in their spectral forms at pressure levels of 25, 100 and 500 mb. The results are displayed in the form of a spectral diagram on Fig. 5.9.1.

At 25 mb, wave numbers 1 and 2 clearly dominate the spectral energy flow, followed by wave numbers 3 and 4. One should note that the CE(n)'s were not computed directly, but were inferred from the computed CE(n)*'s, once the GE(n)'s had been roughly approximated. The spectral generation terms were based on the values computed over the 10-50 mb layer, averaged over the 5-day period of January 12 to 16, 1959. To be consistent with the total eddy generation of available energy used earlier in section 5.8, for the monthly mean case, each GE(n) was doubled. The budget at wave number 1 has a fair balance, assuming that the loss through frictional dissipation at this scale is large and is counteracted by the large positive influence of the pressure interaction term BGE(1) (not shown here). The balances of the budgets of KE(2) and KE(3) are fairly good, and some cancellation effects may be postulated between the pressure interaction process and the frictional dissipation at those scales. On the average, the baroclinic processes are found to decrease with scale. The interaction between the zonal flow and the waves is maximum at the scale of wave 2. Waves 1, 3 and 5 are found to lose kinetic energy to the other waves as wave 4 enjoys the largest gain. It is appropriate here to recall some results from Chapter 4 related to the 5-day non-linear kinetic energy wave interactions which were found to be quite similar to those given by Perry (1966) for January 1963. Over the whole month of January 1959, some reshuffling is found among adjacent wave numbers, as in Teweles (1963) applicable to the period between the beginning of December 1957 to the end of February 1958. Table 5.9.1 has been designed to show how adjacent waves interfere with each other during both the 5-day and the 29-day period of January 1959.

Table 5.9.1. Distribution of the mean kinetic energy non-linear wave interactions over the 5-day and 29-day periods of January 1959. Units: ergs/cm^2 mb sec.

Wave Number n	1	2	3	4	5	6	7
Stratosphere: Jan. 12-16, 1959	-.48	-.73	.48	.32	.35	.08	.12
25 mb: Jan. 2-30, 1959	-.22	.16	-.41	.34	-.44	.19	.20

The table above shows that the origin of the wave energy is less organized over the longer time period. This is not too surprising since the longer period covers many spectral energy regimes, while the 5-day series covers one fairly uniform energy set-up. In this respect, the January 1963 vortex breakdown studied by Perry (1966) was so violent that the spectral regime associated with it was reflected in the monthly mean.

The spectral kinetic energy exchanges between the other modes at 25 mb may be summarized by a baroclinic transfer decreasing with the scales, while the wave number 2 flow assumes the preponderance in the barotropic exchanges to the zonal flow. Consecutive waves exchange energy with each other.

The 100-mb spectral KE-budget is characterized by very small transfers, as was the case for the total eddy study. The CE(n) magnitudes have been obtained through the use of previously calculated 5-day mean GE(n) values. At any rate, the CE and CK processes are small, if not negligible, and the only significant transfer remains in the non-linear interaction of wave energy by the LK(n)-process. Wave 1 kinetic energy is shown to be maintained mainly by the exchanges from waves 2 and 4.

The 500-mb spectral kinetic energy budget is more complete than in the two cases above. Fortunately, Brown (1964) had computed the mean spectral generation of available potential energy for January 1959. His results were integrated graphically to yield values valid between 30°N and 80°N in the tropospheric layer. The residual CE(n)-values are represented by the lower truncated portion of the CE(n)* shaft in Fig. 5.9.1. The upper part of the shaft represents Brown's spectral generation terms. The resulting CE(n) baroclinic process is a maximum at wave number 3 scale, followed by waves 1, 2, 4, 6 and 7, in about equal part. In the non-linear wave interaction domain KE(1) and KE(5) are shown to gain mostly from the loss of KE(3), then from KE(2). The spectral budget would balance if the frictional dissipative and pressure interaction terms were both normally negative in the layer about the 500-mb level. This seems reasonable, from previous results in this report.

In summary, at 500 mb in January 1959, the spectral baroclinic processes and the inter-waves exchanges are shown to be the major processes while the sinks of the spectral kinetic energy are likely the frictional dissipation and the spectral pressure interaction to the layer above most likely.

We have found that the large changes in kinetic energy during January 1959 at 25 mb were mostly explained by the flows at wave numbers 1, 2 and to a small extent, 3. It is interesting to correlate visually both daily changes of kinetic energy at those scales with the corresponding non-linear wave interactions. Figs. 5.9.2 to 5.9.4 exhibit the correlation, while Fig. 5.2.4 may also be used for the actual values of the spectral kinetic energy. The following noteworthy points are discussed in the next few paragraphs.

1. The changes in KE(1) are highly correlated with LK(1) up to about the 27th. On and after this date, the large positive LK(1)-term is counterbalanced by an equally large but negative spectral baroclinic transfer at the same scale.

2. The changes in KE(2) are very well related to the LK(2)-term, except for some instances where the CE(2)-process takes over. Both the 4th-6th and the 19th-22nd periods have transfers of wave 2 kinetic energy to wave 2 available energy, offsetting the LK(2) mechanism. The 19th-22nd

period has a significant average exchange from wave 2 into the zonal flow at a rate of about 0.5 erg/cm^2 mb sec, leading to a further loss in KE(2). The post-27th January 1959 period yields a different situation wherein a large loss of wave 2 kinetic energy to the other waves is replenished by large transfers from available to kinetic energy in wave 2 (rates from 2 to 4 $ergs/cm^2$ mb sec have been computed). Further a moderate energy conversion from KZ is transferred into KE(2) at the same time. An inspection of the 25-mb geopotential-height map on the 29th reveals the existence of two closed low pressure areas symmetric about the North Pole.

3. The " $\partial KE(3)/\partial t$ - LK(3)" correlation was not as high as it was for the two larger scales. Before January 5, the CE(3) averaged about 1 erg/cm^2 mb sec, and explains partially the changes in KE(3). A negative and nearly nil CE(3)-process on the 9th and 10th reduces the KE(3) imbalance then. Large transfers in wave 3 available energy, from the kinetic energy of the same scale, from the 14th to the 16th (averaging more than a unit transfer rate) explain the slight drop in KE(3) over this period even when the other waves feed kinetic energy into this scale at a rate of about 1 unit.

4. Three generally different but typical regimes may be found during the month at 25 mb. Three maxima in the total eddy kinetic energy have been described earlier - they are centred on the 9th-12th, 18th-21st and 28th and are associated with KE(2), KE(1) and KE(2), respectively. A detailed account of the mechanisms involved will be given later in Section 5.11.

5.10 Spectral Available Potential Energy during January 1959

The monthly budget of the spectral available energy at 25, 100 and 500 mb can be seen on the spectral diagram indexed as

Fig. 5.10.1. This is in parallel with the previous section where the spectral kinetic energy budget was investigated.

At 25 mb, waves 1 and 2 are shown to be the most significant scales in the budget of the spectral available energy. Waves 3 and 4 scales show transfers which average about 25% of those of the two first waves. Transfers of scales shorter than that of wave number 4 are insignificant. The budgets of waves 1, 2 and 4 are excellent, while wave 3 shows a small imbalance, but it is probably insignificant with respect to the inherent errors in the computation.

AE(1) is maintained mainly by interactions from both the zonal and wave 2 available energy, in that order. On the whole, it loses energy throughout the month by radiative and baroclinic processes.

AE(2) budget is very similar to AE(1) except for an important difference: it transforms its energy into wave 1 available energy by the non-linear wave interaction process. Because this scale is less baroclinically active than wave 1, it exhibits a slight net increase during the month.

It may be convenient to note at this point that both non-linear wave interaction terms LA(1) and LA(2) have the same sign and about the same magnitudes as found in the corresponding terms averaged over the 12th-16th January period, in the stratosphere. The same may be also found in Table 5.10.1 where these terms are listed at various levels with their associated monthly standard deviation and 95% confidence ranges. A positive LA(4) is found also typical in January 1959. It is to be noted that only the three or four first LA(n)'s are statistically significant at 25 mb and 100 mb while only LA(2) passes the test at 500 mb.

At 100 mb, CA(1), LA(1), LA(2), LA(3) and LA(4) are found to be the only typical transfers for the month. Imbalances of small magnitudes, but relatively significant were found in the AE(1) and AE(2) budgets. All the energy transfers about the 100 mb spectral available energy mode are diminutive mirror images of those at 25 mb, on the average.

Table 5.10.1. Mean January 1959 non-linear wave interaction term LA(n) for wave numbers 1 to 7 at 25, 100 and 500 mb, and their associated standard deviation and 95% confidence ranges.

Mean units: ergs/cm^2 mb sec

LA(n)	25 mb			100 mb			500 mb		
Wave No. n	Mean	St. Dev.	Conf.	Mean	St. Dev.	Conf.	Mean	St. Dev.	Conf.
1	0.52	.36	.12	.18	.48	.16	-.07	1.09	.35
2	-.48	.34	.11	-.34	.50	.16	-.84	1.25	.40
3	.00	.28	.09	.13	.36	.12	.02	1.84	.59
4	.10	.16	.05	.14	.36	.12	-.06	1.04	.33
5	-.01	.12	.04	.06	.40	.13	.16	.85	.27
6	-.02	.14	.04	.02	.45	.15	.21	1.27	.41
7	.01	.06	.02	.05	.35	.11	-.13	.50	.16

The fact that the level of maximum heat transport is usually found near or at the 500 mb level is clearly shown in the lower portion of Fig. 5.10.1. Zonal available energy is converted into waves 1, 5, 6 and 7 at about a rate of 1 erg/cm^2 mb sec while more intense northward heat transport is shown at wave number 2 (1.5 unit) and 3 (2 units). The available energy in wave 2 and to a smaller extent in wave 1 is transferred to the available energy of waves 5 and 6. A similar distribution in the exchanges was found in the troposphere in the earlier 5-day study. The significance of the non-linear transfer from wave 2 is confirmed by Table 5.10.1, where the mean magnitude of LA(2) is found to be -.84 erg/cm^2 mb sec and its confidence range extends to 0.40 unit. Again the GE(n)-terms were those of Brown (1964) for the whole stratosphere in January 1959. The CE(n)-terms are taken as the residuals when GE(n) is abstracted from the computed CE(n)*-terms. The imbalance of the budgets of available energy in wave numbers 1, 2, 4 and 7 are practically nil. AE(3), AE(5) and AE(6) show imbalances of the order of 0.5 erg/cm^2 mb sec. AE(3) imbalance may be inferred from too large a northward heat transport and/or from too small a baroclinic exchange.

Interlevel comparisons give some further clues into process having a vertical significance. January 1959 has been shown to be a month of large northward eddy heat transport at 25 and 100 mb, being limited to waves 1 and 2 scales at the upper level while being fairly well distributed to waves 1 to 7 at the lower level. At 25 mb, the significant baroclinic CE-processes are occurring at waves 1, 2 and to a smaller extent at waves 3 and 4, while at 500 mb, the scales at which these processes occur are predominantly wave numbers 3 followed by 1, with a lower but significant part played by the scales of waves numbers 2, 4, 6 and 7, in about equal intensity. The next important item is the non-linear wave 2 interaction leading to a significant sink of AE(2) energy at all levels. LA(1) channels energy to AE(1) in the stratosphere while it acts as a sink at 500 mb.

The daily spectral changes of the available energy modes will now be analysed to clarify the main processes attached to the current events at 25 mb. The daily variations in the total eddy and spectral (wave number 1, 2 and 3) available potential energy has been plotted in Fig. 5.10.2. This diagram may be compared with Fig. 5.2.4, corresponding to the similar variations in the eddy kinetic energy mode. Note that the plotted scales for AE are four times those of KE since the eddy kinetic energy per mb possesses characteristically a larger magnitude in the stratosphere, while the opposite has been shown to be true in the troposphere. The magnitudes of AE(3) are seen to be negligible during the month. AE(1) is found to explain most of the changes in the total eddy mode, except after the 26th, when AE(2) takes over, and also from the 10th to the 13th when AE(2) reaches almost the magnitude of AE(1).

The daily energy budget of wave number 1 available energy at 25 mb is exhibited in Fig. 5.10.3. It is again based on the relationship:

$$\frac{\partial AE(n)}{\partial t} - CA(n) + CE(n)^* - LA(n) = BAL(n) \qquad (5.10.1)$$

where again: $CE(n)^* = CE(n) - GE(n)$ and BAL(n) is the numerical error associated with the computations. Since the budget of AE(n) is complete, BAL(n) should be a reasonably small number. In Fig. 5.10.3, only BAL-values for which $|BAL(1)| > 0.5$ erg/cm^2 mb sec appear.

The decrease in AE(1) before the 8th is explained by a loss through negative radiative-thermal correlations and the baroclinic transfer to wave number 1 kinetic energy. The more or less continuous increase in AE(1) from the 9th to the 18th is due to three persistent mechanisms which put together explain the warming found at the scale of wave number 1. First the above period reflects a general trend for a net decrease in the mixed baroclinic-generative CE(1)* process. However, the smaller loss of wave 1 available energy through the above mentioned process is almost compensated for by the non-linear wave 1 available energy transfer emanating mostly from the corresponding wave 2 mode. The large and persistent energy transfer from the zonal mode through the northward eddy heat transport process CA(1) contributes finally in the rise of AE(1). From the 18th to the 20th, the large wave 1 oriented thermal field is baroclinically and radiatively relaxed, and it decreases even in the presence of positive non-linear wave interaction originating mainly in AE(2) and an increasing transfer from the zonal mode. From the 20th to the 24th, as CE(1)* stabilizes and CA(1) keeps increasing, AE(1) rebounds again to reach almost the high magnitudes it had on the 18th, the time of maximum warming. A drop in AE(1) from the 24th to the 25th is fairly well indicated by the baroclinic-barotropic exchanges and gains enjoyed by KE(1) and KZ energy reservoirs at about this time. Except for one ephemereal increase in AE(1) the following day, AE(1) reaches negligible magnitude by the end of the month as the whole energy cycle gradually changes its flow direction after the 26th. After subtracting the negative effect due to the generation of wave 1 available energy, a forced circulation in zonal planes results at the scale of wave 1. Simultaneously, AE(1) feeds energy to the zonal available mode as CA(1) becomes negative.

As mentioned above AE(2) sustains two significant rises during the month: the first one on the 13th and the second after the 27th. This is readily depicted in Fig. 5.10.2. Wave number 2 available energy budget is depicted in Fig. 5.10.4, following the same nomenclature as defined for the AE(1)-budget. The general rise of AE(2) up to the 10th can be explained by the northward eddy heat transport process CA(2) overshadowing the transfer by the baroclinic-radiative processes CE(2)*. The further rise until the 13th is not too clearly indicated by the spectral flow diagram. It is to be noted that the rate of change of AE(2) in this period is less than 1 unit, and assuming a low relative error of 10% in the CE(n)* and CA(n) processes (being in the order of 4 units each), then the error made in subtracting one from the other is of the order of magnitude of the AE(2) rates of change themselves. The decrease of AE(2) from the 13th to the 19th is found to be caused by the radiative losses in part, but mostly by the losses associated with the baroclinic transfer and the non-linear wave 2 transfer of available energy mainly to wave 1. These processes overshadow the lesser exchanges from the zonal available energy reservoir (CA(2)). The stabilization and slight rising trend found during the 19th-24th period is characterized by a complete reversal in the exchanges CE(2)* and CA(2). Were it not for the consistent direction of exchanges non-linearly from AE(2) to AE(1) the former would show a much sharper rise; the system is quiescent until both CA(2) and CE(2) change to their previous flow directions and intensities. The above changes occur after the 26th, where in fact the CA(2)-mechanism surpasses the subsequent baroclinic and radiative output of AE(2)-energy.

5.11 Summary of the Monthly Mean and Daily Energetics of January 1959

The results of this section are summarized by the mean January spectral flow diagram on Fig. 5.11.1. The 100 mb spectral conversions have been deleted since the amplitudes were rather small. At 25 mb, baroclinic activity is found in all the significant waves (1 to 4). The transfers between wave 5 and above are weak and flow in the opposite direction. Wave 1 is the dominant in the baroclinic process followed by wave 2. This shows that the post-mid-month minor stratospheric warming has been a wave 1 phenomenon. Perry (1966) studied a strong wave 2 oriented phenomenon; the strength of the bi-polar pattern was also reflected in the monthly mean baroclinic processes. CK(n) is negative for all values of n, leading to exchanges from the wave pattern to the zonal flow, with wave 2 leading in magnitude. It is noted that although KE(2) loses more than the other spectral kinetic energy reservoirs to KZ, it nevertheless gains by the non-linear exchanges: mostly from KE(3) and KE(5) followed by KE(1). The general rise of cold air and subsidence of warm air in the meridional planes leads to a continuous increase of the zonal available energy in cooperation with the zonal generation effect of radiation at 25 mb. The zonal temperature field so produced is eventually deformed longitudinally by the local eddy air motion which strongly pumps available energy into its eddy mode, especially in the scales of wave numbers 1 to 4 while the smaller scales are rather unperturbed by this process. The CA(n) transfers are large at waves 1 and 2 especially, their magnitudes amounting to 5 times those in waves 3 and 4. The wave 1 available energy reservoir is further increased by the re-distribution between the temperature scales, most of the gain of AE(1) being at the expense of AE(2). Because the long wave cooling is strongly negatively correlated to the temperature field, GE(1) leads the negative spectral available energy generation.

The 500-mb mean monthly spectral energy flow is also shown in Fig. 5.11.1. The diagram shows a typical tropospheric active energy flow. Some differences are noted, however. The CK(n)'s are all very small, although in the usual tropospheric direction. This can be traced back to the boundary problem discussed earlier, and to the fact that the strongest barotropic processes were much more active at jet stream levels. The non-linear kinetic wave interaction distribution does not agree with Saltzman and Teweles (1964) and Yang (1967 a, b) whereby wave number 2 and the cyclone waves were feeding both sides of the spectrum at 500 mb. Our results are closer to the Murakami and Tomatsu (1964) mean 1962 500-mb computations where waves 2, 3, 4, 5 and 6 fed the other waves and where wave 1 was receiving a large portion of the exchange. In the present study waves 2, 3, and 4 feed their kinetic energy to the other waves. The persistence of the LK(1)-process in being positive (KE(1) gaining non-linearly from other scales) has been found to be significant within the 95 percent confidence range for the mean. The existence of a persistent blocking circulation has been observed during January 1959. In the mean for the month, at 500 mb, kinetic energy wave numbers 2 to 5, followed by 1, 6 and 7, were found to be the dominant scales, in the given order. The weakness of the barotropic processes requires for balance large frictional dissipation and eddy kinetic energy export across the southern boundaries, whereas possibly, horizontal zonal momentum convergence across the lateral boundaries maintains the zonal kinetic energy in the region of interest.

In order to summarize the distribution in time of the stratospheric events among the various energy modes, a time spectral energy flow diagram for the 25 mb level has been constructed and is presented as Fig. 5.11.2. The relative significance of the transfers is indicated by the arrow intensities given in the legend. The significant "events" during the month are highlighted by the circle-in-square boxes while the other sequential states of the energy reservoirs are circled only. Processes involving sources and sinks of energy have been simply written down. The numbers below the reservoirs or transfers specify the day or days of significant maximum intensities of the corresponding energy modes or transfers.

Three separate periods of high stratospheric eddy kinetic energy appeared during January 1959. The three periods appear to be causally related to blocking flows in the troposphere. The troposphere-stratosphere time pairs in January are the following: 7th and 11th, 18th and 21st, and 24th and 29th. The time differences between the lower and upper events are somewhat variable because the upper events are not only associated with external energy but are also modulated by "in situ" processes such as the barotropic and baroclinic conversions, which may be intense enough to create a local time maximum in the eddy kinetic energy mode. The sequence of processes leading into the separate stratospheric events will be given in summary. The description of the various phases and exchanges may be best understood in relation to the flow chart on Fig. 5.11.2.

a) The rather sharp increase in KE(2) from the 6th to the 9th is mainly due to simultaneous barotropic exchanges from the zonal, wave 1 and wave 3 kinetic energy modes, the baroclinic exchanges at this wavelength and time being rather small. The energy transferred to KE(2) non-linearly via KE(3) originated in the troposphere through a pulse in the BGE(3)-term, while the other non-linear interaction impact on KE(2) from KE(1) was through a moderate baroclinic exchange from AE(1) by the CE(1)-process. KE(2) declined through dissipative effects from the 9th to the 10th, and then rose again as a strengthening baroclinic exchange at the scale of wave number 2 coincided with a pulse in the pressure interaction mechanism BGE(2). The net effect was that KE(2) was maintained through to the 12th, leading to the first "event". The bipolar pattern characterizing the first "event" had some degree of eccentricity as a local maximum of AE(1) on the 11th and of KE(1) on the 11th-12th period can be seen on Fig. 5.10.2 and 5.2.4, respectively.

b) The second event flows out of the first one. It is characterized by increasing eccentric activity in time, in response to i) a rising wave one pressure interaction acting on the 0-25 mb layer, with some help from a similar process in wave number two which peaks on the 15th concurrent with a non-linear transfer from wave two kinetic energy into wave one, and ii) moderate exchanges from AE(1) fed non-linearly by AE(2). AE(1) showed its peak on the 18th and then weakened as KE(1) grew to its monthly maximum over the 18th-21st period. In summary, the second stratospheric "event" evolved from a large eccentricity in the flow pattern caused by three immediate mechanisms given in order of their intensity: i) a strong pressure interaction at the scale of wave number one, originating from the troposphere, ii) a moderate non-linear kinetic energy transfer from wave number two, and iii) a moderate baroclinic transfer from AE(1).

c) The third and last stratospheric event is characterized by the large bipolar flow found at the end of the month. The complex exchanges leading to this state from the highly eccentric state during the 18th-21st period are shown on Fig. 5.11.2. Only the significant processes will be sketched qualitatively here. The higher than average KE(1) energy level leads through a CK-exchange to a KZ-peak on the 18th and then an AZ peak on the 21st. An increase in the northward heat transport follows creating an AE(1)-maximum on the 24th simultaneous with a baroclinic exchange to KE(1). A significant part of the KE(1)-energy is converted into the zonal mode, and KZ exhibits a maximum on the 25th. Possibly under the influence of both the temperature-vertical motion correlation and the solar heating, the zonal available energy attains a local peak on the 27th. This sets up strong northward heat transport at wave number two and a corresponding baroclinic transfer resulting in a large KE(2)-amplification. Two other processes are about equally significant, i.e., the barotropic exchange from the zonal flow after the 27th, and the pressure interaction BGE(2)-term, likely associated with the blocking state found at the end of the month. A weaker process originating in the troposphere at wave number three converts energy into the 25-mb KE(3) mode, and then to KE(2) non-linearly, the mechanism explaining some part of the rise of KE(2).

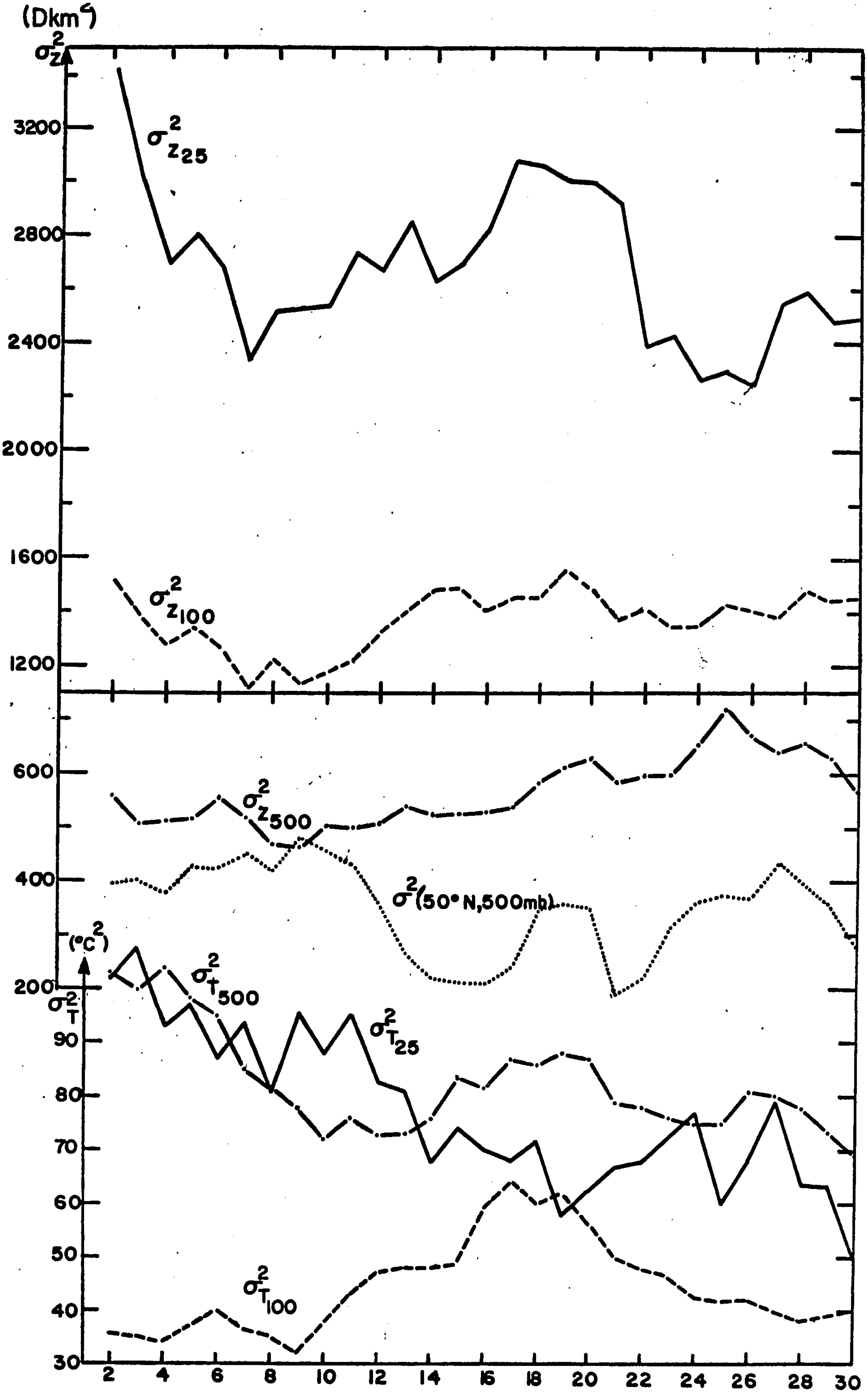

Fig. 5.1.1. Height and temperature variances in January 1959 at 25, 100 and 500 mb

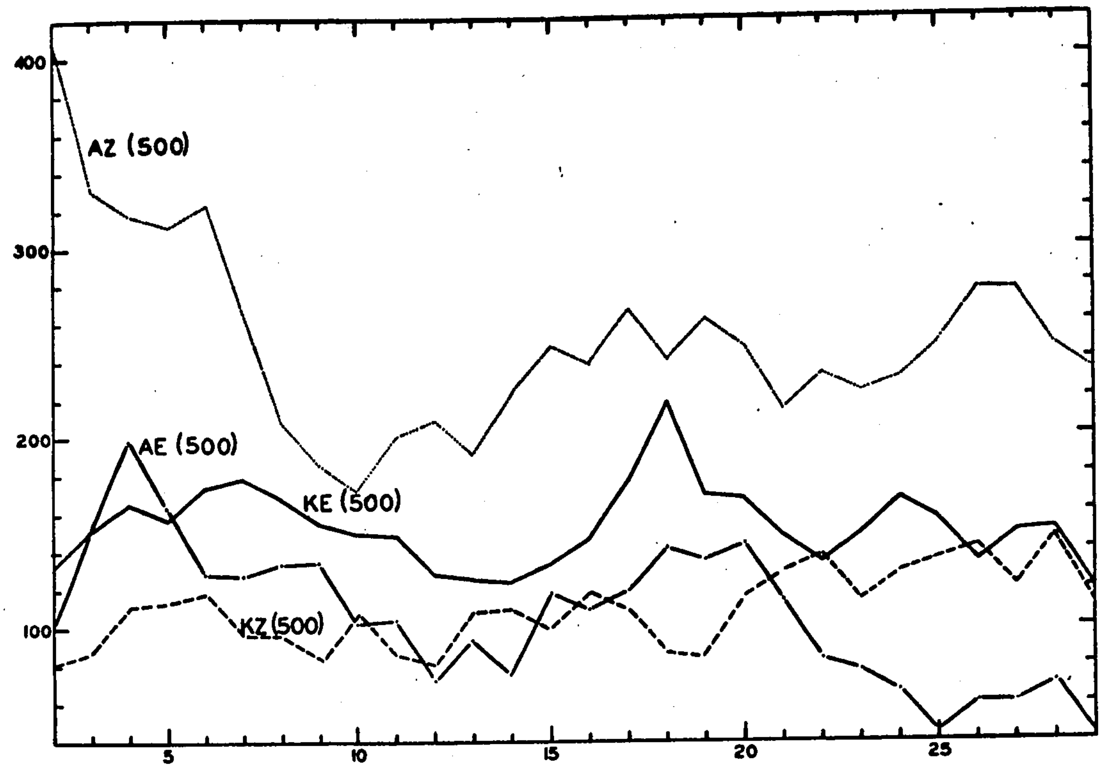

FIG: 5.2.1 DAILY VARIATIONS OF THE VARIOUS ENERGY MODES AT 500MB.
UNITS: 10^4 ERGS/CM^2 MB

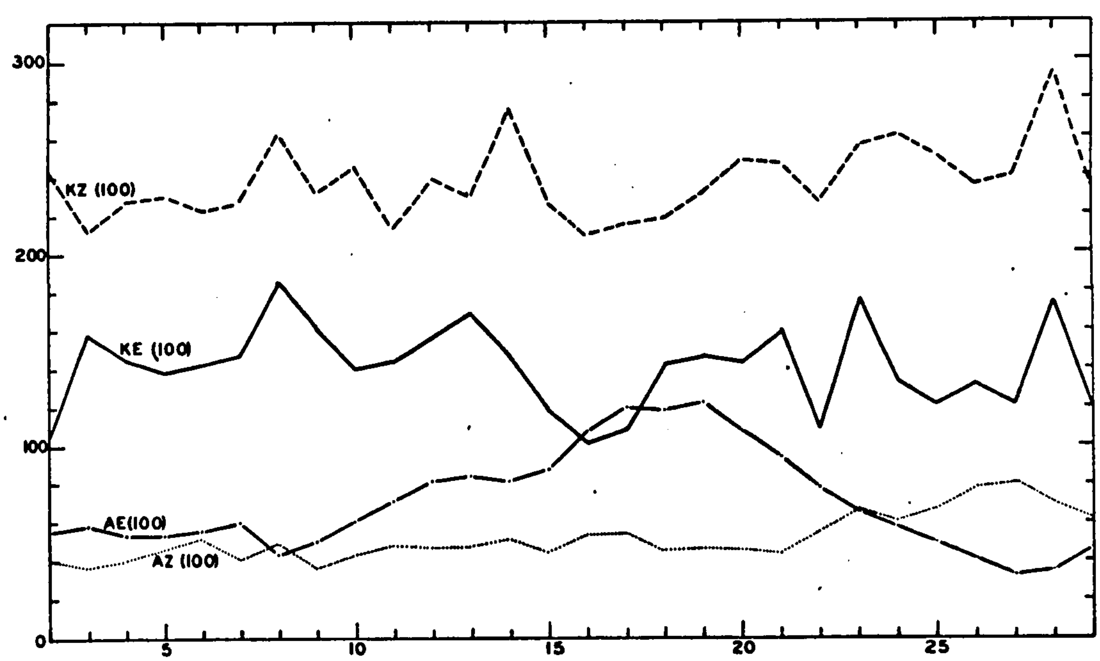

FIG: 5.2.2 DAILY VARIATIONS OF THE VARIOUS ENERGY MODES AT 100 MB.
UNITS: 10^4 ERGS/CM^2 MB

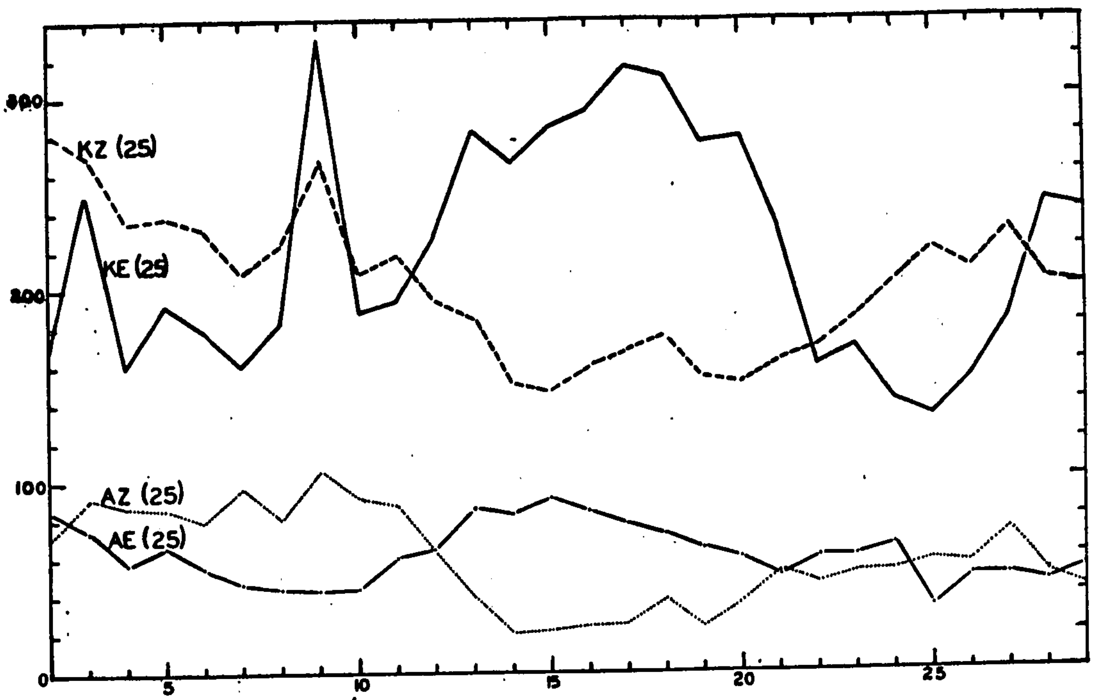

FIG: 5.2.3 DAILY VARIATIONS OF THE VARIOUS ENERGY MODES AT 25 MB.
UNITS: 10^4 ERGS CM^2 MB

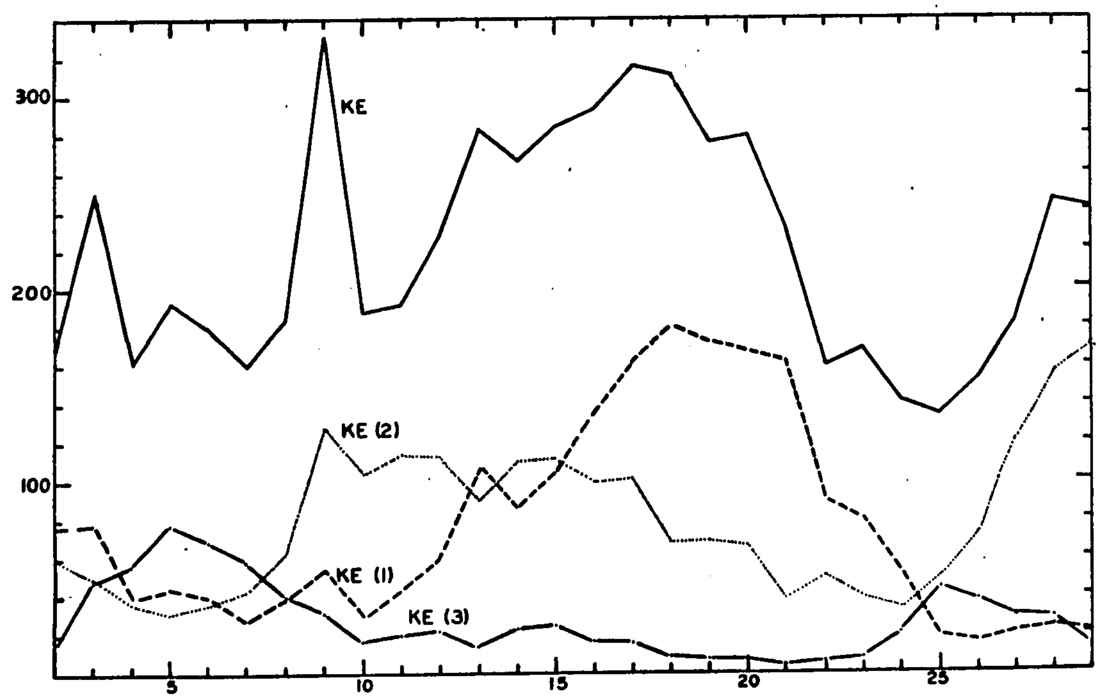

FIG: 5.2.4 SPECTRAL PARTITION OF THE KINETIC ENERGY AT 25 MB IN JANUARY 1959.
UNITS: 10^4 ERGS/CM^2 MB

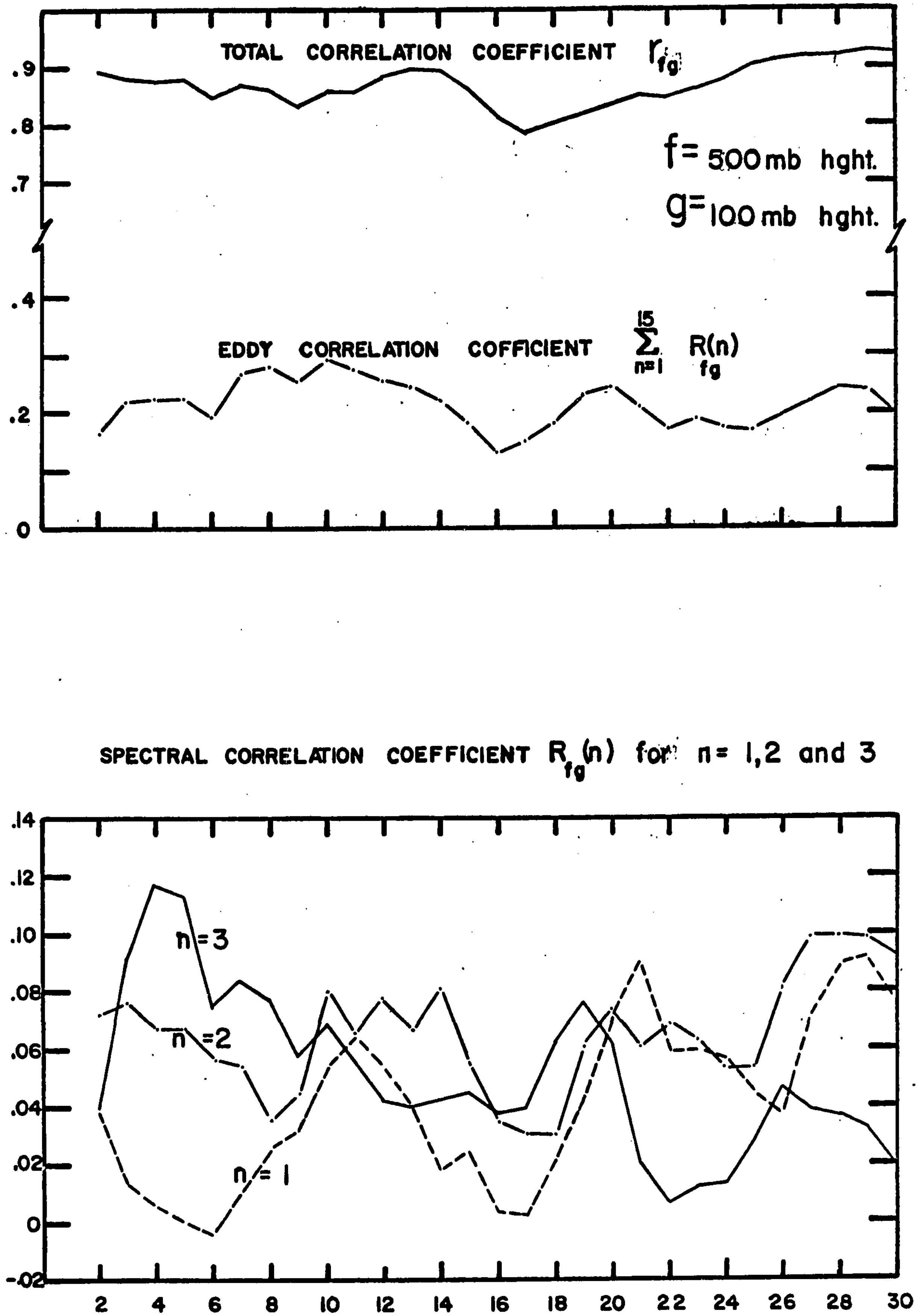

Fig. 5.3.1. Correlation coefficients between the 100-500 mb heights for total, eddy and wave number 1, 2 and 3 cases

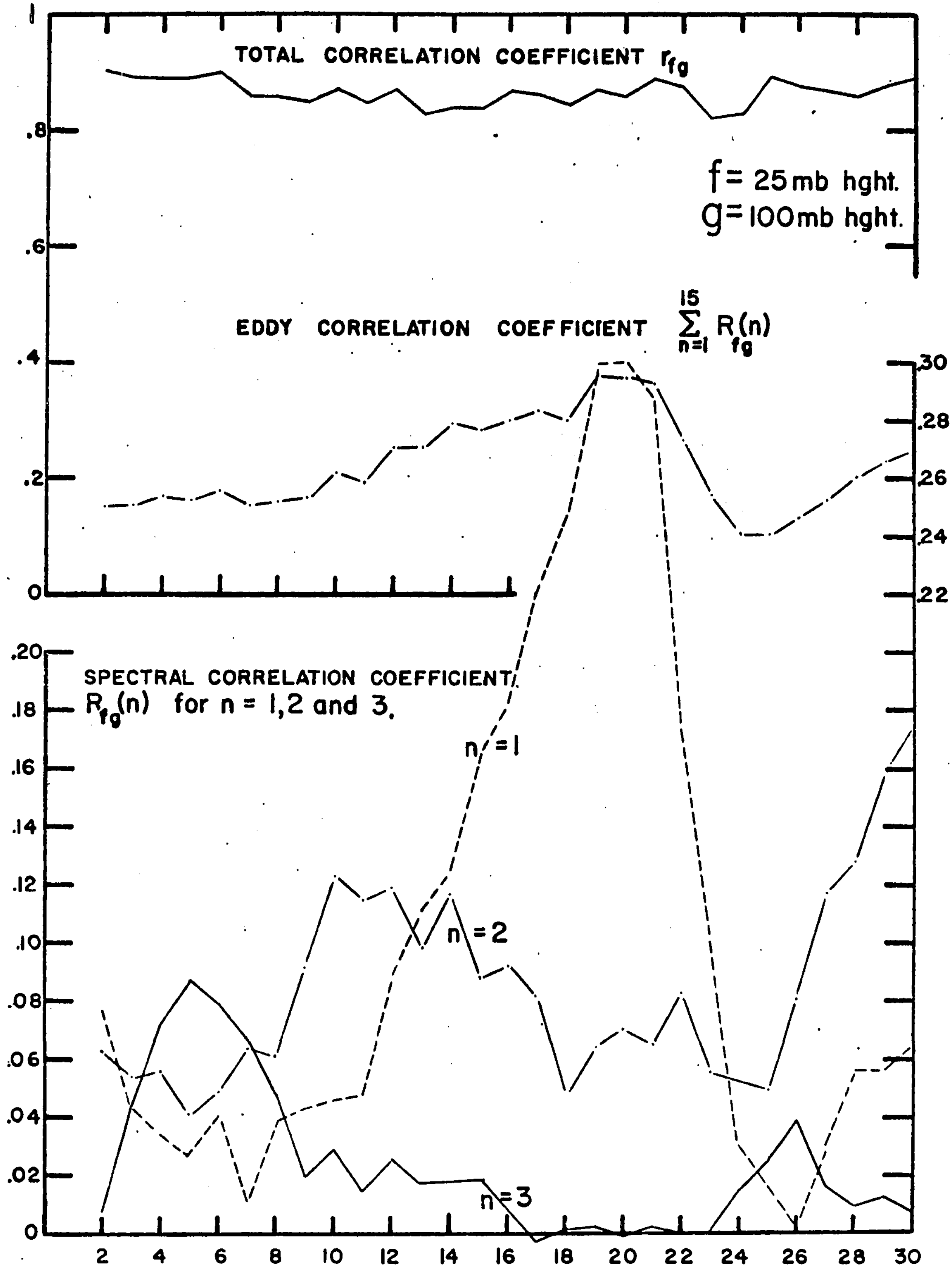

Fig. 5.3.2. Correlation coefficients between the 25-100 mb heights for total, eddy and wave numbers 1, 2 and 3 cases.

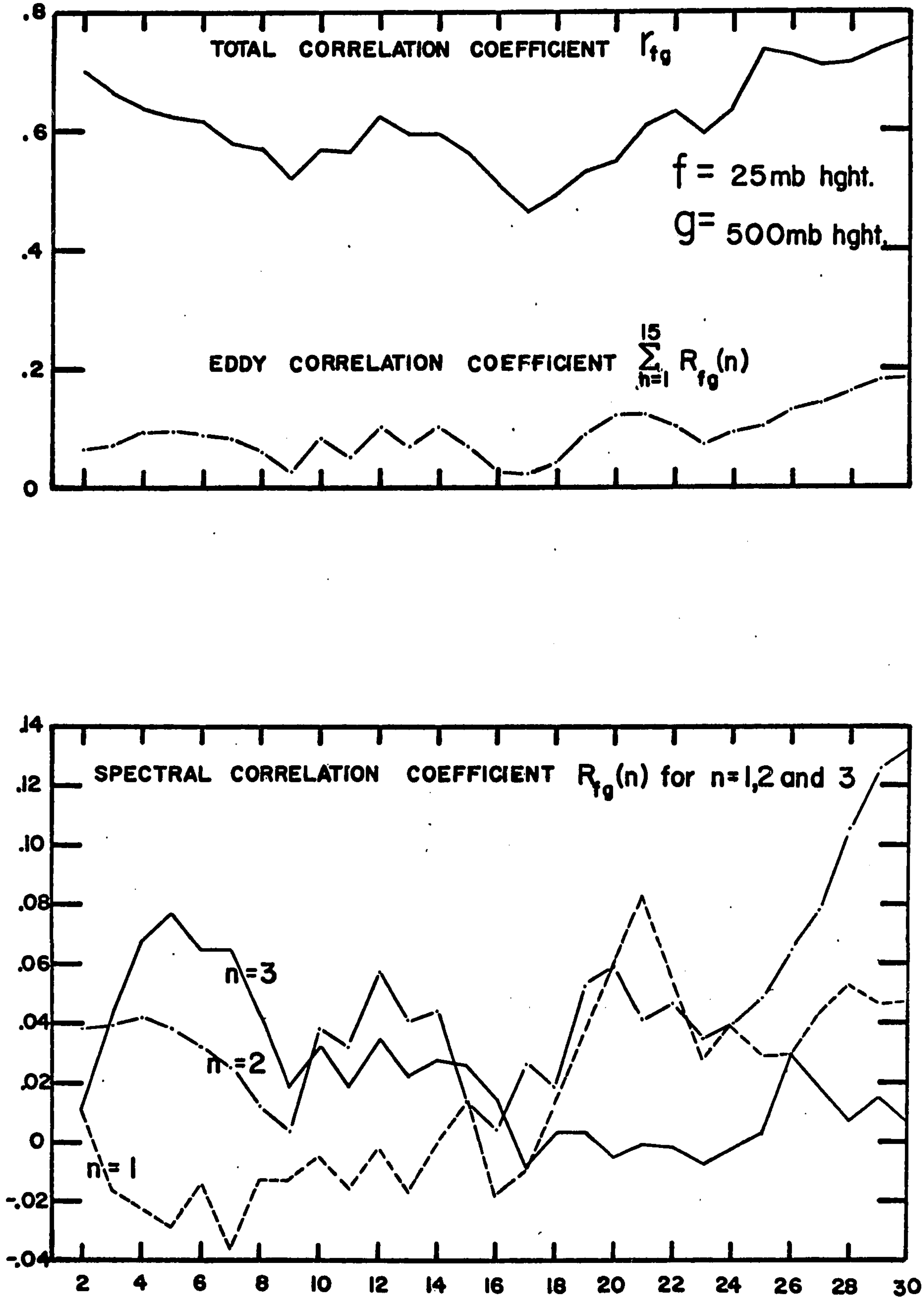

FIG. 5. 3. 3. Correlation coefficient between the 25–500 mb heights for total, eddy and wave 1, 2 and 3 cases.

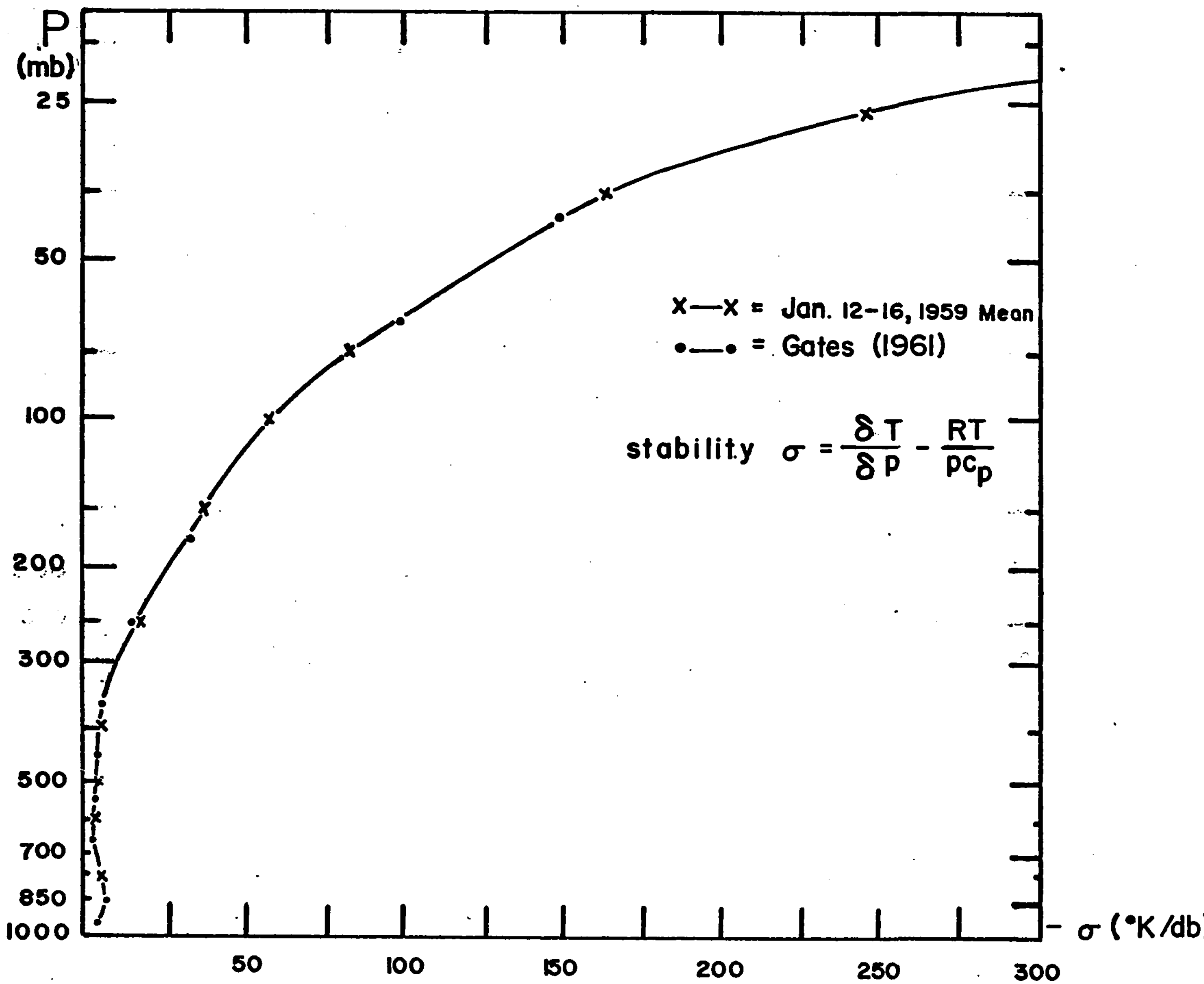

FIG: 5.4.1 Comparison of the mean Jan. 12–16, 1959 profile of the stability against Gates (1961). Units: (°K/db)

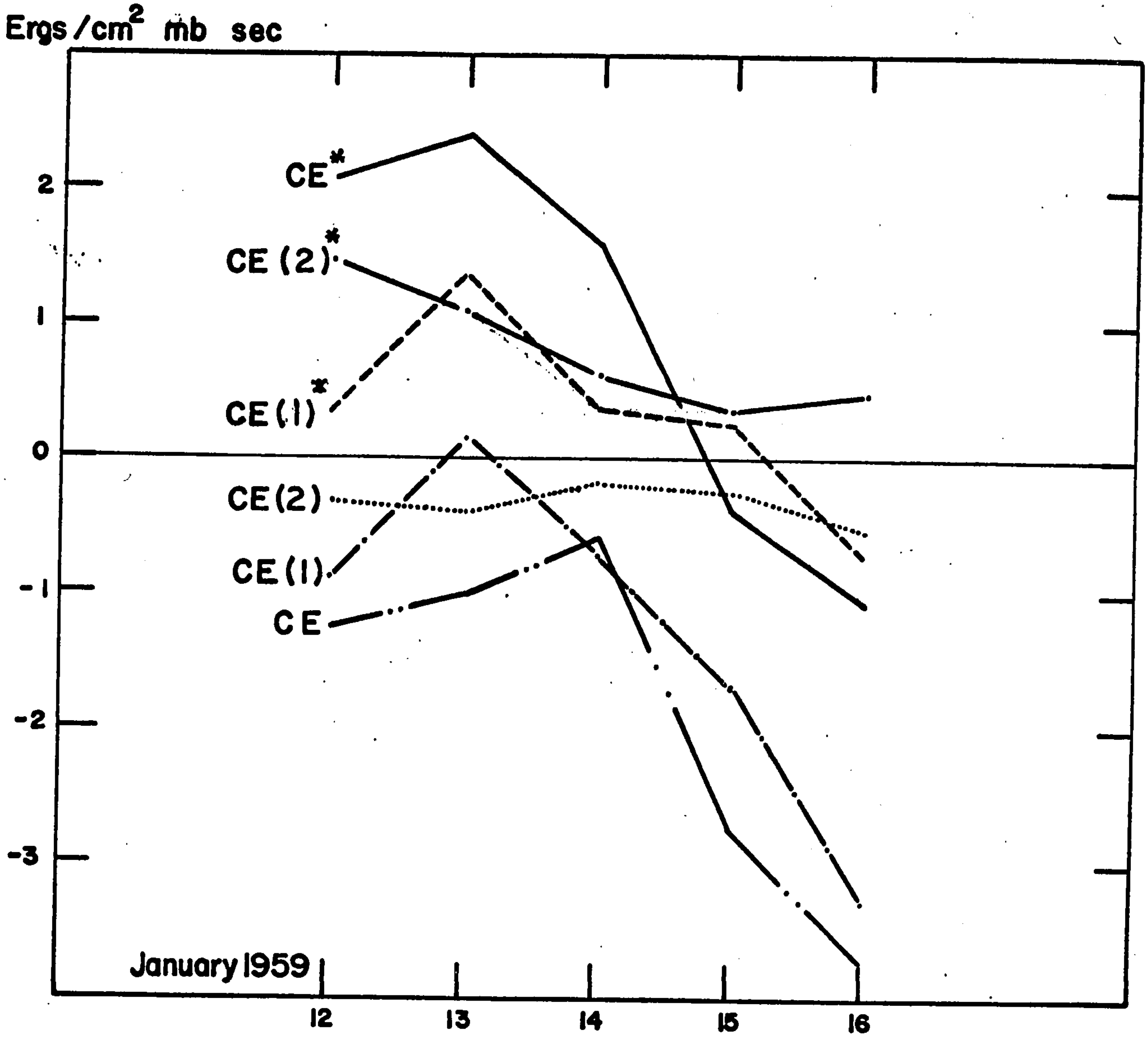

FIG. 5.4.2. Comparisons of computed energy conversions between eddy modes of available to kinetic energy using the diabatic diagnostic method (CE) and the adiabatic thermodynamic method (CE*) for the 25-100 mb layer.
UNITS: Ergs/cm^2 mb sec.

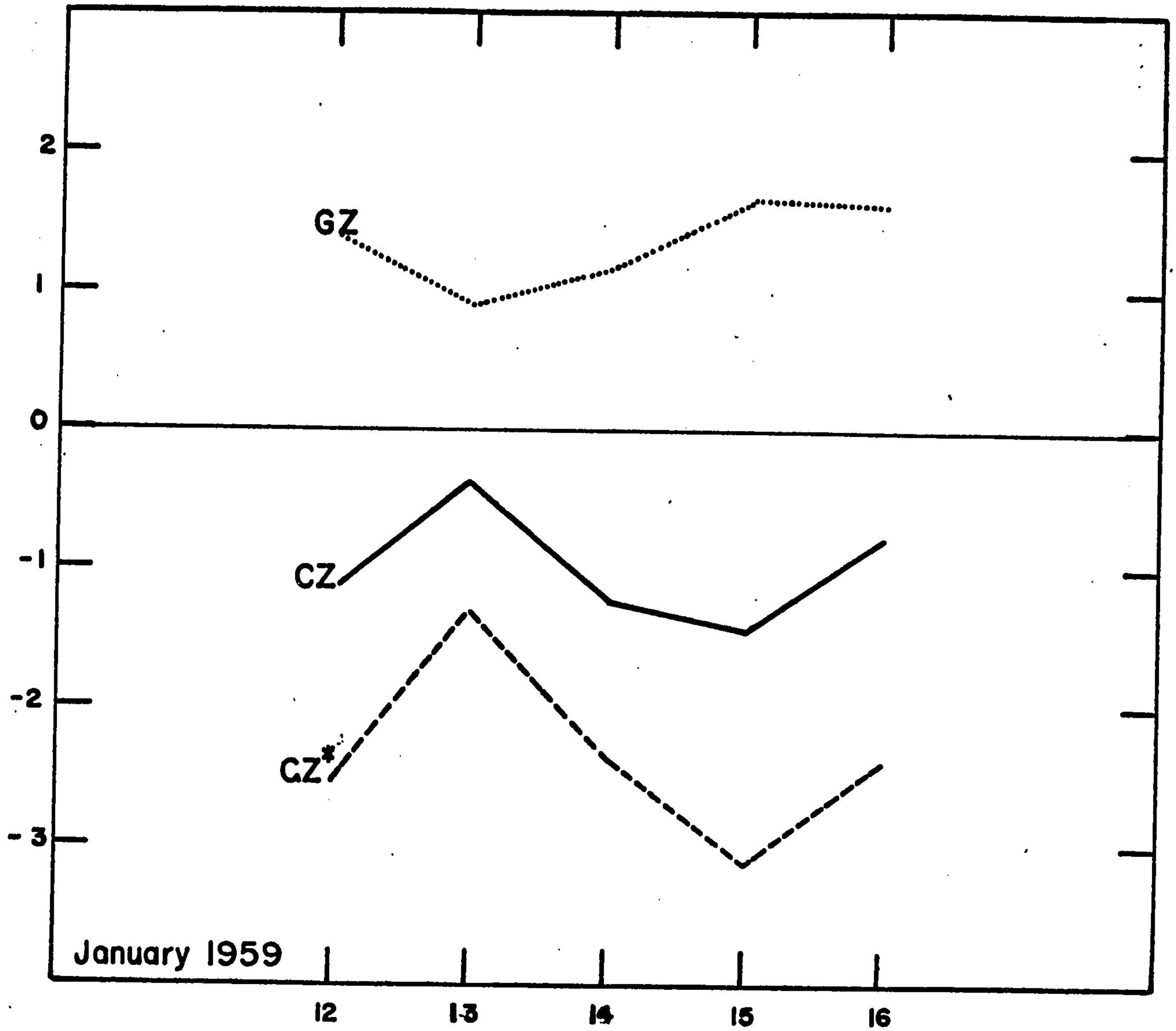

FIG. 5.4.3. Comparisons of computed energy conversions between the zonal modes of available to kinetic energy using the diabatic diagnostic (CZ) method and the adiabatic thermodynamic (CZ^*) method. The zonal generation GZ is given by the residual $CZ - CZ^*$. The computations are valid for the 100–25 mb layer.
UNITS: Ergs/cm^2 mb sec.

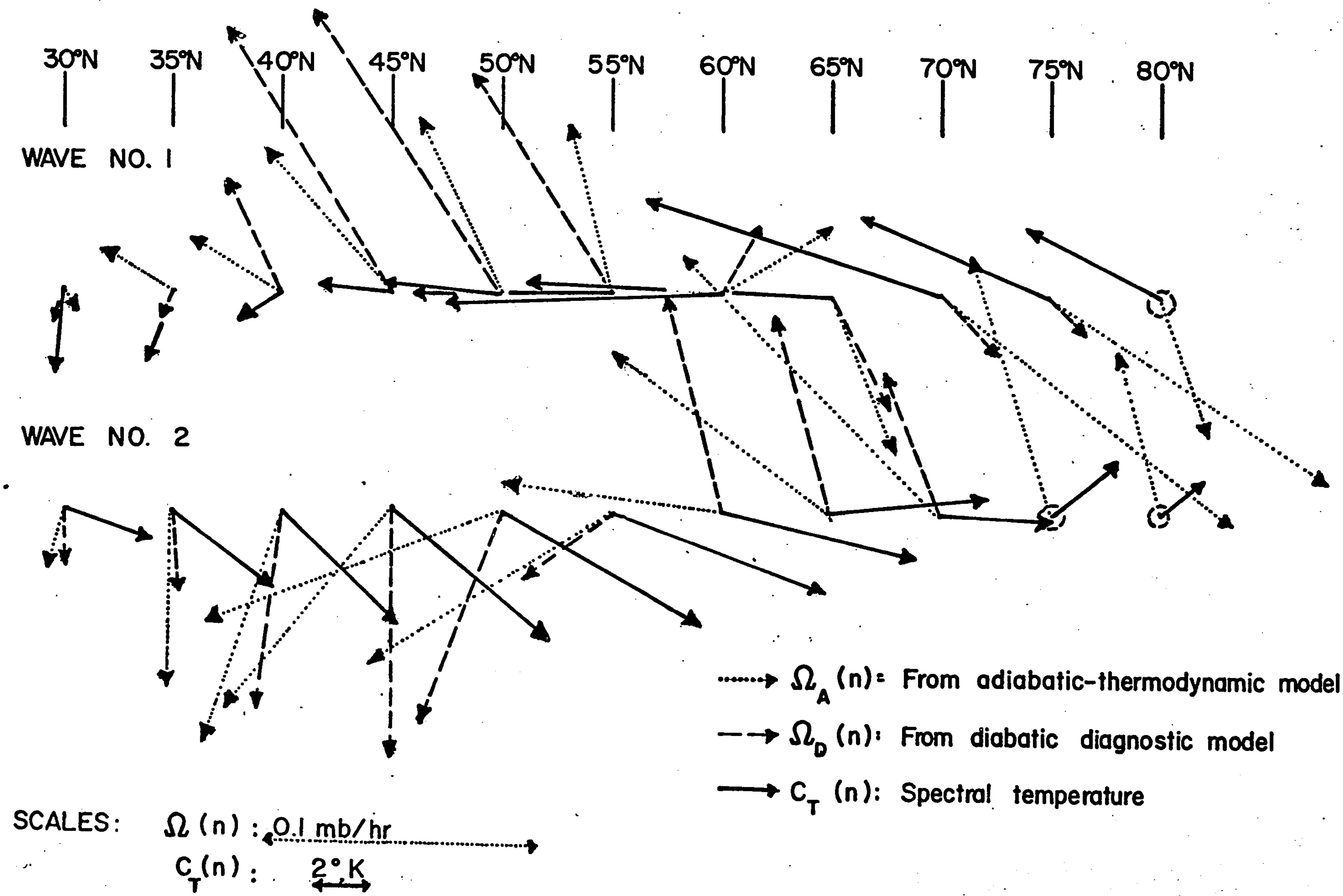

FIG. 5. 4. 4. Spectral vectors for both vertical motion methods and temperature at 25 mb on Jan. 12, 1959.

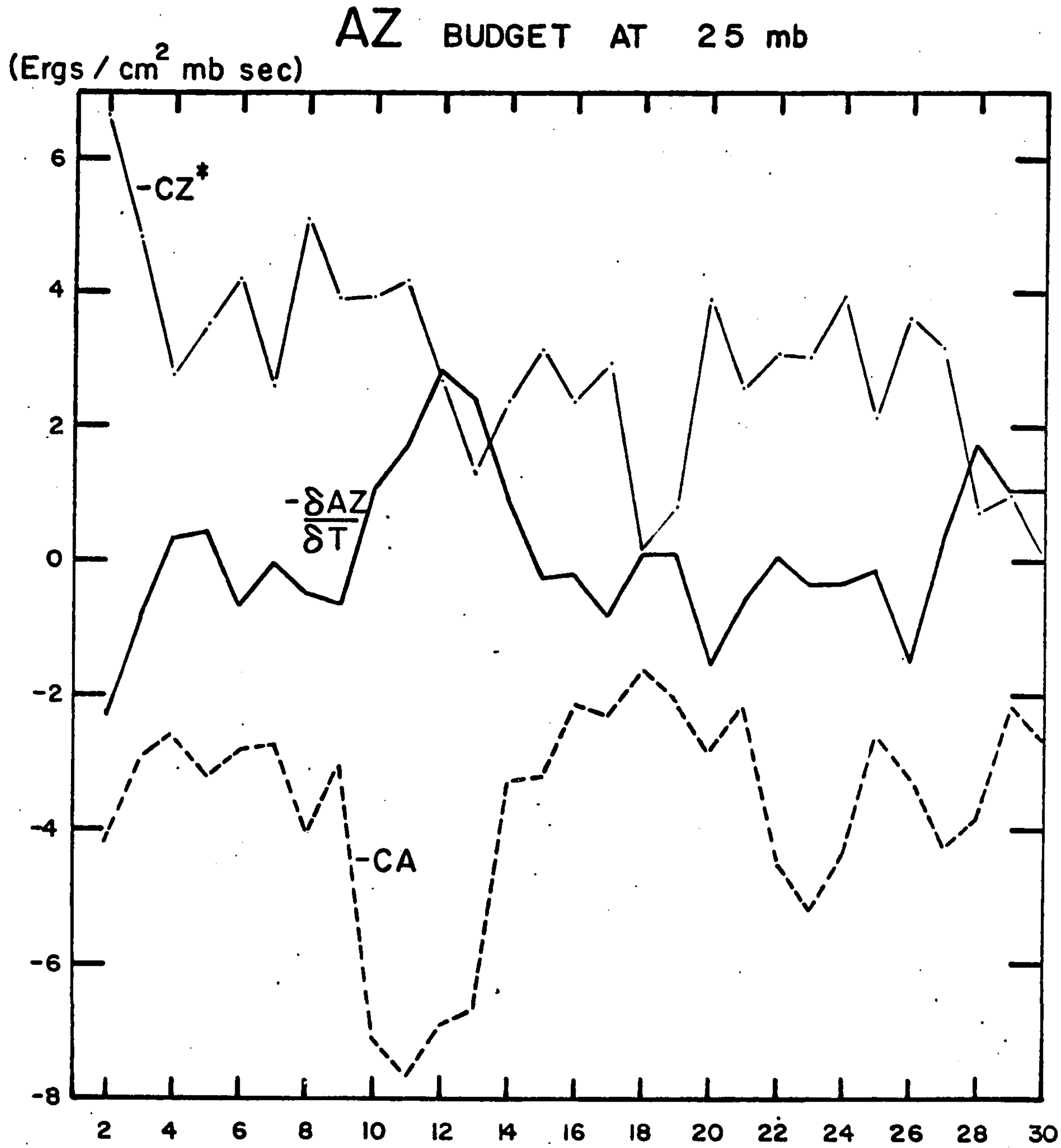

FIG. 5.5.1 : Balance terms in the budget of zonal available energy AZ at 25 mb during January 1959. Units: Ergs/cm^2 mb sec.

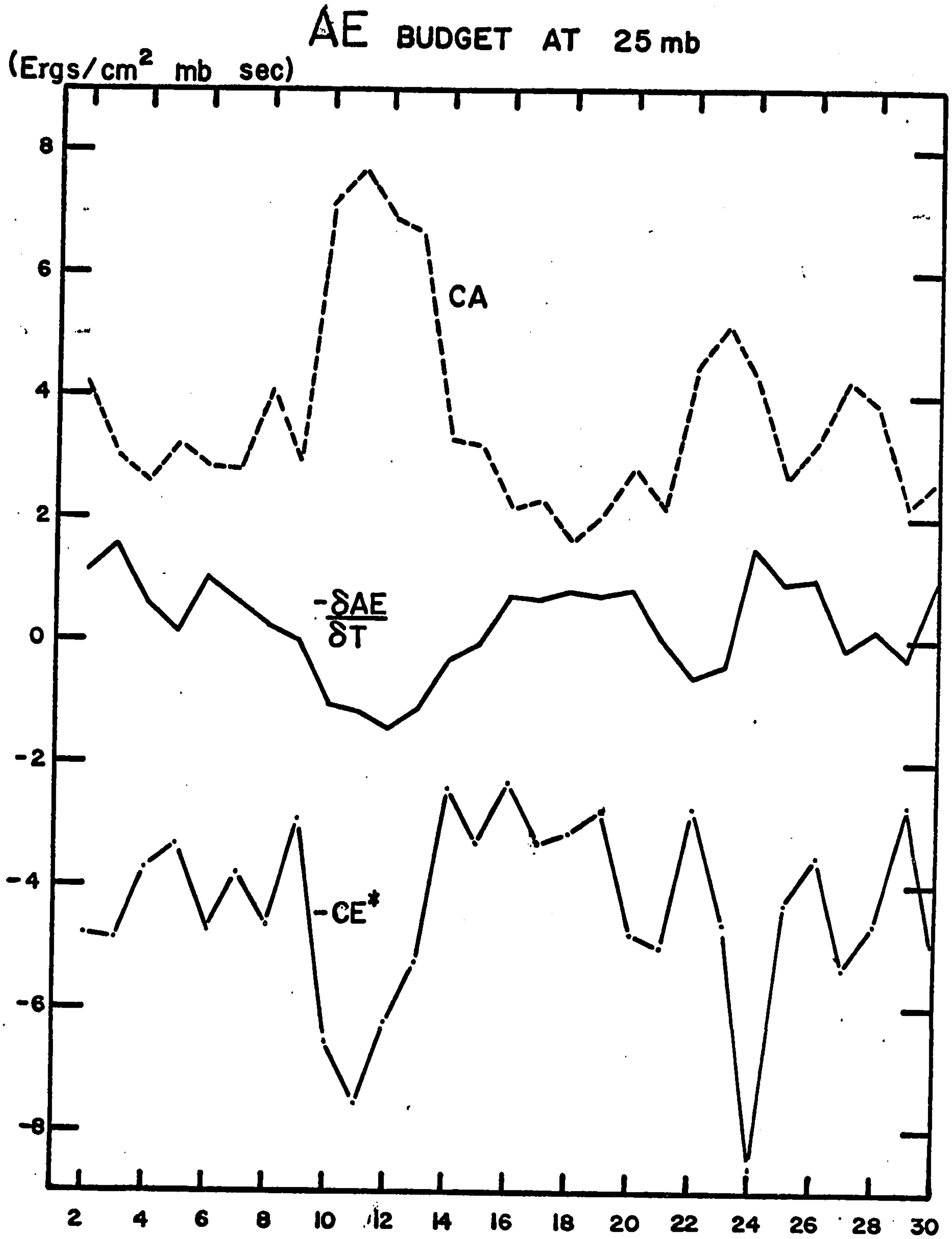

Fig. 5.5.2. Balance terms in the budget of the eddy available energy AE at 25 mb in January 1959

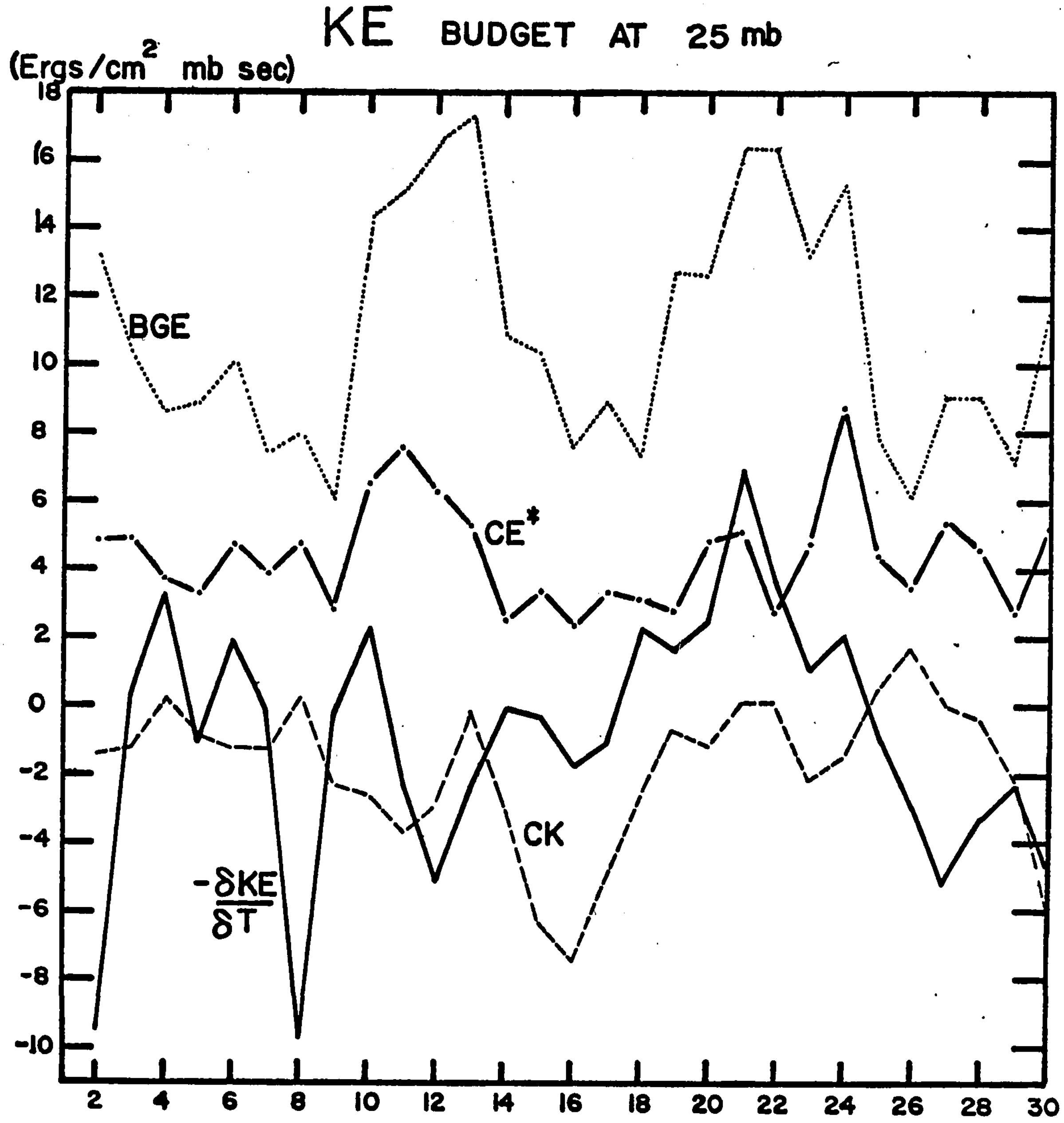

Fig. 5.5.3. Balance terms in the budget of the eddy kinetic energy KE at 25 mb in January 1959

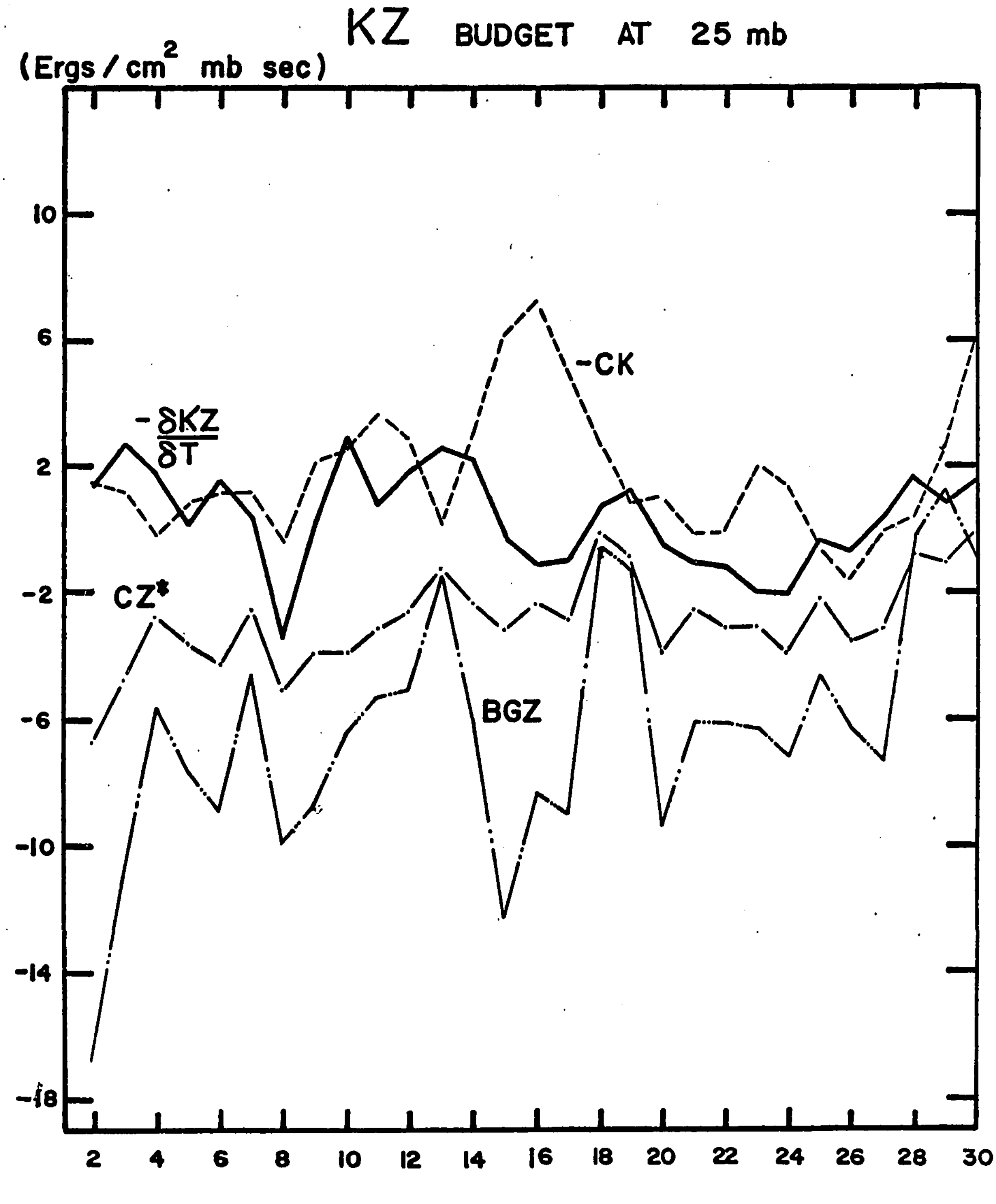

Fig. 5.5.4. KZ budget at 25 mb

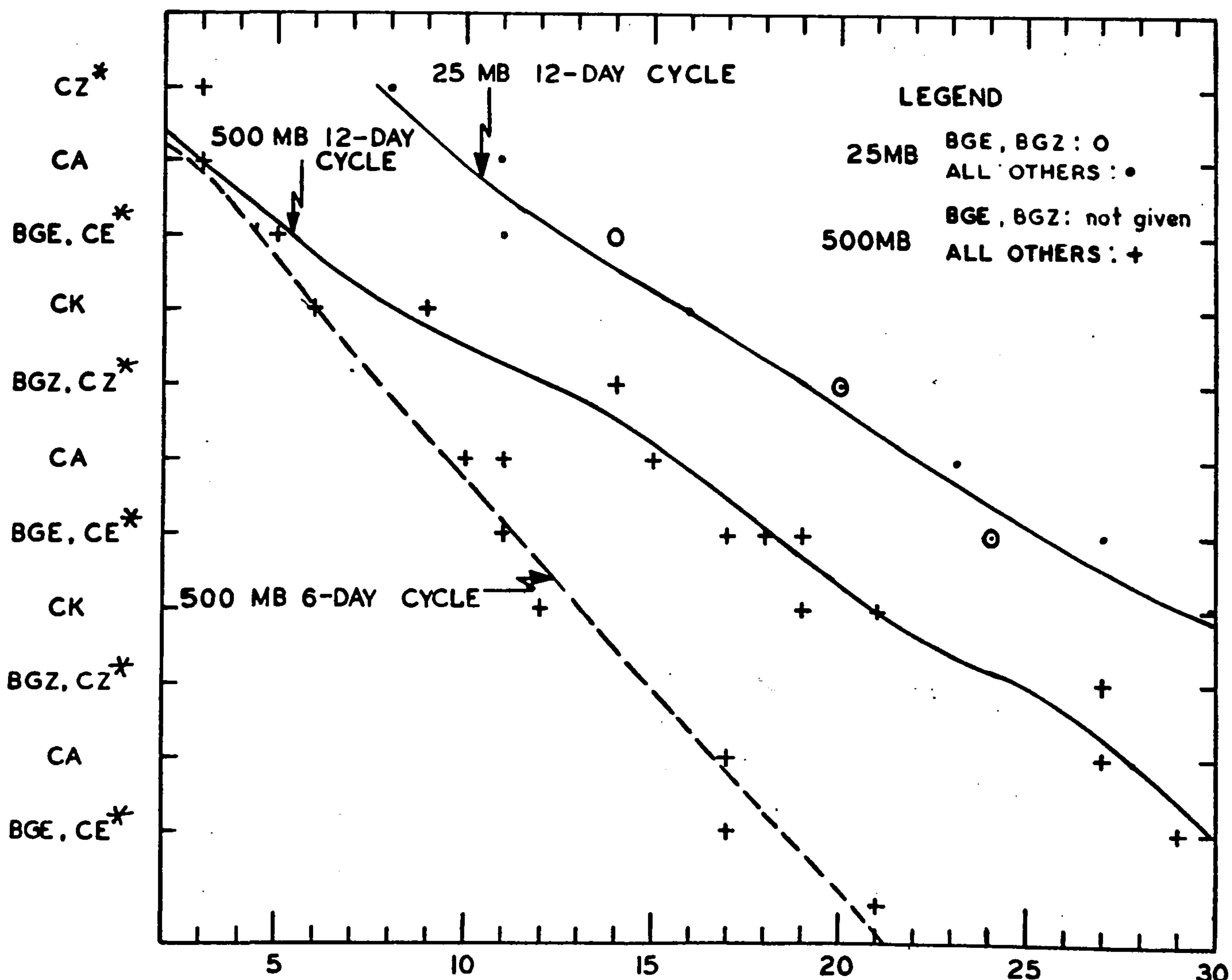

FIG: 5.5.5 TIME LOCI OF ENERGY TRANSFER MAXIMA IN JANUARY 1959 AT 25 AND 500 MB

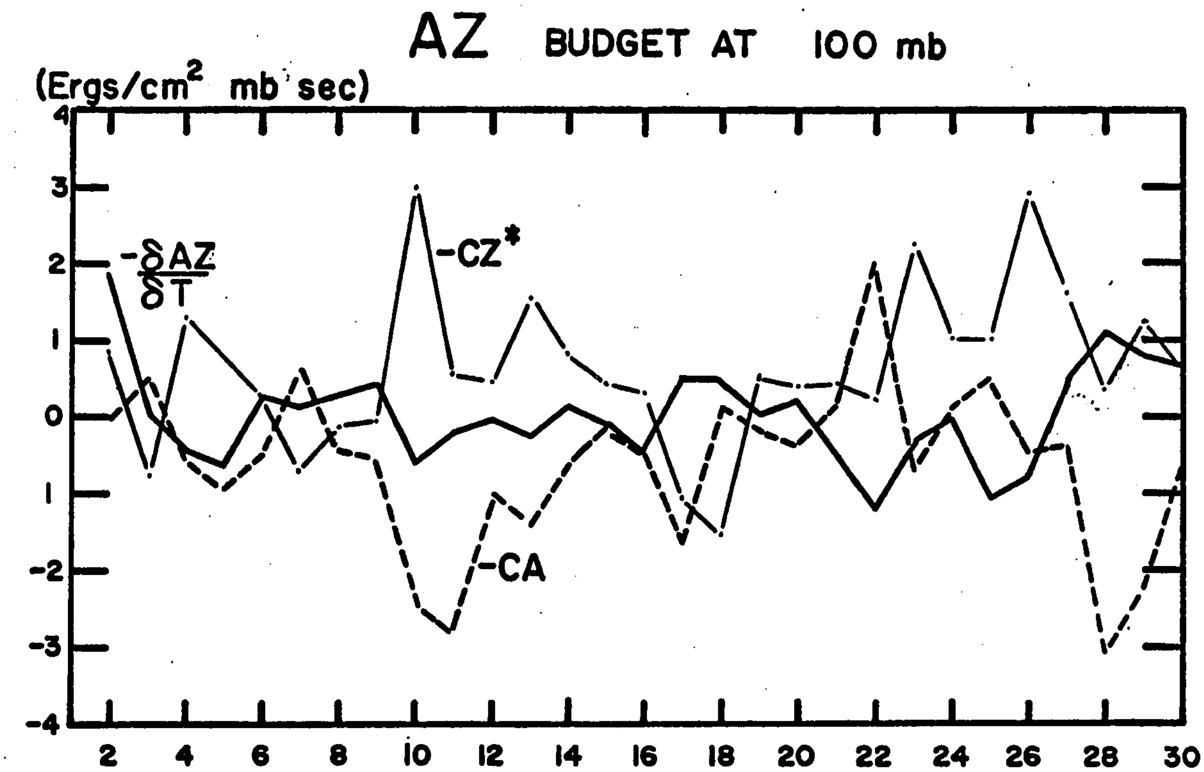

Fig. 5.6.1. Balance terms for the budget of the zonal available energy AZ at 100 mb during January 1959

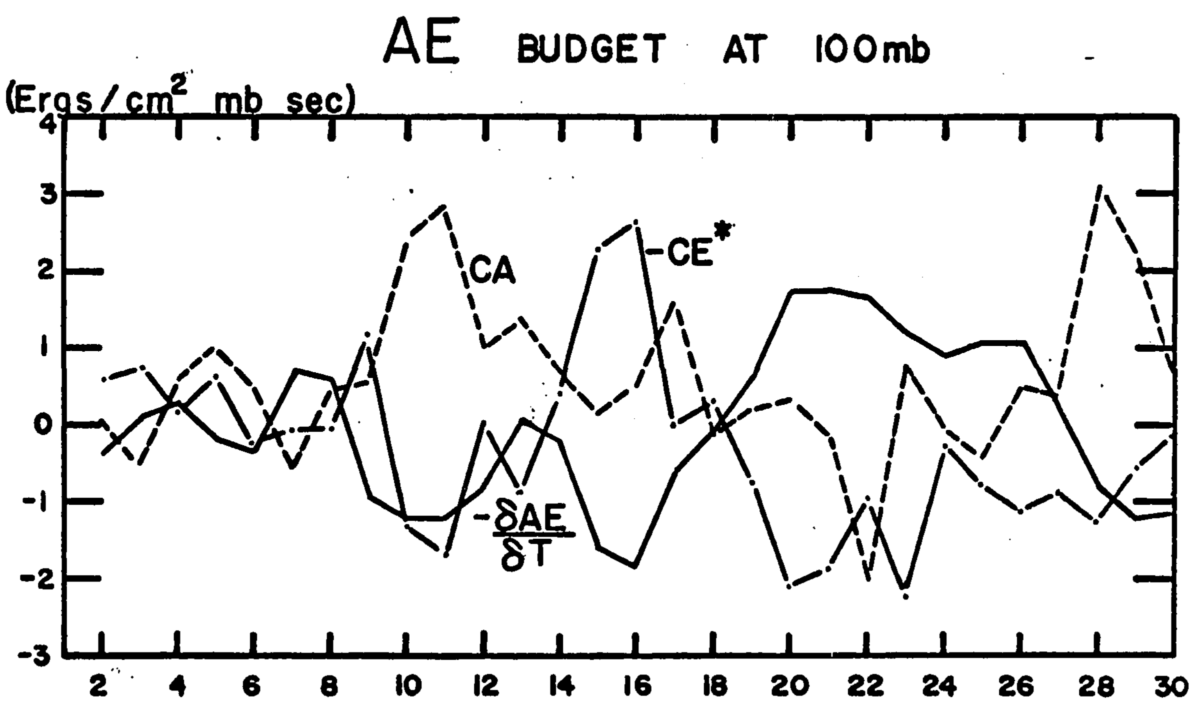

Fig. 5.6.2. Balance terms of the eddy available energy AE at 100 mb during January 1959

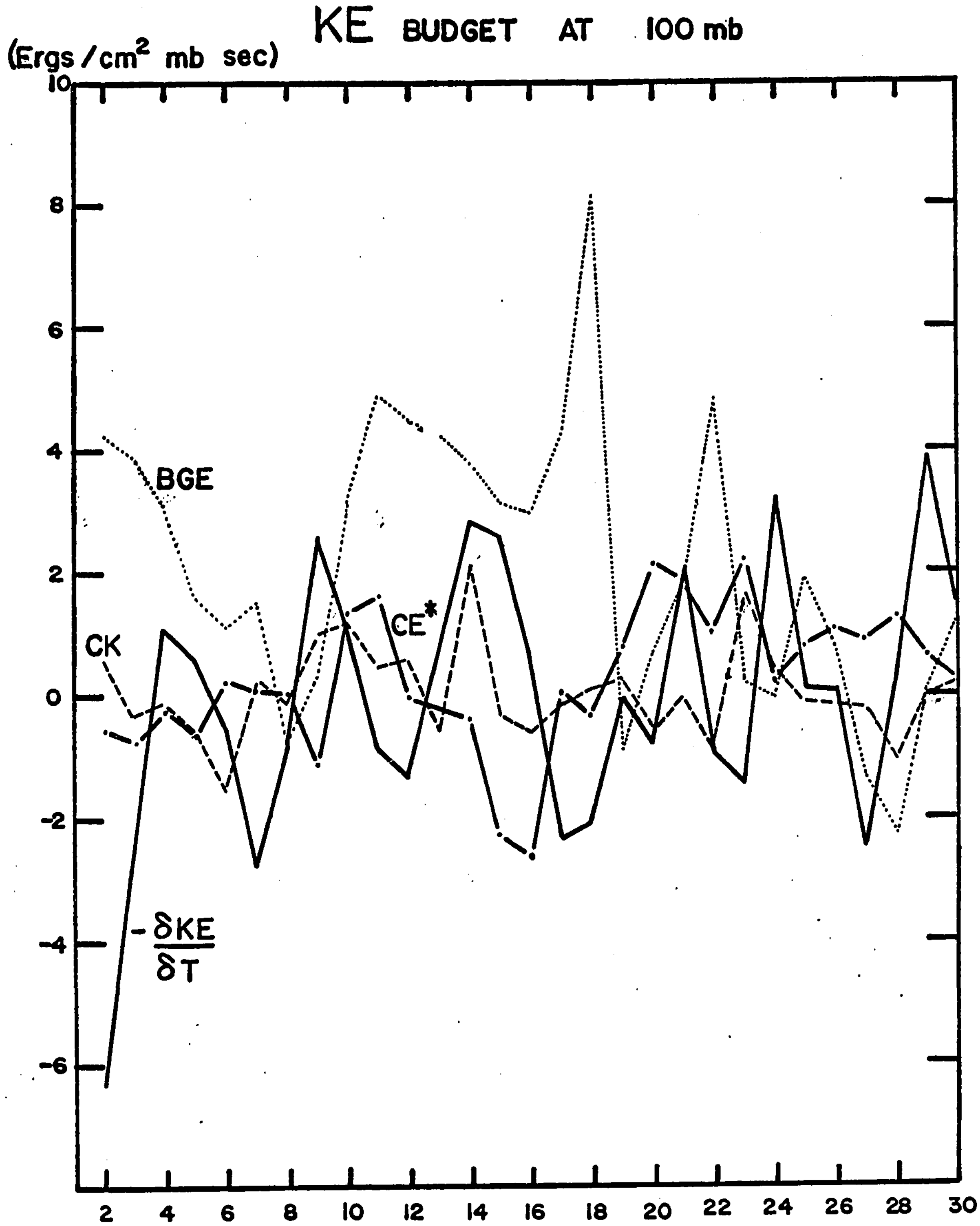

Fig. 5.6.3. Balance terms of the eddy kinetic energy KE at 100 mb during January 1959

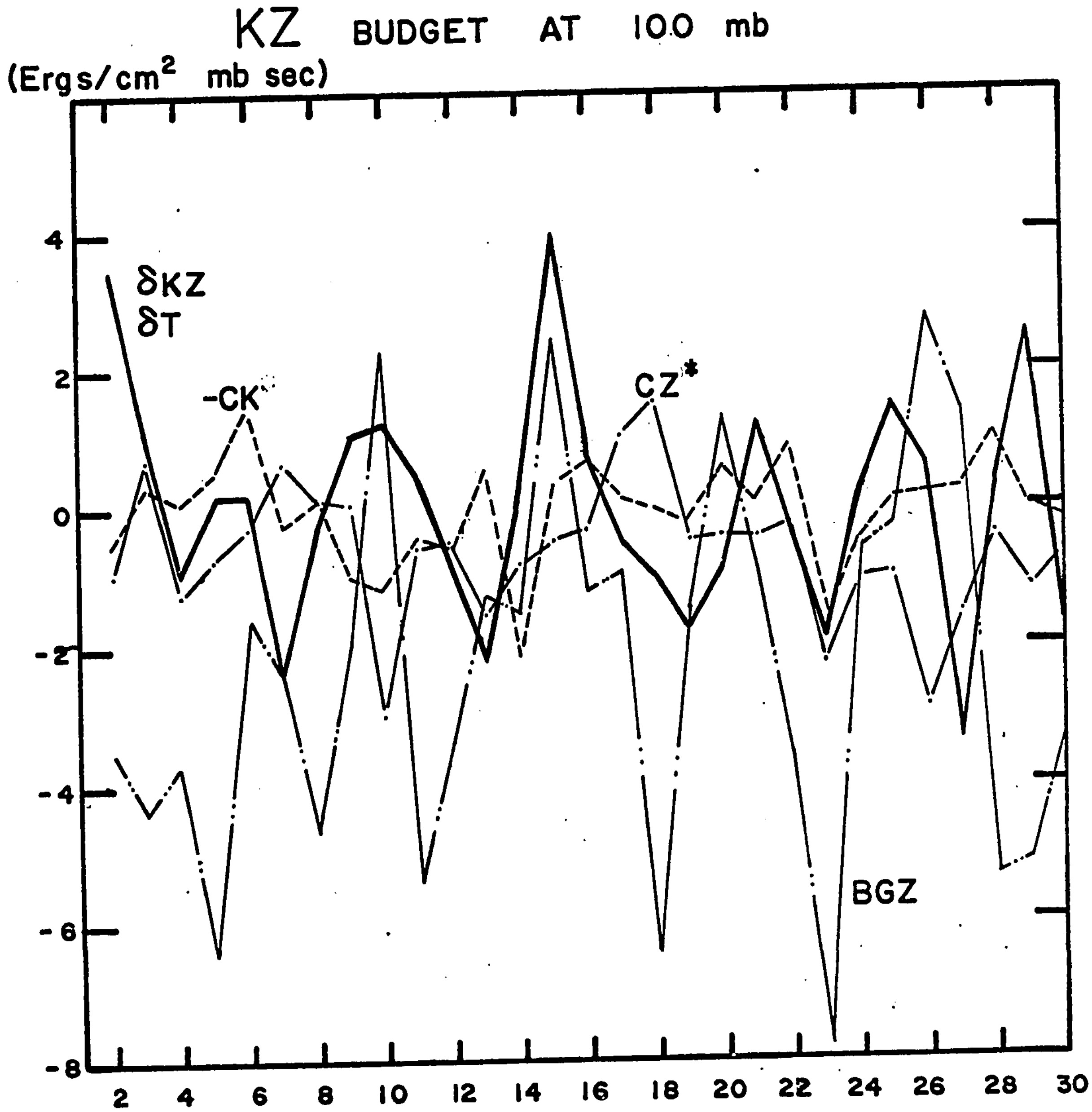

Fig. 5.6.4. Balance of the zonal kinetic energy KZ at 100 mb during January 1959

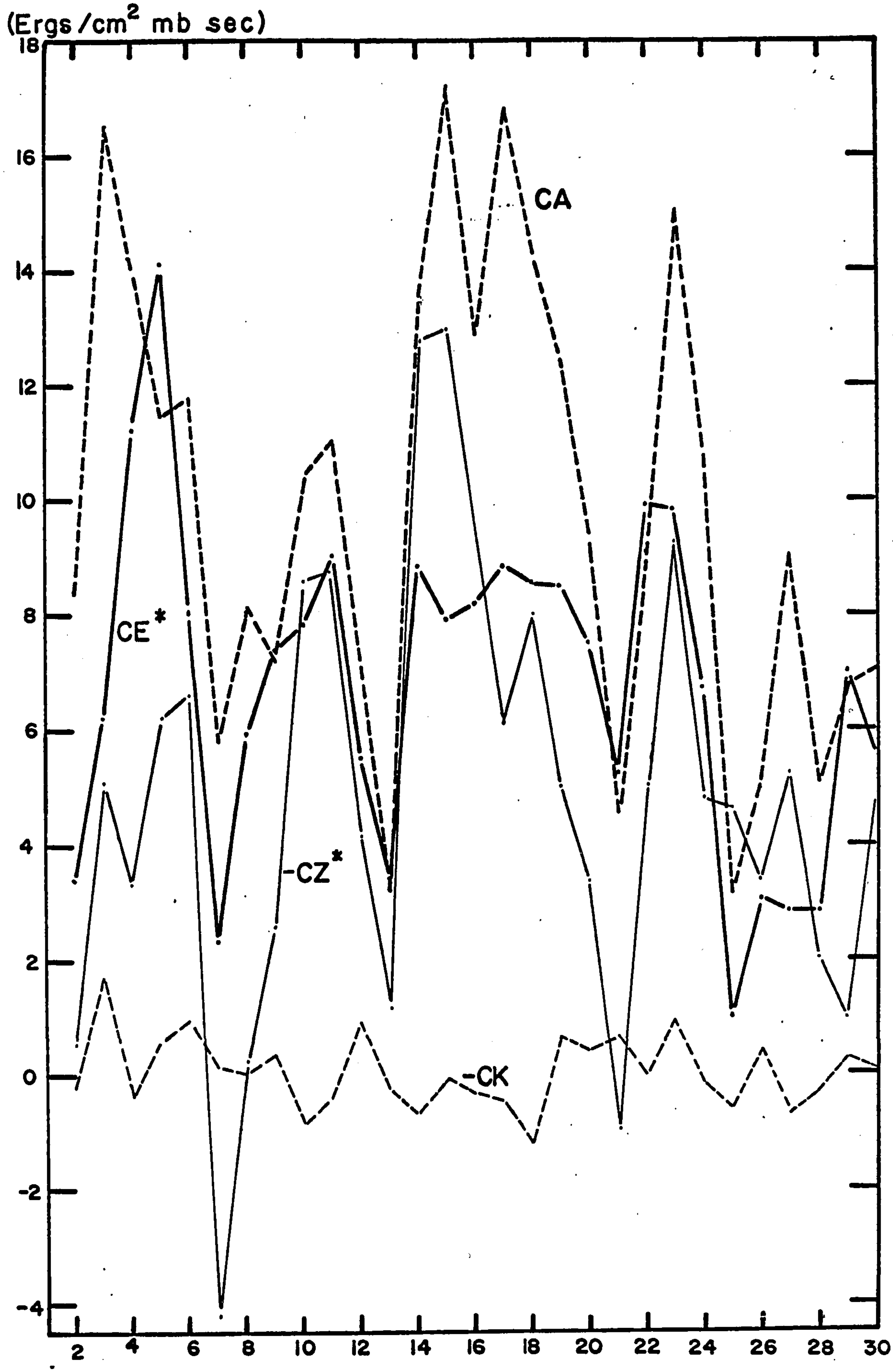

Fig. 5.7.1. Energy transfers at 500 mb in January 1959

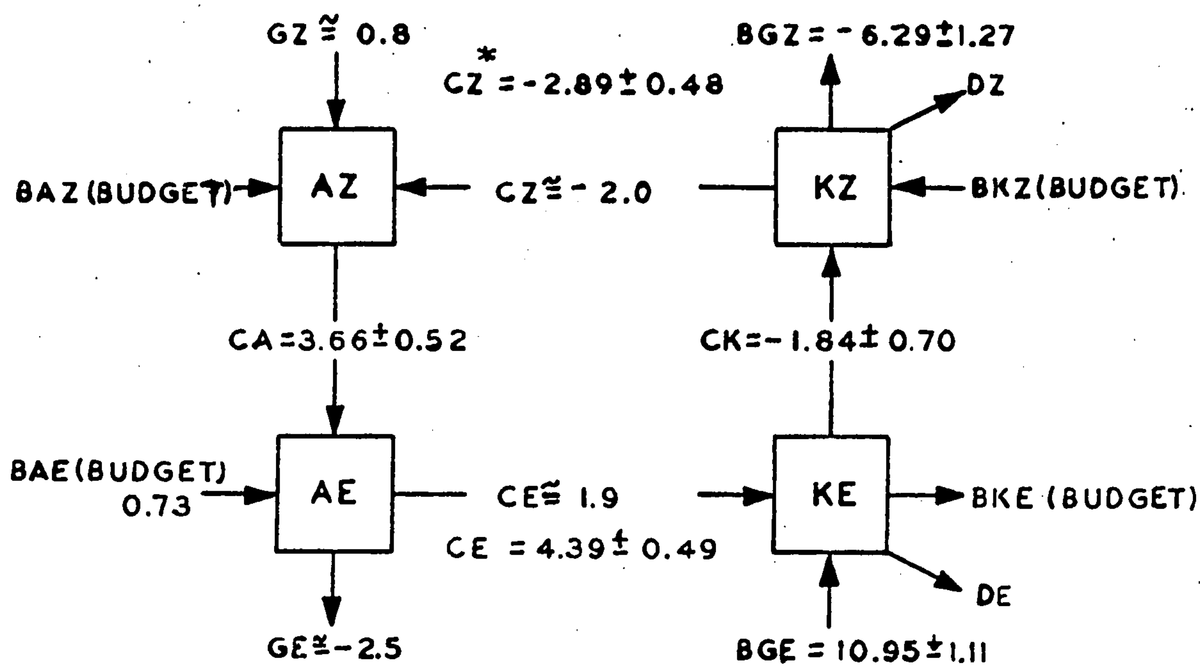

FIG. 5.8.1 MEAN JANUARY 1959 ENERGY TRANSFERS AT 25 MB
UNITS: ERGS/CM^{2}MBSEC

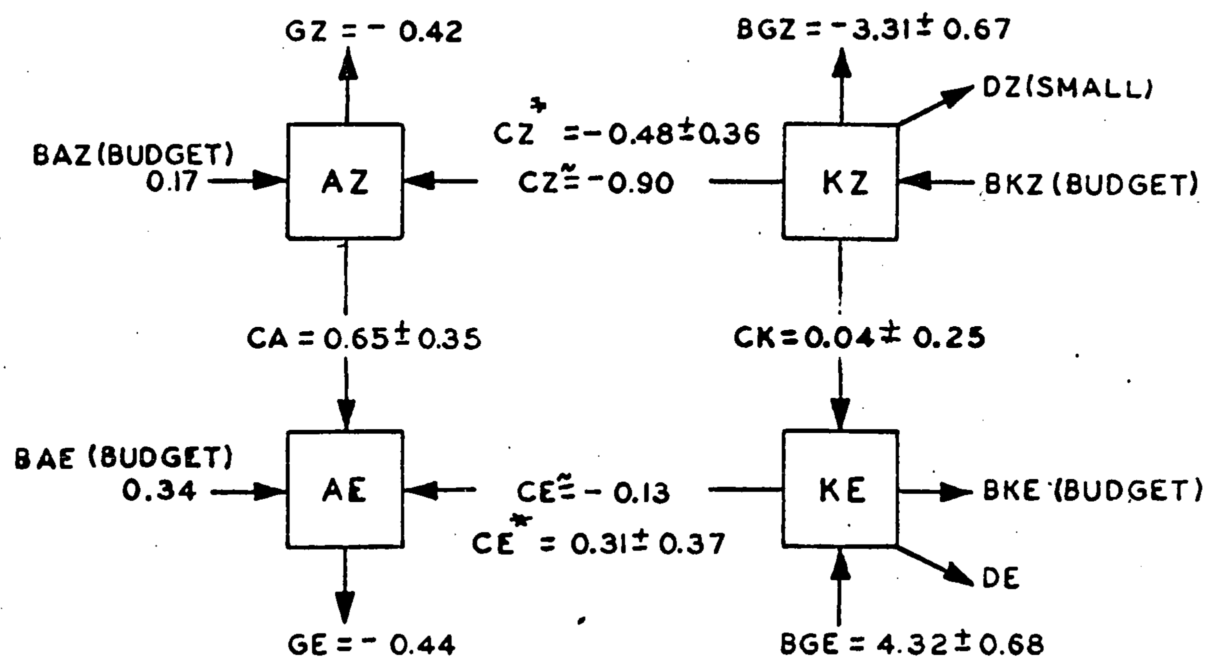

FIG. 5.8.2 MEAN JANUARY 1959 ENERGY TRANSFERS AT 100 MB
UNITS: ERGS/CM^{2}MBSEC

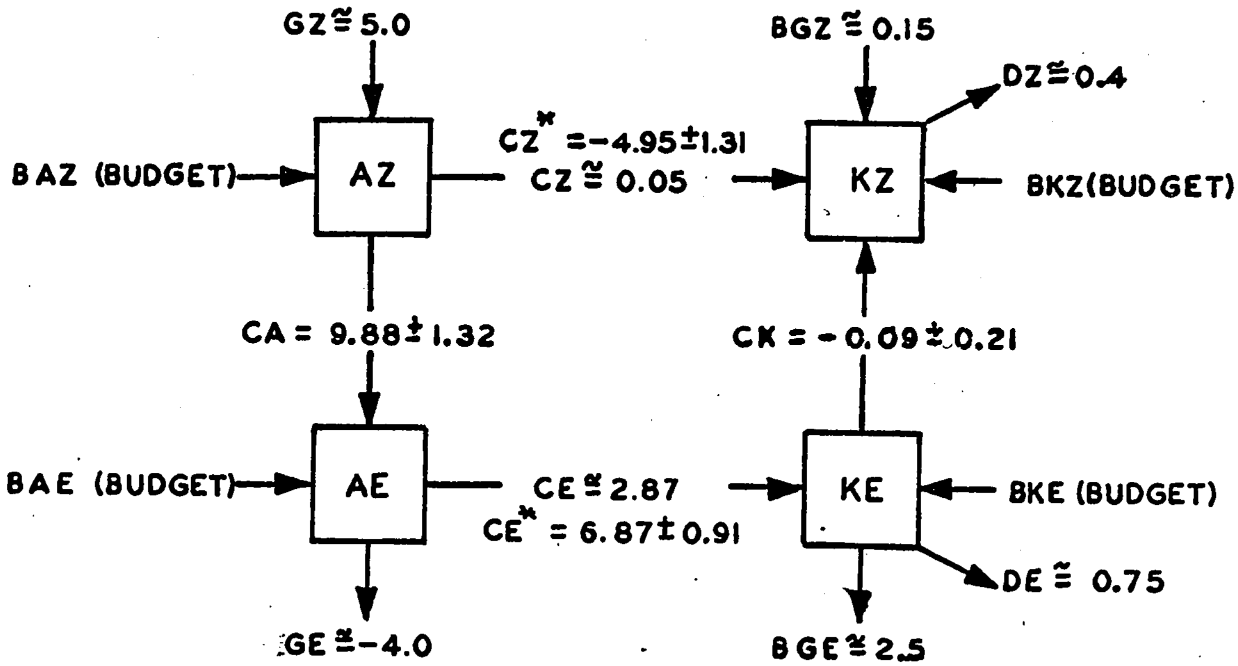

FIG. 5.8.3 MEAN JANUARY 1959 ENERGY TRANSFERS AT 500 MB
UNITS: ERGS/CM^2 MB SEC

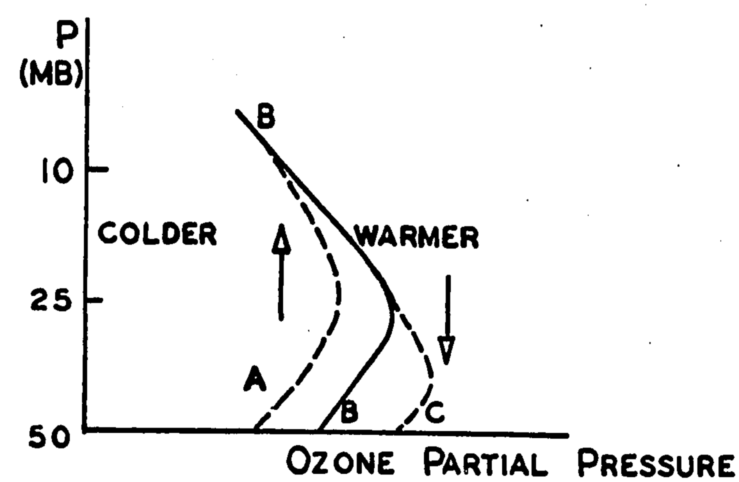

FIG: 5.8.4 SCHEMATIC OZONAGRAM SHOWING THE CHANGES IN THE OZONE VERTICAL PROFILE OF THE MEAN ZONAL CURVE B WHEN INTERACTING WITH UPWARD (CURVE A) OR DOWNWARD (CURVE C) MOTION

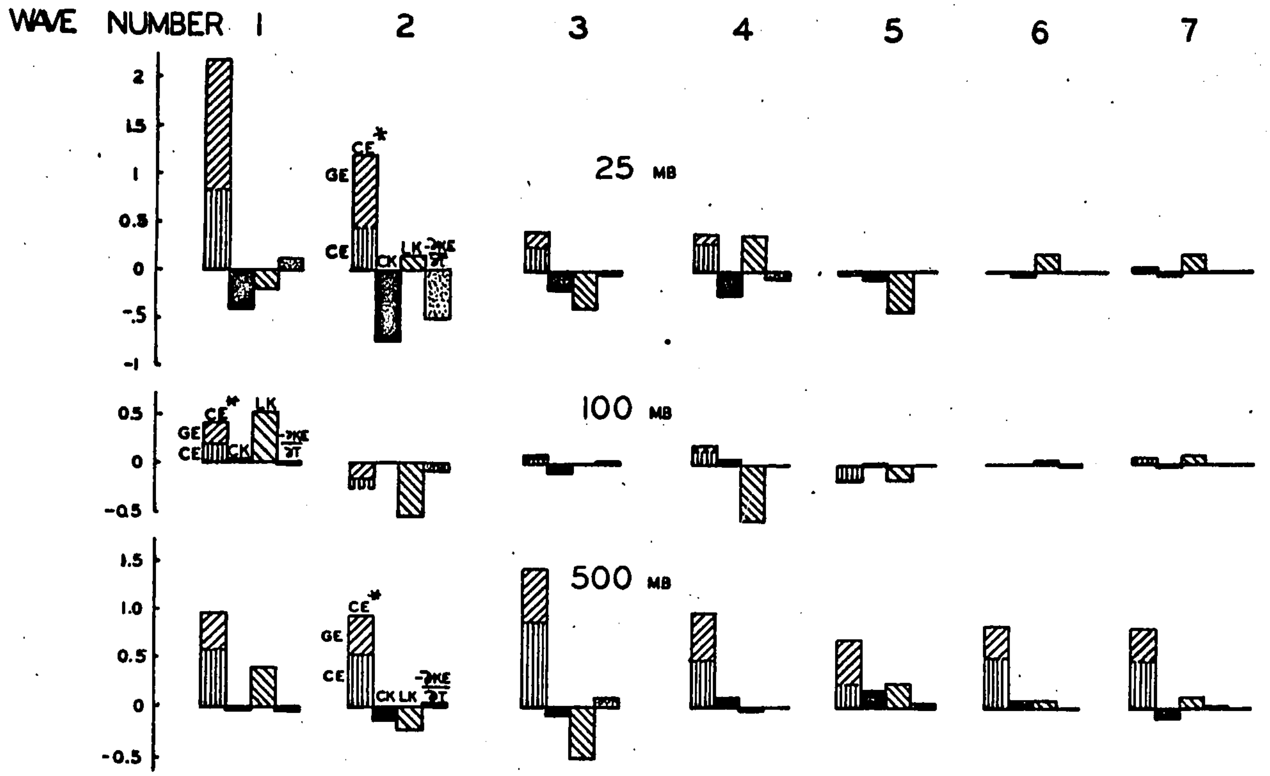

FIG. 5.9.1 MEAN JANUARY 1959 PARTIAL SPECTRAL KINETIC ENERGY BUDGET UNIT: ERGS/CM² MB SEC

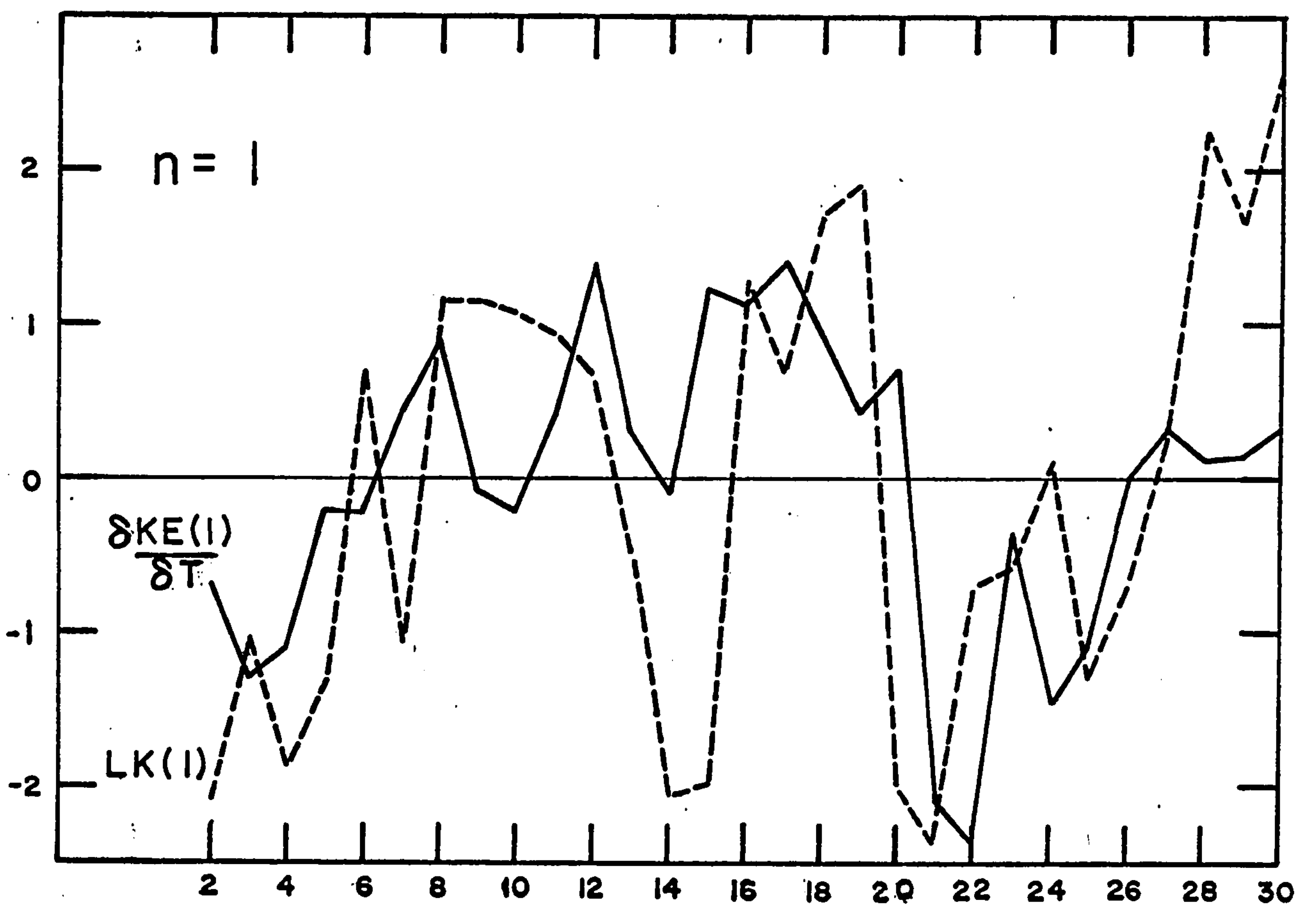

FIG. 5.9.2. Kinetic energy changes and non-linear wave interaction for wave number n = 1 at 25 mb during January 1959.
UNITS: Ergs/cm^2 mb sec.

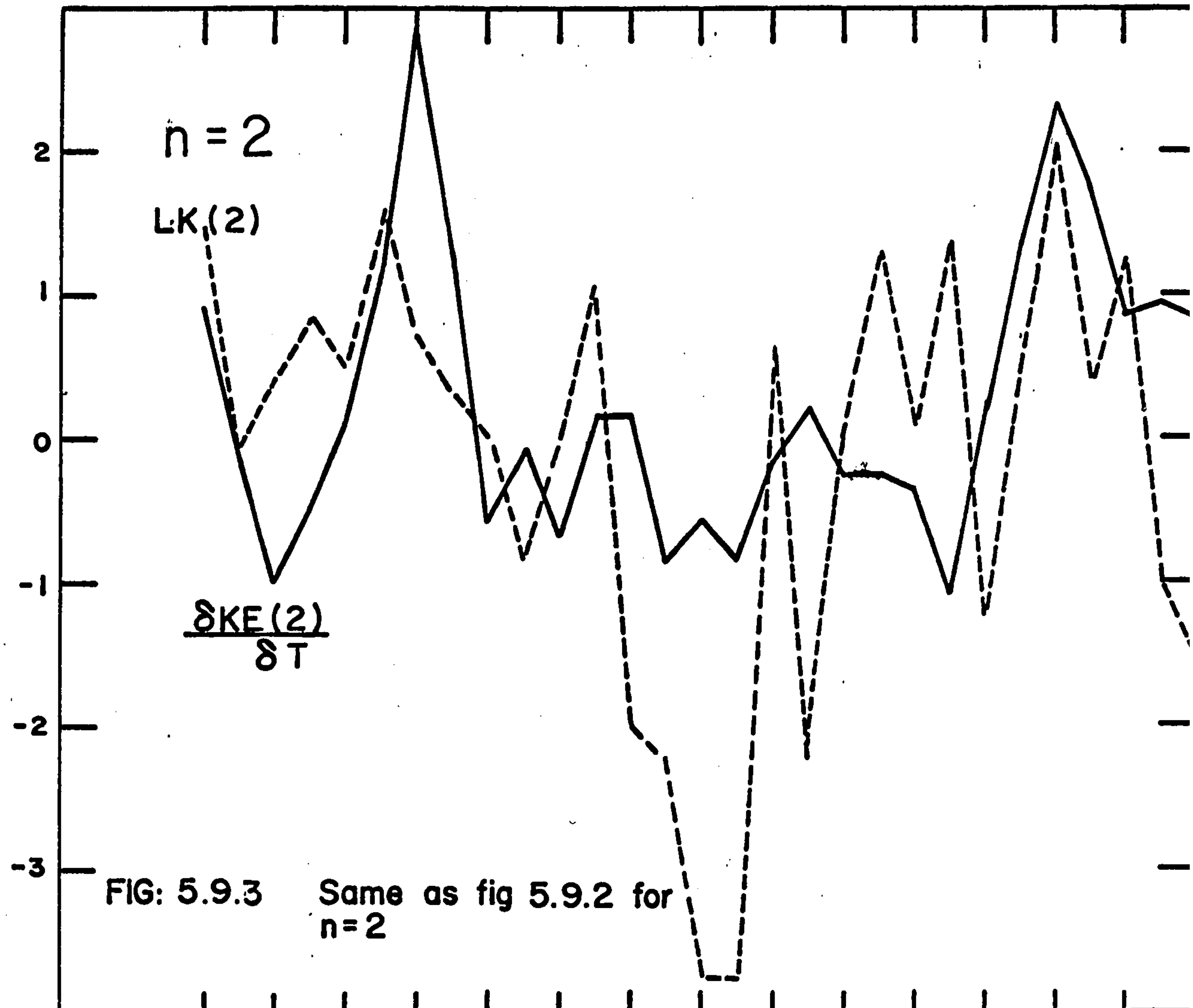

FIG: 5.9.3 Same as fig 5.9.2 for n = 2

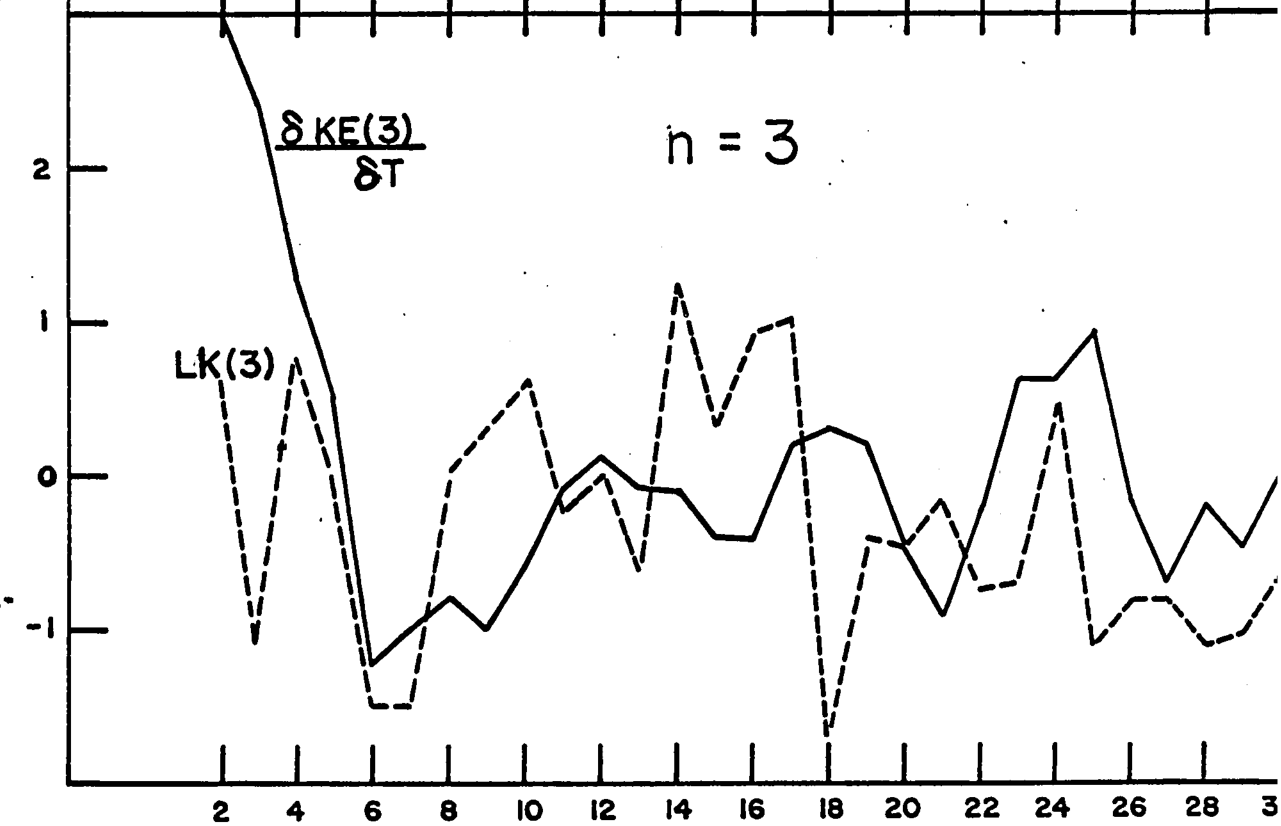

FIG: 5.9.4 Same as fig. 5.9.2 for n = 3 Unit: Ergs/cm^2 mb sec

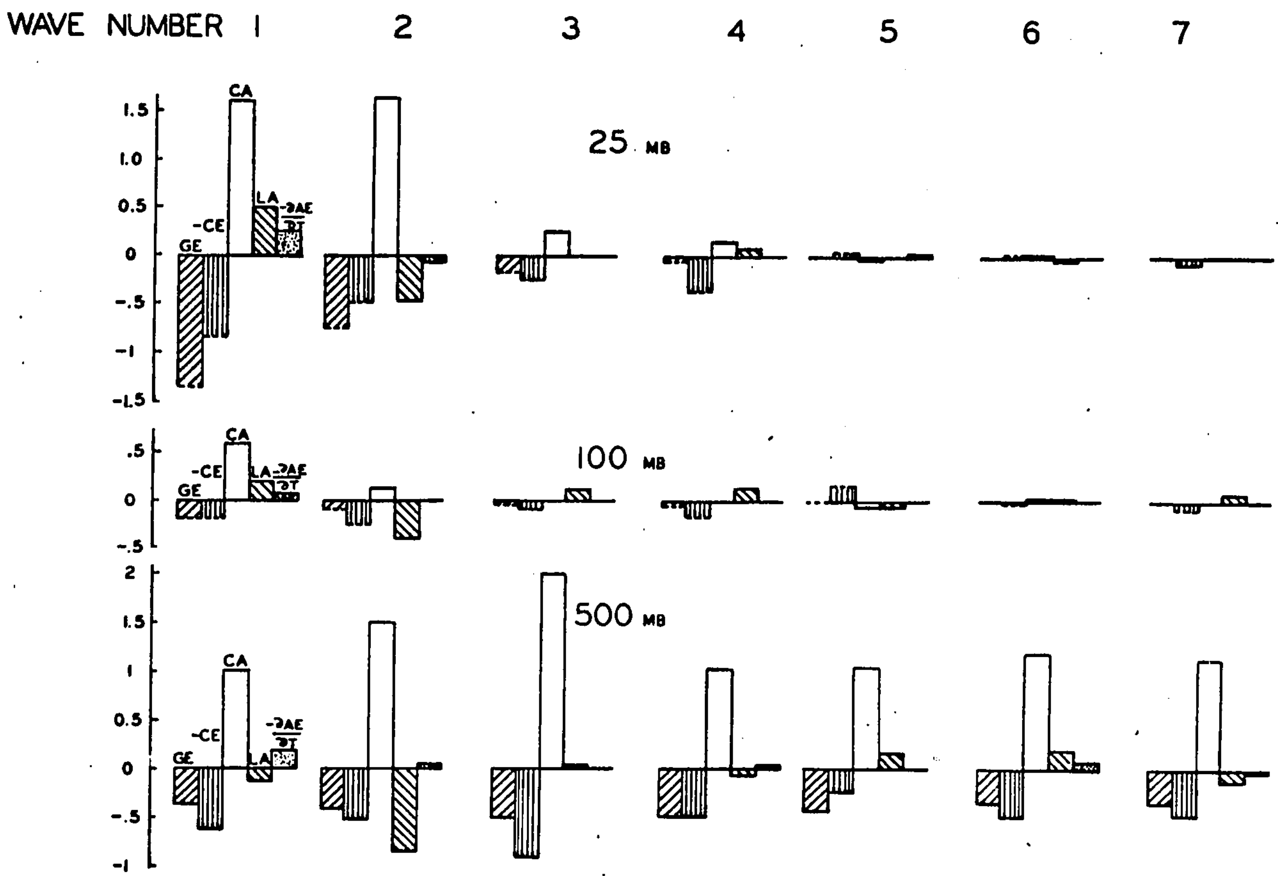

FIG. 5.10.1 MEAN SPECTRAL BUDGET OF THE AVAILABLE ENERGY FOR JANUARY 1959
UNITS: ERGS/CM^2 MB SEC.

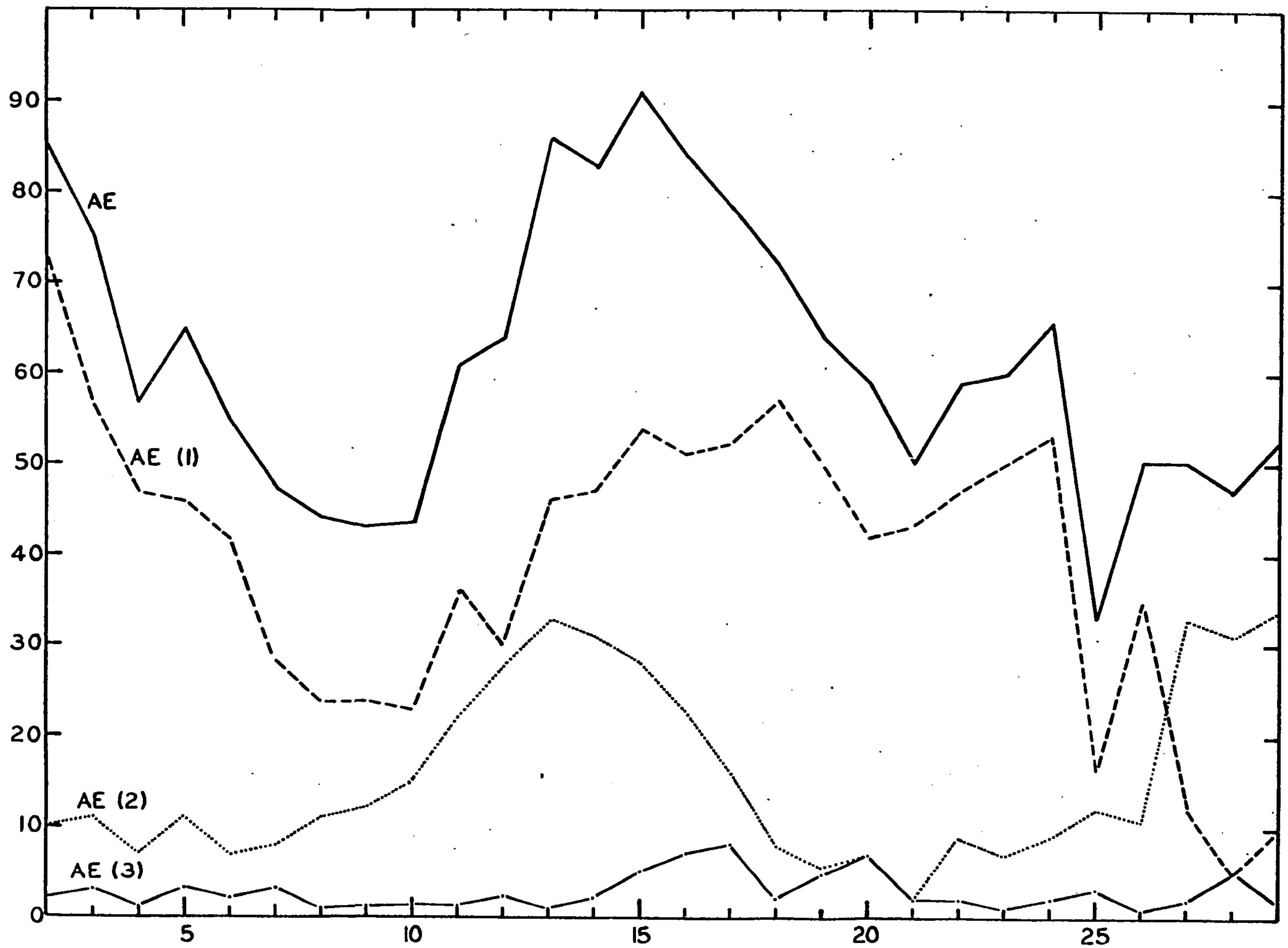

FIG: 5.10.2 TOTAL EDDY AND SPECTRAL AVAILABLE ENERGY FOR N=1,2 AND 3, AT 25 MB DURING JANUARY 1959
UNITS: 10^4 ERGS/CM^2 MB

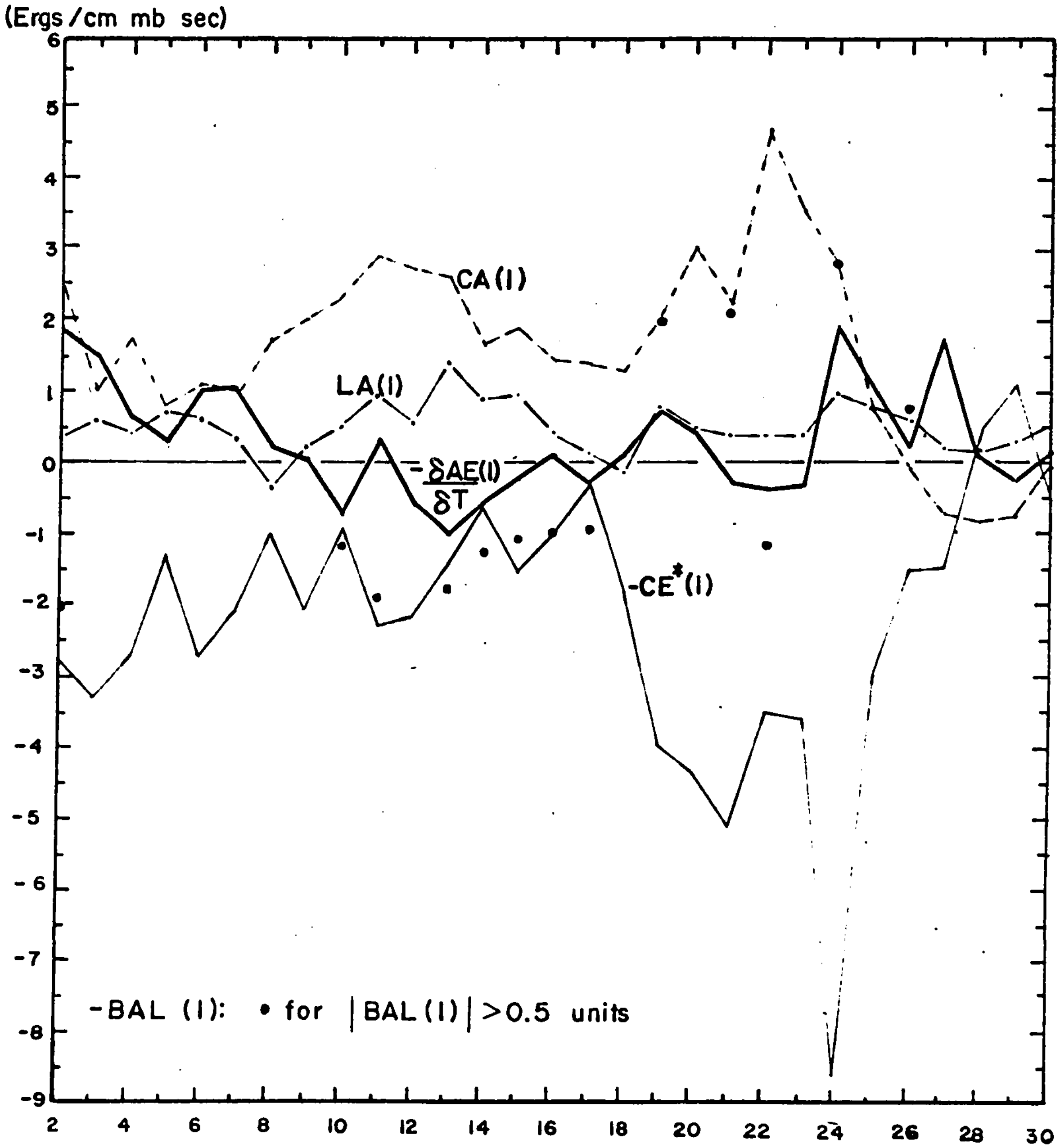

FIG. 5. 10. 3. Daily budget of wave number 1 available energy in January 1959 at 25 mb.
Units: Ergs/cm^2 mb sec.

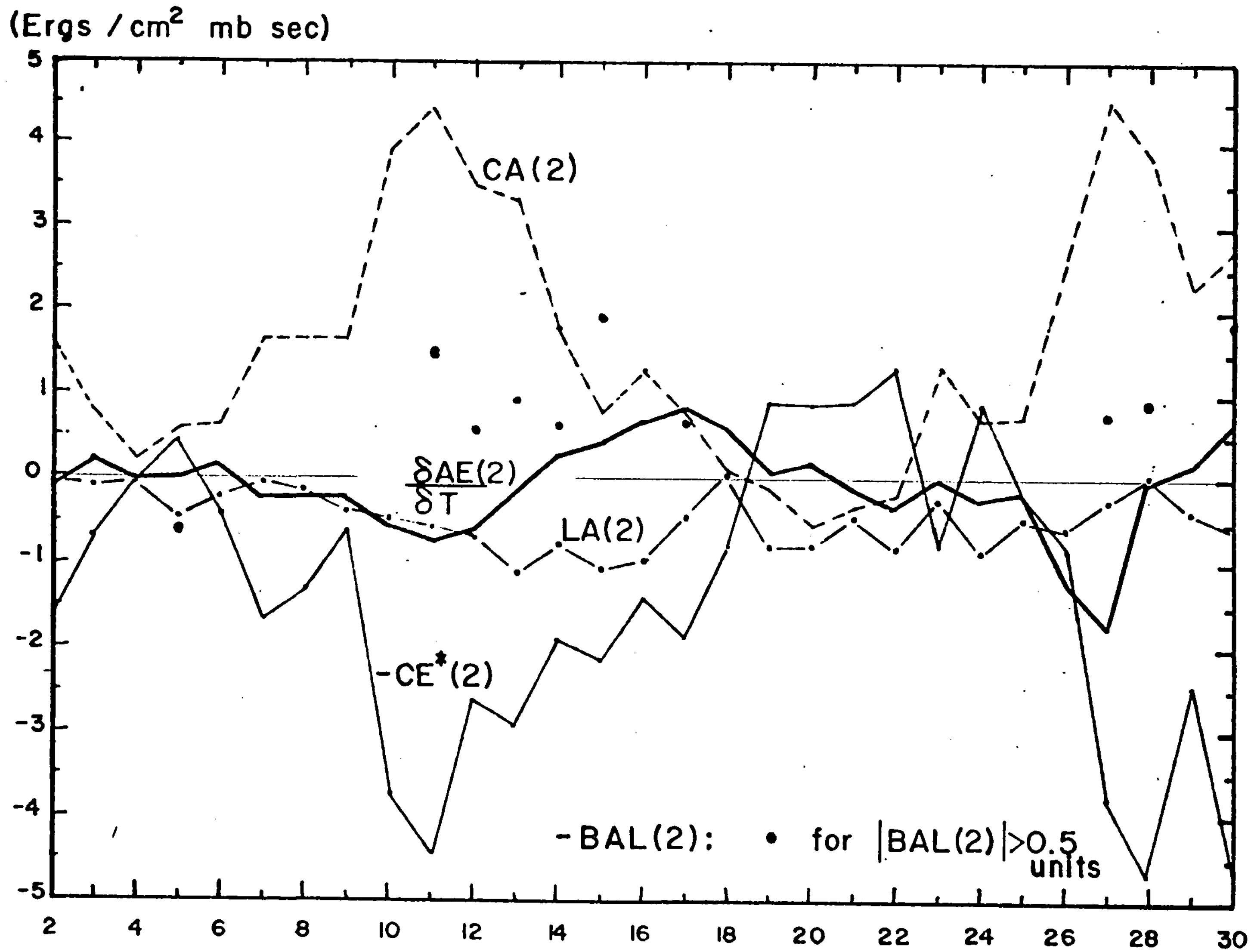

FIG. 5.10.4 : Daily budget of wave 2 available energy in January 1959. Units: Ergs/cm^2 mb sec.

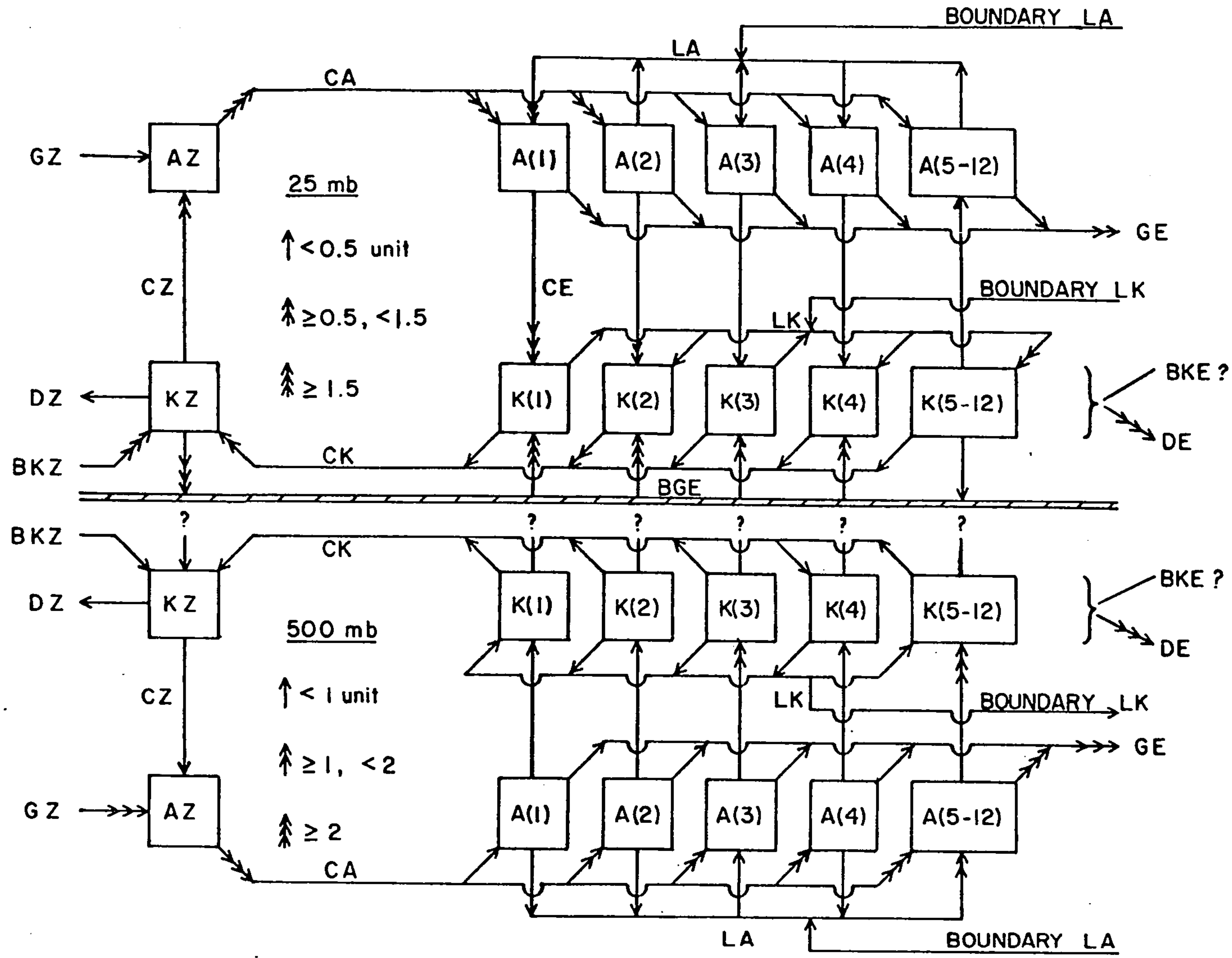

FIG. 5. 11. 1. Spectral energy diagram averaged over January 1959 at 25 and 500 mb. Intensities proportional to arrow heads as indicated in proper diagrams. Units: Ergs/cm^2 mb sec.

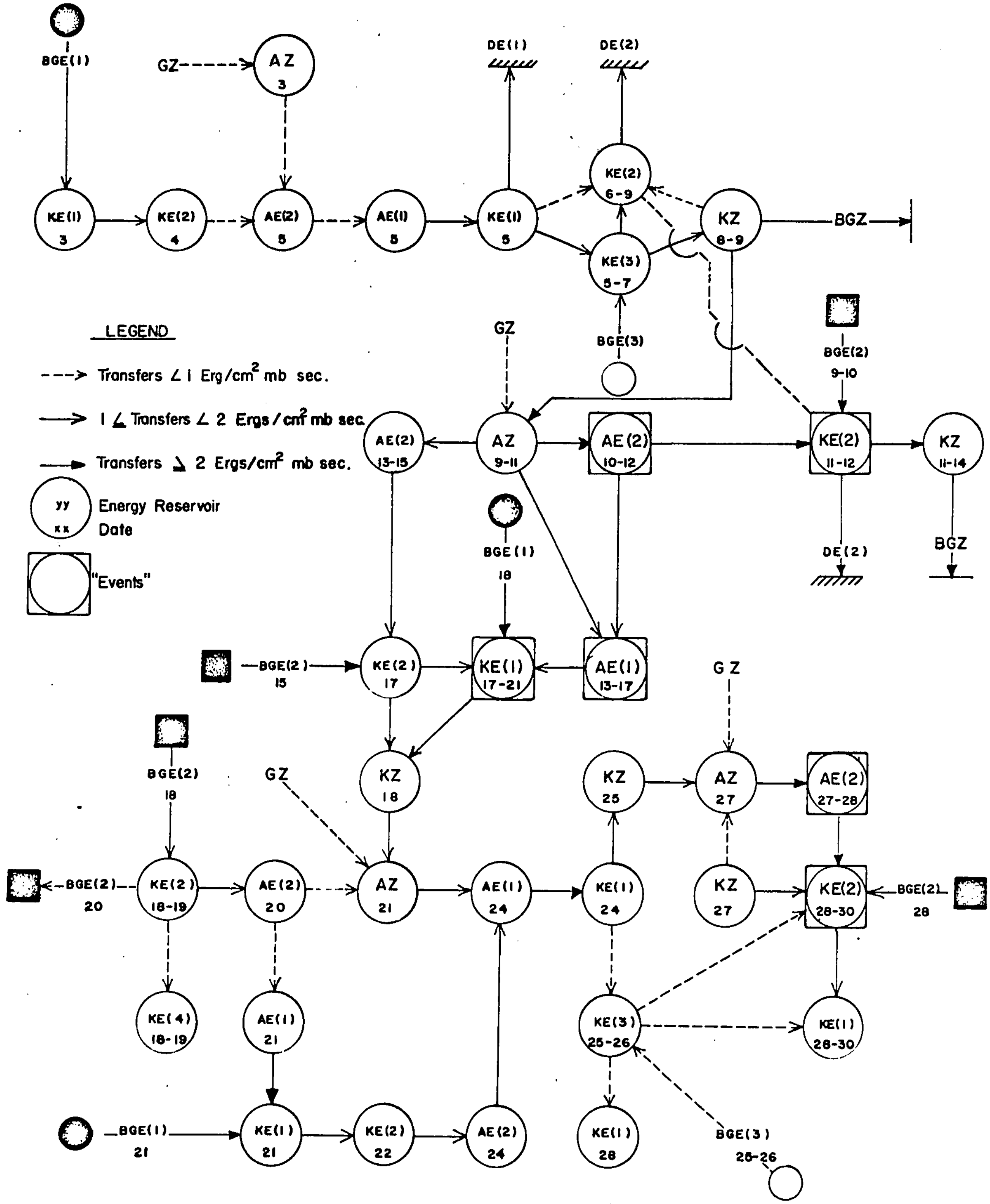

FIG: 5.11.2 Spectral Energy Transfers during January 1959 at 25 mb.

Units: Ergs/cm² mb sec.

CHAPTER 6

SUMMARY AND CONCLUSION

6.1 The Methods of Investigation

The energetics of January 1959 have been assessed through a set of spectral energy equations developed for an open atmospheric system. The study has been divided into two parts. The first considers a mid-January 5-day set, with a high vertical resolution of 10 levels to establish details, and the second considers the full month's data at 3 levels to cover several oscillations in time. For the higher resolution data it was possible to design more elaborate methods of investigation. The following two form original contributions through their development and subsequent applications:

(a) The diagnostic omega-equation has been broken down into its Fourier spectral components and its solution at each wave number has been obtained. In this solution, the static stability was allowed to vary in the latitudinal direction. The model required the solution of 72 simultaneous linear equations each day corresponding to the data gathered at nine levels (850 mb to 10 mb) and eleven latitudes (30^{o}N to 80^{o}N). The radiative diabatic effects were added to the forcing function at stratospheric levels. In general, the model gave realistic results, however, implicit boundary conditions led to excessively smoothed vertical motion wave vectors at the highest level and northermost latitudes.

(b) The stratospheric radiative problem has been partially solved and applied to compute the generation of available potential energy. The solution consists of a hybrid approach using both simple parametric relations (solar ultra-violet absorption) and full radiative transfer calculations in the long-wave spectrum (15-micron carbon dioxide and 9.6-micron ozone absorption). The ultra-violet solar absorption has only latitudinal and time variations. The 15-micron

CO_2 cooling has latitudinal, longitudinal and time variations, being a function of temperature. The 9.6-micron ozone absorption was also hybrid since it used the complete temperature field and only latitudinal variations of the vertical ozone profiles averaged for the month. The resulting heating rates were found to be realistic. Some computations of the generation of available energy, although showing proper sign, were found to be of smaller magnitudes than other dynamical budget computations. This anomaly was probably due to incomplete specifications in the solar ultra-violet absorption (basically a zonal case only) and in the carbon dioxide cooling (a somewhat smoother vertical temperature field than found in the atmosphere).

The validity of the two methods is clearly demonstrated in the spectral and diabatic stratospheric energetics and interactions.

6.2 Summary of the Energetics during January 12 to 16, 1959

The results of the multi-level investigation for the five-day period of January 12 to 16, 1959 are considered with respect to a tropospheric layer and a stratospheric layer. A few analyses are presented for specific levels.

(1) In general the boundary fluxes of the available potential energy are too small to affect either the zonal or eddy modes of this reservoir. While the transfers by vertical kinetic energy fluxes are small, the situation at the lateral boundaries at 30°N shows large influxes of eddy and zonal kinetic energy which have a strong effect on the time variations of these energy reservoirs. The kinetic energy fluxes were larger in the troposphere than in the stratosphere.

(2) Strong pressure interactions were computed between the stratosphere and the troposphere. In the eddy mode, the energy arriving in the stratosphere originated in the troposphere, the effects of the lateral boundary being negligible. In the zonal mode, the stratospheric volume loses energy by the zonal pressure interaction to the exterior: 40 percent of the energy transferred is distributed to

the layer below and 60 percent goes into the lateral adjacent volume. In the mean, the eddy pressure interaction troposphere-to-stratosphere was due to wave numbers 1, 2 and 4. The interaction at the scale of wave number 3 was in the reverse direction.

(3) For the whole stratospheric layer, averaged over five days, the eddy kinetic energy, appearing as a result of the pressure interaction with the troposphere, increases even as it is transformed barotropically into the zonal flow. The zonal kinetic energy suffers some decrease as it transfers its energy to the outside volume by zonal pressure interaction process and to the zonal available energy through the action of the indirect meridional cells. A strong influx of this energy from the lateral boundaries does dampen its decline. A strong northward eddy heat transport into the cold polar stratospheric vortex, leads to a strong transfer from the zonal into the eddy available energy. The small positive generation of zonal available energy is insufficient to balance the zonal available energy budget AZ. The eddy available energy has a net increase in the face of the strong conversion from the zonal available energy and the transfer from the eddy kinetic energy KE. The negative radiative generation of eddy available energy which is found is probably a low estimate. This energy cycle led to a general weakening of the zonal temperature gradient as heat was transported northward by the development and interaction of planetary waves one and two, whose strength defined the stratospheric warming of the period.

(4) Some interlevel radiative interactions have been observed and diagnosed. The generation of eddy available energy was found to be more negative at 50 mb than at 25 mb, this being especially reflected in the scale of wave number one. This is due to radiative transfers between nearby atmospheric layer associated with varying lapse rates.

(5) The tropospheric-stratospheric radiative interaction through the 9.6-micron band of ozone has been clarified. There is a systematic destruction of eddy available energy in stratospheric wave numbers one and two, the effect being maximum at or near 50 mb, through the radiative couple to large-scale dynamically controlled features of the troposphere.

(6) For the whole troposphere, a more or less normal energy cycle has been found. Schematically:

$$AZ \longrightarrow AE \longrightarrow KE \longleftarrow KZ$$

The anomalous barotropic process KZ $\longrightarrow$ KE has been examined and found to be due to the lateral boundaries at 30°N associated with the jet stream near that boundary at 200 and 300 mb. Magnitudes of the transport of zonal kinetic energy across the lateral boundaries indicated that the barotropic process would become more or less normal if the southern lateral boundary were shifted further south to 20°N or 15°N.

(7) The tropospheric energy cycle leads to a vacillating blocking circulation dominated by the scales of wave 1 and 2.

(8) The generation of eddy and zonal available energy has been inferred by residual methods. The values obtained agree reasonably well with other investigations performed during other Januaries.

(9) The dissipation of eddy kinetic energy by the free atmospheric frictional stresses has been computed at each data level as the residual in the balance of the eddy kinetic energy mode. The resulting vertical profile had a very realistic shape, although the dissipation at jet-stream levels was on the large side.

(10) A significant amount of energy seems to be carried aloft by pulse in the geopotential flux creating intermittent signals in the vertical divergence which have reasonable vertical coherence.

(11) Disturbance energy at wave one and also three occasionally propagates downward; the first enhances the energy transfer in the middle and lower stratosphere, while the second connects the upper layers to the surface boundary layer.

(12) The pressure interaction mechanism which stems from a tropospheric blocking pattern in waves one, two and four, is mainly responsible for the increased stratospheric activity at those scales and for the subsequent warming in mid-January 1959.

(13) In the spherical harmonic specification of the height fields

planetary waves of zonal wave numbers one and two showed significant westward tilts with height. The tilts were continuous across both troposphere and stratosphere. On the other hand, zonal wave number 3 coefficients had occasional eastward tilts in the stratosphere. These tilts are associated with different vertical energy propagation as shown earlier.

(14) In the spherical harmonic set ($m = 1, 2, 3$; $n-m = 1, 3, 5$) representing the planetary scale, the following tentative relationships were found regardless of the longitudinal wave number m: the least energy is in the largest latitudinal scale ($n-m = 1$) while the largest contribution comes from the middle scale ($n-m = 3$) in the stratosphere and from the smallest meridional scale ($n-m = 5$) in the troposphere.

(15) The larger scales of the transient waves retrogressed as expected, with a general tendency for the zonal wave numbers two and three to have progression in their shorter meridional scales.

6.3 Summary of the Monthly Energetics during January 1959

The second study in this work spanned the whole month of January 1959, using the daily observations at 500, 100 and 25 mb levels. The major findings are now summarized.

(1) Synoptically, the month of January 1959 may be characterized by a low tropospheric zonal index associated with three minima. The stratosphere also underwent three periods of larger eddy intensities following the period of maximum tropospheric blocking.

(2) The 25-mb energy flow was found to duplicate a normal baroclinic tropospheric cycle, but with a characteristic addition; the important interaction with the lower layers through geopotential flux convergence contributed substantially to the eddy kinetic energy of this layer. The energy cycle is given schematically:

$$\begin{array}{ccccccccc} AZ & \longrightarrow & AE & \longrightarrow & KE & \longrightarrow & KZ & \longrightarrow & AZ \\ & & & & \Uparrow & & \Big| & & \\ & & & & BGE & & BGZ & & \\ & & & & \Big| & & \Downarrow & & \end{array}$$

The pattern underwent daily fluctuations as BGE varied in response to an oscillating pulse in the tropospheric blocking circulation.

(3) The 100-mb energy cycle was characteristically very variable, showing rather small transfer processes.

(4) The 500-mb energy flow showed a normal tropospheric cycle on the average:

$$AZ \longrightarrow AE \longrightarrow KE \longrightarrow KZ$$

(5) A close inspection of the daily variations of the 500 mb and the 25 mb energy transfers gave interesting results. The 500-mb transfers oscillated with periods of about 6 days and 12 days. At 25 mb, the transfers oscillated with a 12-day period. The strengthening of the blocks at 500 mb is followed by larger eddy pressure interaction processes and increases in the 25 mb eddy kinetic energy. It is concluded that a causal relationship existed at these times with the occurrence of a blocking phenomenon at 500 mb and the subsequent kinetic energy rise at 25 mb, the link between the two events being performed by the upward progression of planetary wave energy.

(6) The 25 mb spectral kinetic energy budget showed that:

a) wave numbers one and two were dominant in the kinetic energy spectrum, followed by waves three and four. The first and last eddy kinetic energy maxima were wave number two phenomena, while the largest mid-month increase was from a strong eccentric pattern with some lesser bi-polar quality.

b) on the average, non-linear wave wave interactions were such that consecutive wave numbers exchanged energy with their adjacent members, i. e., the set of wave numbers 1, 3 and 5 transferred their energy into the second set of waves 2, 4, 6 and 7. The period from 12th to 16th of January showed a more organized set-up with waves 1 and 2 feeding the smaller scale waves.

(7) The 100-mb spectral kinetic energy budget was characteristically composed of very small and variable transfers, with waves 1 and 2 leading in the spectral field. The only significant transfers within the waves were into wave one from waves two and four.

(8) The 500-mb spectral kinetic energy budget featured a maximum baroclinic transfer at the scale of wave number 3, while waves 1, 2, 4, 6 and 7 were of fairly even magnitudes. The non-linear wave interaction showed transfers from wave 3 then 2 into waves 1 and 5, with the former receiving most of it.

(9) At 25 mb, a very good correlation exists between the changes in KE (1) and the non-linear kinetic energy transfer into this spectral mode, i.e., the LK (1)-process, up to the 27th of January. The changes of KE (2) are also well correlated to the LK (2)-transfers during the same period.

(10) The 25 mb spectral available energy budget reveals an interplay between transfers mainly at wave numbers one and two. The gains in AE (1) are explained by the non-linear wave interaction transfers and the eccentric northward heat transport, while the losses are produced by the negative generation and baroclinic transfer. The AE(2) reservoir loses through most transfers except the bi-polar northward heat transport mechanism.

(11) The 100 mb AE (n) budget is a mirror image of the 25 mb case above, but the transfers are much smaller in magnitude.

(12) The 500 mb AE (n) - budget is strongly influenced by the transfer from the zonal to eddy available energy with the scales of wave numbers 3 and 2 being dominant, followed by a more or less uniform participation of wave numbers 6, 7, 5, 4 and 1, where the order given follows the decreasing magnitudes of the spectral components.

(13) January 1959 is also characterized by a large northward heat transport at both 500 and 25 mb levels. The scales of wave numbers 1 to 7 dominated at 500 mb while waves 1 and 2 were leading at 25 mb.

(14) At 500 mb, the baroclinic processes are dominated by waves 3 and 1, while 2, 4, 6 and 7 followed suit but at a lower intensity level. At 25 mb, the same processes are mostly in the scales of waves 1 and 2, with lesser contribution from waves 3 and 4.

(15) The non-linear wave interaction process LA(2) contributes to a loss of wave 2 available energy to the other scales at both 500 and 25 mb, when averaged over the month. AE(1) does gain from the above scale at 25 mb but not at 500 mb.

(16) The significant 25 mb monthly mean energy transfers are found in the following:

a) The baroclinic transfers are dominated by wave number 1, followed by wave number 2.

b) The barotropic transfer CK(n) is negative with CK(2) leading.

c) Over the month, LK(2) is positive, as KE(2) receives most of its non-linear transfer from wave 3 followed by 5 and 1.

d) An indirect meridional circulation is indicated by a negative CZ-term.

e) Waves 1 and 2 dominate the northward heat transport at 25 mb.

(17) The 500 mb monthly mean spectral energy flow may be summarized:

a) Typical tropospheric energy exchanges are encountered.

b) Wave 1 kinetic energy is fed non-linearly by waves 2, 3 and 4.

c) The frictional dissipation DE and the eddy flux of kinetic energy are postulated to be large.

d) The zonal kinetic energy is maintained by a large import of this energy across the 30°N lateral boundary.

(18) Major eddy activities in the 25 mb kinetic energy have been termed "events", and the causes have been explained using total and spectral energy descriptions. The three main "events" have been diagnosed:

a) The first "event" which occurred on the 11th-12th of January was of a bi-polar nature. From the 6th to the 9th, KE(2) is increasing under the transfer from the zonal and wave 3 kinetic energy reservoirs, the KE(3) reservoir was simultaneously replenished by the pressure interaction mechanism BGE(3) originating in the troposphere. A large increase in the baroclinic process CE(2) coupled with a surge in the pressure interaction BGE(2) from the 9th to the 12th contributed to the maintenance of KE(2) and the occurrence of an "event" at this scale on the 12th.

b) The strongest "event" occurred on the 12th-21st January period. It was characteristically eccentric in pattern. The maximum eccentricity in the flow was due to a strong pressure interaction at this scale from the troposphere, to a moderate exchange from wave 2 energy into wave 1, and to a moderate baroclinic exchange CE(1).

c) The last "event" centered over the 28th-30th January period was predominantly bi-polar. The increase in KE(2) was not associated with wave 1 or/and 3 interactions, since on the contrary, wave 2 feeds waves 1 and 3. The rise in KE(2) was due to energy gains in the pressure interaction originating in the troposphere at this scale, to barotropic exchanges from the zonal flow and to baroclinic transfers through the CE(2)-process.

6.4 Conclusion

It is felt that the principal objectives of the present study have been fulfilled. A new vertical motion model has been tested and applied to the energetics of the atmosphere with success. A quasi-hemispheric radiative study has been performed in the stratosphere and applied to the energetics of this layer. An energy study of the atmosphere over two space and time domains has been undertaken and the total and spectral results have been analysed and presented. The characteristics of January 1959 have been discussed on a monthly and daily basis in order to explain the continuity of the various events. Interrelationship between the troposphere and the stratosphere has been diagnosed.

6.5 Extension for Future Research

Future research might proceed along two parallel paths emphasizing observational and theoretical studies. The first path would extend this experiment to more quiescent and longer periods. The recently completed McGill three-year data set could then be used to great advantage. The second avenue of endeavour would be an application of the computed energy exchanges to models of the tropospheric-stratospheric complex along the lines of Byron-Scott (1967), but with more scales in the initial boundary conditions.

REFERENCES

Barnes, A.A., 1962: Kinetic and potential energy between 100 mb and 10 mb during the first six months of the IGY. Studies of the stratospheric general circulation. AFCRL-63-435, Dept. of Meteorology, Mass. Inst. of Tech.

Bojkov, R.D., 1965: Vertical distribution of ozone in the earth's atmosphere. Meteorologiia i Gidrologiia, 10, 3-11.

__________, 1966: Differences in the vertical ozone distribution deduced from Umkehr and ozonesonde data at Goose Bay. J. Appl. Meteor., 5, 872-877.

Boville, B.W., 1961: A dynamical study of the 1958-59 stratospheric polar vortex. A.M.R.G. Publication in Meteorology, No. 36, McGill Univ.

__________, 1963: Arctic winter. Atmosphere, 1, No. 1, Canadian Branch Roy. Meteor. Soc.

__________, 1965: Some aspects of the middle stratosphere. A.M.R.G. Publication in Meteorology, No. 75, McGill Univ.

__________, 1966: Planetary-waves in the stratosphere and their upward propagation. Space Research, 7, 20-29. North Holland Publishing Co., Amsterdam.

__________, C.V. Wilson and F.K. Hare, 1961: Baroclinic waves in the polar night vortex. J. Meteor., 18, 567-580.

__________, M.A. McFarlane and H.A. Steiner, 1961: An atlas of stratospheric circulation. A.M.R.G. Publication in Meteorology No. 37, McGill Univ.

Bradley, H.S., 1967: The transient part of the atmospheric planetary waves. Tech. Rep. No. 5, College of Engineering, Dept. of Meteorology and Oceanography, Univ. of Michigan. 113 pp.

Brown, J.A.Jr., 1964: A diagnostic study of tropospheric diabatic heating and the generation of available potential energy. Tellus, 16, 371-388.

__________, 1967: On atmospheric zonal to eddy kinetic energy exchange for January 1963. Tellus, 19, 14-17.

Brunt, D., 1941: Physical and dynamical meteorology. London, Cambridge University Press, 1941.

Burch, D.E., D. Grynvak, E.B. Singleton, W.L. France and D. Williams, 1962: Infrared absorption by carbon dioxide, water vapour and minor atmospheric constituents. Contract No. AF19(604)-2633, Ohio State Univ., 316 pp.

Byron-Scott, R., 1967: A stratospheric general circulation experiment incorporating diabatic heating and ozone photochemistry. A.M.R.G. Publication in Meteorology No. 87, McGill Univ.

Charney, J.G., 1949: On a physical basis for numerical prediction of large-scale motions in the atmosphere. J.Meteor., 6, 371-385.

____________, and P.G. Drazin, 1961: Propagation of planetary wave-scale disturbances from the lower into the upper atmosphere. J. Geophys. Res., 66, 83-109.

____________, and J. Pedloski, 1963: On the trapping of unstable planetary waves in the atmosphere. J. Geophys. Res., 68, 6441-6442.

____________, and M.E. Stern, 1962: On the stability of internal baroclinic jets in a rotating atmosphere. J. Atmos. Sc., 19, 159-172.

Clark, J.H., 1963: Infrared heating due to ozone. M.Sc. Thesis, Dept. of Meteorology, McGill Univ., 52 pp.

Craig, R.A. and W.S. Hering, 1959: The stratospheric warming of January-February 1957. J.Meteor., 16, 91-107.

____________ and M.A. Lateef, 1962: Vertical motion during the 1957 stratospheric warming. J.Geophys.Res., 67, 1839-1854.

Danard, M., 1964: On the influence of released latent heat on cyclone development. J. Appl. Meteor., 3, 27-37.

Davis, P.A., 1961: A re-examination of the heat budget of the troposphere and lower stratosphere. Research Div., College of Engineering, New York Univ.

____________, 1963: An analysis of the atmospheric heat budget. J.Atmos. Sc., 20, 5-22.

Deland, R.J., 1964: Traveling planetary waves. Tellus, 16, 271-273.

____________, 1965a: Some observations of the behaviour of spherical harmonic waves. Mon. Wea. Rev., 93, 307-312.

____________, 1965b: On the scale analysis of travelling planetary waves. Tellus, 17, 527-528.

Deland, R. J., 1967a: On the movement and prediction of travelling planetary-scale waves. Mon. Wea. Rev., 95, 21-31.

__________, 1967b: On the vertical structure of planetary-scale waves. To be published in A.M.R.G. in Meteorology, McGill Univ.

Derome, J., 1966: Some dynamical effects of topography and diabatic heating. A.M.R.G. Publication in Meteorology No. 80, McGill Univ.

Dutsch, H. U., 1964: Uniform evaluation of Umkehr observation from world ozone network. Part III, National Center for Atmospheric Research, Boulder, Colorado. 34 pp.

Eddy, A., 1963: Kinematic divergence and large scale energy conversion. Scientific Report No. 8, AF19(604)-8431, A.R.M.G., McGill Univ.

Finger, F.G., R.B. Mason and H.A. Corzine, 1963: Some feature of the circulation at the 10-mb surface July 1958 through June 1959. Mon. Wea. Rev., 91, 191-205.

Gates, W.L., 1961: Static stability measures in the atmosphere. J. Meteor., 18, 526-533.

Gilman, P.A., 1964: On vertical transport of angular momentum in the atmosphere. Geofisica Pura e applicata, 57, 161-166.

Godson, W.L., 1959: The application of Fourier analysis to meteorological data. TEC-295, Meteorological Branch, Canada.

__________ and C.V. Wilson, 1963: The structure of the Arctic winter stratosphere over a ten-year period. Canadian Meteorological Memoirs, No. 11, Met. Branch. Dept. of Transport. 193 pp.

Gutnick, M., 1962: Mean annual mid-latitude moisture profiles to 31 km. Air Force Surveys in Geophysics, No. 147, AFCRL-62-681, 29 pp.

Haltiner, G.J., L.C. Clarke and G.E. Lawniczak Jr., 1963: Computation of large scale vertical velocity. J. Appl. Meteor., 2, 242-259.

Hering, W.S. and T.R. Borden, Jr., 1965: Mean distribution of ozone density over North America. Env. Res. Papers, No. 162, AFCRL-65-913.

____________________, 1964: Ozonesonde observations over North America. Env. Res. Papers, No. 38. AFCRL-64-30(II).

____________________, 1965: Ozonesonde observations over North America. Env. Res. Papers, No. 133, AFCRL-64-30(III).

Hering, W.S., C.N. Touart and T.R. Borden, Jr., 1967: Ozone heating and radiative equilibrium in the lower stratosphere. J. Atmos. Sc., 24, 402-413.

Hill, C.E., 1963: A multi-level study of heat transport. A. M.R.G. Publication in Meteorology No. 58, McGill Univ.

Hitschfeld, W. and J.T. Houghton, 1961: Radiative transfer in the lower stratosphere due to the 9.6-micron band of ozone. Quart. J. Roy. Meteor. Soc., 87, 562-577.

Jensen, C.E., 1961: Energy transformation and vertical flux processes over the northern hemisphere. J.Geophys.Res., 66, 1145-1156.

Julian, P.R., 1967: Midwinter stratospheric warming in the southern hemisphere: general remarks and a case study. J.Appl.Meteor., 6, 557-563.

__________ and K.B. Labitzke, 1965: A study of atmospheric energetics during the January-February 1963 stratospheric warming. J. Atmos. Sc., 22, 597-610.

Katayama, A., 1967: On the radiation budget of the troposphere over the northern hemisphere(II)- Hemispheric distribution. J.Meteor. Soc., Japan, 45, 1-25.

Kennedy, J.S., 1964: Energy generation through radiative processes in the lower stratosphere. Rep. No. 11, Dept. of Meteorology, Mass. Inst. of Tech. 116 pp.

Knighting, E., 1960: Some computations of the variation of vertical velocity with pressure on a synoptic scale. Quart. J. Roy. Meteor. Soc., 86, 318-325.

Kondrat'yev, K. Ya., 1965: Radiative heat exchanges in the atmosphere. Permagon Press, 62-213.

Krueger, A.F., J.S. Winston and D. Haines, 1965: Computations of atmospheric energy and its transformation for the northern hemisphere for a recent five-year period. Mon. Wea. Rev., 93, 227-238.

Kung, E.C., 1966: Kinetic energy generation and dissipation in the large scale atmospheric circulation. Mon. Wea. Rev., 94, 67-87.

__________, 1967: Diurnal and long-term variations of kinetic energy generation and dissipation for a five-year period. Mon. Wea. Rev., 95, 593-606.

Kuo, H. L., 1951: A note on the kinetic energy balance of the zonal wind systems. Tellus, 3, 205-207.

Labitzke, K., 1965: On the mutual relation between stratosphere and troposphere during the period of stratospheric warming in winter. J. Appl. Meteor., 4, 91-99.

Lateef, M. A., 1964: Energy budget of the stratosphere over North America during the warming of 1957. J. Geophys. Res. 69, 1481-1491.

LaSeur, N. E., 1954: On the asymmetry of the middle-latitude circumpolar current. J. Meteor., 11, 43-57.

Lindzen, R. S., 1967: Cooling rates due to water vapour, carbon dioxide and ozone. To be published.

Lorenz, E. N., 1955: Available potential energy and the maintenance of the general circulation. Tellus, 7, 157-167.

__________, 1960: Energy and numerical weather predictions. Tellus, 12, 364-373.

MacDonald, V., 1963: An atlas of total ozone distribution: October 1958-September 1959. A. M. R. G. Publication in Meteorology No. 61, McGill Univ.

Mahlman, J. D., 1966: Atmospheric general circulation and transport of radioactive debris. Atm. Sc. Paper No. 103, Dept. of Atmospheric Sciences, Colorado State Univ., Fort Collins, Colo.

Manabe, S. and R. F. Strickler, 1964: Thermal equilibrium of the atmosphere with a convective adjustment. J. Atmos. Sc., 21, 361-385.

Mateer, C. L., 1964: A study of the information content of Umkehr observations. Tech. Rep. No. 2, College of Engineering, Dept. of Meteor. and Oceanography, Univ. of Michigan, 199 pp.

Merilees, P., 1966: Harmonic representation applied to large scale atmospheric waves. A. M. R. G. Publication in Meteorology No. 83, McGill Univ., 174 pp.

Miyakoda, K., 1963: Some characteristic features of winter circulation in the troposphere and lower stratosphere. Tech. Rep. No. 14, Dept. of Geophysical Sciences, Univ. of Chicago, 93 pp.

Muench, H.S., 1965: Stratospheric energy processes and associated atmospheric long-wave structure in winter. Env. Res. Papers No. 95, AFCRL-65-236, 73 pp.

Murakami, T., 1963a: Maintenance of the kinetic energy of the disturbances appearing in the monthly weather charts. J. Meteor. Soc., Japan, 41, 15-28.

__________, 1963b: Analysis of various large-scale disturbances and the associated zonal mean motions in the atmosphere. Geofisica Pura e Applicata, 54, 119-165.

__________, 1964: Multiple-level model for the p- and s-coordinate. J. Meteor. Soc., Japan, 42, 1-13.

__________, 1965: Energy cycle of the stratospheric warming in the early 1958. J. Meteor. Soc., Japan, 43, 262-283.

__________, 1967: Vertical transfer of energy due to stationary disturbances induced by topography and diabatic heat sources and sink. J. Meteor. Soc., Japan, 45, 205-231.

__________ and K. Tomatsu, 1964: The spectrum analysis of the energy interaction terms in the atmosphere. J. Meteor. Soc., Japan, 42, 14-25.

Nitta, T., 1967: Dynamical interaction between the lower stratosphere and the troposphere. Mon. Wea. Rev., 95, 319-399.

O'Neil, T.H.R., 1964: Diagnostic studies of vertical motion and precipitation calculations using various grids, analyses and boundary conditions. Ph.D. Thesis, Florida State Univ., 108 pp.

Oort, H.A., 1963: On the energy cycle in the lower stratosphere. Rep. No. 9. Planetary Circulation Project, Dept. of Meteor., Mass. Inst. of Tech., 122 pp.

__________, On estimates of the atmospheric energy cycle. Mon. Wea. Rev., 92, 483-493.

Orvig, S., 1962: Extrapolation and observation of the 25-mb surface height over Canada and Alaska. J. Appl. Meteor., 1, 118-122.

Paulin, G., 1966: Stratospheric heating rates. A.M.R.G. Publication in Meteorology No. 81, McGill Univ., 98 pp.

Perry, J.S., 1966: The energy balance of the atmosphere during a sudden stratospheric warming. Ph.D. Thesis, Univ. of Washington, Seattle, 185 pp.

__________, 1967: Long-wave energy processes in the 1963 sudden stratospheric warming. J. Atmos. Sc., 24, 539-550.

Phillips, N.A., 1956: The general circulation of the atmosphere: a numerical experiment. Quart. J. Roy. Meteor. Soc., 82, 123-164.

__________, 1963: Geostrophic motion. Rev. of Geophys., 1, 2, 123-176.

Plass, G.M., 1956: The influence of the 9.6-micron ozone band on atmospheric infrared cooling rate. Quart. J. Roy. Meteor. Soc., 82, 30-44.

Reed, R.J., 1963: On the causes of the stratospheric sudden warming phenomenon. Meteor. Abhandl., Band XXXVI, 315-334.

__________, J.L. Wolfe and H. Nishimoto, 1963: A spectral analysis of the stratospheric sudden warming of early 1957. J. Atmos. Sc., 20, 256-275.

Rodgers, C.D. and C.D. Walshaw, 1966: The computation of infrared cooling rates in planatery atmospheres. Quart. J. Roy. Meteor. Soc., 92, 67-92.

Saltzman, B., 1957: Equations governing the energetics of the larger scales of atmospheric turbulence in the domain of wave number. J. Meteor., 14, 513-523.

__________, 1958: Some hemispheric spectral statistics. J. Meteor., 15, 259-263.

__________, 1959: On the maintenance of the large-scale quasi-permanent disturbance in the atmosphere. Tellus, 11, 425-431.

__________, 1961: The zonal harmonic representation of the atmospheric energy cycle - A review of measurement. The Travellers Research Center, Report TRC-9, 19 pp.

__________, 1965: On the theory of the winter-average perturbation in the troposphere and the stratosphere. Mon. Wea. Rev., 93, 195-211.

__________, and A. Fleisher, 1960a: Spectrum of kinetic energy transfer due to large-scale horizontal Reynolds stresses. Tellus, 12, 110-111.

______________________, 1960b: The exchange of kinetic energy between larger scales of atmospheric motions. Tellus, 12, 374-377.

Saltzman, B. and A. Fleisher, 1960c: The modes of release of available potential energy in the atmosphere. J. Geophys. Res., 65, 1215-1222.

______, 1961: Further statistics on the modes of release of available potential energy. J. Geophys. Res., 66, 2271-2273.

______, 1962: Spectral statistics on the wind at 500 mb. J. Meteor., 19, 195-204.

______ and S. Teweles, 1964: Further statistics on the exchange of kinetic energy between harmonic components of the atmospheric flow. Tellus, 16, 432-435.

Scherhag, R., 1962a: Meteorologische abhandlungen (10 mb). BAND XXXI/Heft 1, Inst. fur Meteor. und Geophysik der Freien Universitat Berlin.

______, 1962b: Meteorologische abhandlungen(25 mb). BAND XXX/Heft 1, Inst. fur Meteor. und Geophysik der Freien Universitat Berlin.

______, 1962c: Meteorologische Abhandlungen(50 mb). Band XXIX/Heft 1, Inst. fur Meteor. und Geophysik der Freien Universitat Berlin.

Smagorinsky, J., S. Manabe and J.L. Halloway, Jr., 1965: Numerical results from a nine-level general circulation model of the atmosphere. Mon. Wea. Rev., 93, 727-768.

Stark, L.P., 1959: The weather and circulation of January 1959. Mon. Wea. Rev., 87, 33-39.

Steinberg, L., 1965: A spherical harmonic specification of the global 500 mb surface. M.Sc. Thesis, McGill Univ.

Steiner, H.A., 1961: The stratospheric wind regimes of the 1958-59 winter. A.M.R.G. Publication in Meteorology No. 41 McGill Univ.

Teweles, S., 1958: Anomalous warming of the stratosphere over North America in early 1957. Mon. Wea. Rev., 86, 377-396.

______, 1963a: Spectral aspects of the stratospheric circulation during the IGY. Rep. No. 8, Planetary circulations project, Dept. of Meteorology, Mass. Inst. of Tech., 191 pp.

Teweles, S., 1963b: A spectral study of the warming epoch of January-February 1958. Mon. Wea. Rev., 91, 505-519.

__________, 1965: The energy balance of the stratosphere. Tech. Note No. 70, WMO-No. 176. TP.87. 107-122.

Van Mieghem, J., 1952: Energy conversions in the atmosphere on the scale of general circulation. Tellus, 4, 334-351.

__________, 1961a: Le Bilan de l'énergie disponible transformable en énergie cinétique dans l' atmosphere. J. de Méc. et de Phys. de l'Atmo, II-10, 49-71.

__________, 1961b: Zonal harmonic analysis of the northern hemisphere geostrophic wind field. Monographie No. 8, Union Géodésique et Géophysique Internationale. 55 pp.

__________, 1963: New aspects of the general circulation of the stratosphere and mesosphere. Met. Abhandlungen, Bd. 36, Inst. fur Meteor. and Geophysik, Berlin 5-62.

Vernekar, A.D., 1967: On mean meridional circulations in the atmosphere. Mon. Wea. Rev., 95, 705-721.

Walshaw, C.D., 1957: Integrated absorption by the 9.6-micron band of ozone. Quart. J. Roy. Met. Soc., 83, 315-321

White, R.M., 1950: A mechanism for the vertical transport of angular momentum in the atmosphere. J. Meteor., 7, 349-350.

__________, and B. Saltzman, 1956: On conversions between potential and kinetic energy in the atmosphere. Tellus, 8, 3.

Wiin-Nielsen, A., 1959: A study of energy conversion and meridional circulation for large-scale motion in the atmosphere. Mon. Wea. Rev., 87, 319-332.

__________, 1959b: On certain constraints for the time integration of baroclinic models. Tellus, 11, 45-59.

__________, 1964a: Further studies of energy exchanges between the zonal flow and the eddies. Tellus, 16, 168-180.

__________, 1964b: On energy conversion calculations. Mon. Wea. Rev., 92, 161-167.

Wiin-Nielsen, A. and J.A. Brown, 1960: On diagnostic computations of atmospheric heat sources and sinks and the generation of available potential energy. Proceeding of the International Symposium on Numerical Weather Prediction in Tokyo, November 7-13, 1960. Tokyo, Meteor. Soc. of Japan.

__________, and M. Drake, 1964: Further studies of energy exchanges between the zonal flow and the eddies. Tellus, 16, 168-180.

Winston, J.S. and A.F. Krueger, 1961: Some aspects of a cycle of available potential energy. Mon. Wea. Rev., 89, 307-318.

Yang, Chien-hsiung, 1967a: A diagnostic study on non-linear energy exchanges among harmonic components in the atmosphere. To be published in A.M.R.G. Publication in Meteorology No. 88, McGill Univ.

__________, 1967b: Non-linear aspects of the large scale motion in the atmosphere. Tech. Rep., College of Engineering, Dept. of Meteorology and Oceanography, Univ. of Michigan.

APPENDIX A

DIAGNOSTIC OMEGA EQUATION IN THE FOURIER SPECTRAL DOMAIN

Introduction

The formulation and initial results of an experiment designed to produce vertical motions and energy conversions from Fourier coefficients of geopotential height and temperature at selected latitude circles and standard pressure levels, are presented.

The major contribution to energy conversion in the atmosphere comes through the release of potential energy and latent heat in vertical overturnings, and our inability to measure vertical motions creates a serious problem. The vertical motion must be derived either as a time-dependent variable or through the diagnostic property inherent in the hydrostatic approximation. The kinematic method used by Eddy (1963) requires divergence computations from accurate and dense wind data and hence cannot be routinely applied on local, let alone hemispheric, fields.

The adiabatic time-difference method has been used by many authors, e.g. Muench (1964), Reed et al (1963), Barnes (1962), Jensen (1961), Craig and Lateef (1961), to name a few. The results, though valuable, may be strongly biased by the large data observing interval. In addition, Wiin-Neilsen (1964) has shown that energy conversions based on such computations include diabatic contributions. Recently Julian and Labitzke(1965) and Perry (1966) have exploited this apparent deficiency to obtain approximations to the diabatic effects.

The vorticity equation method, used successfully by Perry (1966), also requires time differencing and is not suitable for the longer time intervals in the McGill data.

The diagnostic-omega method, which has gained prominence in numerical weather prediction, has the clear advantage of eliminating time differencing by coupling the vorticity and thermodynamic equations and is applied spectrally in this experiment. Furthermore, the method permits computations of the conversion between available potential energy and kinetic energy which are limited mainly by the resolution inherent in the data and in the mathematical (numerical) model used to process the data.

The mathematical basis for the vertical motion computations and a few results form the body of this review.

Complex Fourier Representation

The complex notation, which is convenient for both analytic and computer manipulations, is reviewed briefly.

If $f(\lambda)$ is a periodic function satisfying Dirichlet conditions, then:

$$f(\lambda) = \sum_{n=-\infty}^{\infty} F(n)\, e^{in\lambda} \qquad (1)$$

where the complex coefficients, F(n) are given by:

$$F(n) = \frac{1}{2\pi}\int_0^{2\pi} f(\lambda)\, e^{-in\lambda}\, d\lambda \qquad (2)$$

$$F(o) = \frac{1}{2\pi}\int_0^{2\pi} f(\lambda)\, d\lambda = \overline{f(\lambda)} \quad \text{, the mean value,} \qquad (3)$$

$$F(-n) = \frac{1}{2\pi}\int_0^{2\pi} f(\lambda)\, e^{in\lambda}\, d\lambda \qquad (4)$$

It is to be noted that F(n) and F(-n) are complex conjugates.

If we let f(λ, ϕ, p, t) be a general meteorological variable, the corresponding Fourier transform pair (f, F) can be related by:

$$f(\lambda, \phi, p, t) = \sum_{n=-\infty}^{\infty} F(n, \phi, p, t)\, e^{in\lambda} \qquad (5)$$

where
$$F(n, \phi, p, t) = \frac{1}{2\pi}\int_0^{2\pi} f(\lambda, \phi, p, t)\, e^{-in\lambda}\, d\lambda \qquad (6)$$

The relation between the Fourier transform pairs of the derivatives in the independent variables n, ϕ, p, t, can be shown to be:

$$\frac{\partial f}{\partial \lambda}(\lambda, \phi, p, t) = \sum_{n=-\infty}^{\infty} inF(n, \phi, p, t)\, e^{in\lambda} \qquad (7)$$

where
$$inF(n, \phi, p, t) = \frac{1}{2\pi}\int_0^{2\pi} \frac{\partial f}{\partial \lambda}(\lambda, \phi, p, t)\, e^{-in\lambda}\, d\lambda \qquad (8)$$

and letting ξ by any of ϕ, p, n, t , we have:

$$\frac{\partial f}{\partial \xi} = \sum_{n=-\infty}^{\infty} \frac{\partial F}{\partial \xi}\, e^{in\lambda} \qquad (9)$$

where
$$\frac{\partial F}{\partial \xi} = \frac{1}{2\pi}\int_0^{2\pi} \frac{\partial f}{\partial \xi} e^{-in\lambda} d\lambda \qquad (10)$$

Let the product of the two functions f(λ) and g(λ) be p(λ),

i. e.
$$p(\lambda) = f(\lambda)\, g(\lambda) \;,$$

then the spectral function P(n) of p(λ) takes the form

$$P(n) = \sum_{m=-\infty}^{\infty} G(m) F(n-m) \qquad (11)$$

where G(ℓ) and F(ℓ) are the spectral functions of g(λ) and f(λ) respectively.

The Diagnostic-Omega Equation

Derivative

When the geostrophic, (or quasi-geostrophic), vorticity equation:

$$\frac{\partial \zeta}{\partial t} + \mathbb{V} \cdot \nabla (\zeta + f) = f \frac{\partial \omega}{\partial p} \qquad (12)$$

is operated on by " $\partial / \partial p$ ", and the thermodynamic equation:

$$\frac{\partial}{\partial t}\left(\frac{\partial Z}{\partial p}\right) + \mathbb{V} \cdot \nabla \left(\frac{\partial Z}{\partial p}\right) - \frac{R \sigma \omega}{g p} = - \frac{R \mathcal{H}}{g p c_p} \qquad (13)$$

is operated by the Laplacian operator ∇^2 , the elimination of the local time derivatives yields the expression:

$$\nabla^2(\sigma\omega) - \frac{pf^2}{R}\frac{\partial^2\omega}{\partial p^2} = -\frac{p}{R} f \frac{\partial}{\partial p}\left[V\cdot\nabla(\zeta+f)\right] - \nabla^2\left(V\cdot\nabla T - \mathcal{H}/c_p\right) \quad (14)$$

which is known as the diagnostic-omega equation. The vorticity, ζ, is given by the relation

$$\zeta = \frac{g}{f}\nabla^2 Z \quad (15)$$

in the geostrophic case, while in the quasi-geostrophic case, it is given by

$$\zeta = \nabla^2\psi \quad (16)$$

where the stream function, ψ, is obtained by the solution of the linear balance equation:

$$g\nabla^2 Z = \nabla\cdot f\nabla\psi \quad (17)$$

The advective terms are derived from either geostrophic or quasi-geostrophic considerations, depending upon the case in question. " σ " is the so-called stability given by:

$$\sigma = \frac{\partial T}{\partial p} - \frac{RT}{pc_p}$$

f is the Coriolis parameter, ω is the individual rate of change of pressure of an air parcel dp/dt, g is the acceleration of gravity, R is the gas constant for dry air, $\mathcal{H}$ is the diabatic heating, Cp is the specific heat coefficient at constant pressure, and T is the temperature in degrees Kelvin.

Operators in the Fourier Domain

The Laplacian takes the following form in spherical coordinates:

$$\nabla^2 = \frac{1}{a^2}\left[\frac{1}{\cos^2\phi}\frac{\partial^2}{\partial\lambda^2} - \tan\phi\frac{\partial}{\partial\phi} + \frac{\partial^2}{\partial\phi^2}\right] \tag{18}$$

Let the height Z(λ, ϕ, p, t) and the vorticity ζ(λ, ϕ, p, t) be expanded in Fourier series as:

$$Z(\lambda,\phi,p,t) = \sum_{n=-\infty}^{\infty} z(n,\phi,p,t)\, e^{in\lambda} \tag{19}$$

and

$$\zeta(\lambda,\phi,p,t) = \sum_{n=-\infty}^{\infty} k(n,\phi,p,t)\, e^{in\lambda} \tag{20}$$

Equivalently, the stream function Ψ(λ, ϕ, p, t) may be expanded as

$$\Psi(\lambda,\phi,p,t) = \sum_{n=-\infty}^{\infty} s(n,\phi,p,t)\, e^{in\lambda} \tag{21}$$

Then depending on whether the geostrophic or quasi-geostrophic case is chosen, the spectral functions for the vorticity are, respectively:

$$k_g(n) = \frac{g}{fa^2}\left[-\frac{n^2 z(n)}{\cos^2\phi} - \tan\phi\,\frac{\partial z(n)}{\partial\phi} + \frac{\partial^2 z(n)}{\partial\phi^2}\right] \tag{22}$$

and $$k_\psi(n) = \frac{1}{a^2}\left[-\frac{n^2 s(n)}{\cos^2\phi} - \tan\phi\,\frac{\partial s(n)}{\partial\phi} + \frac{\partial^2 s(n)}{\partial\phi^2}\right] \tag{23}$$

where the independent variables ϕ, p and t have been omitted and the subscripts "g" and "ψ" differentiate the two cases mentioned above.

The Jacobian $J_a(\alpha,\beta)$ in spherical coordinates is given by:

$$J_a(\alpha,\beta) = \frac{\partial\alpha}{a\cos\phi\,\partial\lambda}\cdot\frac{\partial\beta}{a\,\partial\phi} - \frac{\partial\alpha}{a\,\partial\phi}\cdot\frac{\partial\beta}{a\cos\phi\,\partial\lambda} \tag{24}$$

Let the Fourier transform pair of the Jacobian $J_a(\alpha,\beta)$ be $(J(\lambda), j(n))$, while $(\alpha(\lambda), q(n))$ and $(\beta(\lambda), r(n))$ be the corresponding pairs for the functions α and β. Then following equation (7), (9), (11) and (24):

$$j(n) = \frac{1}{a^2\cos\phi}\left[\sum_{m=-\infty}^{\infty}\left\{i\,m\,r(m)\,\frac{\partial q}{\partial\phi}(n-m) - i\,m\,q(m)\,\frac{\partial r(n-m)}{\partial\phi}\right\}\right] \tag{25}$$

Omega Equations in the Spectral Fourier Domain

It is convenient at this point to tabulate the set of Fourier transform pairs that will be used in the development of the omega-equations. This is the "raison d'etre" of Table A-1. The notation will only be valid for this section. The definition of the various pairs will be given as they appear in the text.

TABLE A-1: Fourier transform pairs of this section.

$f(\lambda)$	Z	$\mathcal{J}$	Q	A_T	A_a	T	$\nabla^2(A_T)$	σ	ω	$\nabla^2\sigma$	$\nabla^2\mathcal{H}/c_p$
$F(n)$	$\mathfrak{z}$	k	q	a_T	a_a	t	L	s	Ω	LS	h

We apply the differential operators ∇^2 and $J(\alpha, \beta)$ to the diagnostic omega equation (14). Note that the stability σ is allowed to vary in all directions and in time. The first term of equation (14) can be expanded into:

$$\nabla^2(\sigma\omega) = \sigma\nabla^2\omega + \omega\nabla^2\sigma + 2\nabla\omega\nabla\sigma \tag{26}$$

We let Q be the absolute vorticity "$\zeta + f$", A_Q and A_T be the advection of absolute vorticity $[\mathbb{V}\cdot\nabla(\zeta+f)]$ and the advection of temperature $[\mathbb{V}\cdot\nabla T]$, respectively. According to this notation, the diagnostic omega equation becomes:

$$\sigma\nabla^2\omega + \omega\nabla^2\sigma + 2\nabla\omega\nabla\sigma - \frac{pf^2}{R}\frac{\partial^2\omega}{\partial p^2} = -\frac{pf}{R}\frac{\partial A_Q}{\partial p} - \nabla^2(A_T - H/c_p) \tag{27}$$

We let $\Delta\phi$ be the numerical difference between any two latitude circles where the data are read off and $2\cdot\Delta p$ be the pressure difference between two pressure intervals. The computations are made to give results in the middle of the pressure intervals, but Δ p is a variable in the vertical depending on the data levels given. Centered difference schemes will be applied.

Applying the definition of "σ" given above, its spectral equivalent becomes

$$s(n) = \frac{\partial t(n)}{\partial p} - \frac{Rt(n)}{pc_p} \tag{28}$$

We will term "data levels", the levels where the data are extracted, while the "omega levels" will be those where "ω" will be found, that is, at the middle of the pressure interval bounded by two data levels. Figure A-1 shows the layering system about an omega-level K.

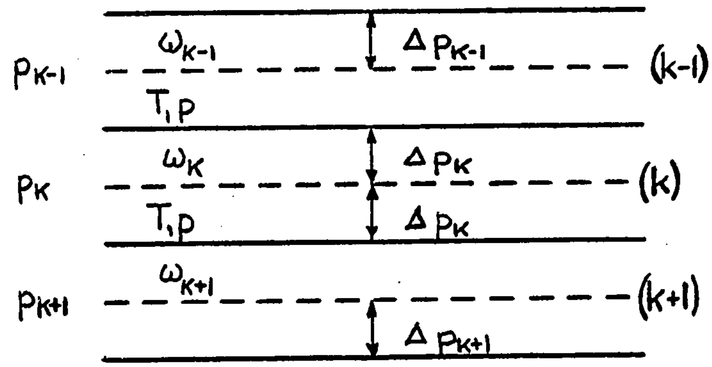

Figure A-1. Layering definition

For simplicity we define the following notation:

$$\alpha^{(k)} = 2f^2 p_K / R(\Delta p)_K^2 \tag{29}$$

$$\alpha^{(k-1)} = 2f^2 p_K / 2R(\Delta p)_K^2 \tag{30}$$

$$\alpha^{(k+1)} = 2f^2 p_K / 2R(\Delta p)_K^2 \tag{31}$$

$$H_K(n) = \frac{f\,p_K}{R}\,\frac{\partial a_0(n)}{\partial p} + L(n) - h(n) \tag{32}$$

It is to be noted that $H_K(n)$ is the spectral form of the forcing function in the omega equation at some level "K" and some given latitude. Using these definitions, the omega-equation (27) can be expanded into the following set of Fourier series:

$$\left(\sum_{n=-\infty}^{\infty}\Omega_K(n)e^{in\lambda}\right)\nabla^2\left(\sum_{m=-\infty}^{\infty}s_K(m)e^{im\lambda}\right)+\left(\sum_{m=-\infty}^{\infty}s_K(m)e^{im\lambda}\right)\nabla^2\left(\sum_{n=-\infty}^{\infty}\Omega_K(n)e^{in\lambda}\right)$$

$$+2\nabla\left(\sum_{n=-\infty}^{\infty}\Omega_K(n)e^{in\lambda}\right)\cdot\nabla\left(\sum_{m=-\infty}^{\infty}s_K(m)e^{im\lambda}\right)=\sum_{n=-\infty}^{\infty}\left\{-\alpha^{(K)}\Omega_K(n)+\alpha^{(K+1)}\Omega_{K+1}(n)+\alpha^{(K-1)}\Omega_{K-1}(n)-H_K(n)\right\}e^{in\lambda} \tag{33}$$

Note that the superscripts attached to the α's are only used to indicate to which spectral $\Omega(n)$ they are related. The subscripts attached to the $\Omega(n)$ refer to the proper omega-levels, as mentioned above.

Having set the vertical differentials, the next step is to expand the horizontal operators affecting the Ω's and the s's. The spectral Laplacian, ∇_n^2 , and the spectral gradient, ∇_n , are applied to equation (33), resulting in the following expression:

$$\left(\sum_{n=-\infty}^{\infty}\Omega_K(n)e^{in\lambda}\right)\sum_{m=-\infty}^{\infty}\frac{1}{a^2}\left[\frac{-m^2 s_K(m)}{\cos^2\phi}-\tan\phi\frac{\partial s_K(m)}{\partial\phi}+\frac{\partial^2 s_K(m)}{\partial\phi^2}\right]e^{im\lambda}$$

$$+\left(\sum_{m=-\infty}^{\infty}s_K(m)e^{im\lambda}\right)\sum_{n=-\infty}^{\infty}\frac{1}{a^2}\left[\frac{-n^2\Omega_K(n)}{\cos^2\phi}-\tan\phi\frac{\partial\Omega_K(n)}{\partial\phi}+\frac{\partial^2\Omega_K(n)}{\partial\phi^2}\right]e^{in\lambda} \tag{34}$$

$$+\frac{2}{a^2}\left(\sum_{m=-\infty}^{\infty}\frac{\partial s_K(m)}{\partial\phi}e^{im\lambda}\right)\left(\sum_{n=-\infty}^{\infty}\frac{\partial\Omega_K(n)}{\partial\phi}e^{in\lambda}\right)-\frac{2}{a^2\cos^2\phi}\left(\sum_{m=-\infty}^{\infty}m s_K(m)e^{im\lambda}\right)\left(\sum_{n=-\infty}^{\infty}n\Omega_K(n)e^{in\lambda}\right)=$$

$$=\sum_{n=-\infty}^{\infty}\left[-\alpha^{(K)}\Omega_K(n)+\alpha^{(K+1)}\Omega_{K+1}(n)+\alpha^{(K-1)}\Omega_{K-1}(n)-H_K(n)\right]e^{in\lambda}$$

The non-linear characteristic of the system is shown by the double summation. Some other non-linear terms are hidden in the $H_K(n)$ term due to the advective terms inside. Recalling from Table 1 that LS(n) is the spectral function corresponding to $\nabla^2\sigma$, letting $\nabla\phi$ be the latitude difference between two latitude circles, letting "j" be the latitude subscript, increasing southward, applying a centered difference scheme in the meridional direction, and using equation (11) for the product of two functions brings about the following system:

$$\sum_{m=-\infty}^{\infty}\left\{\Omega_{j,K}(m)\left[LS_{j,K}(n-m)+\frac{s_{j,K}(n-m)}{a^2}\left(\frac{-m^2}{\cos^2\phi}-\frac{2}{(\Delta\phi)^2}-\frac{2m(n-m)}{\cos^2\phi}\right)\right]\right.$$

$$+\Omega_{j+1,K}(m)\left[\frac{s_{j,K}(n-m)}{2a^2(\Delta\phi)^2}\left(2-\tan\phi.\Delta\phi\right)+\frac{1}{2a^2(\Delta\phi)^2}\left(s_{j+1,K}(n-m)-s_{j-1,K}(n-m)\right)\right]\cdot$$

$$+\Omega_{j-1,K}(m)\left[\frac{s_{j,K}(n-m)}{2a^2(\Delta\phi)^2}\left(2+\tan.\Delta\phi\right)-\frac{1}{2a^2(\Delta\phi)^2}\left(s_{j+1,K}(n-m)-s_{j-1,K}(n-m)\right)\right]\Bigg\}= \tag{35}$$

$$=-\alpha_{j,K}^{(K)}\Omega_{j,K}(n)+\alpha_{j,K}^{(K+1)}\Omega_{j,K+1}(n)+\alpha_{j,K}^{(K-1)}\Omega_{j,K-1}(n)-H_{j,K}(n)$$

System (35) portrays the general solution of the coefficient $\Omega_{j,K}(n)$ of wave number "n", at omega-level "K" and latitude indicator "j", as a function of the coefficients $\Omega(n)$ above and below level "K", the coefficients of all wave numbers at the same level "K" but north and south of latitude "j" and the heating function coefficient at level "K" and latitude "j". System (35) is fairly general as it is diabatic and allows full variation of the stability. System (35) is simplified formally by letting $\epsilon_{j,K}$ (m, n) be the coefficient of $\Omega_{j,K}$ (m), $\delta_{j,K}$ (m, n) be the coefficient of $\Omega_{j+1,K}$ (m) and $\gamma_{j,K}$ (m, n) be the coefficient affecting $\Omega_{j-1,K}$ (m) from which follows

$$\sum_{m=-\infty}^{\infty}\left\{\varepsilon_{j,K}(m,n)\,\Omega_{j,K}(m) + \delta_{j,K}(m,n)\,\Omega_{j+1,K}(m) + \gamma_{j,K}(m,n)\,\Omega_{j-1,K}(m)\right\}$$

$$+\alpha_{j,K}^{(K)}\Omega_{j,K}(n) - \alpha_{j,K}^{(K+1)}\Omega_{j,K+1}(n) - \alpha_{j,K}^{(K-1)}\Omega_{j,K-1}(n) = -H_{j,K}(n) \tag{36}$$

System (36) is a very large system of linear equations to solve. If we have I levels of data available, L latitudes and accept a truncation for N wave numbers, the solution for one coefficient Ω (n) consists in inverting a (I-1) (L-2) (N+1)X (I-1) (L-2) (N+ 1) matrix. If we have 9 levels of information, 11 latitudes and truncate at n = 12, there we will have to invert a 936 x 936 matrix for each of the twelve wave numbers. It is obvious that this method is quite impractical and some simplifications of the system are necessary.

The cause of the large matrix is of course the " $\nabla^2\sigma\omega$ ", where " σ " is a variable in all of λ, ϕ, p and t. Gates (1961) has shown that the main stability variation is in the latitudinal direction in winter (mean January case). The ratio of meridional variation to the longitudinal variation is greatest in the stratosphere. It follows that a minor simplification of the stability term would be to make it a constant in the zonal direction, but a variable in the meridional direction. It is therefore written as:

$$\sigma_{j,K}(\lambda,\phi,p,t) = s_{j,K}(0,\phi,p,t) \tag{37}$$

where n = 0 stands for the zonal mean value of the stability term at latitude "j" and level "K". Introducing the simplification

(37) into equation (34), applying the Fourier transform to the resulting expression and ordering the terms, yields the new expression:

$$\begin{aligned}
&\Omega_{j,K}(n)\left[\frac{1}{a^2}\left(-\tan\phi\,\frac{\partial s_{j,K}(0)}{\partial\phi}+\frac{\partial^2 s_{j,K}(0)}{\partial\phi^2}-\frac{n^2 s_{j,K}(0)}{\cos^2\phi}-\frac{2\,s_{j,K}(0)}{(\Delta\phi)^2}+\alpha_{j,K}^{(K)}\right]\right. \\
&\quad+\Omega_{j+1,K}(n)\left[\frac{s_{j,K}(0)}{a^2}\left(\frac{\tan\phi}{2\Delta\phi}+\frac{1}{(\Delta\phi)^2}\right)-\frac{1}{a^2\Delta\phi}\cdot\frac{\partial s_{j,K}(0)}{\partial\phi}\right] \\
&\quad+\Omega_{j-1,K}(n)\left[\frac{s_{j,K}(0)}{a^2}\left(-\frac{\tan\phi}{2\Delta\phi}+\frac{1}{(\Delta\phi)^2}\right)+\frac{1}{a^2\Delta\phi}\cdot\frac{\partial s_{j,K}(0)}{\partial\phi}\right] \\
&\quad-\Omega_{j,K+1}(n)\left[\alpha_{j,K}^{(K+1)}\right]-\Omega_{j,K-1}(n)\left[\alpha_{j,K-1}^{(K-1)}\right]=-H_{j,K}(n)
\end{aligned} \tag{38}$$

The coefficients of the various Ω (n)'s are redefined:

$\varepsilon_{n,j,K}^{(j)}$ is the coefficient of $\Omega_{j,K}(n)/a^2$,

$\delta_{j,K}^{(j+1)}$ is the coefficient of $\Omega_{j+1,K}(n)/a^2$ and

$\gamma_{j,K}^{(j-1)}$ is the coefficient of $\Omega_{j-1,K}(n)/a^2$

Further we let:

$$R_{j,K}^{(K+1)} = a^2\alpha_{j,K}^{(K+1)} ,$$

$$P_{j,K}^{(K-1)} = a^2\alpha_{j,K}^{(K-1)} \quad \text{and}$$

$$F_{j,K}(n) = -a^2 H_{j,K}(n)$$

Applying these definitions to equation (38), we get the formal relation:

$$\gamma_{j,K}^{(j-1)} \Omega_{j-1,K}(n) + \varepsilon_{n,j,K}^{(j)} \Omega_{j,K}(n) + \delta_{j,K}^{(j+1)} \Omega_{j+1,K}(n) - P_{j,K}^{(K-1)} \Omega_{j,K-1}(n)$$

$$- R_{j,K}^{(K+1)} \Omega_{j,K+1}(n) = F_{j,K}(n) \qquad (39)$$

Given I levels of data with L latitudes, the system (39) will yield (I-1) (L-2) linear equations in exactly the same number of unknowns. In contrast to the general case, a 72 x 72 matrix will need to be inverted instead of a 936 x 936. This inversion is of course needed for each wave number, in both cases. In matrix notation, the problem consists in solving:

$$\left[A(n)\right] \left\{\Omega(n)\right\} = \left\{F(n)\right\}$$

for the vector r(n), where the matrix $\left[A(n)\right]$ is the matrix formed by the coefficients of the $\Omega(n)$'s. Its solution is formally given by:

$$\left\{\Omega(n)\right\} = \left[A(n)\right]^{-1} \left\{F(n)\right\}$$

for each wave number "n". It is interesting to note that the matrix formed by the coefficients of the $\Omega(n)$'s in (39) is a sparse matrix consisting only of five diagonals, the remainder of the elements being zeros. Also out of five diagonals, four of them are independent of the wave number, depending only on the geometry of the model, i.e., δ, γ P and R. ε is a function of the wave number and also of stability. If the stability were defined as a function of pressure only, then A(n) becomes a universal matrix, i.e., it would need to be inverted only once for each wave number.

Some of the practical problems encountered in solving the system such as physical constraints, boundary conditions and numerical approximations are given in the next section.

Numerical and Physical Problems

Data

The available data consisted of a set of 0000Z height and temperature fields for January 12, 1959 to January 16, 1959, at 10 levels: 10 mb, 25 mb, 50 mb, 100 mb, 200 mb, 300 mb, 500 mb, 700 mb, 850 mb and mean sea level surface pressures. No temperatures were available at the lowest level. The data were read from 30N to 80N by 5 degrees latitude steps and 10 degrees longitude steps. Fourier analyses were made at each latitude for each level truncating at wave number 15. Both meridional and vertical derivatives were of the centered-difference type. Taylor expansions were used in the meridional derivatives for the northern and southern boundaries. Analytic fields were used to test the Laplacian and Jacobian operators which were found to be remarkably accurate. The first order numerical derivative was found to have a relative error of 0.390 while the second order numerical derivative had an 8% error.

Boundary conditions

The two usual boundary conditions are made: $\Omega(n) = 0$ at $p = 0$ and $p = 1000$ mb. The boundary conditions on the vertical motion Fourier coefficient are of two types: zonal and wave types.

i) Zonal case: $n = 0$

Murakami (1965) in a similar computation of the mean zonal motion has assumed that it vanishes at 75°N and 20°N, its chosen lateral boundaries. Since our study does not get that far south, we have chosen to take the mean monthly values as found by Perry (1966) for January 1963 at 30°N. These are given in Table A-2.Those values were read off the so-called omega-levels of 0 mb, 17.5 mb, 37.5 mb, 95 mb, 150 mb, 250 mb, 400 mb, 600 mb, 775 mb and 1000 mb.

Table A-2: Mean vertical motion at 30N for January 1963 from Perry (1966).

Omega level (mb)	0	17.5	37.5	75	150	250	400	600	775	1000
ω (cm/sec)	0.0	0.15	0.15	0.15	0.17	0.12	0.05	0.025	0.0	0.0

The vertical motion at 80°N was assumed to be a linear extension of the values found at 70°N and 75°N. Letting j = 1 to j = 11 stand for latitudes 80°N to 30°N, respectively, equation (39) as applied at 80°N and 30°N becomes:

$$\Omega_{2,K}(0)\left[\varepsilon^{(2)}_{n,2,K} + 2\,\gamma^{(1)}_{2,K}\right] + \Omega_{3,K}(0)\left[\delta^{(3)}_{2,K} - \gamma^{(1)}_{2,K}\right] - P^{(K-1)}_{2,K}\,\Omega_{2,K-1}(0) - R^{(K+1)}_{2,K}\,\Omega_{2,K+1}(0) = F_{2,K}(0)$$

$$\gamma^{(9)}_{10,K}\,\Omega_{9,K}(0) + \varepsilon^{(10)}_{n,10,K}\,\Omega_{10,K}(0) + \delta^{(11)}_{10,K}\,\Omega_{11,K}(0) - P^{(K-1)}_{10,K}\,\Omega_{10,K-1}(0) - R^{(K+1)}_{10,K}\,\Omega_{10,K+1}(0) = F_{10,K}(0)$$

Defining:

$$\varepsilon'_{2,K} = \left[\varepsilon^{(2)}_{n,2,K} + 2\,\gamma^{(1)}_{2,K}\right]$$

$$\delta'_{2,K} = \left[\delta^{(3)}_{2,K} - \gamma^{(1)}_{2,K}\right]$$

and carrying the known quantities on the right-hand side:

80°N: $\varepsilon'_{2,K}\,\Omega_{2,K}(0) + \delta'_{2,K}\,\Omega_{3,K}(0) - P^{(K-1)}_{2,K}\,\Omega_{2,K-1}(0) - R^{(K+1)}_{2,K}\,\Omega_{2,K+1}(0) = F_{2,K}(0)$

30°N: $\gamma^{(9)}_{10,K}\,\Omega_{9,K}(0) + \varepsilon^{(10)}_{n,10,K}\,\Omega_{10,K}(0) - P^{(K-1)}_{10,K}\,\Omega_{10,K-1}(0) - R^{(K+1)}_{10,K}\,\Omega_{10,K+1}(0) = F_{10,K}(0) - \delta^{(11)}_{10,K}\,\Omega_{11,K}(0)$

ii) Spectral case

Since by the chosen geometry all wave amplitudes are identically equal to zero at 90°N, we let the amplitudes at 80°N be given by extrapolation this slope to zero from 75°N. We assume that all the coefficients are also zero at the equator and let the amplitude decrease gradually to zero from 35°N. According to this, we have:

80°N: $$\Omega_{j=1}(n) = 2\,\Omega_{j=2}(n)/3$$

30°N: $$\Omega_{j=n}(n) = 6\,\Omega_{j=10}(n)/7$$

When these two relations are substituted in (38), it follows:

80°N $$\Omega_{2,K}(n)\left[\frac{2}{3}\gamma^{(1)}_{2,K} + \varepsilon^{(2)}_{n,2,K}\right] + \delta^{(3)}_{2,K}\Omega_{3,K}(n) - P^{(K-1)}_{2,K}\Omega_{2,K-1}(n) - R^{(K+1)}_{2,K}\Omega_{2,K+1}(n) = F_{2,K}(n)$$

30°N: $$\Omega_{9,K}(n)\gamma^{(9)}_{10,K} + \Omega_{10,K}(n)\left[\varepsilon_{n,10,K} + 6\,\delta^{(11)}_{10,K}/7\right] - P^{(K-1)}_{9,K}\Omega_{9,K-1}(n) - R^{(K+1)}_{9,K}\Omega_{9,K+1}(n) = F_{9,K}(n)$$

It can be seen from the zonal and wave case that we have unknowns at 8 levels and 9 latitudes for each wave number "n", i. e., 72 unknowns. The system being complete since we also have 72 independent linear equations at our disposal.

Variable truncation

Since the original fields at 80°N are usually defined by about 6 to 8 pieces of data, it seems illogical to use 15 wave numbers to specify this ring. It would then be in order to truncate the series at some lower value over the northern regions. Further, we assume that the scale of wave lengths less than a certain size is associated with either reading or instrumental error. We base our truncation on the hypothesis that wave numbers larger than 12 at the lower latitudes (wave length of about 3000 km) are not resolvable in their data. To remain consistent with this logic, the maximum wave number was gradually decreased to 6 at 80N.

Energy invariance constraints

According to Lorentz (1960) the use of the linear balance equation (17) is compatible with the use of the single vorticity equation (12). In this case, the sum of the potential energy, internal energy and kinetic energy of the non-divergent part of the wind is conserved in time. Now, because of the limitations imposed by the use of the geostrophic wind, the deletion of the temperature advection by the ageostrophic or divergent part of the wind in the thermodynamic equation (13) must be compensated by the effect of the horizontal variation of the static stability. Wiin-Nielsen (1959) has shown that in the case of the adiabatic thermodynamic equation, i.e. $\mathcal{H} = 0$, the integration over the whole atmosphere of this equation gives a fictitious temperature production since the " $\sigma\omega$ " correlation is not zero. Since " ω " is zero when integrated over the whole atmosphere, then making σ a constant at any j-level makes the correlation identically zero. However, the diabatic case is not as binding as the adiabatic one since the temperature production can be given by both the heating term and the " $\omega\sigma$ " correlation.

Commenting on the fact that the ageostrophic advection tends to compensate for the effects of variable stability in the horizontal, Danard (1964) has found computationally that the absolute values of the former are smaller than those of the latter. A partial horizontal variation in the stability parameter would tend to make the absolute values of the two terms quantitatively closer to each other.

It is to be noted that the restrictions mentioned above are designed to keep the model stable when integrating in time, and since we are dealing with the instantaneous case, it is not necessary to be so restrictive.

No restriction has been placed on the coriolis parameter "f" following Lorentz (1960). But according to Wiin-Nielsen (1959), at least for a two level model having a linear vertical variation of the wind (also vorticity) and having a vertical motion profile which is parabolic, a variable "f" brings about a fictitious production of thermal vorticity because of a non-vanishing "wf" correlation. This correlation is minimal if the domain boundary is a latitude circle since "f" is a constant there and the mean zonal vertical motion is a very small value. Here again, this error is very small.

Results and Comparison with Other Studies

The computer programme includes the option to use different approximations in the vertical motion computations. The solution may choose either the geostrophic or the linear balance equation, and may be adiabatic or diabatic. The geostrophic-adiabatic solution is portrayed in Figures 2 to 10. It consists of vertical motion computations in mb/hour at "data" levels. The normal values computed at "omega"-levels have been interpolated in the vertical to data-levels using an overlapping fourth degree polynomial where the interpolated level is situated about the middle of the four given values. It is useful to compare normal maximum values at levels with those of other authors. Table A-3 compares such vertical motions, w (cm/sec).

Table A-3. Vertical motion comparisons between various studies and this report.

Author, Remarks	Levels (mb)	w(cm/sec)
Knighting (1966	600	3.5
Diagnostic omega, fixed stability		
Craig and Latief (1961)	50	5
Adiabatic omega	25	8
Miyakoda (1963)	34 (diagnostic)	5
Diagnostic omega, fixed stability	34 (adiabatic)	8
Danard (1964)	800	1.5
Adiabatic	600	4.0
Variable stability	400	7
	200	1.8
O'Neil (1964)	200	2.1
Diagnostic omega	400	14
3° lat. grid	600	11
	800	10
Haltiner, Clarke and Lawniczak (1963)	850	2
Diagnostic omega	700	4
Variable stability	500	7
1977-joint octagonal grid	300	2
Perry (1966)	30	3
Divergence vertical integration		
This Report		
Diagnostic omega	10	3
Variable stability	25	4
	50	3
	100	2.4
	200	2
	300	2
	500	3.2
	700	1
	850	0.5

A rapid survey of Figures A-2 to A-10 shows some scale differences between stratospheric and tropospheric vertical motions. Waves 1 to 3 are seen to meander over the stratosphere. The tropospheric vertical velocity field is much more chaotic with waves up to wave number 7 being observed, but a careful inspection reveals the existance of wave number 3. This fact will be important when the correlation between vertical motion and geopotential is spectrally analysed in a later addition to this report.

Concluding Remarks

The solution of the diagnostic omega equation in the Fourier spectral domain has been described. Some simplification has been made in order to reduce the rather voluminous set of linear equations to be solved. The simplification consists in letting the stability be a constant along a latitude circle but to be variable in the north-south and vertical directions, as well as in time.

Numerical methods for the various derivatives have been shown as well as the boundary conditions. Problems of energy invariance in models have been discussed, and it was inferred that the type of variable stability used is in the proper direction to make terms compensate. It was also shown that letting "f" vary causes minimal error since our boundary is along a latitude circle.

Vertical motion values have been shown to be comparable to other studies, the comparison being at its best in the stratosphere.

The purpose of solving for the spectral values of the vertical motion was to compute the complete set of energy conversions and to study the exchanges associated with them. This study is presently being conducted.

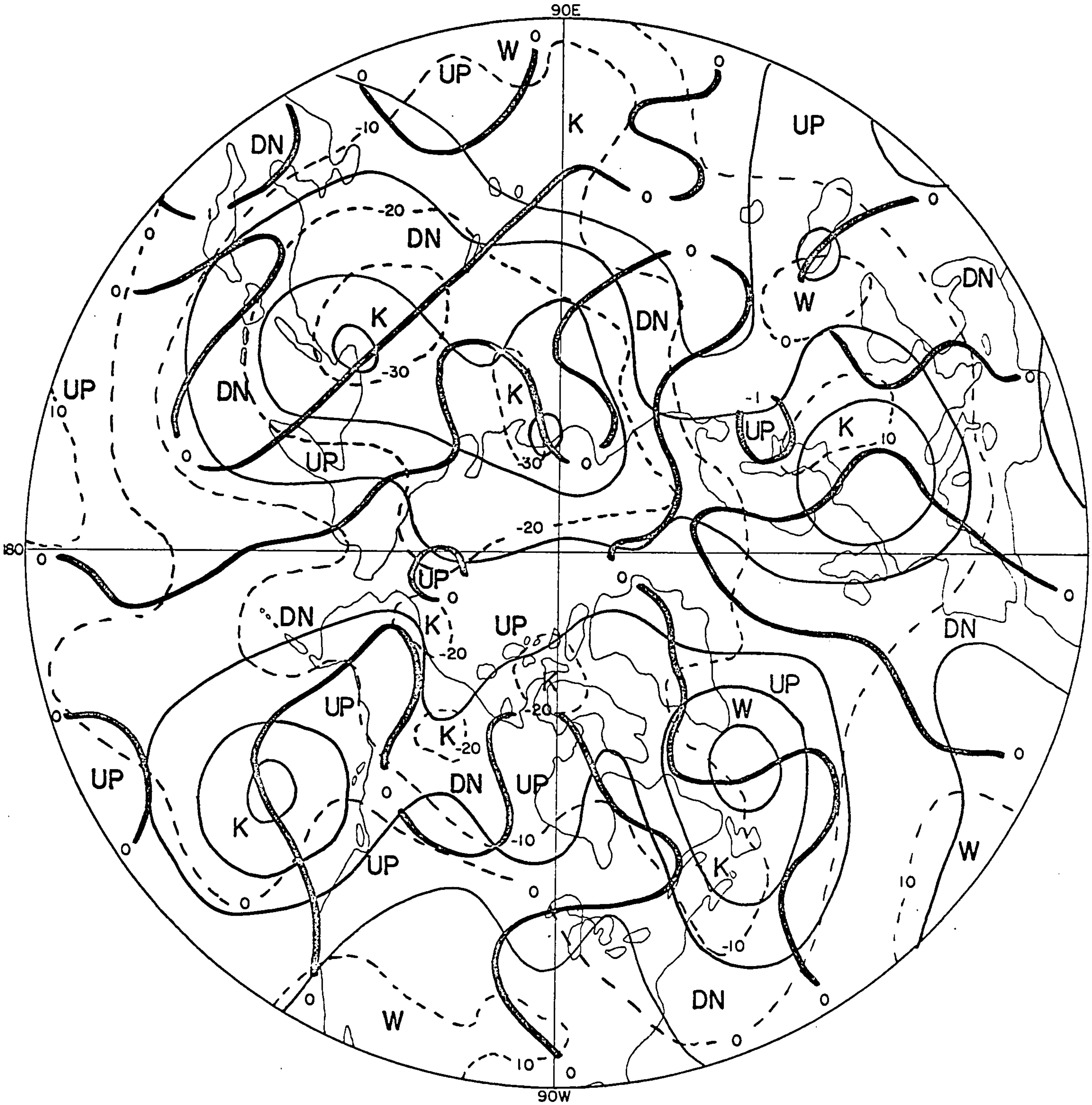

Fig. A-2. VERTICAL MOTION ω (mb/hr) at 850 mb.

12 JANUARY 1959

Fig. A-3. VERTICAL MOTION ω (mb/hr) at 500 mb.

12 JANUARY 1959

Fig. A-4. VERTICAL MOTION ω (mb/hr) at 300 mb.

12 JANUARY 1959

Fig. A-5. VERTICAL MOTION ω (mb/hr) at 100 mb.

12 JANUARY 1959

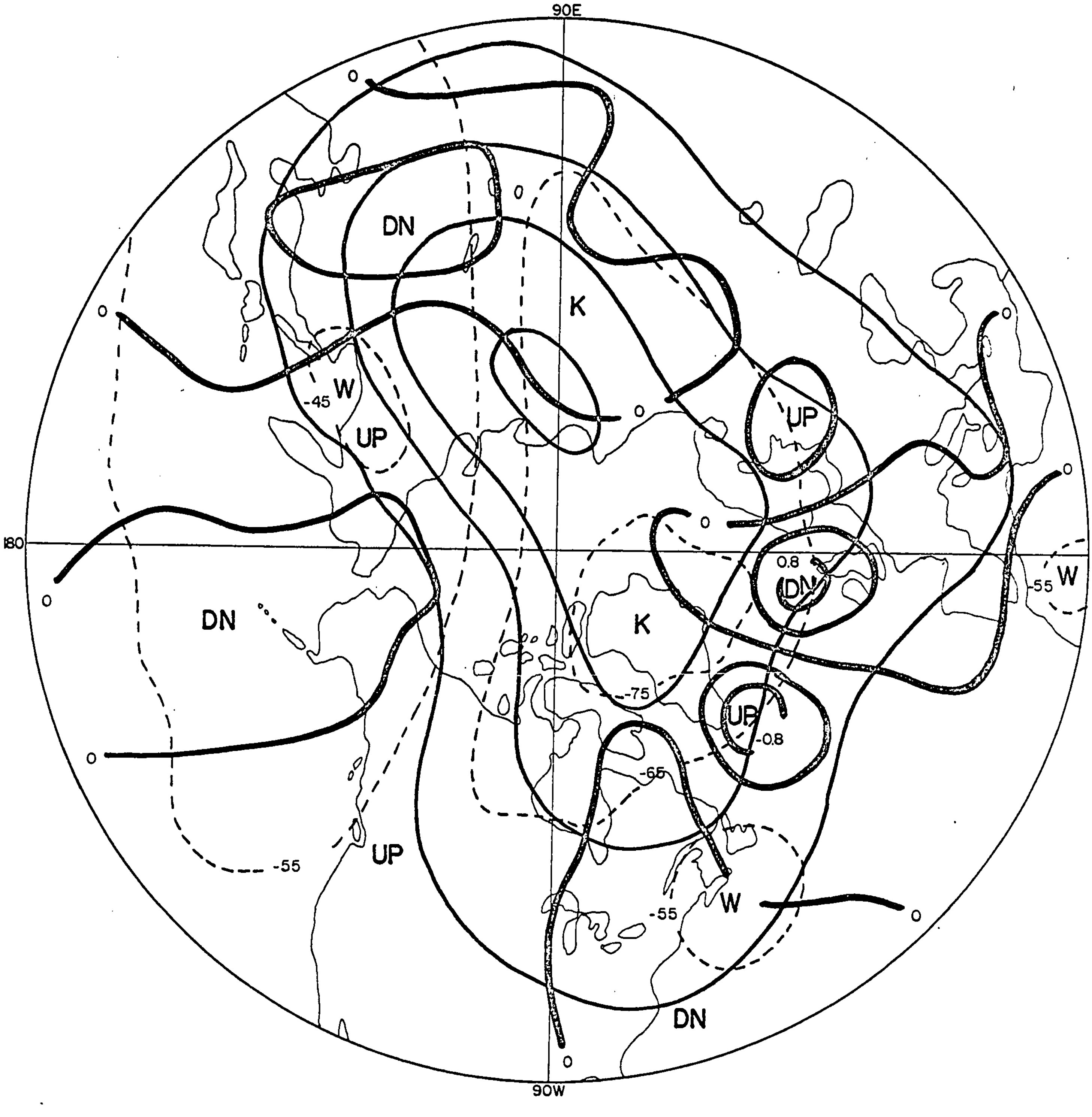

Fig. A-6. VERTICAL MOTION ω (mb/hr) at 50 mb.

12 JANUARY 1959

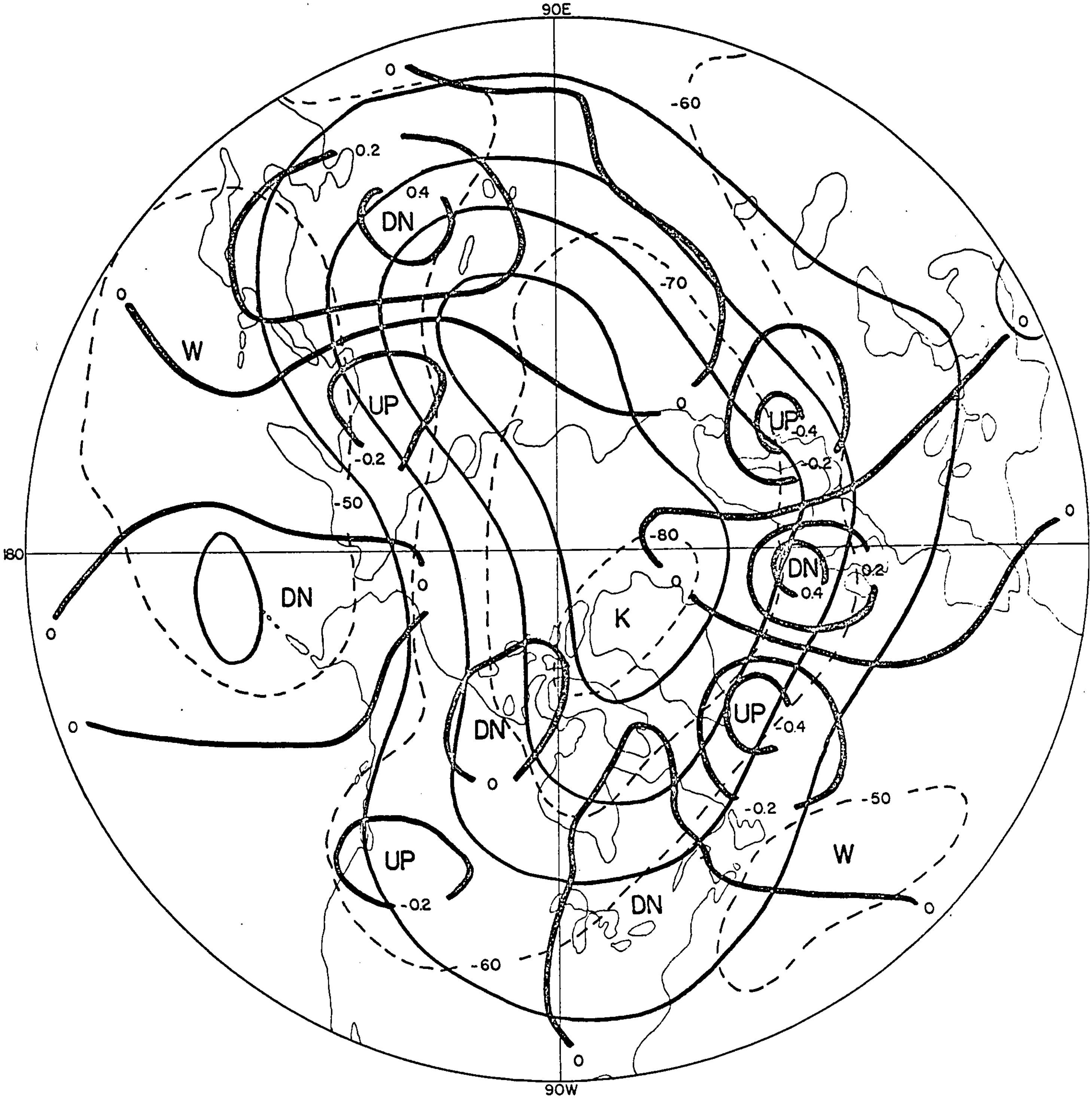

Fig. A-7. VERTICAL MOTION ω (mb/hr) at 25 mb.

12 JANUARY 1959

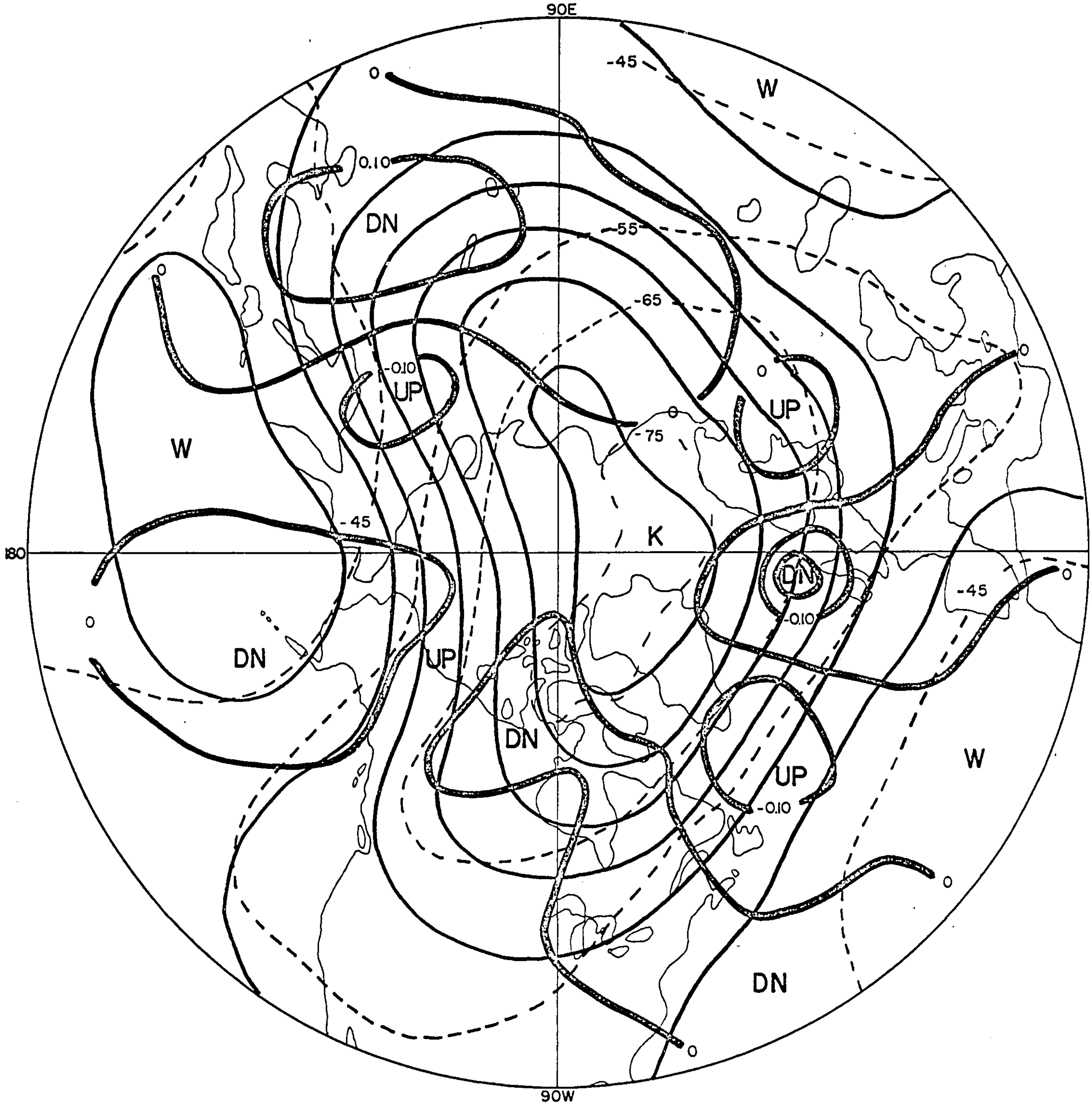

Fig. A-8. VERTICAL MOTION ω (mb/hr) at 10 mb.

12 JANUARY 1959

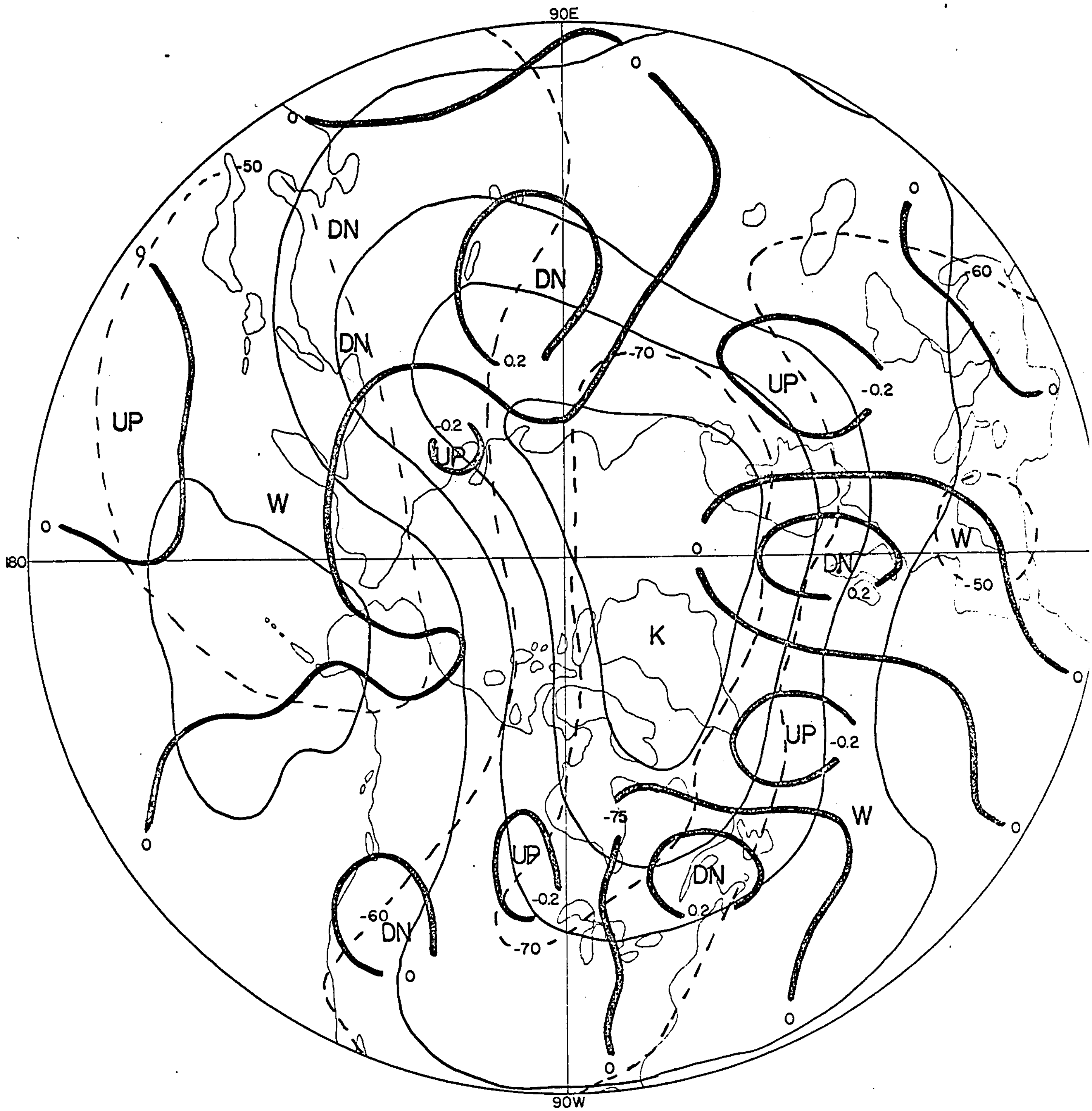

Fig. A-9. VERTICAL MOTION ω (mb/hr) at 25 mb.

14 JANUARY 1959

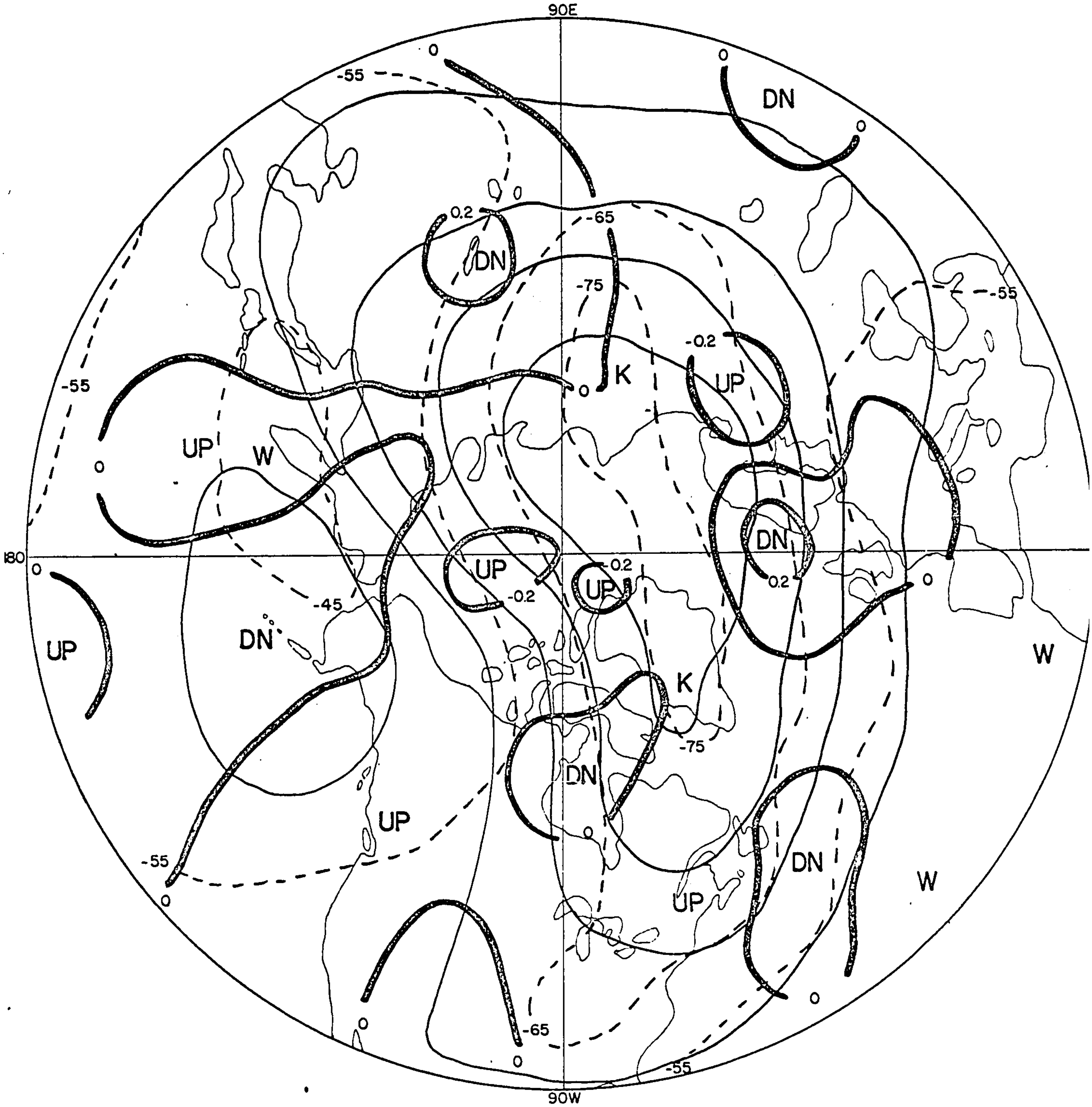

Fig. A-10. VERTICAL MOTION ω (mb/hr) at 25 mb.

16 JANUARY 1959

APPENDIX - B

Radiative Problem in the Stratosphere

Radiative flux computations for the stratosphere have been hampered by the scarcity of observations of absorber concentrations. Of late a few studies have appeared based on ozone data from the Cambridge Research Laboratory (C.R.L.) Ozonesonde network as published by Hering and Borden (1964, 1965). Some have used monthly mean values of the ozonesonde results to compute corresponding statistics (Kennedy, 1964), others have considered daily ozone distributions over North America (Paulin, 1966). In parallel with these studies, and following some of the results of Kennedy (1964), Hering, Touart and Borden (1967) have developed parametric methods to approximate the ozone radiative effects with respect to the solar absorption in the ultraviolet and the water vapour, carbon dioxide, oxygen, methane and nitrous oxide bands effects in the infrared portion of the solar spectrum. Following an intensive study by Rodgers and Walshaw (1966) and some of their results, Lindzen (1967) has advanced simple parametric equations to solve, in an approximate fashion, for the energy transfer in the infrared and ultraviolet.

Results from Kennedy (1964), Hering et al (1967) and Paulin (1966) will be used in order to approximate the daily heating fields in the stratosphere, and to approximate the generation of available potential energy.

Total Solar Heating Rates

Hering et al (1967) found a very strong correlation coefficient between solar heating rates (computed using the lengthy transfer equations) and a combination of solar zenith angle and sunlight duration. The proposed linear relation is the following:

$$\left(\frac{\partial T}{\partial t}\right)_s = a n \overline{M}^{-1/2} + b \qquad \text{(B-1)}$$

where $(\partial T/\partial t)_s$ is the total solar heating rate in °C/day, n is the duration of sunlight in hours, $\overline{M}$ is the magnification of vertical path length for slant path transmission averaged over the daylight hours (Houghton, 1963), and a, b are the linear regressions coefficients listed in Table (B.1).

Table B.1. Correlation coefficients r, standard error σ_e (°C/day) and linear regression constants a and b, for the relationship between $(\partial T/\partial t)_s$ in °C/day and $n\overline{M}^{-1/2}$.

Pressure (mb)	r	σ_e	a	b
25	.990	.056	.142	.071
15	.972	.156	.230	-.081
10	.971	.185	.272	-.109

As noted from Table 1, the correlation is best at 25 mb where the latitudinal variation of ozone is at a minimum, while differences at 15 mb and 10 mb, although small, are systematic and are due to the higher ozone concentrations near the equator and lower concentration in the Arctic.

Hering approximates the "$n\overline{M}^{-1/2}$" term by the relation

$$n\overline{M}^{-1/2} = A + B\cos(2\pi t/365) \qquad \text{(B-2)}$$

where t is the number of days after the summer solstice, and the two constants A and B are given for 10 degree latitude intervals in Table (B-2).

Table B-2. Constants A and B of equation (B-2) as a function of latitude

Latitude (°N)	10	20	30	40	50	60	70	80
A	10.02	9.85	9.56	9.18	8.70	8.36	7.80	7.12
B	0.78	1.58	2.43	3.36	4.43	6.07	7.13	8.30

"$m\overline{M}^{-1/2}$" is approximated within a few percent by eqn. (B-2). Since this study is concerned with latitude intervals of 5 degrees, A and B values at the missing latitudes were interpolated from Table (B-2).

This study combines eqns. (B-1), (B-2) and their associated Tables (B-1) and (B-2) to compute zonal total solar heating in the appropriate period, i.e. January. The values vary slightly from day to day as n and M are functions of time, t.

The corresponding heating rates at 50 mb and 100 mb were taken from Kennedy's January cross-section. These heating rates resulted from energy transfer computations applied to the mean January ozone distribution derived from the ozonesondes reports. The heating rates due to absorption of near-infrared solar radiation were also taken from Kennedy (1964) whose methods were based on Houghton (1963) and whose temperature structure was that of a three-year averaged cross-section for January. Although this last approximation is cruder than the computation at 10 mb and 25 mb, it is validated by the fact that the heating rates are one order of magnitude or more smaller than those at upper levels due to the rapid exponential decrease in the solar radiative fluxes reaching those lower levels.

Infrared Transfer due to Water Vapour

Paulin (1966) concluded that a dry stratosphere having a constant relative humidity of 2% (equivalent to about a mixing ratio of 10^{-3} gm/kgm near 100 mb to about 10^{-2} gm/kgm near 25 mb) would approximate fairly well the Gutnick (1962) measurements of water vapour in the stratosphere. Manabe and Strickler (1964) tried a dry stratospheric mixing ratio of 3×10^{-3} gm/kgm. The value advanced by Craig (1965) is from a relative humidity of 1 to 2%. It is thought that Kennedy's mixing ratio of 2.5×10^{-3} gm/kgm is reasonable, since the heating rates due to water vapour in the infrared are relatively small relative to other stratospheric gases (Paulin, 1966). Kennedy's heating rates for January were accepted at stratospheric levels. Kennedy's computations of infrared transfer due to the rotational water vapour band were based on Davis (1963). Further, Davis (1963) found that mid-tropospheric clouds have little effect on the water vapour rotational band flux divergences in the stratosphere. The resulting cooling rates due to this component vary from about 0.1°C/day at 10 mb to 0.3°C/day at 100 mb.

Infrared Transfer due to the 15-micron Band of Carbon Dioxide

Rodgers and Walshaw (1966) found that the infrared radiative cooling in the stratosphere can be approximated fairly accurately by the cooling-to-space component, which depends on the emitter temperature and the amount of absorber between the emitter and space. Lindzen (1967) has formulated an empirical formula of the "Newtonian" type. The cooling rate due to carbon dioxide in the 15 micron band $(\partial T/\partial t)_{CO_2}$ is given as:

$$\left(\frac{\partial T}{\partial t}\right)_{CO_2} (°C/\text{day}) = a\,(T - T_o) \qquad \text{(B-3)}$$

where $a = 0.73 \times 10^{-4} \exp \quad 7.34\,(1.0 - \exp(-x/2.1))$, (B-4)

where the equilibrium temperature To is:

$$To = 109.3 + 16.8x \qquad \text{(B-5)}$$

and x, the altitude in scale height is:

$$x = \int_0^z \frac{g\,dz}{RT} \tag{B-6}$$

In tests the stratospheric cooling rates based on this approach were found to be too large in comparison to other results using the same temperature distribution. In any case, the differences were larger than those inferred from the Rodgers and Walshaw (1966) results. Because of this and because a relatively fast method of evaluating the cooling rates was available in Kennedy's work, we chose the latter method, which will be described in the next few paragraphs.

The usual constancy of CO_2 concentration is used. The fractional concentration by volume is assumed constant at 0.00031. The heating rate due to infrared transfer in a layer of thickness "Δ p" is:

$$\frac{\partial T}{\partial t} = \frac{g}{c_p} \frac{\Delta F}{\Delta p} \tag{B-7}$$

where Δ F is the net upward flux over a layer Δp mb thick. The spectroscopic data used was that of Burch et al (1962), as applied to the 12 to 18-micron interval. The black body flux for this interval was computed from an expression presented by Davis (1961)

$$B\ (\mathrm{Cal/cm^2\ min}) = 116.435 - 1.6704T + 0.0063T^2 \times 10^{-3}, \tag{B-8}$$

where T is the mean temperature of the layer. Kennedy re-arranged eqn. (B-7) into the form:

$$\frac{dT}{dt}\ (^\circ K/\mathrm{day}) = \frac{gA}{c_p} \sum_{i=1}^{31} \frac{\Delta B_i\, \Delta a_i}{\Delta p} \tag{B-9}$$

where Δa_i is the difference in absorptivities in layer i while ΔB_i is the difference in black body flux in the same layer, and A is a conversion constant. Incidentally, when ΔB_i is in Cal/cm^2 min, Δp is in mb and dT/dt is in $^{\circ}$K/day, the constant "gA/c_p" is 5889.6. Kennedy gives a table for sets of 31 ΔB_i and Δa_i values corresponding to 14 stratospheric layers extending from 200 mb to 5 mb. The heating rates can be found at these 14 layers. The computations require temperatures at 31 atmospheric layers: from surface to 0.6 mb. Kennedy shows that the atmospheric structure below mid-troposphere contributes little to the stratospheric heating rates. The effect then of cloudiness below 500 mb will be negligible in the stratosphere and in the present computations the 500 mb temperature is chosen as the lower boundary. This in turn speeds up the computations by a factor of 1.5, that is only 21 layers are used instead of 31. The temperatures needed at Kennedy's levels were interpolated from the hemispheric data at 500 mb, 300 mb, 200 mb, 100 mb, 50 mb, 25 mb, 10 mb and 2 mb. The heating rates were computed at every grid point separated by 5° latitude and 10° longitude from 30°N to 80°N for the period of January 12 to 16, 1959. The heating at the levels given above are interpolated again from the results. The Fourier coefficients were computed and stored for further use.

Infrared Transfer due to Ozone in the 9.6 μ Band

The infrared radiative transfer method for the 9.6 μ band of ozone used by Paulin (1966) will be described and applied to the data.

The atmosphere is very transparent to black body radiation emitted in the spectral region between about 8 μ and 13 μ. This "window" coincides fairly well with the maximum black body emission of terrestrial radiation. There is an ozone absorption band centered at 9.6 μ. Since the ozone amount in the troposphere is very small, the upcoming flux through this atmospheric window will be effectively absorbed by the much higher amount of ozone in the lower stratosphere where significant heating rates will presumably follow. Of particular interest is the temperature fluctuation of the lower boundary which is assumed to be a black body. Paulin (1966), Kennedy (1964), Clark (1963) have all computed the heating changes following a variable lower boundary temperature. The effects of thick middle clouds will be felt in the resulting heatings taking place in the stratosphere. This differs appreciably from the 15 μ band CO_2 heating where the structure of the lower atmosphere has little effect on the heating in the stratosphere.

The spectroscopic data and corresponding empirical formulae were taken from Walshaw (1957) and the numerical computations were performed in much the same manner as Clark (1963). The method used by Paulin (1966) will be reviewed briefly.

The usual equations relating to the upward flux $F\uparrow(Z)$ and the downward flux $F\downarrow(Z)$ at any height Z are:

$$F\uparrow(Z) = \int_{Z'=Z}^{0} \int_{\theta=0}^{\pi/2} \sin 2\theta \int_{\nu_1}^{\nu_2} B_\nu(Z')\, dA_\nu(Z,Z')\, d\nu\, d\theta \qquad \text{(B-10)}$$

$$F\downarrow(Z) = \int_{Z'=Z}^{\infty} \int_{\theta=0}^{\pi/2} \sin 2\theta \int_{\nu_1}^{\nu_2} B_\nu(Z')\, dA_\nu(Z,Z')\, d\nu\, d\theta \qquad \text{(B-11)}$$

where $B_\nu(Z')$ is the monochromatic black body flux at the temperature of the height Z', θ is the zenith angle and $dA_\nu(Z, Z')$ is the difference in absorptivity across an infinitessimal layer of absorber of thickness dZ' at height Z'. Since the 9.6 μ band is a very complex one, some simplifications are needed to solve eqns. (B-10) and (B-11). We let $B(Z')$ be the black body flux appropriate to the mid-point of the band (ν = 1043 cm^{-1}). The band area A_r is given by

$$A_r(Z, Z') = \int_{BAND} A_r \, d\nu \qquad \text{(B-12)}$$

where ν is taken over the whole band. If we choose the band width to be 138 cm^{-1}, then there exists a number $\overline{A_r(Z, Z')}$ such that the band area $A_r(Z, Z')$ is given by:

$$A_r(Z, Z') = \overline{A_r(Z, Z')} \cdot 138 \qquad \text{(B-13)}$$

Walshaw (1957) formulates eqn. (B-13) empirically by a complex function of ozone masses. The laboratory designed empirical relations are applied to the non-homogeneous atmospheric layer through the Curtis-Godson approximation. (Godson, 1961: Lecture notes). The average pressure over a layer is weighted according to this approximation using the amount of ozone absorbing mass in the layer. Plass (1956) has shown that this approximation is valid for strong and weak absorption regions only. Using the computation for individual lines in the 9.6 μ band performed by Hitschfeld and Houghton (1961) as a standard, Clark (1963) found that his results on the whole agree well with theirs but differs mostly where the lines are neither weak nor strong. A word of caution should be added at this point. Kennedy (1964) while doing similar computation has not used the Curtis-Godson approximation. He used the so-called pressure scaling whereby the ozone path length is reduced by multiplying it by the factor $(p/p_o)^{0.3}$, where p is the pressure at the level in question and p_o is the standard surface pressure. Letting $\overline{p}$ be the new mean pressure of the layer, we have the formal relation for the absorptivity A_r:

$$A_r = A_r(U, \overline{p}) \qquad \text{(B-14)}$$

where U is the layer effective ozone mass. The integration over the zenith angle, Θ , is done by assuming isotropy, i.e., multiplying the ozone mass by the factor 1.66. This simplification has been used by Hitschfeld and Houghton (1961) and also advanced and discussed by Kondrat'yev (1965). Equation (B-14) then takes the form:

$$A_r = A_r(1.66U, \bar{p}) \qquad \text{(B-15)}$$

Following this approximation to A_r, and the assumption on the effective black body flux $\overline{B(Z')}$, the two flux equations become in a finite difference form:

$$F\uparrow(Z) = \sum_{Z'=Z}^{0} \overline{B(Z')} \left[A_r(Z,Z') - A_r(Z,Z'+\Delta Z)\right] \qquad \text{(B-16)}$$

$$F\downarrow(Z) = \sum_{Z'=Z} \overline{B(Z')} \left[A_r(Z,Z'+\Delta Z) - A_r(Z,Z')\right] \qquad \text{(B-17)}$$

where $A_r(Z, Z')$ is the absorption due to the absorber in the layer Z to Z'. The atmosphere was divided into 18 quasi-equal layers, except that the troposphere up to 314 mb was taken to be the lowest layer, because the amount of ozone is very small across this interval. The ground or the overcast cloud tops were assumed black bodies while the top of the atmosphere was taken to be at 0°K. Defining the net flux through height Z to be the difference between $F\uparrow(Z)$ minus $F\downarrow(Z)$, Paulin (1966) shows that the numerical equivalent to (B-10) and (B-11) can be expanded into a matrix product of the form:

$$
\begin{bmatrix} F_{net}(Z_1) \\ F_{net}(Z_2) \\ F_{net}(Z_4) \\ | \\ | \\ | \\ F_{net}(Z_{18}) \\ F_{net}(Z_{19}) \end{bmatrix}
=
\begin{bmatrix}
2A_r(1,1) & A_r(1,2) & A_r(1,4) - & - A_r(1,18) & A_r(1,19) \\
A_r(2,1) & A_r(2,2) & A_r(2,4) - & - A_r(2,18) & A_r(2,19) \\
A_r(4,1) & A_r(4,2) & A_r(4,4) - & - A_r(4,18) & A_r(4,19) \\
 & | & & & | \\
 & | & & & | \\
 & | & & & | \\
A_r(18,1) & A_r(18,2) & A_r(18,4) - & - A_r(18,18) & A_r(18,19) \\
A_r(19,1) & A_r(19,2) & A_r(19,4) - & - A_r(19,18) & A_r(19,19)
\end{bmatrix}
\times
\begin{bmatrix} \overline{B(Z_1)} - 0 \\ \overline{B(Z_3)} - \overline{B(Z_1)} \\ \overline{B(Z_5)} - \overline{B(Z_3)} \\ | \\ | \\ | \\ \overline{B(Z_{19})} - \overline{B(Z_{17})} \\ 0 - \overline{B(Z_{19})} \end{bmatrix}
\qquad \text{(B-18)}
$$

where the arguments (i, j) of the absorptivities refers to the layering system Zi to Zj, and Zm of $\overline{B(Zm)}$ refers to the black body flux at the temperature of the level Zm.

The local rate of temperature change at level Zi+1 is given by the same relation (B-7), which in our new system becomes:

$$
\frac{\partial T}{\partial t} = \frac{g}{c_p} \left[\frac{F_{net}(Z_{i+2}) - F_{net}(Z_i)}{(p_{i+2} - p_i)} \right] \qquad \text{(B-19)}
$$

If F net is in Cal/sec cm^2 and p is in mb, and $\partial T / \partial t$ is in ($^{\circ}$C/day), (B-19) becomes:

$$
\frac{\partial T}{\partial t} (^{\circ}C/day) = 35.3376 \times 10^{4} \left[\frac{F_{net}(Z_{i+2}) - F_{net}(Z_i)}{(p_{i+2} - p_i)} \right] \qquad \text{(B-20)}
$$

It was considered useful to approximate the effect of cloudiness on the heating rates in the stratosphere. The problem becomes one of incorporating Eqn. (B-20) into our data.

First, one must define a hemispheric ozone distribution representative of the month of January. Dütsch (1964) has presented seasonal vertical ozone distribution over selected latitudes, based on the Umkehr method. Bojkov (1965) has also presented ozone vertical profile over the world based on both the Umkehr method (3700 cases) and on ozonesonde reports (about 200). Because of the much greater number in the former cases the statistics will be normally biased towards the Umkehr determinations. There has been some criticism of the Umkehr method; Mateer's (1964) study of the Umkehr method has shown its limitations as far as the number of independent pieces of information is concerned, and inferences from specific profiles. Bojkov (1966) confirmed the difficulties encountered in comparing the two methods. On the other hand Kennedy (1964) has computed average ozone cross-sections based on January-February 1963 ozonesonde reports over North America. Hering, and Borden (1965) have abstracted mean seasonal cross-sections from the 2-year period 1963-1964. Although these observations were mostly over North America and far less numerous than the compiled Umkehr determinations, it is felt that the ozonesonde reports and statistics would be more representative and physically more acceptable. Following these arguments the winter mean cross-sections as given by Hering and Borden (1965) were adopted as representative of hemispheric distributions.

As indicated earlier, the temperature at the lower boundary has a one-to-one correspondence to the heating encountered in the lower stratosphere. The next point is to define the synoptic cloud patterns over our region. In a study such as the present, we are only interested in the synoptic cloud system so as to be able to measure the signal emanating from the tropospheric lower boundary via the 9.6 μ absorption band. This signal will be modified by the vertical ozone profile. The southernmost ozone profile has its maximum concentration at a higher altitude, is more sharply defined and shows a larger concentration, whereas the arctic profile is broader and has a lower concentration at its level of maximum concentration. From this it follows that the magnitude of the heating will decrease with latitude, for a similar temperature profile. In addition, the temperature structures of the southern and the northern regions in winter are quite different. The temperature difference between the lower boundary and the level of maximum heating is much larger in the southern regions. The amplitude of the signal change received between the clear-to-cloudy areas becomes of the order of the error in computing heating rates over the northern regions. Table B-3 shows example of computation at various latitudes using our selected ozone profile.

Table B-3. Heating rates (^{o}C/day) due to the absorption of terrestrial radiation by the 9.6 μ band with variable lower boundaries.

Latitude	30N	50N	70N
Clear Conditions	0.56	0.20	0.04
Overcast tops at 500 mb	0.24	0.14	0.03
Overcast tops at 300 mb	0.10	0.05	0.03

In view of the results of Table B-3, it was decided to omit the cloud effects for the regions north of 50^{o}N. For the regions bounded by 30^{o}N and 50^{o}N, one of the two lower boundary temperatures (850 mb and 500 mb) was accepted, 850 mb being the lowest temperature level available in this study. This can be taken as a very conservative level since it approximates the temperature of the low cloud tops, on the non-synoptic scale, especially applicable over oceanic areas. The 500 mb temperature was chosen in case of a synoptic cloud cover. This is a conservative estimate of the highest clouds behaving as black bodies. The next step was to define the cloud patterns from the available data. The decision to call a region cloudy or not was based on three different tests. At

500 mb, areas of dew point depression less or equal to $2^{o}C$ were contoured. Areas of observed overcast conditions were also defined. Thirdly, using dynamical tools, areas of positive vorticity advection were also determined. Finally the intersection of these areas were formally called overcast with tops at 500 mb.

The temperature structure at each grid point was interpolated to fit the radiative model. The resulting heating rates were re-interpolated at the four stratospheric mandatory levels of 100 mb, 50 mb, 25 mb and 10 mb for each grid point and for the five days included in the period January 12 to 16, 1959. It was thought that in following those rules, the signal received in the stratosphere from the troposphere in the 9.6 μ band would be appropriately defined; even if the amplitudes were somewhat conservative, the phase of the signal should be relatively accurate. These mean zonal heating rates due to the 9.6 μ band are a bit lower on the average than those computed by Kennedy. This is due mainly to three causes. The use of pressure scaling by Kennedy versus the Curtis-Godson approximation will cause some change in the results. Probably more important systematic effects are the inclusion of clouds in our model, which decrease the mean zonal heating and the systematic use of the 850 mb temperature as the emitting lower boundary. Smaller differences may also be due to the layering system in the model and to the difference between the real temperature fields against a climatological mean temperature.

The Fourier coefficients of the heating fields were computed and stored for later use.

At the end, the Fourier coefficients of all the heating components were added together to give the daily heating fields in the stratosphere. Fig. B-1 to Fig. B-4 show the semi-hemispheric distribution obtained with the corresponding temperature fields on January 12, 1959.

The components of the heating fields were added together to give the total heating field due to the absorption of solar and terrestrial radiation at 10 mb, 25 mb, 50 mb and 100 mb, over a 5-day period starting on 12 January, 1959 and ending on 16 January, 1959. The zonal heating configurations were given by the solar absorption by ozone in the ultra-violet and the solar absorption in the near infrared by water vapour, carbon dioxide, oxygen, methane and nitrous oxides bands. The eddy heating fields were generated by the heating or cooling rates associated with the infra-red transfer due to the stratospheric absorption by the 9.6 micron band of ozone and by the 15 micron band of carbon dioxide, respectively.

The diabatic fields are used in the determination of the spectral diagnostic vertical motion, as shown in Appendix A. They are also used to compute the energy generation terms in stratospheric energy budgets for the two periods in question.

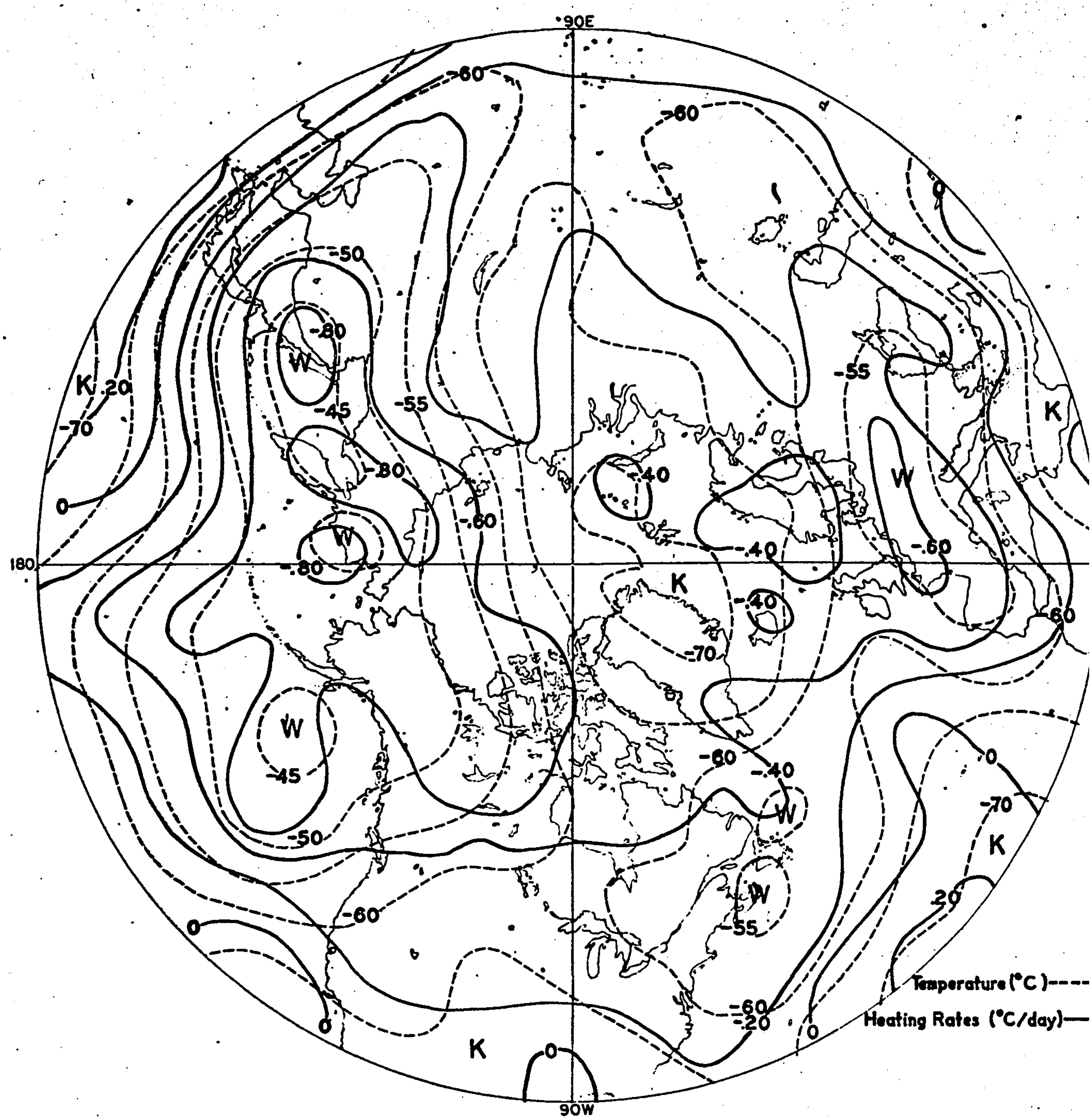

FIG. B. 1. HEATING RATES (°C/DAY) AND TEMPERATURE (°C) AT 100 MB 12 JANVIER 1959

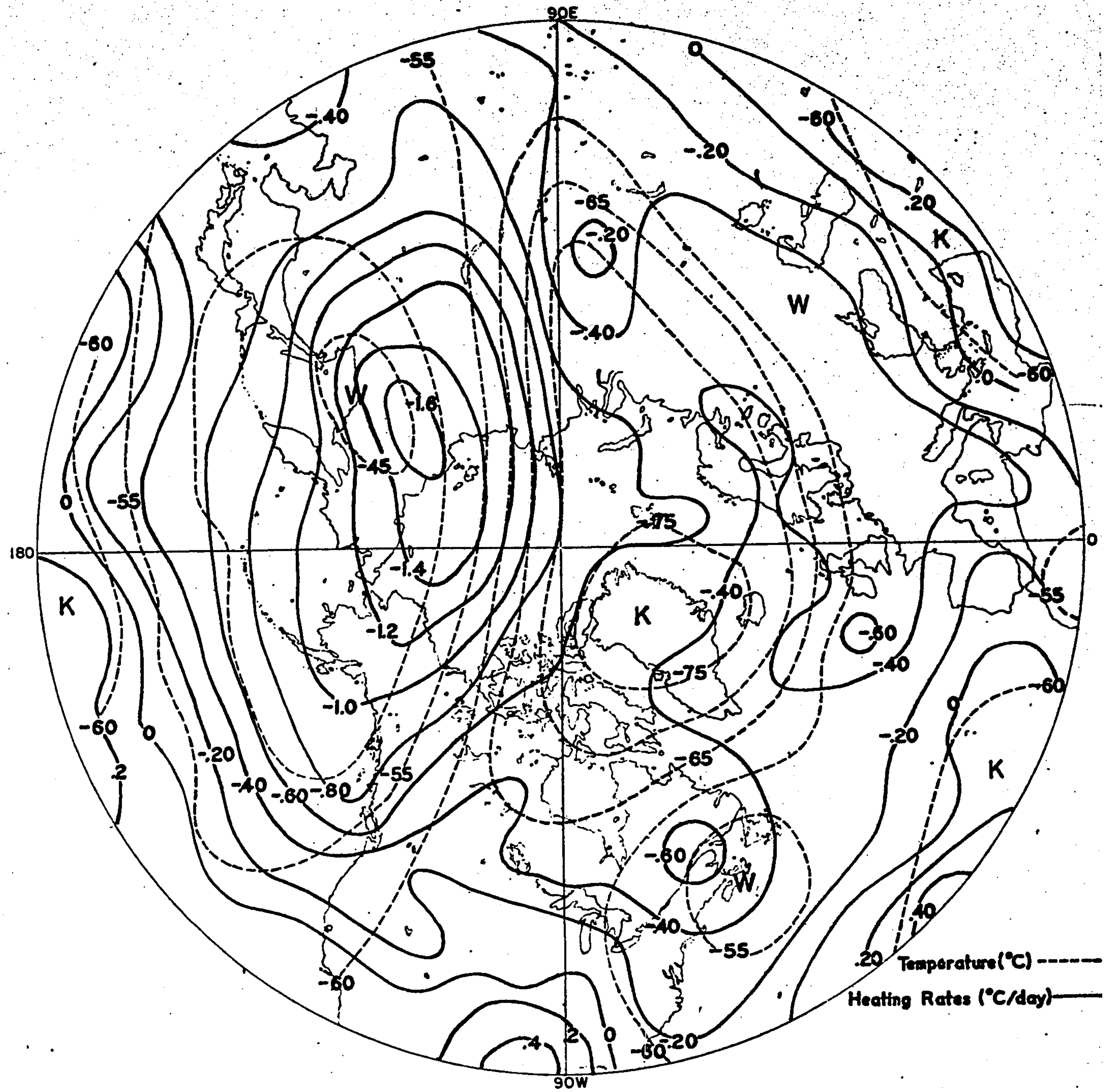

FIG. B. 2. HEATING RATES (°C/DAY) AND TEMPERATURE AT 50 MB 12 JANUARY 1959

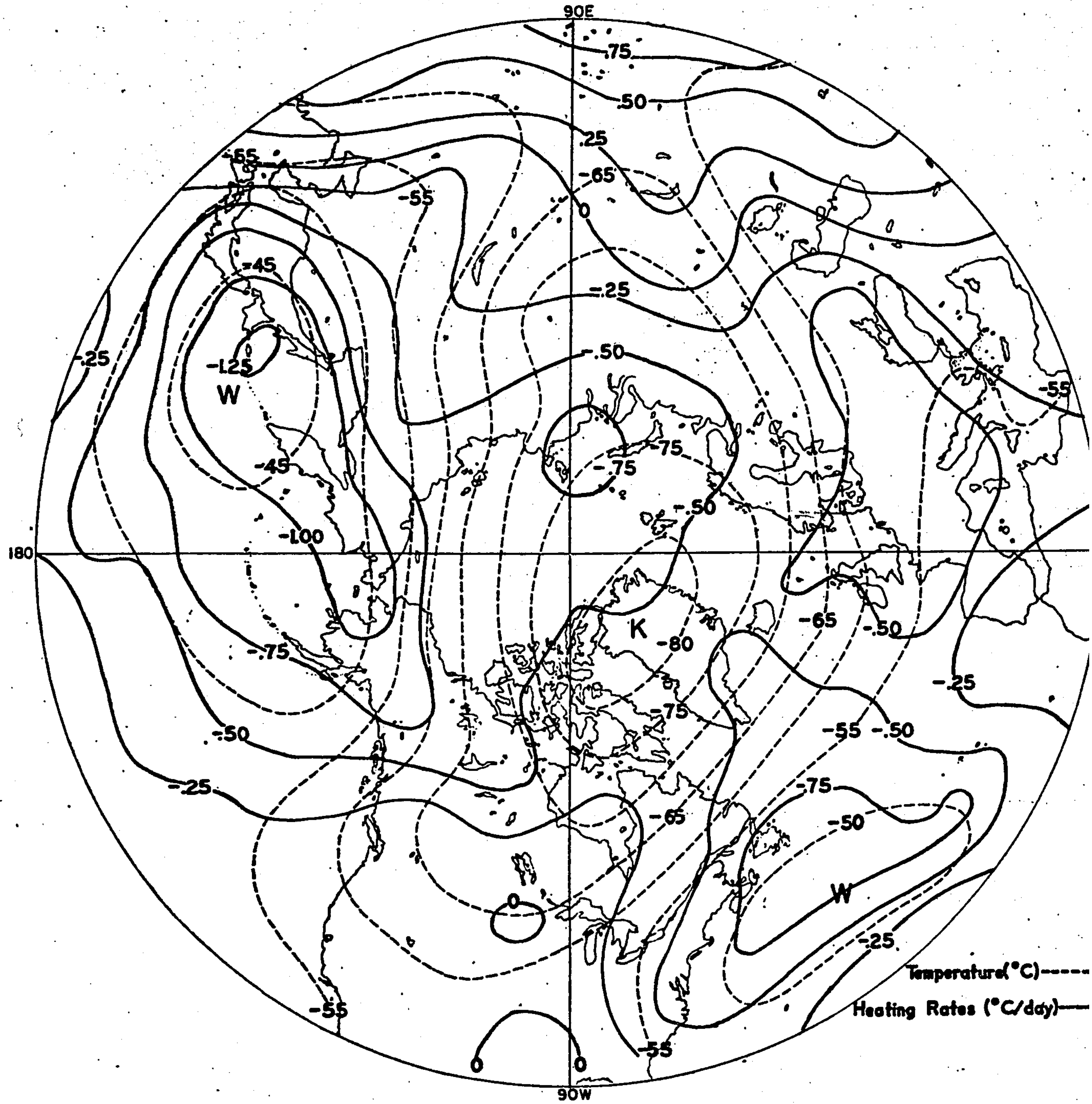

FIG. B.3. HEATING RATES (°C/DAY) AND TEMPERATURE (°C) AT 25 MB 12 JANVIER 1959

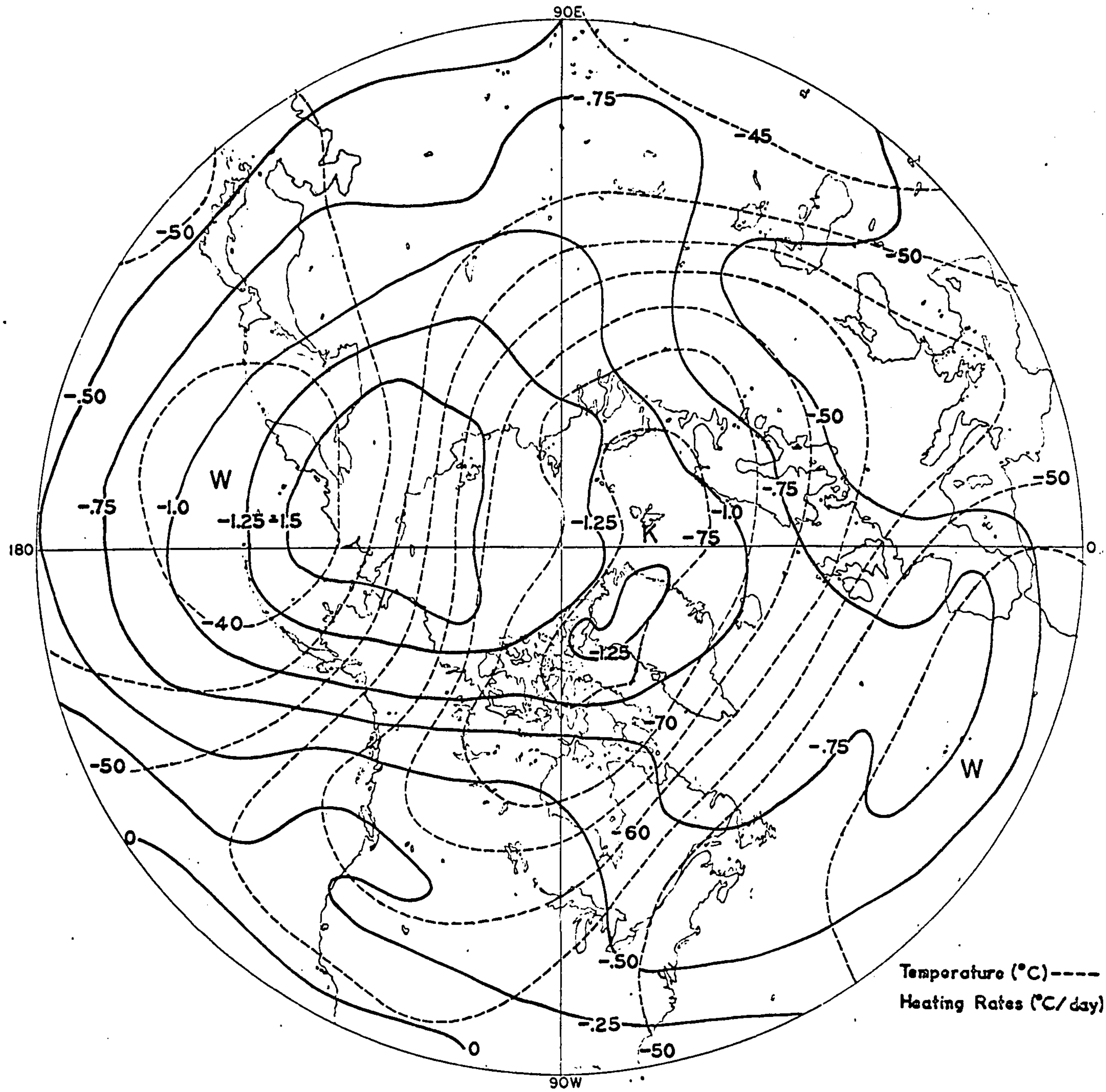

FIG. B. 4. HEATING RATES (°C/DAY) AND TEMPERATURE AT 10 MB. 12 JANUARY 1959.

Appendix C.

FURTHER EXTENSION ON THE COMPLEX FOURIER METHOD

It has been shown in Appendix A that the spectral function J(n) of the product f(λ)g(λ) is given by the multiplication theorem as:

$$J(n) = \sum_{m=-\infty}^{\infty} F(n-m)\,G(m) - \sum_{m=-\infty}^{\infty} G(n-m)\,F(m) \qquad \text{(C-1)}$$

In the case n = 0, this yields Parseval's Theorem:

$$J(0) = \overline{fg}^{\lambda} = \sum_{m=-\infty}^{\infty} F(-m)\,G(m) = F(0)\,G(0) + \sum_{m=1}^{\infty} F(-m)G(m) + F(m)G(-m) \qquad \text{(C-2)}$$

Defining the second term at the extreme right of (C-2) as $\Phi_{fg}(n)$, the relationship becomes:

$$J(0) = \overline{fg}^{\lambda} = \overline{f}^{\lambda}\,\overline{g}^{\lambda} + \sum_{m=1}^{\infty} \Phi_{fg}(m) \qquad \text{(C-3)}$$

If f = g, then:

$$\overline{f^2}^{\lambda} = \overline{f}^{\lambda^2} + \sum_{m=1}^{\infty} \Phi_{fg}(m) = \overline{f}^{\lambda^2} + 2 \sum_{m=1}^{\infty} \left| F(m) \right|^2 \qquad \text{(C-4)}$$

It is then evident that $\sum_{m=1}^{\infty} \Phi_{fg}(n)$ is the covariance between f and g while $\sum_{m=1}^{\infty} \Phi_{f^2}(n)$ is the variance of f.

When S(n) is the spectral function corresponding to the triple product d(λ)f(λ)g(λ), it may be expanded as follows:

$$S(n) = F(0)G(0)D(0) + F(0)\sum_{\substack{m=-\infty \\ \neq 0}}^{\infty} G(m)D(n-m) + G(0)\sum_{\substack{\ell=-\infty \\ \neq 0}}^{\infty} F(\ell)D(n-\ell)$$

$$+ \sum_{\substack{\ell=-\infty \\ \neq 0}}^{\infty} F(\ell) \sum_{\substack{m=-\infty \\ \neq 0}}^{\infty} G(m)D(n-\ell-m) \tag{C-5}$$

Inserting n = 0, i.e., averaging S(n) zonally:

$$S(0) = \overline{dfq}^{\lambda} = \overline{d}^{\lambda}\,\overline{f}^{\lambda}\,\overline{q}^{\lambda} + \overline{f}^{\lambda}\sum_{m=1}^{\infty}\Phi_{qd}(m) + \overline{q}^{\lambda}\sum_{m=1}^{\infty}\Phi_{fd}(m) + \overline{d}^{\lambda}\sum_{m=1}^{\infty}\Phi_{fq}(m)$$

$$+ \sum_{\substack{\ell=-\infty \\ \neq 0}}^{\infty} F(\ell)\sum G(m)D(-\ell-m) \tag{C-6}$$

Since:

$$\overline{dfq}^{\lambda} = \overline{d}^{\lambda}\,\overline{f}^{\lambda}\,\overline{q}^{\lambda} + \overline{f}^{\lambda}\,\overline{q'd'}^{\lambda} + \overline{q}^{\lambda}\,\overline{f'd'}^{\lambda} + \overline{d}^{\lambda}\,\overline{f'q'}^{\lambda} + \overline{f'q'd'}^{\lambda},$$

$$\sum_{m=1}^{\infty}\Phi_{qd}(m) = \overline{q'd'}, \quad \sum_{m=1}^{\infty}\Phi_{fd}(m) = \overline{f'd'}^{\lambda} \quad \text{and} \quad \sum\Phi_{fq}(m) = \overline{f'q'}^{\lambda} \tag{C-7}$$

then:

$$\overline{f'q'd'}^{\lambda} = \sum_{\ell=-\infty}^{\infty} F(\ell)\sum_{\substack{m=-\infty \\ \neq 0 \\ \neq -\ell}}^{\infty} G(m)D(-\ell-m) \tag{C-8}$$

and
$$\overline{d}^{\lambda}\,\overline{f'g'}^{\lambda} + \overline{f'g'd'}^{\lambda} = \sum_{\ell=-\infty}^{\infty} F(\ell) \sum_{\substack{m=-\infty \\ \neq 0}}^{\infty} G(m)\, D(-\ell-m)$$
$$= \sum_{\ell=1}^{\infty} \sum_{\substack{m=-\infty \\ \neq 0}}^{\infty} G(m) \left[F(\ell)\, D(-\ell-m) + F(-\ell)\, D(\ell-m) \right]$$
$$= \sum_{\ell=1}^{\infty} \sum_{\substack{m=-\infty \\ \neq 0}}^{\infty} G(m)\, \Psi_{fd}(m,\ell) \qquad \text{(C-9)}$$
$$= \overline{d\, f'g'}^{\lambda}$$

where

$$\Psi(m,\ell) = F(\ell-m)\,G(-\ell) + F(-\ell-m)\,G(\ell) \qquad \text{(C-10)}$$

It is to be noted that for m = 0,

$$\Psi(0,\ell) = F(\ell)\,G(-\ell) \qquad F(-\ell)\,G(\ell) = \Phi_{fg}(\ell) \qquad \text{(C-11)}$$

and also:

$$\Phi_{ff_{\lambda}}(\ell) = -i\ell\, F(\ell)\, F(-\ell) + i\ell\, F(-\ell)\, F(\ell) \equiv 0. \qquad \text{(C-12)}$$

Eqn. (C-9) represents then the zonal average of the triple product of the field d and the deviations of f and g.